ABSTRACT

SAGUES, WILLIAM JOSEPH. Systems Modeling & Product Development for Biomass-Enabled Carbon-Negative Technologies. (Under the direction of Dr. Sunkyu Park & Dr. Hasan Jameel).

Technologies that remove atmospheric CO_2 must be developed and deployed rapidly if we are to avoid the worst effects of climate change. Engineered carbon-negative technologies, including bioenergy with CO_2 capture and biomass carbonization, require significant advancements to reduce costs and increase scale without environmental or social harm. Additionally, the U.S. bioeconomy is in need of innovative biomass conversion technologies that utilize existing policy incentives and are capable of near-term deployment. Here, we develop and assess a multitude of biomass-enabled carbon-negative technologies that satisfy the aforementioned needs through impactful concept creation, granular system design and modeling, and robust product development, where applicable. We take a systems-level approach to design and model three new integrated biosystems and a product development approach to assess two new bioproducts. From the systems-level approach, we find that direct air capture, dietary protein, ammonia fertilizer, and pulp and paper technologies can all be enhanced through synergistic integration with carbon-negative biosystems. From the product development approach, we find that carbon fibers and electrochemical battery anodes can be enhanced through innovative biomass-enabled carbon-negative technologies. Moving forward, we believe researchers interested in carbon-negative bioproducts should take a similar, integrated approach to innovation, involving both systems-level modeling and experimental product development. This dissertation provides stakeholders in the U.S. bioeconomy with near-term opportunities to leverage existing federal policies for carbon-negative bioproduct development and deployment.

Systems Modeling & Product Development for Biomass-Enabled Carbon-Negative Technologies

by
William Joseph Sagues

A dissertation submitted to the Graduate Faculty of
North Carolina State University
in partial fulfillment of the
requirements for the degree of
Doctor of Philosophy

Forest Biomaterials

Raleigh, North Carolina
2020

APPROVED BY:

Dr. Sunkyu Park Committee Co-Chair	Dr. Hasan Jameel Committee Co-Chair
Dr. Fanxing Lee	Dr. Richard Venditti

BIOGRAPHY

William (Joe) Sagues was raised in Orlando, Florida. Joe attended the University of Florida from 2009 – 2012 where he graduated with a B.S. in Agricultural & Biological Engineering. From 2012 – 2015, he worked as a Bioprocess Engineer at the Stan Mayfield Biorefinery, a private-public partnership between Georgia Pacific LLC and the University of Florida. From 2015 – 2017, he attended the University of Florida where he graduated with M.S. degrees in Chemical Engineering and Agricultural & Biological Engineering. In 2018, he worked as a Technology-to-Market Scholar at the Department of Energy's Advanced Research Projects Agency (ARPA-E). In 2020, he worked as an Office of Science Graduate Student Research Fellow at the Department of Energy's National Renewable Energy Laboratory (NREL). His interests include boating, cycling, hiking, and participating in other outdoor activities with his wife and two dogs.

ACKNOWLEDGEMENTS

This work was made possible through a collaborative effort involving my committee members, departmental faculty, fellow graduate students, interinstitutional colleagues, and family. I would like to thank Dr. Sunkyu Park and Dr. Hasan Jameel for their sincere support, undivided attention, and relentless ambition to answer difficult research questions and conduct impactful work. I would like to thank Dr. Daniel Sanchez for his unwavering positive attitude, sincere generosity, innovative contributions, and commitment to collaborate and pursue impactful research projects. I would like to thank Dr. Richard Venditti for his support and mentorship while I co-developed and co-lectured new online courses focused on the bioeconomy. I would also like to thank Shana McAlexander for improving my teaching philosophy through the use of proven pedagogical techniques. I would like to thank Dr. Fanxing Li for providing valuable technical input to my research. I would like to thank Dr. Mark Davis and Dr. Mark Nimlos from the National Renewable Energy Laboratory for their incredible support during my time as an Office of Science Graduate Student Research Fellow with the Department of Energy. I would like to thank Dr. Madhav Acharya for his mentorship during my time as a Technology-to-Market Scholar at the Advanced Research Projects Agency - Energy. I would like to thank Dr. Argyropoulos for providing the opportunity to incorporate coursework into my dissertation. I would like to thank Dr. Steve Kelley for his endless encouragement and overall positive attitude. I would like to thank members of Dr. Park's lab group for always being there for support if needed. I am so thankful to have all of the aforementioned people as close colleagues as I begin the next chapter in my career. Finally, my wife, Natalie, made enormous efforts to allow me the freedom and flexibility to complete my PhD in a timely fashion and in remote locations, and I am incredibly grateful to have such an amazing and loving spouse.

TABLE OF CONTENTS

LIST OF FIGURES

LIST OF TABLES

Chapter 1 - Introduction

Carbon-negative technologies (CNTs) play a prominent role in climate change mitigation strategies consistent with limiting global warming to well below 2°C; by definition, a CNT provides a service or product which results in a net reduction in atmospheric CO2. A variety of biomass-enabled CNTs show great promise for low-cost, near-term deployment, including bioenergy with carbon capture and sequestration (BECCS) and graphitic carbon materials (GCM). Herein, innovative BECCS and GCM technologies are developed and assessed to provide valuable knowledge and impactful opportunities to stakeholders in CNT development and deployment. In total, three BECCS technologies are assessed from a systems-level perspective, and two GCM technologies are assessed from an experimental product development perspective.

1.1 Systems-Level Modeling of Carbon-Negative Technologies

Direct air capture (DAC) and bioenergy with carbon capture and sequestration (BECCS) are the two leading engineered CNTs currently under development. Major limitations to scaling DAC and BECCS technologies include high demands for energy and natural resources, respectively. To date, there has been almost no research on the synergies between DAC and BECCS technologies. Existing BECCS technologies are designed for energy generation, while existing DAC technologies are presumed to be powered by low-carbon energy sources such as solar, wind, or nuclear. The use of biomass as an energy source for DAC has been largely overlooked in prior literature. Here, we conduct a techno-economic and geospatial analysis to understand the economic and carbon removal potential of coupled BECCS and DAC technologies. The aforementioned limitations to BECCS and DAC technologies are curtailed when coupled into one system. This analysis takes a significant step forward in the development

of CNTs by demonstrating the technical and economic viability of coupled BECCS-DAC systems capable of removing significant quantities of CO_2 with lower cost and environmental impact.

The decarbonization of agriculture faces many challenges and has received a level of attention insufficient to abate the worst effects of climate change and ensure a sustainable bioeconomy. Agricultural emissions are caused both by fossil-intensive fertilizer use and land-use change, which in turn are driven in part by increasing demand for dietary protein. To address this challenge, we present a synergistic CNT in which organic waste-derived biogas (a mixture of methane and carbon dioxide) is converted to dietary protein and ammonia fertilizer. This system produces low-carbon fertilizer inputs alongside high-quality protein, addressing the primary drivers of agricultural emissions. If the proposed system were implemented across the United States utilizing readily available organic waste from municipal wastewater, landfills, animal manure, and commercial operations, we estimate 30% of dietary protein intake and 127% of ammonia usage could be displaced while reducing land use, water consumption, and greenhouse gas emissions.

The pulp and paper industry utilizes more biomass for stationary heat and power than any other industry in the United States. In total, pulp and paper mills in the US emit ~150 million metric tons of CO_2 each year, of which 77% is biogenic. Thus, the pulp and paper industry has significant potential to indirectly remove atmospheric CO_2 through bioenergy with CO_2 capture and storage (BECCS). In addition, avenues for CO_2 utilization exist in pulp and paper processing. Here, we analyze the technical and economic potential of integrating carbon capture, utilization, and sequestration (CCUS) technologies at pulp and paper mills in the US through top-down, industry-wide screening and bottom-up, chemical process modeling techniques. We

estimate costs of capturing and transporting CO_2 from pulp and paper mills using post-combustion amine chemisorption in the year 2026 with application of the existing federal tax credit for carbon capture and sequestration (Section 45Q). Costs are highly dependent on scenario-specific details, such as waste heat or power generation at the mill, idling or stranded assets, and proximity to suitable geologic storage opportunities. Some CCS implementation scenarios produce significant economic returns for pulp and paper mills, indicating a near-term opportunity to accelerate CCS in the US. Finally, we qualitatively assess alternative techniques for CO_2 capture through process innovation, and opportunities for CO_2 utilization at pulp and paper mills.

1.2 Product Development for Carbon-Negative Technologies

Single component lignin-derived carbon fibers have been under development for many years, but strength properties are still inferior to those of commercial carbon fibers. With careful lifecycle accounting, ligin-derived carbon fibers are capable of being carbon-negative products. The extent of graphitization is an overlooked limitation to lignin-derived carbon fiber development, particularly for high-modulus fibers treated at high temperatures. The tensile moduli of commercial carbon fibers increase with temperature during graphitization, however, lignin-derived carbon fiber moduli stay the same or decrease. We expose the inability of lignin-derived carbon fibers to graphitize in a manner similar to commercial carbon fibers, thereby providing rationale for the aforementioned discrepancy in tensile moduli-temperature trends and offering possible tangible future areas of research and development.

Demand for battery-grade graphite is growing rapidly, and new, sustainable methods of production are needed. A multitude of biomass resources of varying molecular composition are converted to high quality graphite for use in lithium-ion anodes using a simple, scalable, and

green process. With careful lifecycle accounting, biomass-derived graphite anodes are capable of being carbon-negative products. Low-cost, earth abundant iron powder is used to catalyze the conversion of softwood, hardwood, cellulose, glucose, organosolv lignin, and hydrolysis lignin biomaterials to crystalline graphite at relatively low temperatures (< 1200°C). Kraft lignin is the only biomaterial incapable of graphitization at the processing conditions used in this study due to high sulfur content. Biographite materials are characterized and compared based on graphite mass yield, graphite crystallite size, degree of graphitization, graphite uniformity, iron catalyst distribution, and graphite crystallite morphology. Particle size, heating method, and intermediate liquid phase formation, among other factors, play important roles in the graphitization process. Molten eutectic iron carbides act as graphite reactors, solubilizing disordered carbon and precipitating graphite platelets of crystal size comparable to commercial graphite (Lc ~ 20 - 30nm). Softwood-derived biographite is of the highest quality and demonstrates excellent electrochemical performance as anode material in a lithium-ion coin cell.

Chapter 2 - Enhanced Carbon Dioxide Removal from Coupled Direct Air Capture-Bioenergy Systems

2.1 Introduction

Engineered CO2 removal technologies—such as direct air capture (DAC) and bioenergy with carbon capture and sequestration (BECCS)—hold large promise for rapid and reliable CO2 removal consistent with stringent climate change mitigation.2.1–2.3 However, DAC and BECCS remain commercially and technically immature.2.4 The Intergovernmental Panel on Climate Change (IPCC) insists that DAC and BECCS technologies must scale up rapidly as the necessity for CO2 removal increases.2.3 To meet stringent climate targets set forth by the IPCC, the United States is expected to sequester 1 GtCO2 per year in 2050 and 3 GtCO2 per year in 2100.2.5 To meet such ambitious targets, research, development, and demonstration of CO2 removal technologies must rapidly accelerate.2.3,2.6,2.7

BECCS refers to the utilization of renewable biomass resources for energy and the subsequent capture and sequestration of CO_2 via injection into geologic formations.[2.3,2.5,2.6] The advantages of using BECCS for engineered CO_2 removal include relatively low cost and the existence of established technologies for both biomass conversion and CO_2 capture and sequestration.[2.6] The major drawbacks of BECCS technologies are their substantial land requirements, sustainability impacts at scale, limited resource potential, and social barriers to acceptance.[2.8–2.10] Nonetheless, the US National Academy of Sciences recently classified BECCS as one of four CO_2 removal technologies ready for immediate deployment.[2.6] DAC refers to the direct removal of CO_2 from the atmosphere and subsequent sequestration. Two leading DAC technology platforms employ liquid solvents and solid sorbents.[2.2,2.11] Several companies are currently commercializing technologies that use these platforms, including Carbon Engineering,

which uses a liquid alkaline solvent for thermal energy-driven calcium looping,[2.12] and Global Thermostat and Climeworks, which use solid-supported amine sorbents for thermal energy-driven adsorption/desorption.[2.13,2.14] The advantages of using DAC for engineered CO_2 removal include flexibility in site location, low land footprint, and potentially limitless scale. However, DAC technologies suffer from high costs, substantial energy requirements, and commercial immaturity.[2.2] The US National Academy of Sciences recently reported the levelized costs of CO_2 removal via DAC to be uneconomical in current policy environments.[2.6,2.15]

The energy-intensive nature of liquid solvent and solid sorbent DAC technologies contribute to their high costs of operation. The majority of such DAC technologies under development require substantial quantities of thermal energy for regeneration (Figure 2.1). Liquid solvent based calcium looping requires high temperature thermal energy to liberate CO_2 from calcium carbonate. A direct heating, oxygen-fired calciner using natural gas for fuel is utilized in Carbon Engineering's pilot plant in Squamish, BC, which they describe as their 'baseline' process in recent literature.[2.12] To ensure their process results in a net removal of CO_2, Carbon Engineering envisions the sequestration of CO_2 produced from natural gas combustion along with that from the atmosphere. Similarly, solid-supported amine adsorption/desorption requires a significant quantity of low-to-medium temperature thermal energy for CO_2 liberation and sorbent regeneration.[2.6,2.13,2.14] Carbon Engineering recently published a detailed techno-economic analysis of their pilot-scale liquid solvent process in which levelized costs were estimated to vary between \$126 - \$170 per t-CO_2 for an n^{th}-of-a-kind plant with a net removal of 0.98 Mt-CO_2 per year (12). The US National Academy of Sciences estimates costs of solid sorbent CO_2 removal to vary between \$89 - \$877 per t-CO_2 for an n^{th}-of-a-kind plant utilizing low temperature thermal energy with a net removal of ~1 Mt-CO_2 per year[6]; the wide range of

costs is due to the different sources of energy used in their modeling, namely solar, nuclear, natural gas, and coal (biomass was not included).

Many emerging DAC innovators claim that fossilized hydrocarbons, renewable electricity, or nuclear energy will provide the thermal energy necessary for operation.[2.6] Biomass, however, is frequently neglected in such analyses: for instance, recent energy system modelling of DAC integration into low-carbon heat and power systems did not consider biomass as an energy source.[2.16] Biomass combustion technologies hold several advantages over other low-carbon technologies for providing thermal energy for DAC, including high heating efficiencies, high technology readiness, and the ability to contribute to CO_2 removal (Figure 2.1).[2.17,2.18]

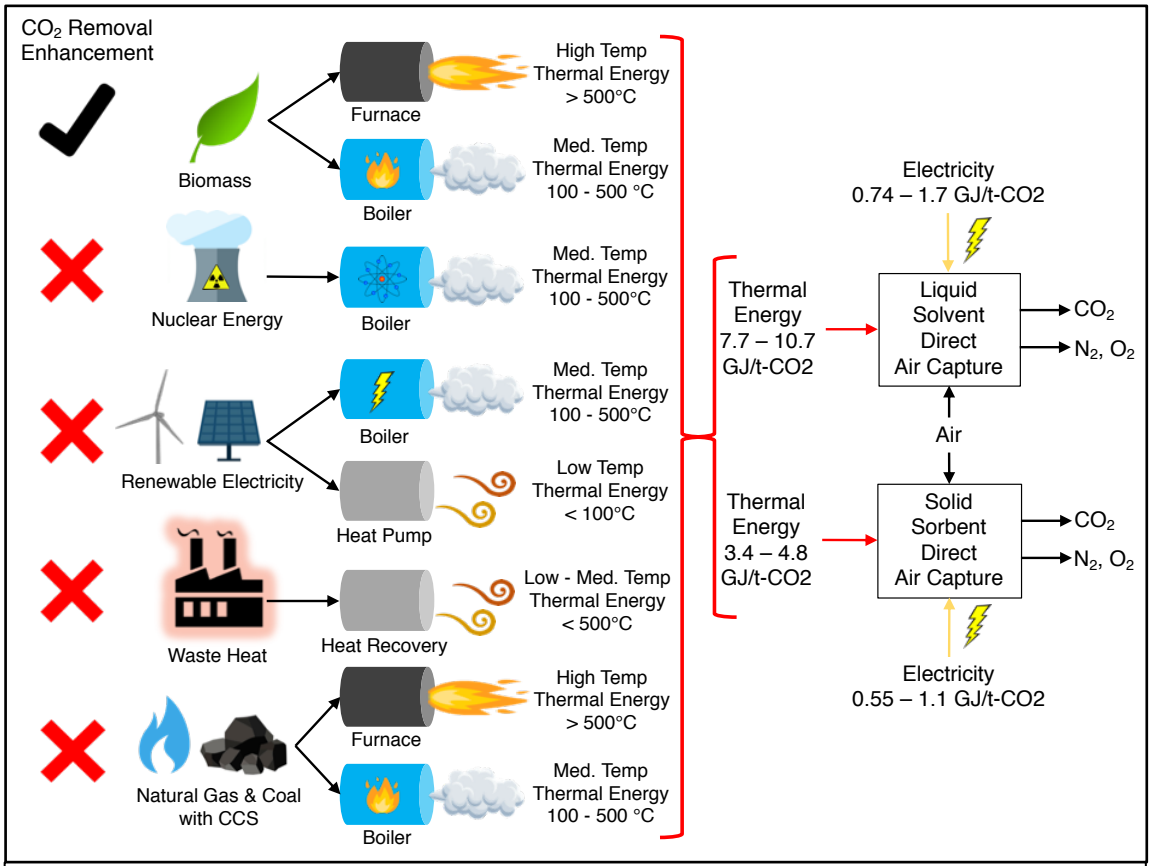

Figure 2.1 Commercially established, low-carbon methods for obtaining thermal energy and their applicability towards carbon dioxide removal via direct air capture (left).[2.17] Ranges of thermal and electrical energy demands for direct air capture recently reported by the US National Academy of Sciences (right) (values do not include energy required for CO_2 compression).[2.6]

The use of biomass for thermal energy-driven DAC technologies remains relatively unexplored, despite the ability of BECCS to provide carbon-negative heat and power to DAC processes. Here, we demonstrate that integration of BECCS and DAC systems reduces costs, increases CO_2 removal, and extends the impact of scarce biomass resources. To demonstrate this, we estimate the levelized costs of CO_2 removal and performance of two hybrid BECCS-DAC systems and compare them to commonly proposed standalone CO_2 removal systems.

2.2 Methodology

2.2.1 System Design & Modeling

We design, model, and analyze four CO_2 removal systems by scaling and integrating detailed technologies from published literature and using conservative assumptions to estimate performance and costs.[2.6,2.12,2.19–2.21] The integration of technologies considered in this study demonstrate the benefits of synergizing bioenergy and direct air capture systems relative to standalone reference systems. We compare a natural gas plus liquid solvent direct air capture (NG + LS-DAC, Figure 2.2A) system to a biomass gasification plus liquid solvent direct air capture (BG + LS-DAC, Figure 2.2B), mimicking a biomass-enhanced DAC system. Subsequently, we compare a biomass boiler plus solid sorbent carbon capture (BB + SS-CC, Figure 2.2C) system to a biomass boiler plus solid sorbent direct air capture (BB + SS-DAC, Figure 2.2D) system, mimicking a DAC-enhanced BECCS system.

We design our biomass-DAC systems to demonstrate the inherent advantages biomass has as an energy source for DAC. Each system is modeled as a greenfield plant. We define system boundaries as inside the battery limits of the chemical processing facilities, with compressed CO_2 as the final product. Table A2.1 provides a basic overview of the four CO_2 removal systems. Figure A2.1 shows the generalized approach to designing, modeling, and

analyzing the four systems. Table 2.1 provides pertinent technical information about the four CO_2 removal systems.

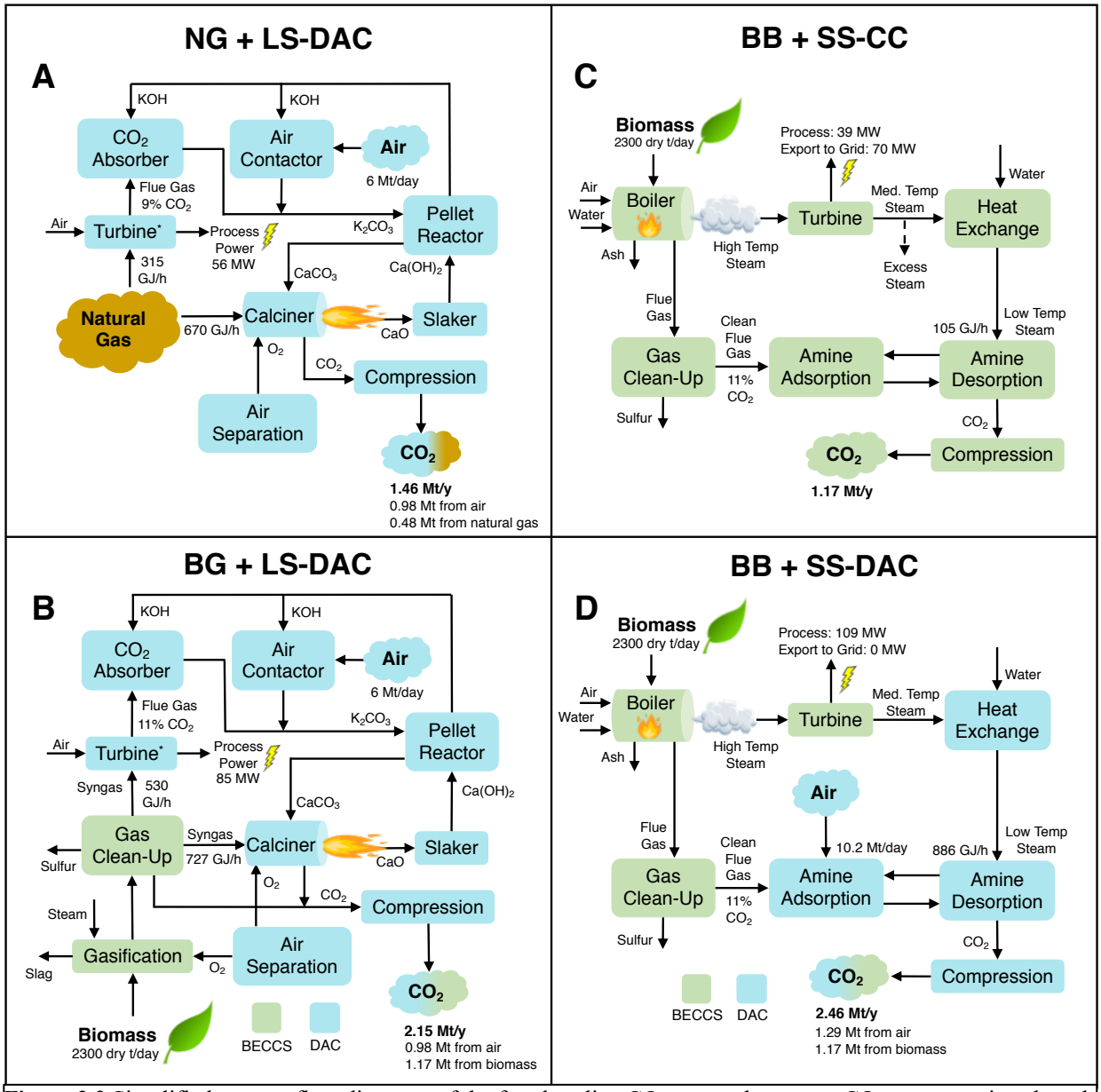

Figure 2.2 Simplified process flow diagrams of the four baseline CO_2 removal systems. CO_2 concentrations based on volume. **A)** Natural Gas plus Liquid Solvent Direct Air Capture (NG + LS-DAC) system, adapted from Carbon Engineering's baseline DAC system.[2.12] Turbine* includes a gas turbogenerator and a heat recovery steam generator. **B)** Biomass Gasification plus Liquid Solvent Direct Air Capture (BG + LS-DAC) system.[2.6,2.19] **C)** Biomass Boiler plus Solid Sorbent Carbon Capture (BB + SS-CC) system.[2.6,2.20] **D)** Biomass Boiler plus Solid Sorbent Direct Air Capture (BB + SS-DAC) system.[2.6,2.20]

Table 2.1 Technical details for the four baseline CO_2 removal systems analyzed in this study. The parameters for the natural gas plus liquid solvent (NG + LS-DAC) system were taken from Keith et al.'s technical analysis of Carbon Engineering's baseline direct air capture technology.[2.12]

	NG + LS-DAC	**BG + LS-DAC**	**BB + SS-CC**	**BB + SS-DAC**
Air flow rate (Mt/day)	6.0	6.0	--	10.2
Biomass flow rate (dry t/day)	--	2300	2300	2300
Air-derived CO_2 capture (Mt-CO_2/year)	0.98	0.98	--	1.29
Air-derived CO_2 capture efficiency (t-CO_2 removed/t-CO_2 in air)	74.5%	74.5%	--	65%
Natural-gas derived CO_2 captured (Mt-CO_2/year)	0.47	--	--	--
Biomass-derived CO_2 captured (Mt-CO_2/year)	--	1.17	1.17	1.17
Flue gas CO_2 capture efficiency (t-CO_2 removed/t-CO_2 generated)	90% nat. gas	90% biogenic	90% biogenic	90% biogenic
Biogenic carbon capture ratio (t-CO_2/t-biomass)	--	1.55	1.55	1.55
Total CO_2 removal capacity (Mt-CO_2/year)	0.98	2.15	1.17	2.46
% Increase in CO_2 removal capacity relative to reference system	0% (reference)	119%	0% (reference)	109%
Energy content of biomass fuel (25% moisture) (LHV) (GJ/tonne)	--	12.6	12.6	12.6
Fuel energy (LHV) to electrical energy 1st law conversion efficiency	~52% (fuel = nat. gas)	44.9% (fuel = biomass)	24.5% (fuel = biomass)	24.5% (fuel = biomass)
Electrical energy demand (GJ/t-CO_2) * denotes energy demand without accounting for biogenic CO_2	~1.8	1.2 2.6*	1.0	1.3 2.4*
Electrical energy demand (MW)	~55.8	84.6	39.6	109.5
Thermal energy demand (GJ/t-CO_2) * denotes energy demand without accounting for biogenic CO_2	~5.6	2.8 6.1*	0.71	2.8 5.4*
Thermal energy demand (GJ/h)	~624	727	105	886
Pressure of compressed CO_2 (bar)	151	151	151	151
Purity of CO_2 [% CO_2]	97%	97%	97%	97%

Equation 1 is used to calculate the minimum work required for separation of CO_2 from various gaseous streams.[2.21]

$$Minimum\ work\ for\ CO_2\ separation = w_{min} = RT \begin{bmatrix} \left(n_{r,CO_2} \ln\left(X_{r,CO_2}\right) + n_r \ln\left(X_r\right)\right) \\ +\left(n_{p,CO_2} \ln\left(X_{p,CO_2)}\right) + n_p \ln\left(X_p\right)\right) \\ -\left(n_{i,CO_2} \ln\left(X_{i,CO_2}\right) + n_i \ln\left(X_i\right)\right) \end{bmatrix} \quad (1)$$

$n_{x,CO_2} = moles\ of\ CO_2\ in\ stream\ x$
$n_x = moles\ of\ nonCO_2\ component\ in\ stream\ x$
$X_{x,CO_2} = mole\ fraction\ of\ CO_2\ in\ stream\ x$
$X_x = mole\ fraction\ of\ nonCO_2\ components\ in\ stream\ x$
$r = residual\ stream$
$p = product\ stream$
$i = inlet\ stream$

The process flow diagrams shown in Figure 2.2, as well as Figures S2 – S5, include major unit operations only. Each operation contains process equipment not shown, such as pumps, compressors, mixers, and reactors. Detailed diagrams including such equipment can be found in the published techno-economic analyses that are used for process scaling (Figures S2-S5).[2.6,2.12,2.19,2.20] The biomass gasification and two solid sorbent systems do not undergo intensive engineering optimization, which could further decrease costs and improve performance. We expect future studies to investigate system configurations different than those presented here. For instance, there is potential to integrate emerging, biomass-based solid chemical looping technologies with liquid solvent DAC.[2.22,2.23]

2.2.2 Economic Analysis

To ensure consistency when calculating levelized costs of CO_2 removal, we follow the method of economic analysis used by Keith et al. for the four CO_2 removal systems.[2.12] Keith et al.'s methodology for economic analysis, which is adequate for early-stage cost estimations, requires five primary inputs: 1) itemized capital costs, 2) energy and non-energy operating costs, 3) plant utilization, 4) capital intensity, and 5) a capital recovery factor (CRF). To validate our economic model, we independently reproduce economic figures for Carbon Engineering's baseline liquid solvent DAC process. The levelized costs calculated by the independent

economic analysis match Keith et al.'s published values, as shown in Table A2.4. Itemized capital and operating costs along with Equations 2 – 10 allow for reasonable estimates of levelized costs of CO_2 removal by the four systems.

$$Levelized\ Cost\ of\ CO_2\ Removal = Levelized\ Capital\ Cost + \ Net\ Operating\ Cost \quad (2)$$

$$Net\ Operating\ Cost = \frac{NonEnergy\ Cost + Energy\ Cost - Byproduct\ Revenue}{CO_2\ Capacity} \quad (3)$$

$$Levelized\ Capital\ Cost = Capital\ Intensity \times \frac{Capital\ Recovery\ Factor}{Utilization} \quad (4)$$

$$Capital\ Intensity = \frac{Total\ Capital\ Cost}{CO_2\ Capacity} \quad (5)$$

$$Capital\ Recovery\ Factor = \frac{i(i+1)^N}{(1+i)^N - 1} \quad (6)$$

$$\begin{aligned} Weighted\ Average\ Cost\ of\ Capital = i \\ = (Interest\ on\ Debt\ Capital) \times (\%\ Debt\ Financing) \\ + \ (Return\ on\ Equity\ Capital) \times (\%\ Equity\ Financing) \end{aligned} \quad (7)$$

$$N = Project\ life\ (years) \quad (8)$$

$$Total\ Capital\ Cost = Direct\ Capital + Indirect\ Capital \quad (9)$$

$$Direct\ Capital\ Cost = \sum_i Reference\ Cost_i \times \left(\frac{New\ Capacity_i}{Reference\ Capacity_i}\right)^{Scale\ Factor} \quad (10)$$

We perform a sensitivity analysis on the levelized cost of CO_2 removal by varying CRF values and biomass costs. CRF is a metric that considers financing details including weighted average cost of capital (i) and project life (N) (Equations 6, 7 & 8). Table A2.2 provides CRF values with varying i and N values. Keith et al.'s economic analysis used CRF values of 7.5% and 12.5%, whereas this study uses values ranging from 2.5% to 17.5%. CRF values above 12.5% are reflective of stringent financial obligations that might be used for nascent CO_2 removal technologies. A CRF value of 2.5% requires a very low cost of capital, which might be

possible with strong government support. Several financing uncertainties are therefore taken into account by varying the CRF.[2.12] As in Keith et al.'s economic analysis, corporate taxes are not included in this method of early-stage cost estimation. The biomass costs used for analysis range from $20 - $100 per short ton, a range that includes the majority of potential biomass resources characterized in the US DOE's Billion-Ton Report.[2.24] Conservative contingency costs are used in the economic analyses of the new systems, as shown in Table 2.2.

Table 2.2 Baseline economic details for the four CO_2 removal systems analyzed in this study. The parameters for the natural gas plus liquid solvent system were taken from Keith et al.'s economic analysis of Carbon Engineering's baseline direct air capture technology.[2.12]

	NG + LS-DAC	**BG + LS-DAC**	**BB + SS-CC**	**BB + SS-DAC**
Plant utilization	90%	90%	90%	90%
Project year	2016	2016	2016	2016
Natural gas price ($/GJ)	3.5	--	--	--
Capital scaling factor	--	0.8	0.8	0.8
Indirect capital costs (% direct capital)	35%	35%	35%	35%
Capital cost contingency (% direct & indirect capital)	12.5%	20%	30%	30%
Excess electricity sold to grid (MW)	--	--	70	--
Purchase cost of byproduct electricity ($/kWh)	--	--	$0.05	--
Excess thermal energy sold as byproduct steam (GJ/h)	--	--	780	--
Purchase cost of byproduct steam (~230C)($/t-steam)	--	--	$7.02	--

The capital contingency cost for the NG + LS-DAC system is for an nth-of-a-kind plant with a relatively low level of uncertainty, whereas the contingency costs for the bioenergy-integrated systems are for early-stage plants with higher levels of uncertainty. To remain conservative in our economic assessments, contingencies of 20% and 30% are used for the BG + LS-DAC and BB + SS-CC/DAC systems, respectively; these contingencies were conservatively selected based on industry practices.[2.25] The NG + LS-DAC system has undergone intensive development and is currently being commercialized[2.12], whereas the bioenergy-integrated

systems are less robust and therefore require higher contingencies. The bioenergy-integrated solid sorbent systems have a higher contingency cost than the liquid solvent system because of the increased uncertainty in the heat exchange subsystem that is used to generate and distribute clean, low temperature steam for amine desorption, as well as the overall technical immaturity of solid sorbent DAC systems.

To account for upstream emissions, additional analyses are conducted in which emission penalties are applied to natural gas and biomass fuels.[2.1] The techno-economic results presented here are conservative, early-stage estimations with some uncertainty; however, they allow direct comparison between standalone and biomass-integrated DAC technologies.

2.2.3 Upstream Emissions Accounting

Baseline scenarios assume no leakage of natural gas during extraction and transportation and carbon neutrality for cultivation, harvest, and transportation of biomass. Penalty scenarios are constructed to account for upstream emissions (Tables 2.5 and S14). The Penalty scenario for the NG + LS-DAC system assumes the quantity of natural gas-carbon leaked during extraction and transportation is equal to 3% of the natural gas-carbon captured on-site. A global warming potential of 25 is assigned to leaked natural gas. The Penalty scenarios for the three biomass systems assume the quantity of carbon emitted to the atmosphere during cultivation, harvest, and transportation of biomass is equal to 15% of the biogenic carbon captured on-site.[2.26] Severe No Bio penalty scenarios for the BG + LS-DAC and BB + SS-DAC systems are constructed in which none of the biogenic carbon captured on-site is included in the net removal of CO_2. A detailed life cycle assessment including the global warming impact of the four cases presented would provide a more accurate accounting of emissions and should be considered in future studies.

2.2.4 Geospatial Analysis

To understand the potential for gigaton-scale CO_2 removal by the proposed BECCS-DAC systems in the US, we conduct a geospatial analysis based on methods developed by Baik et al.[2.8] Our geospatial analysis considers the amount of biomass economically available for under $100 per dry short ton in every US county, the locations of suitable geologic formations for permanent CO_2 sequestration, and the CO_2 removal capacity of the BECCS-DAC systems.

2.2.5 System Descriptions

2.2.5.1 Natural Gas plus Liquid Solvent Direct Air Capture (NG + LS-DAC)

The Natural Gas plus Liquid Solvent Direct Air Capture system (NG + LS-DAC, Figure 2.2A) is adapted from Carbon Engineering's baseline liquid solvent technology that uses alkaline chemistry for CO_2 capture.[2.12] Carbon Engineering's baseline technology uses natural gas as the sole energy source for both thermal and electrical energy. The itemized capital and operating costs are presented by Keith et al. This system is analyzed and compared with the BG + LS-DAC system.

2.2.5.2 Biomass Gasification plus Liquid Solvent Direct Air Capture (BG + LS-DAC)

The Biomass Gasification plus Liquid Solvent Direct Air Capture system (BG + LS-DAC, Figure 2.2B) integrates biomass gasification with the NG + LS-DAC system by substituting natural gas with biomass-derived syngas. The biomass gasification technology is modeled using robust process information obtained from a techno-economic analysis (TEA) published by the US National Renewable Energy Laboratory (NREL).[2.19] NREL is a leading institute in the field of biomass conversion technology development and has published detailed TEAs of multiple biomass conversion technologies. The biomass gasification technology involves a high temperature, entrained-flow, slagging gasifier, which has been commercially

proven by GE, Siemens, Shell, and ConocoPhillips. Corn stover is used as the model biomass feedstock with 25% moisture and an energy content of 12.6 GJ per tonne (16.8 GJ per dry tonne) (LHV); corn stover's mass composition (47% C, 5% H, 41% O, 0.2% S, 0.8% N, and 6% ash) serves as an adequate representation of lignocellulosic biomass. The original design by NREL involves biomass gasification plus catalytic conversion of syngas to liquid fuels. Extraneous operations involved with liquid fuel synthesis are not included in the BG + LS-DAC model; NREL's detailed mass and energy flows for each unit operation allow for complete system integration with a liquid solvent DAC technology. The syngas is cleaned via scrubbing of particulates, ammonia, hydrogen sulfide, and some CO_2. Syngas has been shown to be a suitable replacement to natural gas as fuel for gas turbines.[2.19,2.27,2.28] A complete water-gas shift reaction could be incorporated to remove CO_2 pre-combustion and generate a pure stream of hydrogen instead of syngas,[2.4] however, we did not model such a configuration. The costs associated with removing CO_2 from turbogenerator flue gas were deemed acceptable because of the large quantity of liquid solvent already on-site for CO_2 removal from air; Carbon Engineering's baseline design incorporates post-combustion removal of CO_2 from turbogenerator flue gas. The biomass feed rate of 2300 dry tonnes per day provides energy to remove 0.98 Mt-CO_2/year from air, which is equivalent to that of the NG + LS-DAC system. The syngas turbogenerator and heat recovery steam generator supply enough heat (727 GJ/h) and power (84.6 MW) to operate the entire BG + LS-DAC system. The 1st law efficiency of converting biomass energy (LHV) to electricity is 44.9%, accounting for the gas turbogenerator and heat recovery steam generator. Electrical energy produced from the steam slaker excess heat is conservatively taken to be zero. The BG + LS-DAC system captures more total CO_2 than the NG + LS-DAC system due to the relatively high carbon/hydrogen ratio of biomass. Similar to coal, biomass produces more CO_2

than natural gas per unit energy harnessed via combustion.[2.21] The CO_2 concentrations of air and syngas combustion flue gas are 0.04% and 11% by volume, respectively. The percentages of CO_2 captured from air and flue gas are 74.5% and 90%, respectively, and the end purity is 97%, equaling those in the NG + LS-DAC system. Therefore, according to Equation 1, the theoretical minimum energy inputs required for separation of CO_2 from air and flue gas are 20.38 kJ/mol (463 MJ/t-CO2) at 25°C and 8.34 kJ/mol (190 MJ/t-CO2) at 90°C, respectively (not including compression). The real work required for CO_2 separation by the BG + LS-DAC system is determined by scaling heat and power demands of the NG + LS-DAC system. The relatively large quantity of CO_2 produced from the BG + LS-DAC system requires more absolute thermal and electrical energy than the NG + LS-DAC system, particularly for calcination and compression. However, the increased net removal of CO_2 by the BG + LS-DAC system results in lower thermal and electrical energy demands per t-CO_2 removed, when compared to the NG + LS-DAC system; see Table 2.1 for further details. Approximate mass and energy flows are provided in Tables 2.1 and S2.5 and Figure A2.3.

The itemized capital costs are scaled using appropriate scaling factors, as shown in Table A2.6. Biomass cost is the sole contributor to energy operating cost with feedstock prices varying from $20 – $100 per short ton. The non-energy operating costs are comprised of those associated with biomass gasification and liquid solvent CO_2 removal.[2.12,2.19] The non-energy operating costs associated with the gasification subsystem are comprised of steam, cooling water, other raw materials, waste disposal, and fixed costs. Fixed costs for the gasification subsystem include salary, overhead (60% of total salaries), and maintenance (2% of total installed equipment cost). The non-energy operating costs associated with liquid solvent CO_2 removal

include make-up streams and fixed costs (including raw materials, maintenance, labor, and waste disposal).

2.2.5.3 Biomass Boiler plus Solid Sorbent Direct Air Capture (BB + SS-DAC)

The Biomass Boiler plus Solid Sorbent Direct Air Capture system (BB + SS-DAC, Figure 2.2D) integrates a proven biomass boiler technology with an emerging solid sorbent amine CO_2 removal technology. The system is scaled to have the same biomass feed rate as the BG + LS-DAC system. The biomass boiler technology is modeled using process information from a techno-economic analysis published by NREL.[2.20] The solid sorbent technology is modeled using technical information from the National Academy of Sciences.[2.6] Emerging solid sorbent technologies are designed to capture CO_2 from gaseous streams concentrated in CO_2 (flue gas) as well as from streams dilute in CO_2 (air).[2.13,2.14] The biomass boiler features a live-bottom grated fuel bin, combustor, boiler, and turbogenerator. The biomass boiler flue gas is cleaned via particulate removal and desulfurization. As with the BG + LS-DAC system, corn stover is the model biomass feedstock with 25% moisture and an energy content of 12.6 GJ per tonne (16.8 GJ per dry tonne) (LHV). The biomass boiler and turbogenerator generate enough heat (886 GJ/h) and power (109 MW) to operate the solid sorbent CO_2 removal system. All of the generated heat and power are used for direct air capture, with no excess. The 1st law conversion efficiencies of biomass energy (LHV) to heat and power are 55% and 24.5%, respectively.[2.18] A heat exchange network converts the medium temperature steam (~230°C) from the turbine outlet to low temperature saturated steam (~100°C) for CO_2 desorption.[2.6] The solid sorbent system works by temperature/pressure swing for adsorption/desorption with a cycle time of 16 minutes (90 cycles per day).[2.6] The adsorbent material lifetime and CO_2 removal capacity are 0.5 year and 1.3 t-CO_2/kg/year, respectively.[2.6] The biomass boiler flue gas is

comprised of 11% CO_2 by volume and at a temperature of 60°C. Air is comprised of 0.04% CO_2 by volume and at a temperature of 25°C. The amine sorbent subsystem is modeled as two components (Figure A2.4): one component removes CO_2 from air with an efficiency of 65% and the other removes CO_2 from biomass boiler flue gas with an efficiency of 90%. The CO_2 end purity is 97%. Therefore, according to Equation 1, the theoretical minimum energy inputs required for separation of CO_2 from air and biomass boiler flue gas streams are 20.1 kJ/mol-CO_2 (458 MJ/t-CO_2) and 7.66 KJ/mol-CO_2 (174 MJ/t-CO_2), respectively (not including compression). The real work required for solid sorbent amine separation of CO_2 from air is taken to be 5900 MJ/t-CO_2 (4800 MJ/t-CO_2 from heat and 1100 MJ/t-CO_2 from electricity), correlating to a 2nd law efficiency of 7.76%[2.21]; the real work values are conservatively taken from the high-energy demand scenario in reference 1.[2.6] The real work required for solid sorbent amine separation of biomass boiler flue gas is taken to be 870 MJ/t-CO_2 (708 MJ/t-CO_2 from heat and 162 MJ/t-CO_2 from electricity), correlating to a 2nd law efficiency of 20%.[2.21] Approximate mass and energy flows are provided in Tables 2.1 and S2.8 and Figure A2.4.

The itemized capital costs were scaled using appropriate scaling factors, as shown in Table A2.9. Biomass cost is the sole contributor to energy operating cost with feedstock prices varying from $20 – $100 per short ton. The non-energy operating costs are comprised of those associated with the biomass boiler and solid sorbent CO_2 removal. The non-energy operating costs associated with the biomass boiler are comprised of makeup water, other raw materials, and fixed costs. Fixed costs include salary, overhead (60% of total salaries), and maintenance (2% of total installed equipment cost). Uncertainty exists in the capital cost of the heat exchange subsystem that is used to generate clean, low temperature steam for amine desorption; the 30% contingency takes this uncertainty into account. The non-energy operating costs associated with

solid sorbent CO_2 removal include adsorbent material replacement, maintenance, and fixed costs (including other raw materials and waste disposal). The adsorbent material price is $50/kg, and therefore adsorbent material replacement contributes greatly to the final levelized cost of CO_2 removal.[2.6] Due to lack of information, the salary and overhead costs associated with the solid sorbent CO_2 removal subsystem are taken to be the same as that for the biomass boiler subsystem.

2.2.5.4 Biomass Boiler plus Solid Sorbent Carbon Capture (BB + SS-CC)

The Biomass Boiler plus Solid Sorbent with Carbon Capture (BB + SS-CC, Figure 2.2C) is the same as the BB + SS-DAC system, but without any direct air capture. An excess of 70 MW of power and 780 GJ/h of heat in the form of steam are sold to generate byproduct revenue. The biomass boiler flue gas is the only gaseous stream input to the solid sorbent subsystem and has the same composition as the flue gas in the BB + SS-DAC system. Approximate mass and energy flows are provided in Tables 2.1 and S2.11 and Figure A2.5.

The itemized capital costs were scaled using appropriate scaling factors, as shown in Table A2.12. Biomass is the sole contributor to energy operating cost with feedstock prices varying from $20 – $100 per short ton. The contributors to non-energy operating costs are the same as those for the BB + SS-DAC system. An excess of 70 MW of power is sold to the grid at varying prices (Table 2.4) and an excess of 780 GJ/h of heat in the form of steam is sold at $7.02/tonne.[2.25]

2.3 Results & Discussion

As shown in Tables 2.3A & B, levelized costs of CO_2 removal by the BG + LS-DAC system range from $54 - $187 per t-$CO_2$ across analyzed parameters, a significant improvement over the NG + LS-DAC system's range of $65 - $268 per t-$CO_2$. Only air-derived CO_2 may be

taken into account when calculating levelized costs of CO_2 removal by the NG + LS-DAC system, as natural gas-derived CO_2 does not contribute to a net removal of atmospheric CO_2. The BG + LS-DAC system's use of renewable biomass allows for biogenic CO_2 to contribute towards net CO_2 removal, resulting in a more cost-effective approach. In addition to improving economics, CO_2 removal capacity increases by 119% when biomass-derived syngas is used in place of natural gas, and the energy demand per t-CO_2 removed is significantly reduced.

As shown in Tables 2.3C & D, with an electricity selling price of $0.05/kWh, the levelized costs of CO_2 removal range from $80 - $186 and $106 - $165 per t-$CO_2$ for the BB + SS-CC and BB + SS-DAC systems, respectively, across analyzed parameters. The high operating cost of replacing adsorbent material every 6 months makes the BB + SS-DAC system economically unfavorable when the costs of fuel (biomass) and capital are low; however, the integrated system still out performs its reference standalone system (BB + SS-CC) in 45% of the analyzed scenarios. The economics of the BB + SS-DAC system become more favorable, relative to the BB + SS-CC system, when the cost of grid electricity is low, as shown in Table 2.4. The CO_2 removal capacity increases by 109% when DAC is incorporated into a more traditional, steam-driven BECCS system like BB + SS-CC. For both the liquid solvent and solid sorbent platforms analyzed, the levelized costs of the reference systems (Tables 2.3A and C) are relatively more sensitive to the costs of fuel and capital, as shown by the stark color change in the heat maps across analyzed parameters.

Table 2.3 Heatmaps showing levelized costs of CO_2 removal ($/t-$CO_2$) by the baseline systems with variation in fuel cost and capital recovery factor (CRF).

$54 — $268

A NG + LS-DAC

CRF	Natural Gas Price ($/GJ)				
	$1.50	$3.50	$5.50	$7.50	$9.50
2.5%	$65	$83	$100	$118	$136
7.5%	$109	$127	$145	$162	$180
12.5%	$153	$171	$189	$206	$224
17.5%	$197	$215	$233	$250	$268

B BG + LS-DAC

CRF	Biomass Price ($/short ton)				
	$20	$40	$60	$80	$100
2.5%	$54	$62	$70	$77	$85
7.5%	$88	$96	$103	$111	$119
12.5%	$122	$130	$137	$145	$153
17.5%	$156	$164	$171	$179	$187

$80 — $186

C BB + SS-CC

CRF	Biomass Prices ($/short ton)				
	$20	$40	$60	$80	$100
2.5%	$80	$94	$108	$122	$137
7.5%	$96	$111	$125	$139	$153
12.5%	$113	$127	$141	$155	$170
17.5%	$129	$144	$158	$172	$186

D BB + SS-DAC

CRF	Biomass Prices ($/short ton)				
	$20	$40	$60	$80	$100
2.5%	$106	$113	$120	$127	$134
7.5%	$117	$124	$131	$137	$144
12.5%	$128	$134	$141	$148	$155
17.5%	$138	$145	$152	$159	$165

The ever-present deployment of low-cost renewable electricity, particularly from wind and solar energy, threatens the economic viability of BECCS systems that are optimized for power distribution.[2.29,2.30] Such BECCS systems typically produce power at a higher cost than solar or wind energy systems.[2.31] For these reasons, utilizing heat from biomass combustion to operate thermal-energy intensive DAC systems may be a more attractive prospect than its use for grid power generation, depending on electricity and CO_2 price. Levelized costs of CO_2 capture from the BB + SS-CC system significantly increase as electricity prices decrease, as shown in Table 2.4; additionally, levelized costs are much higher when the steam byproduct generates zero revenue, as shown in Table A2.15. The interaction between BECCS and future electricity grids is

uncertain and may involve complexities not discussed herein, but the prospect of using bioenergy for direct air capture is intriguing considering the critical role carbon removal will play in mitigating climate change. A conceivable future scenario could involve a coupled BECCS-DAC system that operates in a similar fashion to that of a peaking power plant: when electricity is priced high, the BECCS-DAC system shifts its use of bioenergy from DAC to generating excess electricity for sale to the grid. In such a scenario, the BECC-DAC system's rates of biomass combustion and biogenic CO_2 removal remain constant, ensuring the CO_2 removal subsystem remains largely operable and doesn't experience significant downtime.

Table 2.4 Levelized costs of CO_2 removal ($/t-$CO_2$) by the baseline BB + SS-CC system with variation in biomass price and electricity selling price. CRF constant at 12.5%.

BB + SS-CC

$113 — $193

Biomass Price ($/short ton)	Electricity Selling Price ($/kWh)					
	$0.00	$0.01	$0.02	$0.03	$0.04	$0.05
$20	$136	$132	$127	$122	$118	$113
$40	$151	$146	$141	$136	$132	$127
$60	$165	$160	$155	$151	$146	$141
$80	$179	$174	$170	$165	$160	$155
$100	$193	$188	$184	$179	$174	$170

The levelized costs presented up to this point assume zero upstream net emissions from extraction and transportation of natural gas or cultivation, harvest, and transportation of biomass. We conduct sensitivity analyses where emissions penalties of varying severity are applied to both natural gas and biomass.[2.1] Figure 2.3 shows the reduced quantities of net CO_2 removal due to the emissions penalties and Tables 2.5 and S2.14 show an increase in levelized costs.

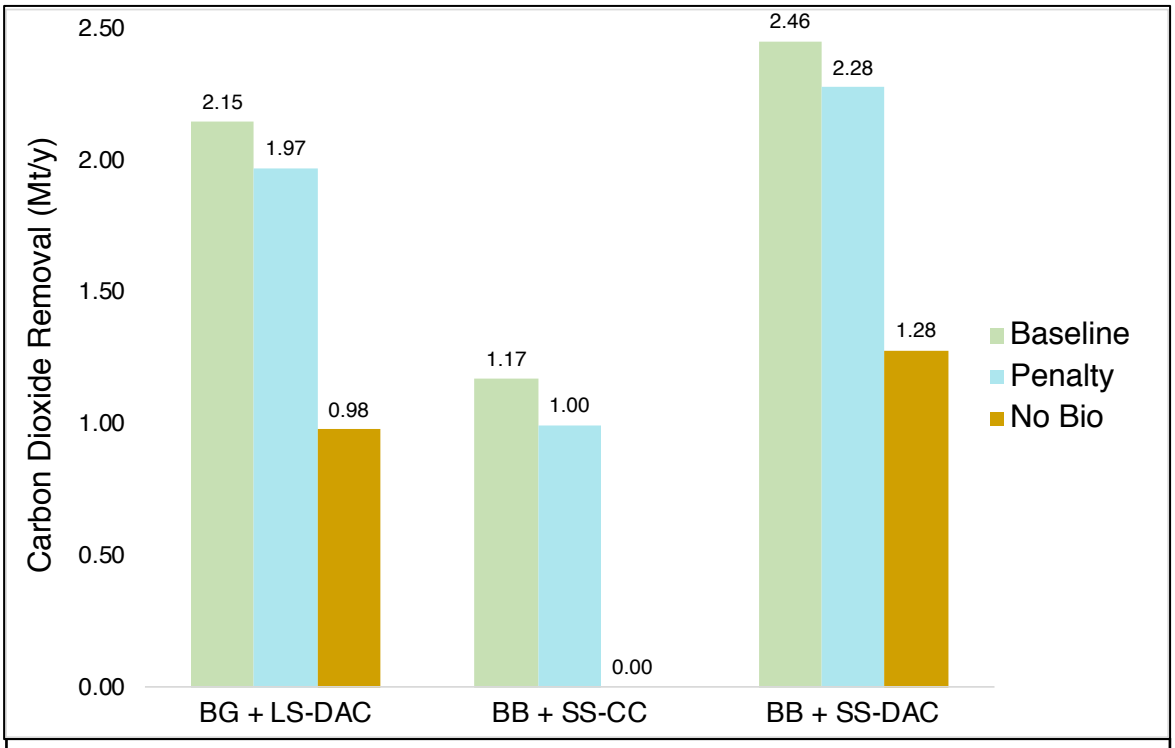

Figure 2.3 Net carbon dioxide removal (Mt/y) by the biomass-enabled systems under Baseline, Penalty, and No Bio scenarios.

For the BG + LS-DAC system, the Penalty and No Bio scenarios increase costs by 9% and 119%, respectively, relative to Baseline. For the BB + SS-DAC system, the Penalty and No Bio scenarios increase costs by 8% and 92%, respectively, relative to baseline. Removing all biogenic carbon from economic calculations (No Bio scenario) results in levelized costs in the $300 - $400 range for the more feasible parameters analyzed, a range which more closely aligns with estimated costs of DAC found in the academic literature.[2.6,2.11,2.32] Removing 15% of biogenic carbon from economic calculations (Penalty scenario) results in a relatively small increase in levelized costs, thereby demonstrating the ability of BECCS-DAC systems to retain cost-effectiveness without biomass carbon neutrality. Additionally, the levelized costs of CO_2 removal by biomass enhanced DAC systems are less sensitive to upstream emissions than their

standalone reference systems. These sensitivity scenarios further demonstrate the potential cost benefits of using biomass as fuel for DAC operations.

Table 2.5 A) Levelized costs of CO_2 removal ($/t-$CO_2$) by the BG + LS-DAC system with variation in biomass price and CRF. Baseline scenario assumes biomass is carbon neutral. Penalty scenario assumes a quantity of carbon equivalent to 15% of the biogenic carbon captured on-site is emitted to the atmosphere during biomass cultivation, harvest, and transportation. No Bio scenario accounts only for air-derived CO_2 in cost calculations. **B)** Levelized costs of CO_2 removal by the BB + SS-DAC system with variation in biomass price and CRF. All scenarios same as A.

A

BG + LS-DAC

$54 — $409

	Biomass Price ($/short ton)														
	$20			$40			$60			$80			$100		
CRF	Baseline	Penalty	No Bio	Baseline	Penalty	No Bio	Baseline	Penalty	No Bio	Baseline	Penalty	No Bio	Baseline	Penalty	No Bio
2.5%	$54	$59	$118	$62	$67	$135	$70	$76	$152	$77	$84	$169	$85	$93	$186
7.5%	$88	$96	$193	$96	$104	$210	$103	$113	$227	$111	$121	$244	$119	$129	$261
12.5%	$122	$133	$267	$130	$141	$284	$137	$150	$301	$145	$158	$318	$153	$166	$335
17.5%	$156	$170	$341	$164	$178	$358	$171	$187	$375	$179	$195	$392	$187	$203	$409

B

BB + SS-DAC

$106 — $317

	Biomass Price ($/short ton)														
	$20			$40			$60			$80			$100		
CRF	Baseline	Penalty	No Bio	Baseline	Penalty	No Bio	Baseline	Penalty	No Bio	Baseline	Penalty	No Bio	Baseline	Penalty	No Bio
2.5%	$106	$115	$204	$113	$122	$217	$120	$129	$230	$127	$137	$243	$134	$144	$256
7.5%	$117	$126	$224	$124	$133	$237	$131	$141	$250	$137	$148	$263	$144	$155	$276
12.5%	$128	$137	$244	$134	$145	$257	$141	$152	$270	$148	$159	$283	$155	$167	$296
17.5%	$138	$149	$265	$145	$156	$278	$152	$163	$291	$159	$171	$304	$165	$178	$317

Deployed at scale, BECCS-DAC systems enable gigaton-scale CO_2 removal in the US without long-distance biomass or CO_2 transport, thereby overcoming a significant barrier to near-term deployment.[2.8] Figure 2.4 shows the technical potential for CO_2 removal by BB + SS-DAC system in all counties of the Continental US by the year 2030 based on estimates in the US Department of Energy's 2016 Billion Ton Study.[2.24] Total CO_2 removal potential is 2.9 Gt-CO_2 and 1.5 Gt-CO_2 per year for the entire US and counties collocated with suitable geologic formations, respectively. In comparison, the BB + SS-CC system would only remove 1.4 and 0.7 Gt-CO_2 per year, respectively, when utilizing equivalent biomass inputs.

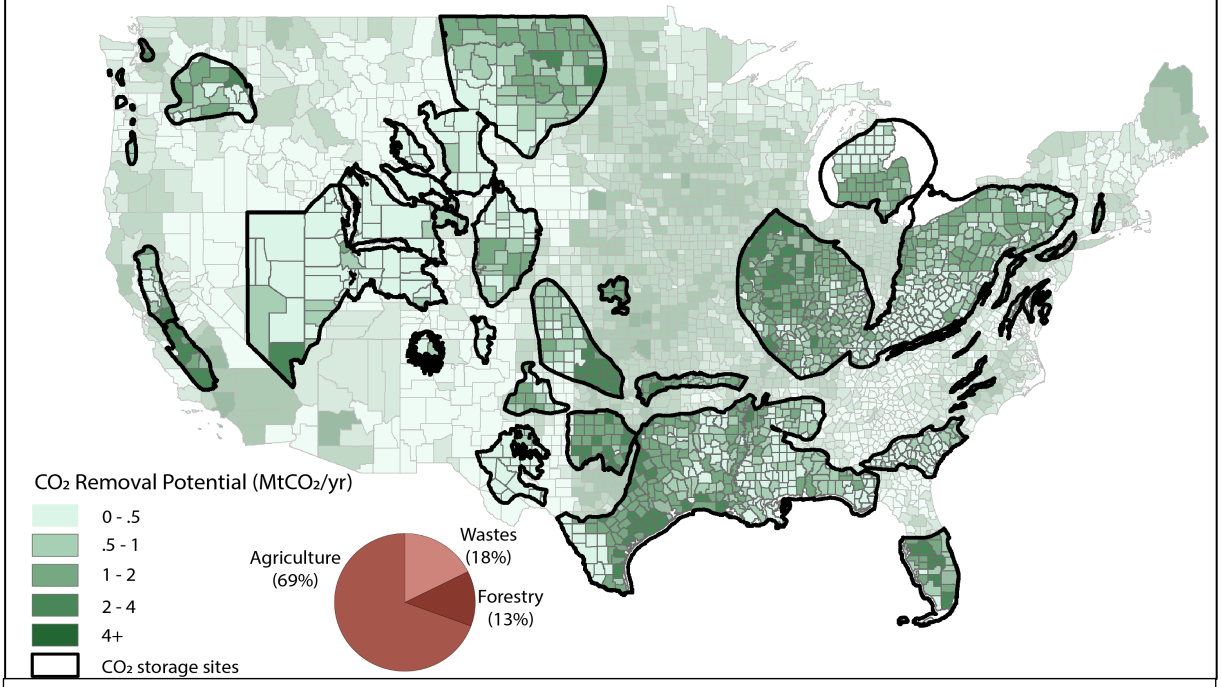

Figure 2.4 County-level CO_2 removal potential of biomass integrated DAC (BB + SS-DAC) systems in the US for the year 2030 overlaid with potential geologic storage sites for CO_2. CO_2 removal potential is 2.9 Gt-CO_2 and 1.5 Gt-CO_2 per year for the entire US and counties collocated with suitable geologic formations, respectively.

DAC technologies have significant locational flexibility: as a result, they can easily be sited where suitable geologic storage capacity exists.[2.33] This locational flexibility also imparts advantages to bioenergy systems, which rely on geographically dispersed, low-energy density biomass resources. Therefore, BECCS-DAC systems extend the impact of scarce biomass resources, a primary constraint on deployment of net-zero emissions energy systems.

2.4 Conclusions

The coupling of BECCS and DAC technologies enables cost-effective removal of CO_2 on a gigaton scale. Biomass is a suitable energy source for DAC through its ability to provide high, medium, and low temperature thermal energy at relatively low cost while enhancing CO_2 removal capacity, as well as its inability to provide electricity at costs competitive with other

renewable resources, such as wind and solar. However, DAC technologies are in their infancy and require substantial development to increase technical readiness and decrease uncertainty prior to integration with BECCS technologies. In addition, social acceptance, environmental protection, and appropriate political incentives are necessary for large-scale deployment of CO_2 removal systems fueled by biomass.[2.6,2.9] Fortunately, the US Department of Energy has conducted thorough assessments of sustainable biomass availability to help minimize environmental and social harm as CO_2 removal systems continue to advance.[2.24] Historically, the lack of US policies placing a value on CO_2 has been a barrier to the deployment of BECCS and DAC technologies, however, the US congress recently enhanced the Section 45Q carbon oxide sequestration tax credit to help overcome this barrier.[2.34] Two BECCS-DAC systems were designed and analyzed to demonstrate their economic and environmental advantages over standalone reference systems. Techno-economic analyses indicate the BECCS-DAC systems increase net CO_2 removal by 109 - 119% at lower costs than standalone reference systems. Moving forward, BECCS-DAC systems can drive efficient, cost-effective, and locationally-optimized usage of biomass resources for engineered CO_2 removal. As the level of attention towards CO_2 removal technology development continues to grow, BECCS-DAC systems deserve serious consideration.

Chapter 3 - Decarbonizing Agriculture through the Conversion of Animal Manure to Dietary Protein and Ammonia Fertilizer

3.1 Introduction

The agricultural subsector of the industrial economy will be difficult to decarbonize due in part to its heavy reliance on energy-intensive nitrogenous fertilizers, such as ammonia, and its inefficient methods of producing dietary protein in the form of livestock. Agriculture as a whole represents ~9% of total emissions in the US, with livestock management contributing ~4% [3.1]. Nearly 50% of the energy consumed by an average US farm is embodied in nitrogenous fertilizers, resulting in substantial carbon dioxide emissions since over 90% of the ammonia produced in the US is derived from natural gas; the methane in natural gas is reformed to generate hydrogen and carbon dioxide, with the hydrogen being used for ammonia production and the carbon dioxide being emitted to the atmosphere [3.2,3.3]. Decarbonizing the production of ammonia is challenging due to the necessity of energy-dense chemical feedstocks (e.g. natural gas), and therefore carbon-free electricity (solar and wind power) by itself does not provide an impactful solution. Over 80% of total agricultural production in the US is for animal feed, resulting in significant land use and greenhouse gas emissions [3.4]; privately owned pasture and rangeland account for 27% of all land area in the contiguous US, with the majority of such used for cattle grazing [3.5]. A growing global population and shifting social demographics are increasing the demand for food rich in high quality protein, and the US is expected to play a significant role in meeting future demand [3.6]. The global demand for animal-based protein is expected to double by 2050 [3.6]. As the demand for dietary protein grows, the US agricultural system will strain due to lack of arable land and freshwater, and the environment will be impacted through a continued rise in greenhouse gas emissions. Therefore, the agricultural

subsector of the industrial US economy is ripe for innovative solutions that conserve land and water and reduce greenhouse gas emissions without limiting dietary protein production.

Microalgae have the potential to serve as a sustainable source of high quality protein for human health. *Chlorella* and *Spirulina* are established nutritional supplements due to their proven health benefits [3.7–3.9]. Microalgae strains commonly used for biofuel research, including *Nannochloropsis*, *Scenedesmus*, and *Dunaliella*, have recently shown great potential as nutritional supplements [3.7]. Animal feed is another promising application for microalgae supported by a multitude of successful trials in which corn and soy diets were partially substituted with whole and defatted algal biomass for cattle, pigs, chicken, and salmon [3.10–3.15]. However, large scale deployment of microalgae-substituted animal feed is currently challenged due to the high costs of algal biomass production, remaining uncertainty in feed effectiveness, and the strict nutrient profiles required by commercial animal feed producers. Therefore, incorporating microalgae in the human diet might be more feasible in the near-term since direct consumption of microalgae by humans is potentially more cost-effective, metabolically efficient, and environmentally beneficial than indirect consumption via animal feed. The essential amino acid indices (EAAI) of the aforementioned algal strains are close to 1.0, meaning the protein compositions include amino acids essential for optimal human health. In addition to high quality protein, microalgae provide nutritious omega 3 & 6 fatty acids, vitamins, and essential minerals; some strains exhibit anti-cancer, anti-inflammatory, and anti-oxidant properties [3.7]. The environmental benefits of substituting animal and plant-based proteins with microalgae are substantial, including reduced land use, water consumption, and greenhouse gas emissions; compared with soy, microalgae produce approximately 15 times more protein per unit area [3.16]. Therefore, a shift towards meeting dietary protein demand with microalgae has great potential to

benefit society and the environment. Unfortunately, the costs associated with constructing and operating freshwater microalgae farms are significant, as detailed by the US National Renewable Energy Laboratory's (NREL) recent techno-economic analysis [3.17]. Additionally, the bioavailability of microalgal proteins must be enhanced though energy-intensive processing prior to human consumption [3.16]. However, technological advancements, government support, and a renewed interest in optimizing microalgae farms for food and feed production, instead of biofuels, are lowering costs and pushing microalgae farms closer to reality [3.17]. According to NREL's techno-economic model, nutrients comprise 78% of the variable operating costs of an open pond microalgae farm; the costliest nutrients are carbon dioxide, ammonia, and diammonium phosphate (DAP) [3.17]. Currently, the vast majority of carbon dioxide and ammonia produced in the US is derived from fossilized carbon resources. Ideally, microalgae farms of the future will use nutrients sourced from renewable sources of carbon, such as biogas from anaerobic digestion.

NREL has analyzed the feasibility of producing biogas from major organic waste streams in the US, namely those associated with wastewater, landfills, animal manure, and commercial waste [3.18]; commercial waste includes industrial, institutional, and commercial organic waste. NREL considers these organic waste resources as "low-hanging fruit" due to their underutilization and low cost [3.18]. The biogas potential for the US is much greater if lignocellulosic biomass resources are included with organic waste resources. The majority of research and development into biogas technologies has focused on using the methane component (~60% of biogas) as a substitute to natural gas for power production. Converting the renewable chemical energy locked within biogas to electricity may not be best the method of utilization given the aforementioned difficulties with decarbonizing the agricultural subsector of the

industrial economy. Instead, dedicating biogas to the production of chemical energy-dense agricultural products, such as ammonia and dietary protein, is an interesting approach that has received little attention. Herein, we use data from NREL's detailed analyses on biogas and microalgae production to design a synergistic system for the conversion of organic waste-derived biogas to algal protein and ammonia fertilizer, as shown in Figure 1 [3.17,3.18].

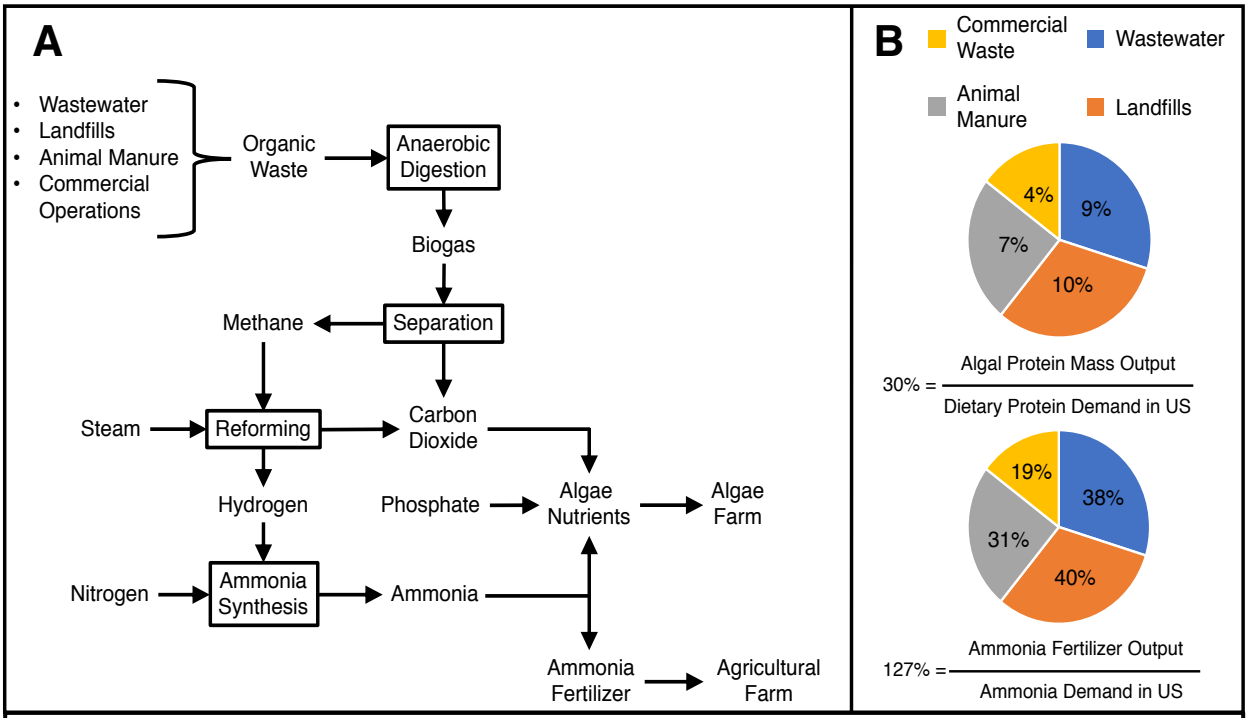

Figure 3.1 A) A synergistic system in which organic waste is converted to algal protein and ammonia fertilizer [3.17,3.18]. B) The potential for displacement of dietary protein and ammonia fertilizer if full utilization of organic waste sources across the US is realized. Commercial waste includes industrial, institutional, and commercial organic waste.[3.3,3.19]

3.2 Materials & Methods

The synergistic system is designed and modeled using process data, assumptions, and conversion efficiencies as detailed in Table 3.1 and the Supplementary Information. The system is modeled to account for all mass flows, without any inclusion of energy flows since this information is not pertinent to the study.

Table 3.1 Technical parameters used in modeling the synergistic system.	
Density of biogas (kg/m^3)	1.15
Density of CH_4 (kg/m^3)	0.67
Density of CO_2 (kg/m^3)	1.84
Biogas vol% CH_4	60%
Biogas vol% CO_2	40%
Biogas separation CO_2 yield	95%
Biogas separation CH_4 yield	95%
Reforming H_2 yield	90%
Reforming CO_2 yield	90%
NH_3 synthesis yield	90%

Biogas is assumed to be generated at each source of organic waste and then cleaned, dehydrated, pressurized, and transported via pipeline to a centralized facility for separation of methane and carbon dioxide, ammonia synthesis, and microalgae cultivation. The sources of organic waste include those associated with wastewater, landfills, animal manure, and commercial waste [3.18]; commercial waste includes industrial, institutional, and commercial organic waste. The quantities of biogas available from each source of organic waste are taken from NREL's review, which includes a geospatial plot of biomethane availability [3.18]. Small scale steam methane reforming is used to synthesize ammonia and provide a stream of CO_2 for microalgae cultivation. The design of the microalgae farm is based on the freshwater open pond biorefinery developed by NREL, in which high purity nutrients are used to cultivate microalgae (*Scenedesmus* sp.) [3.17]; the composition (wt%) of the microalgae are 13.2% protein, 30.1% lipids, 52.8% carbohydrates, 2.4% ash, and 1.6% cell mass. The techno-economic model for microalgae

production developed by NREL is used to quantify mass flows for a 1000 acre operation [3.17]. Dietary Reference Intakes established by the National Institute of Health are used to estimate the total daily protein intake by all men, women, and children in the US [3.19]; the average daily protein intakes (g protein/ kg body weight) are 0.87 for ages 1-3, 0.76 for ages 4-13, 0.72 for ages 14-18, and 0.66 for ages above 19. See the Supplementary Information for total protein consumption by men and women of all ages in the US.

3.3 Results and Discussion

If all available organic wastes are fully utilized, this system has the potential to supply 127% of the entire US demand for ammonia and 30% of the demand for dietary protein while reducing net greenhouse gas emissions and opening up vast areas of pasture and rangeland for other purposes. NREL's geospatial plot showing the potential biomethane production from various organic wastes across the US is used to estimate the potential production capacity of algal protein in each US county, as shown in the Supplementary Information [3.18]. Interestingly, the areas with the largest potential for biogas generation are also suitable for microalgae growth[3.20].

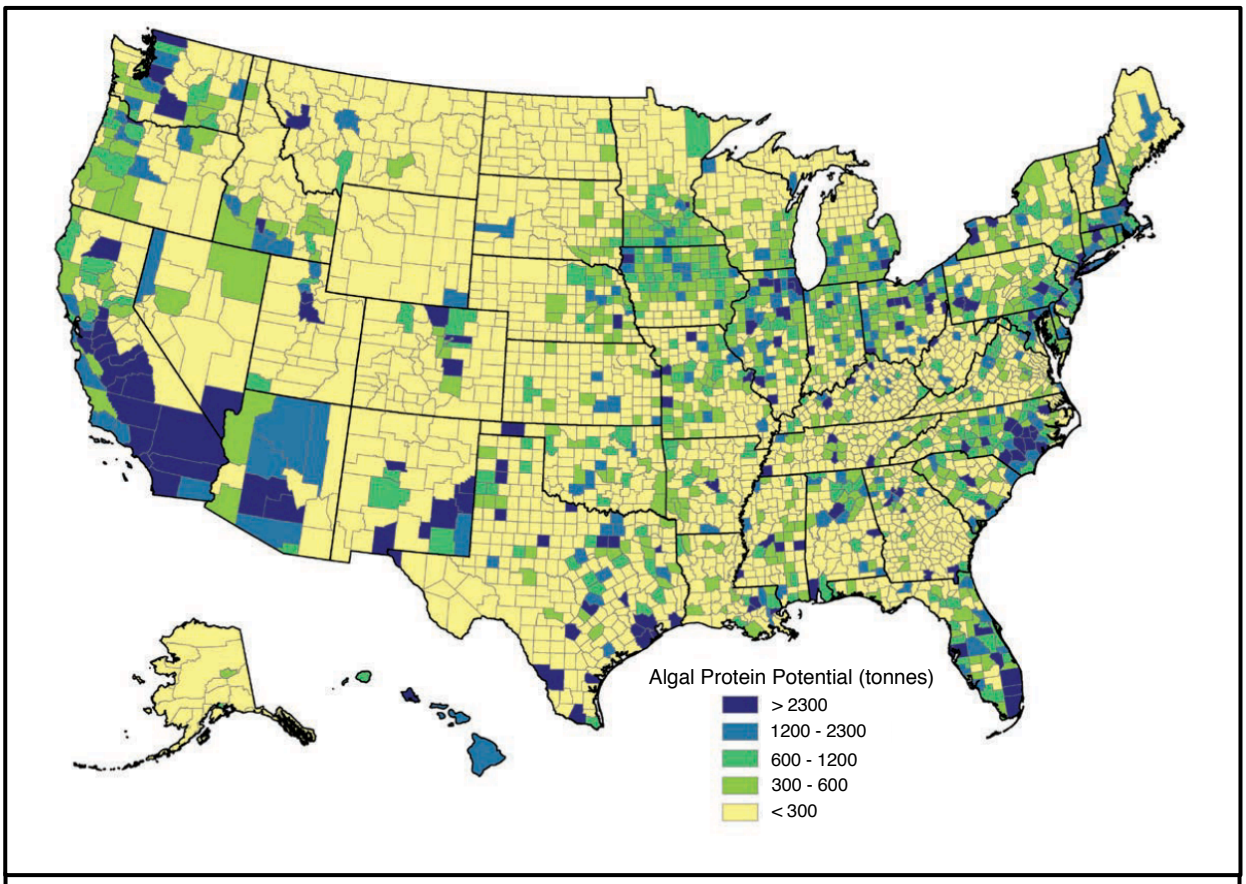

Figure 3.2 A geospatial plot showing the annual potential algal protein production in every US county if all organic waste sources are utilized by the proposed system in Figure 1; adapted, with permission, from work published by the US National Renewable Energy Laboratory.[3.18]

Many researchers have investigated the use of anaerobic digestates as nutrient sources to microalgae growth, but this approach is technically difficult to implement for food production due to the variation in digestate composition and concerns over fecal pathogens, among other factors [3.21–3.23]; NREL's work indicates first generation microalgae farms will require high purity nutrients for reliable, continuous operation [3.17]. Only one strain of microalgae was considered in the analysis (*Scenedesmus* sp.) with a protein content of 13.2%, and therefore the potential for dietary protein substitution could be greater if other strains of microalgae are used – other strains have >40% protein. Notably, less than 2% of the ammonia produced by the system is used for microalgae growth, thereby generating excess ammonia in an amount equal to 127% of US

ammonia demand. In addition, 32.2 Mt-CO_2 are utilized for microalgae production per year if implemented across the US. See Table 2 for a summary of the input and output mass flows and land area required for conversion of all organic wastes in the US to ammonia and algal protein using the synergistic system.

Among the various sources of organic waste, we believe animal manure has the greatest potential for near-term impact using the proposed system. We envision farming areas where feed crops are grown for livestock and organic waste is anaerobically digested to serve as biogas inputs to a centralized microalgae farm (1000 acres), as shown in Figure 2. Methane reforming and ammonia synthesis technologies have historically operated at large scale using the Haber-Bosch process, however, recent advancements are enabling the use of modular systems to synthesize ammonia with high efficiency [3.24]. Therefore, the centralized microalgae farms cost-effectively produce ammonia on a relatively small scale (122 t-NH_3/day). A total of 93 centralized microalgae farms of 1000 acres each are required to utilize all the available biogas from animal manure in the US, and 384 farms of the same size to fully utilize biogas from all organic waste streams. Notably, the microalgae farm land area required for complete conversion of organic waste-derived biogas to algal protein would demand less than 1% of pasture and rangeland used today in the US [3.5]. The algal protein would be sold for human consumption and the excess ammonia fertilizer would be purchased by local farming communities.

Table 3.2 Summary of the input and output mass flows and land area required for conversion of all organic wastes in the US to ammonia and algal protein using the synergistic system.

	Synergistic System Inputs & Outputs (Mt/year)				
	Wastewater	Landfills	Animal Manure	Commercial Waste	Total
Biogas	6.71	7.04	5.47	3.32	22.55
Biogas: CH_4	2.22	2.33	1.81	1.10	7.46
Biogas: CO_2	4.09	4.29	3.33	2.02	13.72
Reformed H_2	1.00	1.05	0.81	0.49	3.36
Reformed CO_2	5.50	5.77	4.48	2.72	18.47
CO_2 to Algae Farm	9.59	10.06	7.81	4.74	32.20
Total NH_3	5.10	5.35	4.15	2.52	17.13
NH_3 to Ag. Farm	5.00	5.25	4.07	2.48	16.80
NH_3 to Algae Farm	0.10	0.10	0.08	0.05	0.33
Algal Protein	0.51	0.54	0.42	0.25	1.72
Algal Lipids	1.17	1.23	0.95	0.58	3.93
	Land Area (acres)				
	Wastewater	Landfills	Animal Manure	Commercial Waste	Total
Land Area of Algae Farms	114185	119829	92997	56517	383527
% of US Pasture & Rangeland	0.022%	0.023%	0.018%	0.011%	0.073%

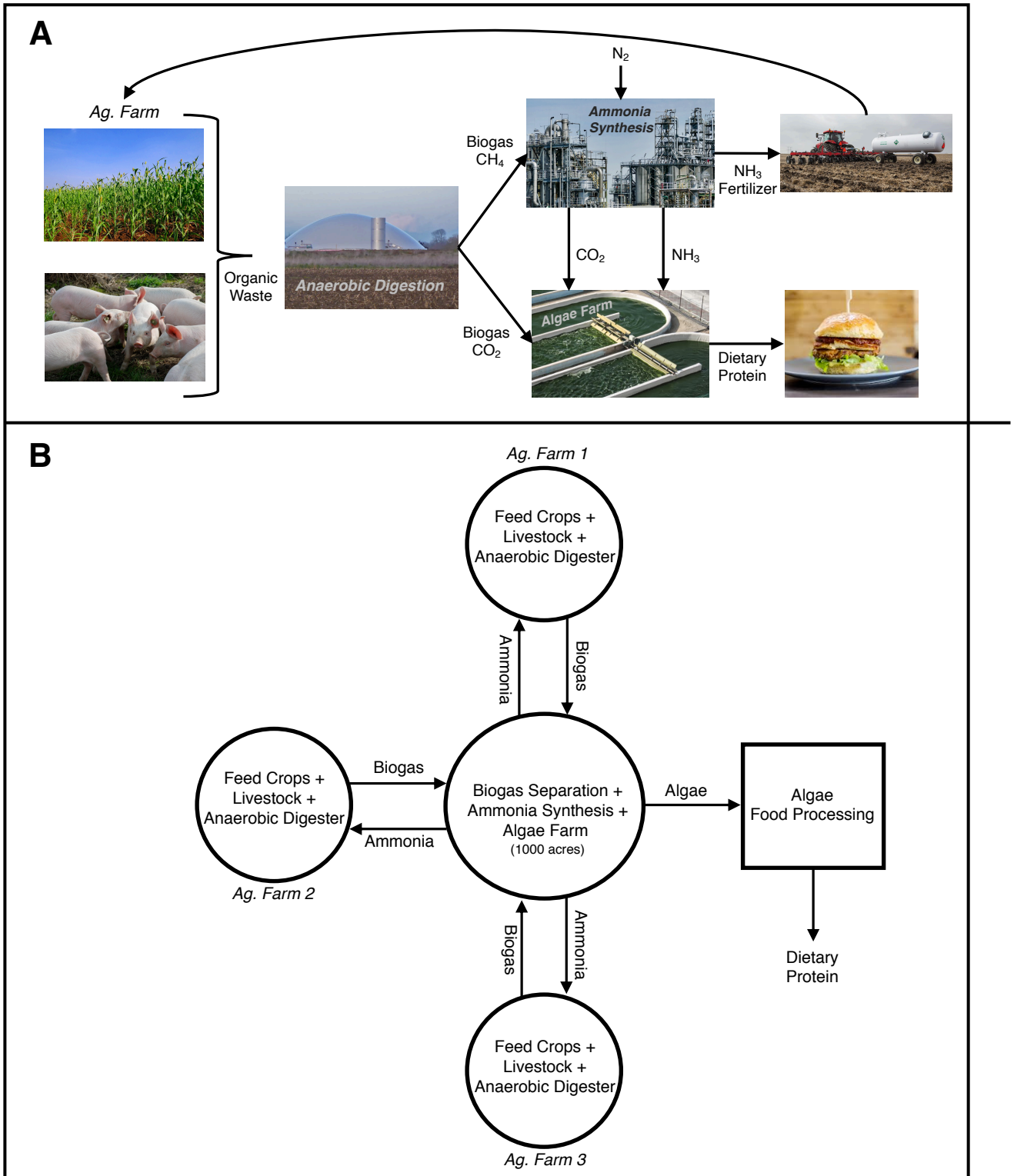

Figure 3.3 A) A simplified diagram showing the flow of mass from an agricultural farm to final products; see Figure 1 for a more detailed mass flow diagram. B) An example of a synergistic system with 3 agricultural farms and 1 centralized algae farm. A total of 93 centralized algae farms of 1000 acres each are required to utilize all the available biogas from animal manure in the US, and 384 farms of the same size to fully utilize biogas from all waste streams.

Further comprehensive investigation into the economic viability of such a system is required, however, published studies indicate the economics of microalgal food products are more favorable than microalgal fuel products [3.7–3.9]. In addition, the localized production of ammonia fertilizer should reduce costs for nearby farming operations. Regarding policy support, microalgae production has seen impressive policy gains in recent years, the largest milestone being the recent 2018 Farm Bill, which designated algae a high-priority for research and extension initiatives, as well as amending the Biomass Crop Assistance Program to allow for algae [3.25]. For this vision to become realty, social acceptance of algae-based food products must continue to advance through innovative culinary practices and public studies demonstrating health benefits. Developing and optimizing systems such as the one presented herein will help maintain the United States' status as a world leader in agricultural production as the stresses of climate change, global population, and a shifting socio-economic spectrum stress the fossil carbon-, land-, and water-demanding agricultural system society is reliant upon.

3.4 Conclusions

The level of attention aimed at decarbonizing agriculture has been insufficient to ensure a sustainable future. The global demand for dietary protein is increasing rapidly, thereby requiring the development of innovative agricultural practices. Agricultural products are highly dependent on ammonia-based fertilizers derived from fossilized carbon precursors dense in chemical energy, such as natural gas. Therefore, renewable, energy-dense sources of carbon, such as biomethane, deserve serious consideration as sustainable alternatives for the production of agricultural products. The proposed system provides an impactful option to fully utilize biogenic sources of carbon for the production of agricultural products, namely ammonia and algal protein.

Chapter 4 - Prospects for Bioenergy with Carbon Capture & Storage (BECCS) in the United States Pulp and Paper Industry

4.1 Introduction

To meet the stringent climate targets set forth by the Intergovernmental Panel on Climate Change's (IPCC) Fifth Assessment Report, the United States (US) must deploy bioenergy with CO_2 capture and sequestration (BECCS) to a scale of 1 Gt-CO_2 per year by 2050.[4.1] Commercial CO_2 capture, utilization, and storage (CCUS) operations must rapidly accelerate to meet such an ambitious target.[4.2] Near-term opportunities to develop, demonstrate, and deploy CCUS technologies can reduce costs, improve performance, and clarify their sustainable scale. Previous work has highlighted the opportunities to deploy CCUS on existing biogenic CO_2 emissions as a first market for engineered carbon removal. For instance, sequestration of biogenic CO_2 emissions from bioethanol refineries is considered to be a viable opportunity due to its technical and commercial maturity (current emissions are 45 Mt-CO_2 per year) and low-cost of capture, transport, and sequestration.[4.3] Analyses that identify opportunities to leverage existing infrastructure, technologies, and policies can enhance both near-term and long-term mitigation efforts by deploying existing technologies and developing experience in CCS.[4.4]

As the largest industrial source of existing biogenic CO_2 emissions in the US, the pulp and paper industry represents a viable opportunity for utilizing and/or sequestering biogenic CO_2 emissions. Many pulp and paper mills involve multiple energy-intensive operations that emit CO_2-containing waste streams, as shown in Figure 4.1.[4.5] Some streams are of relatively high purity CO_2 and therefore may be ideal candidates for CCUS. Recent technological innovations in CO_2 capture offer opportunities to cost-effectively integrate CO_2 capture at existing pulp and paper mills.[4.6–4.15] However, the complexity of operations is a challenge that must be addressed.

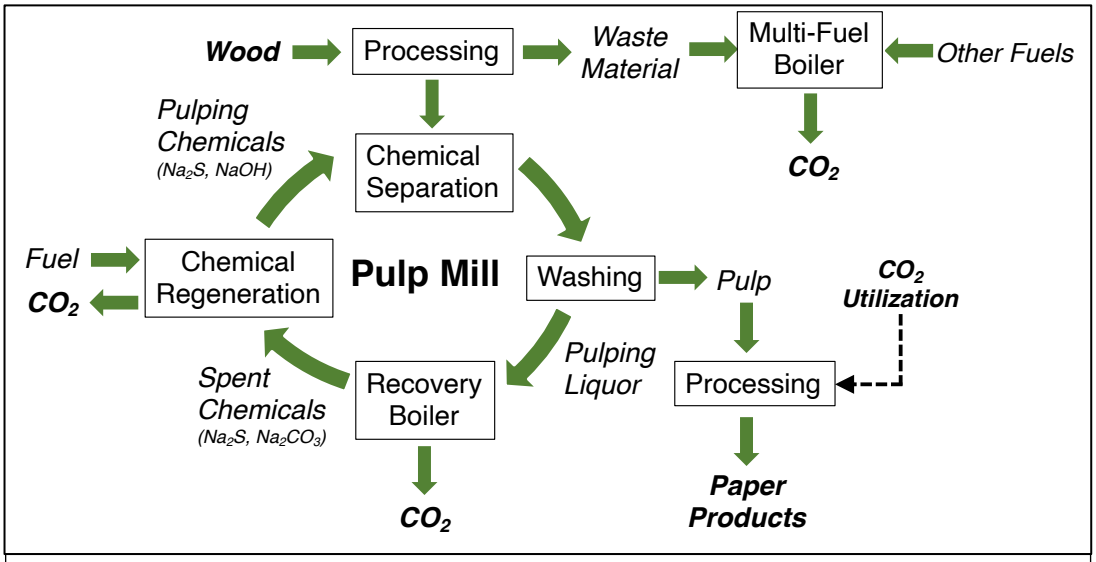

Figure 4.1 A simplified process flow diagram of a Kraft pulp mill.

The federal government of the US has developed several policies to accelerate innovation and deployment of CCUS. Most notably, Congress has recently revised the Section 45Q tax credit for utilizing or sequestering point-source CO_2.[4.16] This tax credit will change with time, increasing from \$19 to \$35 per t-CO_2 for utilization and \$31 - \$50 per t-CO_2 for sequestration in geological formations for years 2019 to 2026, after which point the value will remain constant (indexed to inflation). The 45Q tax credit does not distinguish between biogenic and non-biogenic sources of CO_2. Further, the US Department of Energy Loan Guarantee Program can be combined with 45Q federal tax credits to help enable large-scale projects involving advanced technologies. The Department of Energy has \$8.5 billion in unutilized loan guarantee authority for innovative fossil energy technology, including carbon capture and low-carbon power systems.[4.17] Existing pulp and paper mills that directly utilize CO_2 may be immediately eligible for the 45Q utilization tax credit with minimal upfront costs. In particular, pulp and paper products that contain calcium carbonate fillers and coatings, including multiple grades of paperboard, may be immediately eligible for the tax credit. Additionally, some Kraft pulping mills are currently implementing

technologies that utilize CO_2 to precipitate lignin from black liquor, thereby potentially enabling downstream products to be eligible for the 45Q utilization tax credit.[4.18] Detailed lifecycle assessments (LCAs) are necessary to ensure these products meet the federally-established requirements.

Previous studies have investigated the economic feasibility of capturing CO_2 from pulp and paper mills using traditional amine chemisorbents[4.9–4.11], but none have involved an industry-wide, geospatial assessment that quantifies the costs of capturing and transporting biogenic and fossil-derived CO_2 emissions from mills located in the US, with high granularity regarding fuel type and unit operation used for combustion, CO_2 concentrations, and economic impact of the 45Q tax credit. Onarheim et al. conducted a thorough investigation into the techno-economic feasibility of capturing CO_2 emitted from two pulp and paper mills: 1) a generic Kraft market pulp mill and 2) a generic integrated Kraft pulp and board mill.[4.9,4.10] Their analysis involved highly detailed chemical process simulations for multiple scenarios, but did not involve an industry-wide analysis. Nabinger et al. quantified the greenhouse gas emissions from a select number of pulp and paper mills in the US, but did not involve a techno-economic analysis for capturing the emissions.[4.19] Psarras et al. estimated the costs of capturing CO_2 via amine chemisorbents for 21 sectors in the US industrial economy, including the pulp and paper industry.[4.11] However, in their assessment, emissions are quantified using a dataset from the EPA that does not consistently include biogenic emissions, emissions are not quantified for mill-specific unit operations, emissions are not categorized by fuel type, emissions from different product grades are not assessed, idling assets are not assessed, detailed process simulations are not conducted, and potential revenues from the 45Q tax credit are not taken into account. Regarding CO_2 utilization, to the best of our knowledge, there have been no studies published on

integrating CO_2 utilization in the pulp and paper industry though process intensification and innovation for the purpose of removing atmospheric CO_2 and improving process economics through the 45Q tax credit. Thus, there has yet to be an extensive investigation into the economic feasibility of incorporating CCUS technologies into US pulp and paper mills.

Here, we assess the technical and economic feasibility of indirectly removing atmospheric CO_2 through the capture, compression, transportation, and sequestration of CO_2 emissions from the pulp and paper industry in the continental US. This is accomplished by first assessing the entire industry using a top-down approach to identify favorable mills, followed by an assessment of a select number of favorable mills using a bottom-up approach with process engineering methods. All techno-economic analyses use post-combustion amine chemisorption technologies for CO_2 capture. Additionally, alternative techniques for CO_2 capture through process innovation are assessed qualitatively. Finally, pathways for CO_2 utilization at existing pulp and paper mills are assessed qualitatively.

4.2 Methodology

4.2.1 Top-Down Analysis, Part I: Industry-Wide Screening

Operable pulp and paper mills in the continental US are assessed for their potential for CO_2 capture and sequestration. All 205 mills included in this analysis meet the eligibility requirements for the Section 45Q utilization tax credit, which places a lower limit on captured mill emissions to 25,000 metric tons per year; 135 mills (66% of total) meet the eligibility requirements for the sequestration tax credit, which places a lower limit of 100,000 metric tons per year.[4.16] A high level of granularity is taken to assess the CO_2 emissions for each mill, involving the quantification of CO_2 emitted from 1) the entire mill, 2) each fuel consumed, 3)

each major operation on-site, and 4) the production of each major product grade, as shown in Figure 4.2.

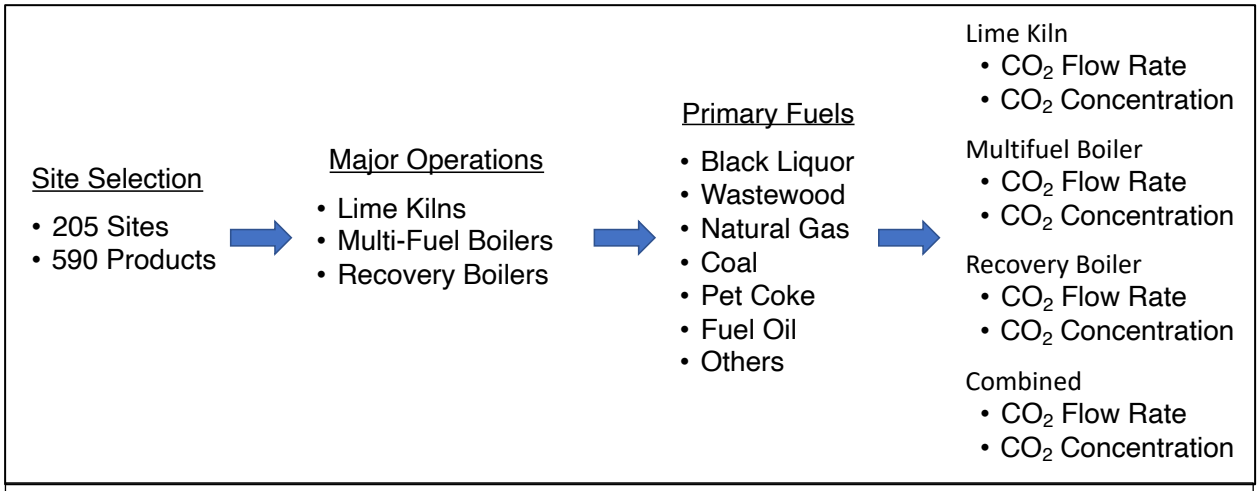

Figure 4.2 Logic flow to quantify CO_2 emissions in multiple ways for each site. (Year: 2018)

Emission stream compositions are quantified using fuel composition and combustion properties typical for each of the major operations.[4.20] A significant portion of the basis process data used in calculations is derived from the Fisher*Solve* Platform for the year 2018.[4.21] Visual Basic is used to program an automated model with data inputs from multiple sources and outputs that are presented herein. The major operations include lime kilns, multi-fuel boilers, and recovery boilers; multi-fuel boilers vary considerably in their configuration. As shown in Figure 4.2, six primary fuels are used at pulp and paper mills to drive the three major operations: black liquor, wastewood, natural gas, coal, petroleum coke, and fuel oil; other minor fuels include diesel, methanol, and tires, to name a few. Emissions are also quantified with respect to eight major product grades: containerboard, market pulp, printing and writing, cartonboard, tissue and towel, specialties, packaging paper, and newsprint.

Abiding by the laws of thermodynamics, the minimum energy required for separation of CO_2 from each emission stream at each mill is calculated using Equation 1.[4.22] The incoming and

outgoing concentrations of CO_2 and the percent capture rate are the most influential variables with respect to system energy demand for CO_2 capture (Equations 1 – 5). The outgoing concentration of CO_2 is taken to be 97 mol% and the capture rate is taken to be 90% for all cases. The 2nd law efficiency for separation of CO_2 is estimated for each stream at each mill using Equations 2 - 4. The actual energy required for separation of CO_2 is estimated using Equation 5.

$$Min.energy\ for\ CO_2\ separation = w_{min} = RT\begin{bmatrix} \left(n_{r,CO_2}\ln\left(X_{r,CO_2}\right) + n_r\ln\left(X_r\right)\right) \\ +\left(n_{p,CO_2}\ln\left(X_{p,CO_2)} + n_p\ln\left(X_p\right)\right)\right. \\ \left. -\left(n_{i,CO_2}\ln\left(X_{i,CO_2}\right) + n_i\ln\left(X_i\right)\right)\right. \end{bmatrix} (1)$$

$n_{x,CO_2} = moles\ of\ CO_2\ in\ stream\ x$

$n_x = moles\ of\ nonCO_2\ component\ in\ stream\ x$

$X_{x,CO_2} = mole\ fraction\ of\ CO_2\ in\ stream\ x$

$X_x = mole\ fraction\ of\ nonCO_2\ components\ in\ stream\ x$

$r = residual\ stream$

$p = product\ stream$

$i = inlet\ stream$

$$2nd\ law\ efficiency = \eta = 1 \times 10^{-5} + 0.0014\alpha + 0.0087\ (2)$$

$$\alpha = \frac{capture\ rate}{\log C_f}\ (3)$$

$$C_f = \frac{[CO_2]_{out}}{[CO_2]_{in}}\ (4)$$

$$Actual\ energy\ for\ CO_2\ separation = \frac{w_{min}}{\eta}\ (5)$$

For each mill, existing capital assets are assessed because of their potential to reduce costs. Finally, a geospatial analysis is conducted to determine which mills are co-located with geology suitable for long-term CO_2 sequestration, following methods developed by Sanchez et al.[4.23]

4.2.2 Bottom-Up Analysis: Case Studies

Chemical process models are developed and assessed using AspenTech process simulation software and process data obtained from the literature to provide engineering metrics necessary for estimating levelized capital and operating expenses for capturing (including compression) CO_2 at four select mills[4.24,4.25]. The top-down industry-wide screening is used to select the four mills for detailed analysis, with motivating information provided in Table 4.1. For Mill 4, we assume on-site waste heat is of sufficient quality to be used in the CO_2 capture system. For each of the four select mills, costs of CO_2 capture ($/t$CO_2$) are estimated for four baseline scenarios, resulting in a total of sixteen baseline cost estimates; see Figure 4.3 for the logic flow of analysis. All amine chemisorbent systems modeled use biomass fuel for heat and power to ensure a large net removal of CO_2.

Table 4.1 Descriptions of the four mills selected for detailed analysis.

Site Name	Site Type	Products	CO_2 Capacity	Motivation from Top-Down, Industry-Wide Analysis
Mill 1	Virgin & Recycled Integrated	Containerboard	Lime Kiln: 0.204 $MtCO_2/y$ Combined: 2.59 $MtCO_2/y$	• High CO_2 concentration of combined emissions (14.83 mol%) • Integrated site that produces pulp and board products • Co-located with suitable geological storage • Eligible for 45Q sequestration tax credits
Mill 2	Virgin Integrated	Cartonboard	Lime Kiln: 0.223 $MtCO_2/y$ Combined: 2.89 $MtCO_2/y$	• Largest quantity of CO_2 emissions of all sites (2.89 $MtCO_2/y$) • High percentage biogenic emissions (> 85%) • Integrated site that produces pulp and board products • Co-located with suitable geological storage • Eligible for 45Q sequestration tax credits
Mill 3	Virgin Integrated	Market Pulp	Lime Kiln: 0.417 $MtCO_2/y$ Combined: 2.00 $MtCO_2/y$	• High CO_2 concentration of lime kiln emissions (27.15 mol%) • High percentage biogenic CO_2 (> 85%) • Co-located with suitable geological storage • Eligible for 45Q sequestration tax credits
Mill 4	Virgin & Recycled Integrated	Containerboard, Cartonboard	Lime Kiln: 0.183 $MtCO_2/y$ Combined: 1.23 $MtCO_2/y$	• Large quantity of waste heat available on-site • Integrated site that produces pulp and board products • Co-located with suitable geological storage • Eligible for 45Q sequestration tax credits

As shown in Figure 4.3A, “Steam” scenarios incorporate a biomass boiler subsystem without a turbogenerator, wherein 100% of the steam demand is met from the boiler and 100% of the electrical power is purchased from the grid. “Steam and Power” scenarios incorporate a biomass boiler subsystem with a turbogenerator wherein 100% of the steam and power demands are met by the boiler and turbogenerator. Biomass is the only fuel source used by the boiler subsystem in this analysis. The major unit operations of the biomass boiler subsystem include live-bottom grated fuel bin, dryer, combustor, particle cyclone, electrostatic precipitator, boiler, and turbogenerator.[4.26] The major unit operations of the amine chemisorption subsystem include pumps for amine circulation, an absorber column with packed bedding, a stripper column with partial reflux, heat exchangers to preheat the stripper column inlet and cool various operations, a water knockout unit to remove water from the CO_2 stream via direct contact condensation, and compressors to pressurize the pure CO_2 stream.[4.24,4.27] A summary of pertinent baseline engineering metrics are presented in Table 4.2; unless noted, the metrics are consistent across all baseline scenarios. The engineering metrics are determined through a combination of process simulation and literature review.[4.12,4.14,4.27–4.32] To take reboiler duty variation into account, we conduct a sensitivity analysis across multiple duty values; reboiler duties are defined and used as independent variables in the process models. In addition, we conduct a sensitivity analysis of amine solvent loss rate. The process models developed for each scenario do not undergo intensive engineering optimization and there is some uncertainty; however, the most influential parameters are accounted for, assumptions are conservative, and analyses are conducted consistently to allow for direct comparison between scenarios. A summary of pertinent baseline economic metrics are presented in Table 4.3; unless noted, the metrics are consistent across all scenarios. The project year is taken to be 2026, when the 45Q sequestration tax credit plateaus

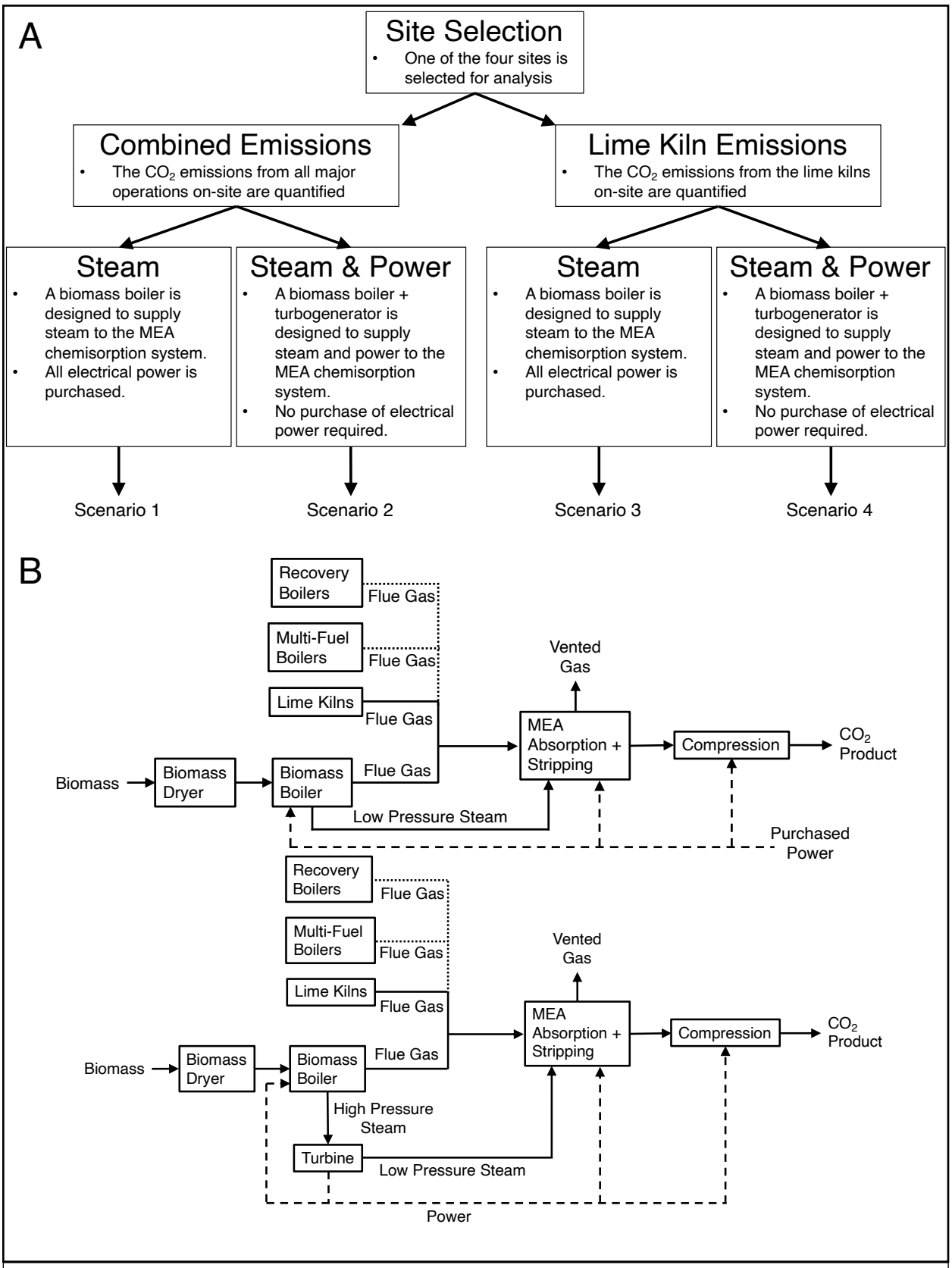

Figure 4.3 A) Descriptions of the four scenarios investigated for each of the four select sites. B) Simplified process flow diagrams of the "steam" (top) and "steam & power" (bottom) processes.

Table 4.2 Baseline technical details consistent with all scenarios, unless noted otherwise.	
Energy content of biomass fuel (LHV) (GJ/dry tonne)	16.8
1st law conversion efficiency of fuel energy (LHV) to steam enthalpy (Steam scenario: S, Steam & Power scenario: S&P)	S: 80% S&P: 69%
1st law conversion efficiency of fuel energy (LHV) to electrical power (Steam & Power scenario)	S&P: 11%
Biogenic emissions from boiler (tCO_2/t-biomass)	1.51
CO_2 concentration of boiler flue gas (mol%)	15.5%
Amine chemisorbent (MEA) concentration (wt%)	30%
Temperature of absorber column	~ 50°C
Temperature of stripper column	~ 120°C
Rate of amine loss (kg MEA/tCO_2 captured)	2.3
Reboiler Duty (GJ/tCO_2)	3.5
Total CO_2 capture rate (tCO_2 captured/tCO_2 generated)	90%
Concentration of CO_2 output (mol%)	97%
Pressure of CO_2 output (bar)	150
CO_2 compression power demand (kWh/tCO_2)	132

Table 4.3 Baseline economic metrics consistent with all scenarios, unless noted otherwise.	
Plant utilization	90%
Project year	2026
Capital scaling factor	0.7
Indirect capital costs (% of total direct capital)	35%
Capital cost contingency (% of total direct & indirect capital)	10%
Debt financing	0%
Debt interest rate	n/a
Equity financing	100%
Return on equity	5%
Payback period (years)	20
Capital recovery factor (CRF)	8%
Cost of biomass ($/dry short ton)	$60
Cost of excess steam (4.5 bar) ($/tonne)	$8.6
Cost of MEA chemisorbent ($/kg)	$5.9
Cost of electricity ($/kWh)	$0.07

At \$50 per tonne CO_2. A 2% rate of inflation is used to adjust costs for the year 2026. Capital costs for the biomass boiler subsystem are determined through cost scaling techniques using reference costs from a detailed techno-economic analysis published by the US National Renewable Energy Laboratory.[4.26] Capital costs for the amine chemisorption subsystems are determined through cost scaling techniques using reference costs from the Aspen Process Economic Analyzer.[4.24] The major capital costs for the biomass boiler subsystem are broadly broken down into preprocessing, boiler, turbogenerator, gas cleaning, and other accessories. The capital costs for the amine chemisorption subsystem are broadly broken down into compressors, pumps, heat exchangers, absorber column, stripper column, and water knockout. Operating costs are broadly broken down into biomass feedstock, MEA material, cooling water, electricity (for Steam & Power scenarios), other operating and maintenance, and fixed costs (including salaries).[4.24,4.25,4.27,4.32,4.33] A value is placed on excess steam in the Steam & Power scenarios with the assumption that such steam will be used on-site for pulp and paper processing. Itemized capital and operating costs for each baseline scenario are provided in the Supplementary Information. To ensure consistency when calculating levelized costs of CO_2 capture, we follow the method of economic analysis used by Keith et al. for CO_2 removal systems.[4.14] Keith et al.'s methodology for economic analysis, which is adequate for early-stage cost estimations, requires five primary inputs: 1) itemized capital costs, 2) operating costs, 3) plant utilization, 4) capital intensity, and 5) a capital recovery factor (CRF). Levelized costs of CO_2 capture are calculated for each scenario using Equations 6 – 14. A CRF of 8% is used for all scenarios investigated because it corresponds to a 20 year payback period and 5% return on equity. We assume the funding of CO_2 capture systems at existing pulp and paper mills will be through private equity with a guaranteed return of 5%. Therefore, the levelized costs include a 5% return on equity over

20 years. Sensitivity analyses are conducted to account for variation in the cost of biomass, cost of electricity, and return on equity. In addition, scenarios are modified to understand the potential for reducing costs by utilization of existing boilers and turbogenerators on-site.

$$Levelized\ Cost\ of\ CO_2\ Capture\ \&\ Compression = Levelized\ Capital\ Cost + \ Net\ Operating\ Cost \quad (6)$$

$$Net\ Operating\ Cost = \frac{Operating\ Costs}{CO_2\ Capacity} \quad (7)$$

$$Levelized\ Capital\ Cost = Capital\ Intensity \times \frac{Capital\ Recovery\ Factor}{Utilization} \quad (8)$$

$$Capital\ Intensity = \frac{Total\ Capital\ Cost}{CO_2\ Capacity} \quad (9)$$

$$Capital\ Recovery\ Factor = \frac{i(i+1)^N}{(1+i)^N - 1} \quad (10)$$

$$Weighted\ Average\ Cost\ of\ Capital = i = (Interest\ on\ Debt\ Capital) \times (\%\ Debt\ Financing) + \ (Return\ on\ Equity\ Capital) \times (\%\ Equity\ Financing) \quad (11)$$

$$N = Project\ life\ (years) \quad (12)$$

$$Total\ Capital\ Cost = Direct\ Capital + Indirect\ Capital \quad (13)$$

$$Direct\ Capital\ Cost = \sum_i Reference\ Cost_i \times \left(\frac{New\ Capacity_i}{Reference\ Capacity_i}\right)^{Scale\ Factor} \quad (14)$$

4.2.3 Top-Down Analysis, Part II: Industry-Wide Cost Assessment

A nonlinear multivariate regression (Equation 15) is constructed using results from the bottom-up analysis combined with published results of cost estimates for a variety of CO_2 capture systems to ultimately estimate costs of capturing CO_2 at all 205 mills across the US.

$$
\begin{aligned}
Levelized\ Cost = {} & A1(FlowRate)^{B1} + A2(CapRate)^{B2} + A3(Conc)^{B3} \\
& + A4(FlowRate * CapRate)^{B4} \\
& + A5(FlowRate * Conc)^{B5} \\
& + A6(CapRate * Conc)^{B6} \\
& + A7(FlowRate * CapRate * Conc)^{B7}
\end{aligned}
\qquad (15)
$$

$$
\begin{aligned}
&A1 = 1001,\ B1 = 0.0275,\ A2 = 281.7,\ B2 = -0.0511, A3 = -8475, \\
&B3 = 5.712,\ A4 = -22.83,\ B4 = 0.1539,\ A5 = 95.15, B5 = 0.7852, \\
&A6 = -1379, B6 = 0.0115, A7 = 0.0022,\ B7 = 0.6771, R^2 = 0.8533
\end{aligned}
$$

The nonlinear regression is computed using the Gekko package in Python[4.34] and a total of 39 data sets, with each set containing four data points: CO_2 flow rate, CO_2 capture rate, CO_2 concentration, and levelized cost of capturing CO_2. Of the 39 data sets used in the regression, 15 are from the bottom-up analysis conducted herein, and the remaining 24 are derived from work published by Psarras et al.[4.11] wherein techno-economic studies were conducted on CO_2 capture systems for a variety of emission types. Using two separate data sets provides a wide range of operational parameters (CO_2 flow rate, capture rate, and concentration), thereby generating a robust regression. See the Supplementary Information for a detailed explanation of the multivariate regression. The year 2026 is taken to be the year for cost estimation because the 45Q sequestration tax credit levels off at \$50 per t-CO_2 at this time; a 2% rate of inflation is assumed between the years of 2016, which is the year for cost estimation by the multivariate regression, and 2026, which is the year for cost estimation in this analysis. We assume biomass intake, fuel intake, production capacity, and CO_2 emissions remain constant at all mills between the years 2018 – 2026. Levelized costs are quantified in three ways to provide stakeholders with an understanding of how CO_2 capture will influence their respective operations: 1) cost per tonne CO_2, 2) cost per tonne product, and 3) percent of manufacturing cost. Finally, transportation costs are quantified for each of the 205 mills using results from the geospatial analysis and methods developed by Sanchez et al.[4.23]

4.3 Results

4.3.1 Top-Down Analysis, Part I: Industry-Wide Screening

Approximately 150 million metric tons of CO_2 are emitted annually from the 205 pulp and paper mills selected for this analysis, of which 77% are biogenically derived (Table 4.4). Compared to other industrial commodities, the production of pulp and paper products is heavily reliant on biogenic fuels, which positions the industry favorably if future carbon emissions policies provide premium incentives for capturing biogenic CO_2. Details regarding the contributions of various fuels across all mills and respective operations are shown in Figure 4.4 and Table 4.5.

Table 4.4 Cumulative CO_2 emissions differentiated by origin of fuel.

Total CO_2 Emissions ($MtCO_2/y$)		
Fossil	34	23%
Biogenic	115	77%
Total	149	100%

The lime kilns and multi-fuel boilers use multiple fuels and therefore the emission CO_2 concentrations vary for particular operations across mills. Emissions from lime kilns are derived from fuel combustion and carbonate calcination, and therefore these emission streams have relatively high concentrations of CO_2 (Table 4.5)[4.35]; stoichiometric reactions for fuel combustion: $C_xH_yO_z + O_2 \rightarrow xCO_2 + \frac{y}{2}H_2O$ and calcium carbonate calcination: $CaCO_3 \rightarrow CaO + CO_2$. Overall, the total contribution of CO_2 from lime kilns is relatively small (~9%), whereas the contributions from multifuel boilers and recovery boilers are approximately the same (~43, ~48%). The energy demanded by CO_2 separation is most heavily influenced by the concentration of CO_2, which is evident from the relatively low energy demand for capturing

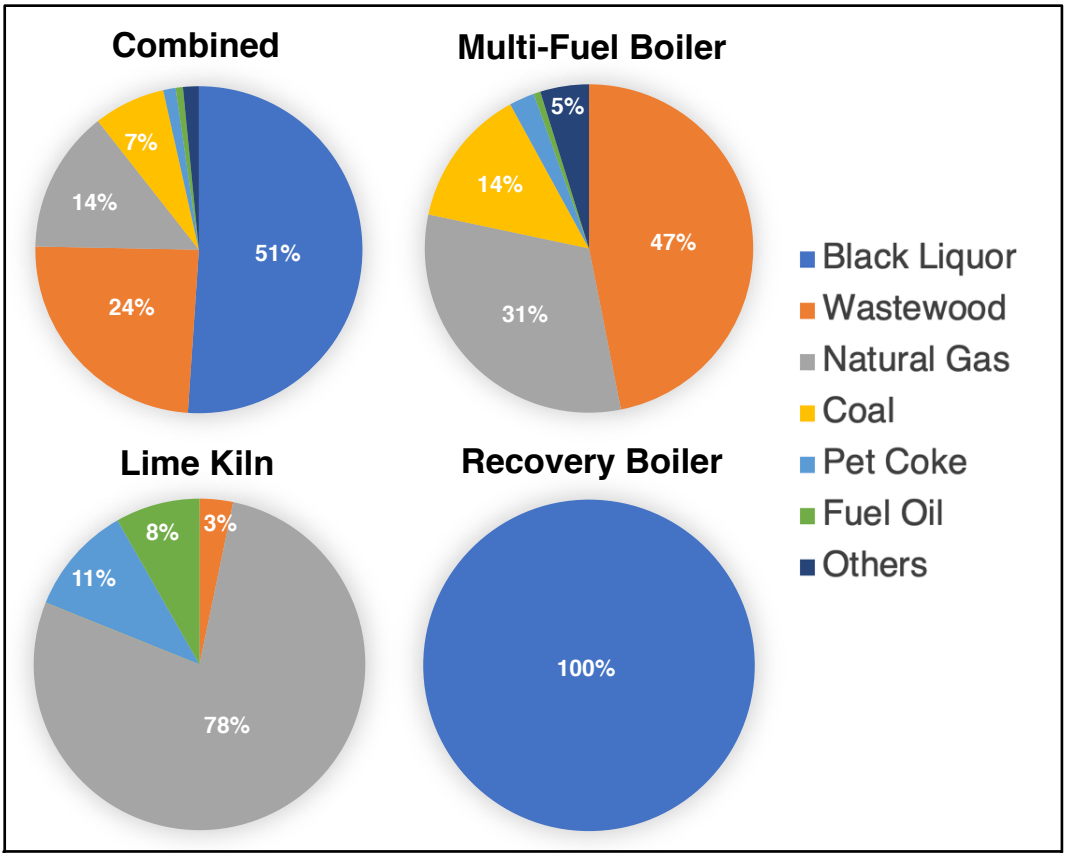

Figure 4.4 Contributions to CO_2 emissions by various fuels for the major operations across all pulp and paper mills in the US.

Table 4.5 Cumulative CO_2 emissions by operation and their contribution to total emissions. Average CO_2 concentration in emission streams from the respective operations and the corresponding energy required for CO_2 separation; energy demand for CO_2 separation not including compression.

CO_2 Emissions by Operation				
Operation	**CO_2 Emissions ($MtCO_2/y$)**	**Contribution to Total Emissions**	**Avg. CO_2 Concentration (mol%)**	**Energy Demand ($kJ/mol\text{-}CO_2$)**
Lime Kiln	13.7	9%	21%	13.1
Multi-Fuel Boiler	64.1	43%	9%	40.7
Recovery Boiler	71.4	48%	13%	24.9
Combined	149.2	100%	10%	37.4

CO_2 from lime kiln emissions. Natural gas has a high H/C ratio relative to solid fuels such as biomass, petroleum coke, and coal, and therefore natural gas generates effluent streams with high concentrations of water and low concentrations of CO_2.[4.20] Thus, natural gas-derived CO_2 emitted from multi-fuel boilers is generally more energy-intensive to capture than that derived from solid fuels. The production rates and corresponding CO_2 emissions of the eight major product grades are shown in Figure 4.5. As shown in Figures 4.5 and 4.6, the production of containerboard constitutes the largest quantity of CO_2 emissions per year, yet has a relatively low emission intensity due to its high production volume and relatively low-energy processing. Newsprint is also produced using a relatively mild, low-energy process.

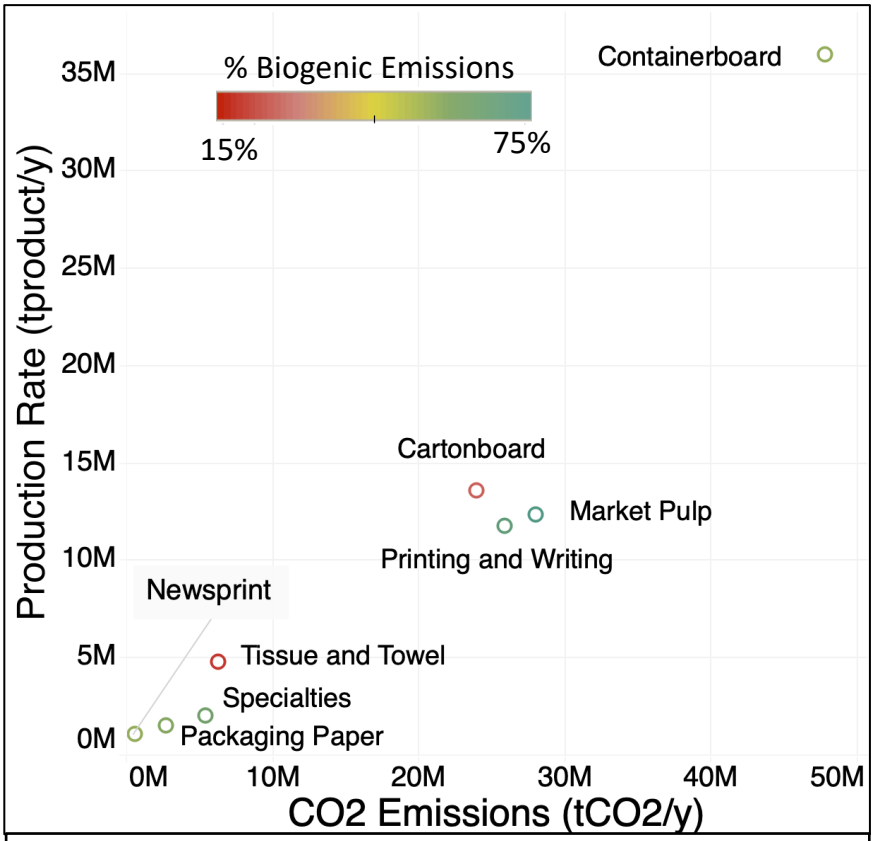

Figure 4.5 Annual production rates of the eight major product grades and their corresponding CO_2 emissions. The percentage of biogenic emissions for each major product grade shown via color.

Tissue and towel and cartonboard are often produced independent from wood pulping and processing, and therefore the on-site fuel consumption for their production is primarily fossil-derived and considerably lower than that for other products that are made at Kraft pulping mills. Thus, newsprint, tissue and towel, and cartonboard have relatively low emission intensities. Emissions from the production of all grades are primarily biogenically sourced, aside from cartonboard and tissue and towel, as shown in Figure 4.5. As shown in the Table 4.6, a substantial quantity of idling kilns and boilers are potentially available to drive new processes, such as CO_2 capture. The costs of capturing CO_2 could decrease if capital expenditures are reduced through the use of idling or stranded assets. In addition, waste heat, if available in sufficient quantity and quality, could reduce costs of capturing CO_2. A geospatial analysis is conducted to determine which mills are co-located with geology suitable for permanent CO_2 sequestration (Figure 4.7).[4.23] Of the 205 mills selected for analysis, 88 (43%) are located on geology suitable for sequestration and therefore do not require long-distance transportation of CO_2. Of the 117 mills that are not located on suitable geology, the average pipeline transportation distance to suitable geology is 134km.

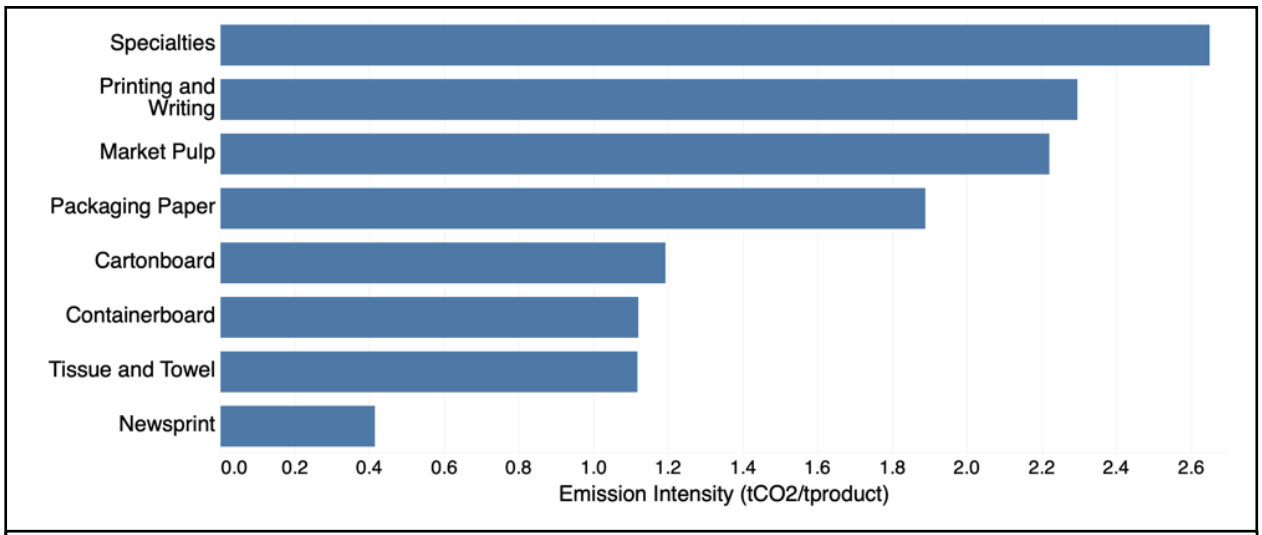

Figure 4.6 Emission intensities from on-site manufacturing for eight grades of pulp & paper products.

Table 4.6 Quantities of operating and idling assets across all sites.

Site Assets		
Operation	**# Operating**	**# Idling**
Lime Kiln	124	14
Multi-Fuel Boiler	406	103
Recovery Boiler	150	16

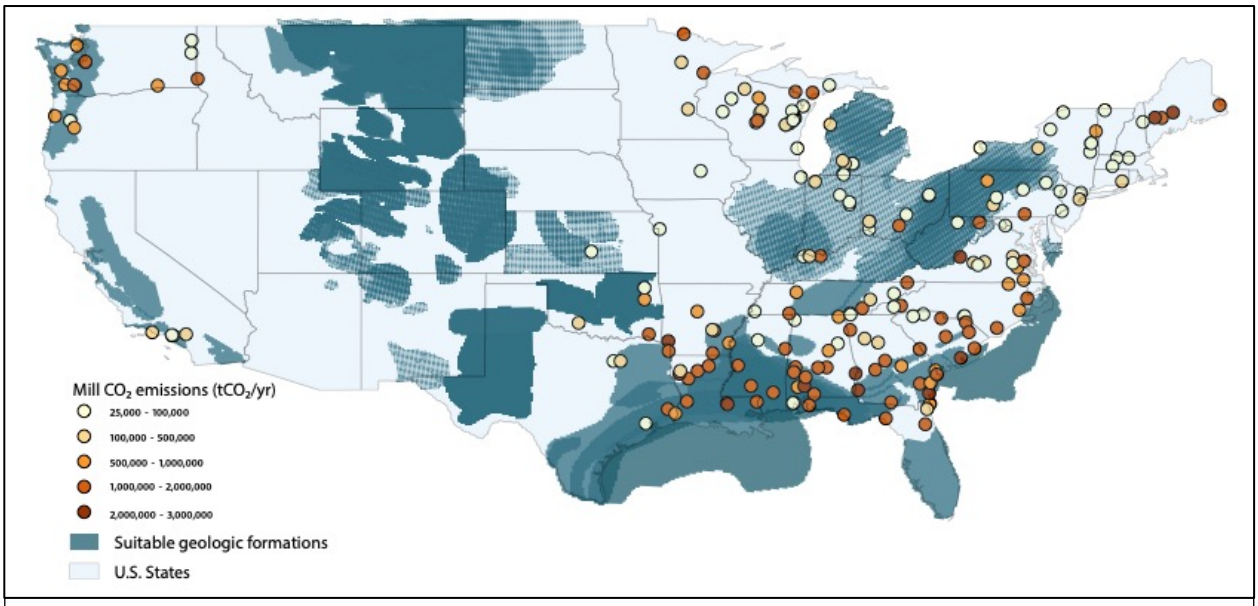

Figure 4.7 Geospatial plot showing the location and relative CO_2 capacity of all 205 pulp and paper mills. Suitable geology for sequestration overlaid in green.

4.3.2 Bottom-Up Analysis: Case Studies

Levelized costs of capturing CO_2 (including compression) from the four select mills are estimated over a range of scenarios, as shown in Figure 4.3A. The initial top-down, industry-wide analysis indicated the energy demands for capturing CO_2 from lime kiln emissions are the lowest of the three major operations, hence the inclusion of a scenario with only lime kiln emissions in this bottom-up analysis. Table 4.7 shows pertinent process data and cost estimates for the four baseline scenarios outlined in Figure 4.3A. Costs are estimated in year 2026 and the 45Q sequestration tax credit of $50 per tonne CO_2 is applied to all scenarios.

Table 4.7 Pertinent process data and cost estimates of CO_2 capture ($/t$CO_2$) for the four baseline scenarios outlined in Figure 3A. Waste heat at Mill 4 is assumed to be of high enough quality for use as steam in the amine subsystem reboiler. Year of cost estimation: 2026. 45Q tax credit: $50/tCO2.

Baseline Scenario 1: Steam + Combined Emissions				
	Mill 1	Mill 2	Mill 3	Mill 4
P&P Mill Biomass Flow Rate (dry short ton/day)	4225	5263	7320	3444
CO_2 System Biomass Flow Rate (dry short ton/day)	3140	3162	2438	831
CO_2 Concentration (mol%)	15.1%	13.0%	14.9%	13.1%
CO_2 Captured (tCO_2/y)	4.01E+06	4.03E+06	3.11E+06	1.60E+06
Power Demand (MW)	61	63	47	24
Steam Demand (GJ/h)	1600	1611	1242	640
Cost of Capture & Compression ($/$tCO_2$)	$2	$5	$4	$2

Baseline Scenario 2: Steam & Power + Combined Emissions				
	Mill 1	Mill 2	Mill 3	Mill 4
P&P Mill Biomass Flow Rate (dry short ton/day)	4225	5263	7320	3444
CO_2 System Biomass Flow Rate (dry short ton/day)	3939	4088	3026	1859
CO_2 Concentration (mol%)	15.1%	13.2%	14.9%	13.6%
CO_2 Captured (tCO_2/y)	4.37E+06	4.45E+06	3.38E+06	2.07E+06
Power Demand (MW)	77	80	59	36
Steam Demand (GJ/h)	1744	1778	1349	827
Cost of Capture & Compression ($/$tCO_2$)	-$3	$0	-$2	$1

Baseline Scenario 3: Steam + Lime Kiln Emissions				
	Mill 1	Mill 2	Mill 3	Mill 4
P&P Mill Biomass Flow Rate (dry short ton/day)	4225	5263	7320	3444
CO_2 System Biomass Flow Rate (dry short ton/day)	247	243	506	0
CO_2 Concentration (mol%)	18.8%	18.6%	21.4%	20.9%
CO_2 Captured (tCO_2/y)	3.16E+05	3.10E+05	6.45E+05	1.83E+05
Power Demand (MW)	4.9	4.8	9.9	2.9
Steam Demand (GJ/h)	126	124	258	73
Cost of Capture & Compression ($/$tCO_2$)	$23	$23	$12	-$19

Table 4.7 (continued)

Baseline Scenario 4: Steam & Power + Lime Kiln Emissions				
	Mill 1	Mill 2	Mill 3	Mill 4
P&P Mill Biomass Flow Rate (dry short ton/day)	4225	5263	7320	3444
CO_2 System Biomass Flow Rate (dry short ton/day)	320	314	640	296
CO_2 Concentration (mol%)	18.4%	18.2%	20.8%	18.2%
CO_2 Captured (tCO_2/y)	3.48E+05	3.42E+05	7.06E+05	3.16E+05
Power Demand (MW)	6.2	6.1	12.5	5.8
Steam Demand (GJ/h)	139	137	282	126
Cost of Capture & Compression ($/$tCO_2$)	$18	$18	$8	$3

Cost estimates below $0 indicate the tax credit acts a source of income for the particular scenario. Figure 4.8 provides a breakdown of the levelized capital and operating costs for each baseline scenario investigated. As can be seen in Figure 4.8, operating costs contribute significantly more than capital costs to the levelized costs of CO_2 capture. As can be seen in Table 4.7 & Figure 4.8, the cost estimates for the Combined emission scenarios are near to $0, ranging from -$3 to $5 per tonne CO_2, whereas the cost estimates for the Lime Kiln emission scenarios vary considerably, ranging from -$19 to $23 per tonne CO_2. The levelized costs of capturing CO_2 for the Steam & Power + Combined Emissions scenarios are negative for Mills 1-3, and slightly positive for Mill 4, thereby demonstrating the economic feasibility of these scenarios. The lowest cost of CO_2 among the baseline scenarios is the Mill 4, Steam + Lime Kiln Emissions scenario (-$19/$tCO_2$) in which on-site waste heat (217 GJ/h) is sufficient for the entire operation and new biomass boiler steam generation is not necessary. Mill 4 is the only mill of the selected four that has waste heat potentially available to use for CO_2 capture.

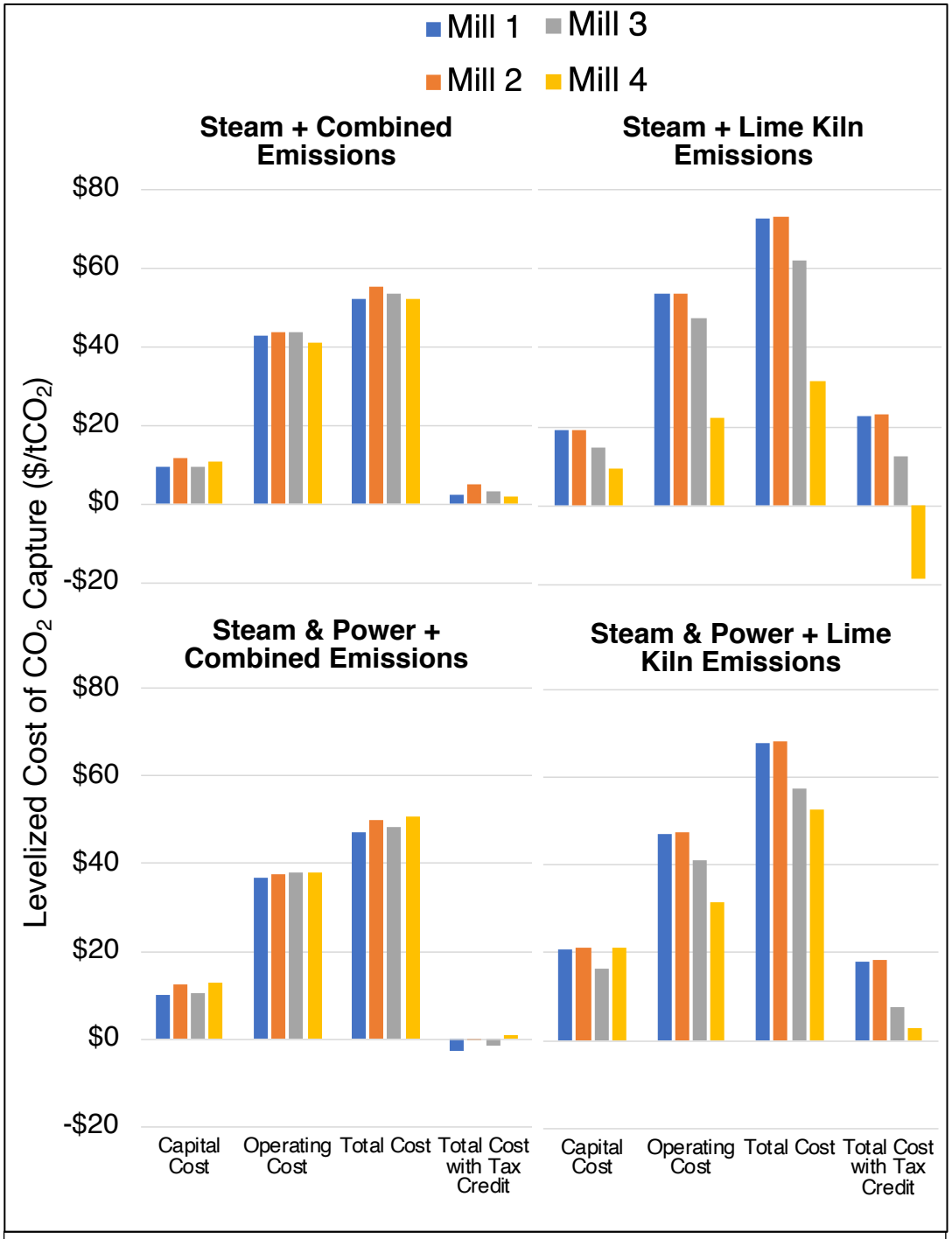

Figure 4.8 Levelized capital, operating, and total costs of CO_2 capture for baseline scenarios. Year of cost estimation: 2026. 45Q tax credit: $50/t$CO_2$.

We assume the waste heat is of high enough quality to be used as steam (4.5 bar, 150°C) in the amine subsystem reboiler. Interestingly, the costs of capturing CO_2 for the other three Mill 4 scenarios are not as low as that for the Steam + Lime Kiln Emissions scenario. This observation can be explained by the fact that the other three scenarios require capital expenses for a biomass boiler subsystem and operating expenses for biomass feedstock, thereby significantly increasing the levelized cost of CO_2 capture. The availability and quality of heat at Mill 4 must be validated before accepting these cost estimates. Nevertheless, this exercise demonstrates the significant potential for cost reduction through the use of on-site waste heat.

According to results from the bottom-up analysis, cost estimates for capturing CO_2 from lime kiln emissions are generally higher than those from combined emissions, which contradicts the energy demand trend determined in the initial top-down analysis; lime kiln emissions require less energy to process than emissions from other operations due to the high concentrations of CO_2. This contradiction can be explained by the relatively small flow rates of CO_2 from lime kilns and thus the lack of economies of scale. The scales of operation for the Combined Emission scenarios are significantly larger in size than those for the Lime Kiln Emission scenarios, evident by the differences in biomass flow and CO_2 capture rates (Table 4.7). Therefore, the scaling factor (0.7) in the Combined Emissions scenarios outweighs the cost benefits of higher CO_2 concentrations in the Lime Kiln Emissions scenarios. Notably, the biomass input required by the CO_2 capture system for the Mill 1, Steam & Power + Combined Emissions scenario is 3939 tonnes biomass per day, which is 93% of the biomass input to pulp and paper operations at Mill 1. Overall, the Combined emissions scenarios demand significant quantities of biomass, thereby warranting investigation into local availability of biomass resources to determine feasibility[4.37]; a sensitivity analysis varying biomass costs is conducted to help understand this feasibility.

Mill 4 demands a relatively small quantity of biomass for the Combined Emissions scenarios (831 – 1859 t-biomass/day), because of the on-site waste heat utilization which allows for less biomass consumption. The most effective way to reduce biomass demand is to reduce the reboiler duty and/or utilize existing waste heat. A sensitivity analysis is conducted by varying reboiler duty to help understand how different amine solvents might affect costs. The high costs associated with the Lime Kiln Emissions scenarios are largely due to the small scale of operation. Small biomass boiler systems of capacities in the range of 200 – 300 tbiomass/day have high capital intensities ($/t$CO_2$) relative to large systems due to economies of scale.[4.38] The Steam & Power scenarios that use biomass to entirely meet steam and power demands have lower levelized costs of CO_2 capture than the Steam scenarios that purchase power. This observation is interesting because scenarios that purchase power do not require large capital expenditures for turbogenerators, and the quantities of biomass required for operation are considerably less than for scenarios that generate steam and power. A sensitivity analysis varying electricity costs is conducted to better understand this observation.

4.3.2.1 Sensitivity Analyses:

Sensitivity analyses are conducted to understand the effects of important variables on levelized costs of CO_2 capture (Figures 4.9 – 4.15). Specifically, reboiler duty, biomass cost, electricity cost, rate of MEA loss, and return on equity are varied. Costs due to transportation are negligible for all four mills since they sit atop suitable geology for long-term sequestration, however, we conduct a sensitivity analysis by varying transportation distances to understand the effects transportation would have if these sites were not located on suitable geology.

Regarding reboiler duty, Figure 4.9 shows the inflection point at which levelized costs transition from negative to positive is ~3.0 GJ/tCO_2 for the Steam + Combined Emissions and

~3.5 GJ/tCO_2 for the Steam & Power + Combined Emissions scenarios. All mills except Mill 4 have positive costs for the Lime Kiln Emissions scenarios, due to reasons explained in the previous section. Notably, the cost associated with Mill 3, Steam + Lime Kiln Emissions and a reboiler duty of 1.5 GJ/tCO_2 is approximately $0 per tonne CO_2, or break even; Mill 3's lime kiln emissions are of a relatively high concentration of CO_2, hence the lower costs. Scenarios that generate steam only, namely Steam + Combined Emissions and Steam + Lime Kiln Emissions, are more sensitive to reboiler duty values, evident by the larger variation in levelized costs of CO_2 capture when compared to scenarios that generate steam and power. Commercial MEA solvents used at concentrations of 30 wt% in a manner similar to that used in this analysis typically have reboiler duties in the range of 3.0 – 5.0 GJ/tCO_2, and advanced amine solvents currently under development have shown the potential for duties less than 2.0 GJ/tCO_2.[4.2,4.12] Therefore, the low reboiler duties analyzed in this sensitivity analysis are proxies for advanced amine solvents.

Regarding MEA loss, Figure 4.10 shows the inflection point at which levelized costs transition from negative to positive is ~1.7 kg/tCO_2 for the Steam + Combined Emissions and ~2.6 kg/tCO_2 for the Steam & Power + Combined Emissions scenarios. All mills except for Mill 4 have positive costs for the Lime Kiln Emissions scenarios, due to reasons explained in the previous section. Costs associated with Mill 4, Steam + Lime Kiln Emissions are highly sensitive to MEA rate loss, with a minimum cost of -$26/$tCO_2$; the contribution of MEA cost to overall operating cost is significant for this particular scenario since no biomass is consumed. Notably, the cost associated with Mill 3, Steam & Power + Lime Kiln Emissions and a MEA loss rate of 1.1 kg/tCO_2 is approximately $0/$tCO_2$, or break even; Mill 3's lime kiln emissions are of a relatively high concentration of CO_2, hence the lower costs. Relative to Steam only scenarios, the

Steam & Power scenarios are overall more sensitive to MEA loss rates because of the increased biomass flow rate rates and thus larger quantities of CO_2 to process.

Regarding biomass cost, Figure 4.11 shows the inflection point at which levelized costs transition from negative to positive is ~$50/tbiomass for the Steam + Combined Emissions and ~$60/tbiomass for the Steam & Power Combined Emissions scenarios. Costs associated with Mill 3, Steam & Power + Lime Kiln Emissions are negative with a biomass cost of $20/tbiomass, but all other costs for Mill 3, Lime Kiln Emissions are positive. The costs associated with Mill 4, Steam + Lime Kiln Emissions do not change with biomass cost because this particular scenario relies entirely on waste heat and does not require biomass energy for operation. Relative to Steam only scenarios, the Steam & Power scenarios are more sensitive to biomass cost because of the increased biomass flow rates. The use of natural gas-fueled boiler and turbogenerator systems would likely reduce costs of CO_2 capture due to the very low cost of natural gas energy in the US, relative to biomass energy. However, the net removal of CO_2 from the atmosphere would be reduced if natural gas was used in place of biomass fuel.

Regarding electricity cost, Figure 4.12 shows the inflection point at which levelized costs transition from negative to positive is ~$0.045/kWh for the Steam + Combined Emissions scenarios. The costs for all Steam & Power scenarios do not change from baseline with variation in electricity price since all power necessary for operation is derived from biomass. Costs associated with Mill 4, Steam + Lime Kiln Emissions are highly sensitive to electricity cost, with a minimum cost of -$27/t$CO_2$; the contribution of electricity cost to overall operating cost is significant for this particular scenario since no biomass is consumed.

Regarding return on equity, Figure 4.13 shows the inflection point at which levelized costs transition from negative to positive is ~2.0% for Steam + Combined Emissions and ~5.0% for

Steam & Power + Combined Emissions. All mills except for Mill 4 have positive costs for the Lime Kiln Emissions scenarios, due to reasons explained in the previous section. Relative to Steam only scenarios, the Steam & Power scenarios are more sensitive to return on equity due to the larger capital expenditure required. For a return on equity of 10%, which is common for industrial investments, all mills except Mill 4 have positive costs of CO_2 capture. Therefore, near-term investments into CO_2 capture at pulp and paper mills in the US will likely not be driven solely by economics, but rather a combination of economics and environmental stewardship.

Regarding transportation distance, Figure 4.14 shows the effects of increasing transportation distance on levelized costs of capturing and transporting CO_2. The four mills selected for the bottom-up analysis are co-located with suitable geology and thus do not require transportation of CO_2 for long-term sequestration, however, understanding how transportation could affect cost is important. The average transportation distance among the 117 mills that do not sit atop suitable geology for long-term sequestration is ~130km, and thus 130km is selected as the median point in the sensitivity analysis. As can be seen in Figure 4.14, the lime kiln scenarios are affected by transportation distance more than the combined scenarios, which is due to economies of scale; constructing pipeline to transport CO_2 is highly expensive for relatively small CO_2 flow rates. There are only two scenarios with negative costs for transporting CO_2 a distance of 130km (the average distance for mills not co-located with suitable geology), namely Mill 1, Steam & Power + Combined Emissions and Mill 4, Steam + Lime Kiln Emissions. Thus, the majority of scenarios are not economical for the average transportation distance of 130km, and stakeholders should prioritize mills that are co-located with suitable geology.

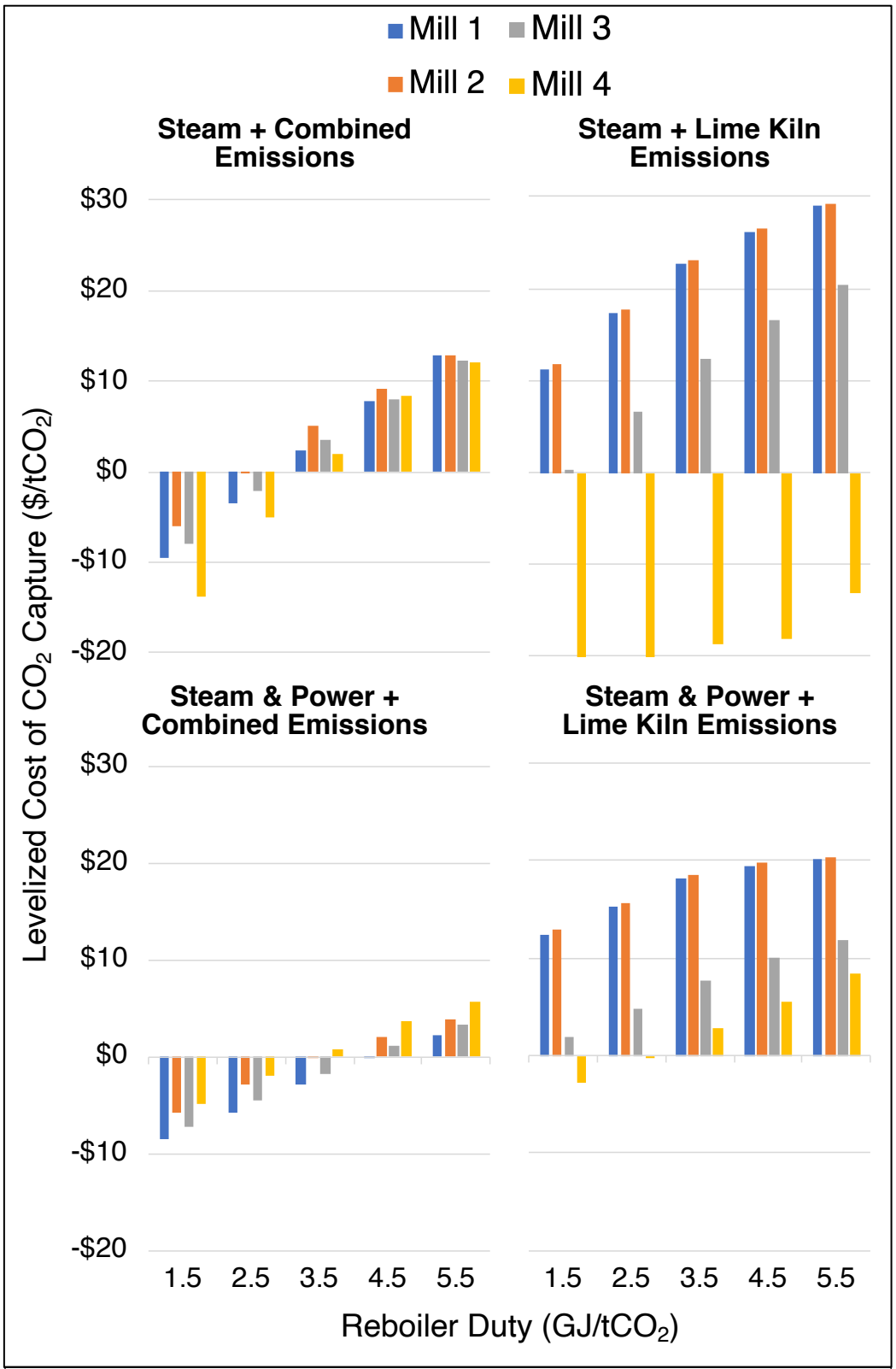

Figure 4.9 Sensitivity analysis showing levelized costs of CO_2 capture ($/tCO$_2$) with variation in reboiler duty. Year of cost estimation: 2026. 45Q tax credit: $50/tCO$_2$.

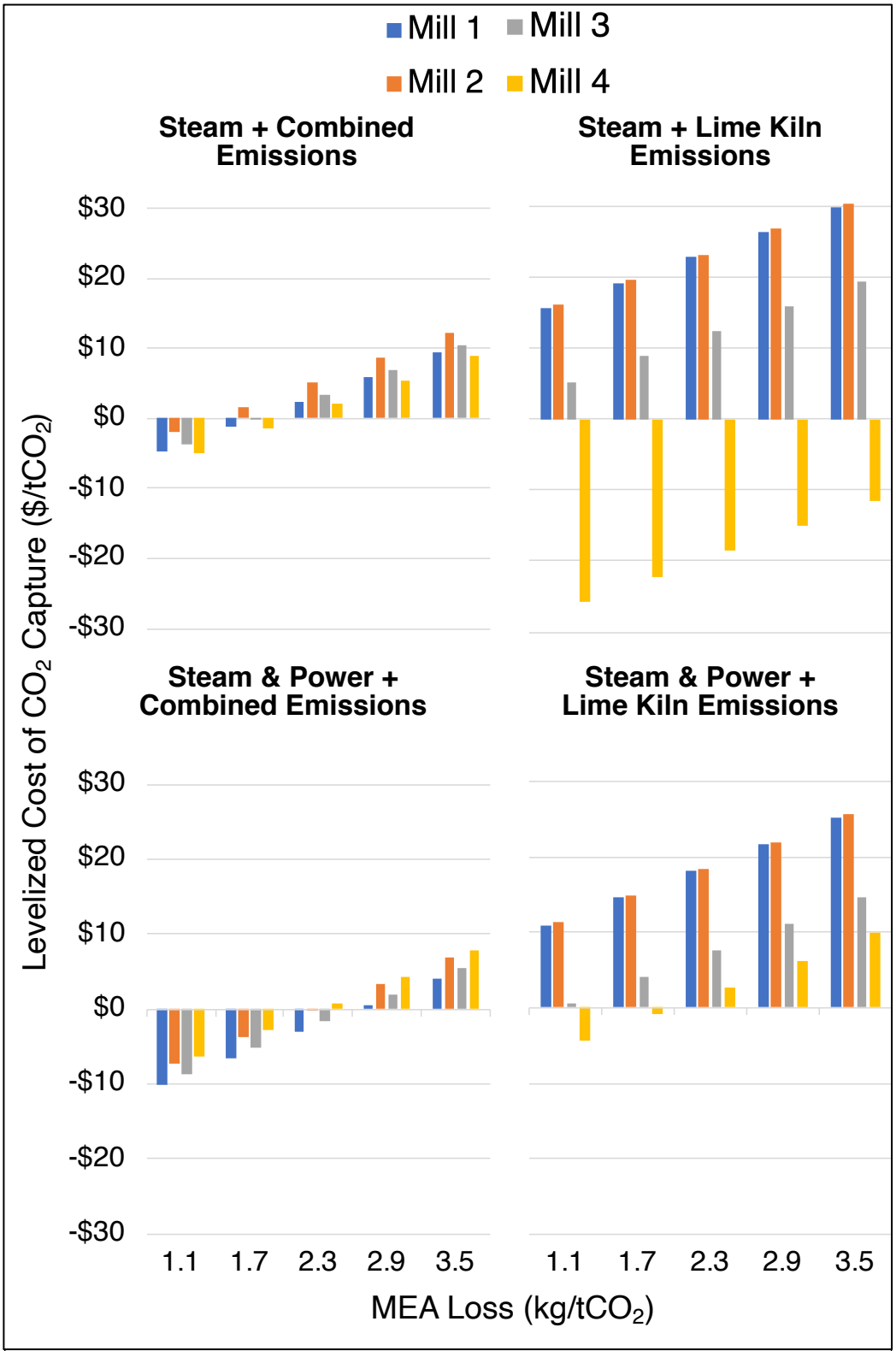

Figure 4.10 Sensitivity analysis showing levelized costs of CO_2 capture ($/t$CO_2$) with variation in rate of monoethanolamine (MEA) loss. Year of cost estimation: 2026. 45Q tax credit: $50/t$CO_2$.

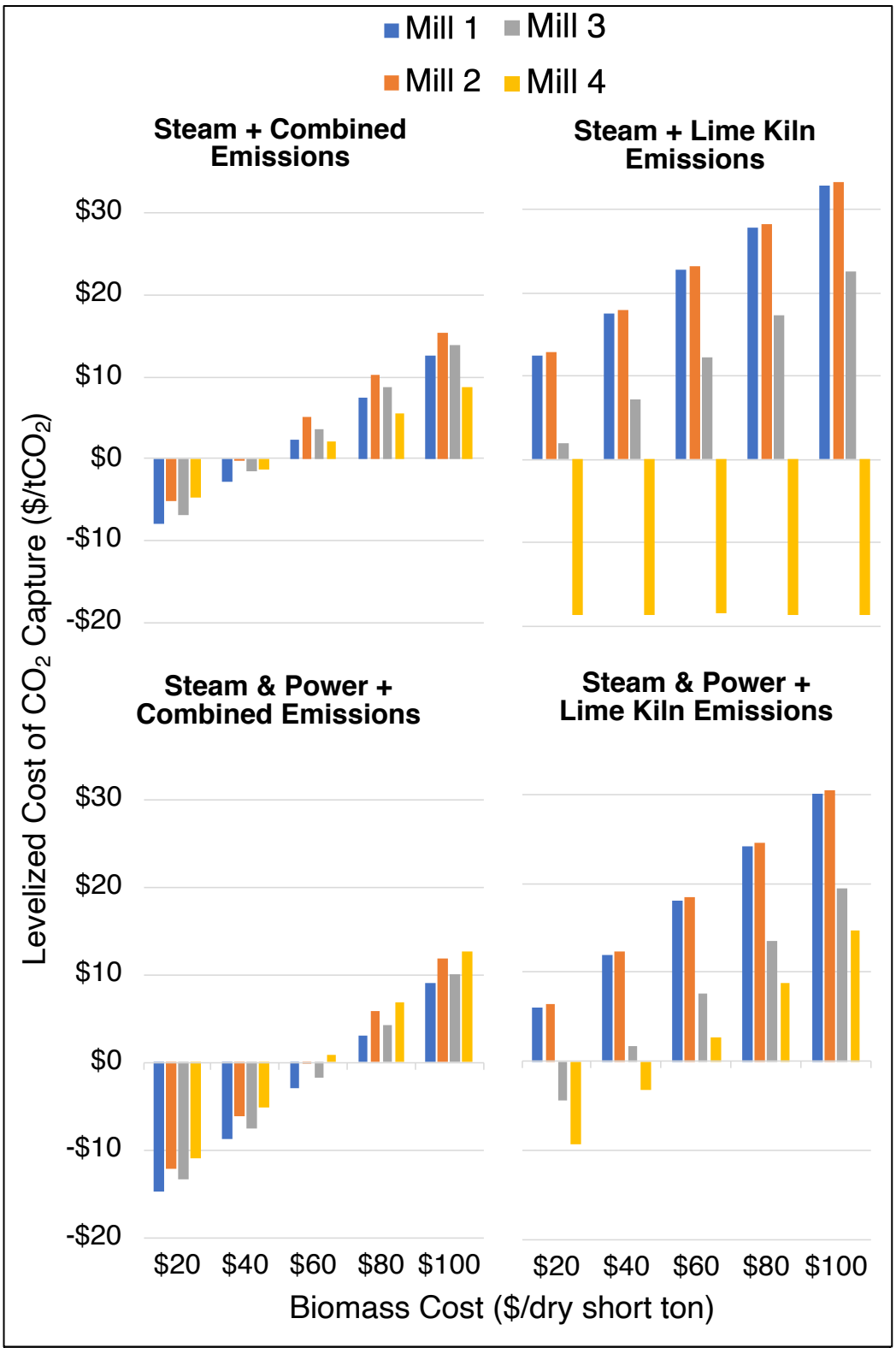

Figure 4.11 Sensitivity analysis showing levelized costs of CO_2 capture ($/t$CO_2$) with variation in biomass cost. Year of cost estimation: 2026. 45Q tax credit: $50/t$CO_2$.

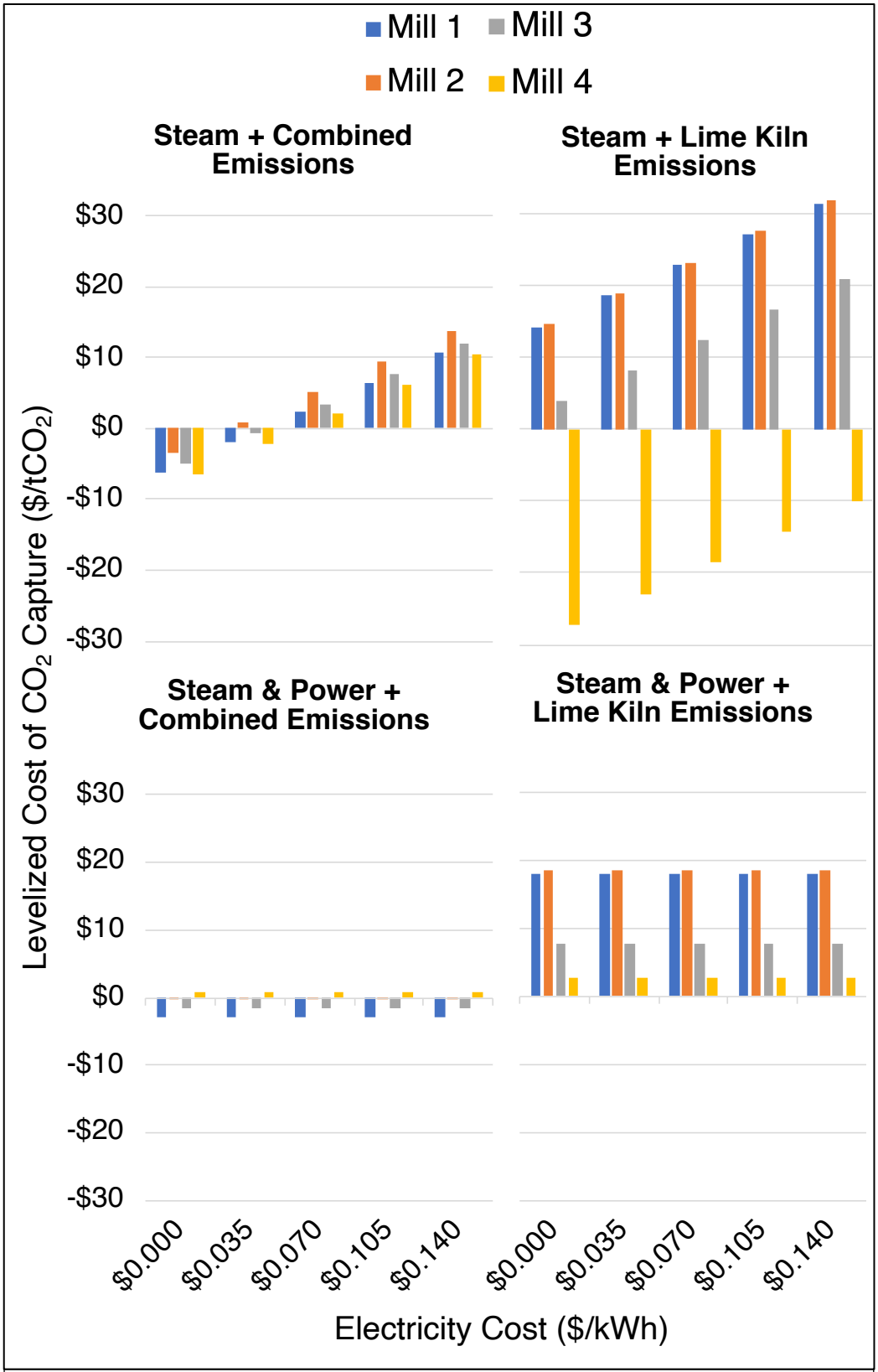

Figure 4.12 Sensitivity analysis showing levelized costs of CO_2 capture ($/t$CO_2$) with variation in electricity cost. Year of cost estimation: 2026. 45Q tax credit: $50/t$CO_2$.

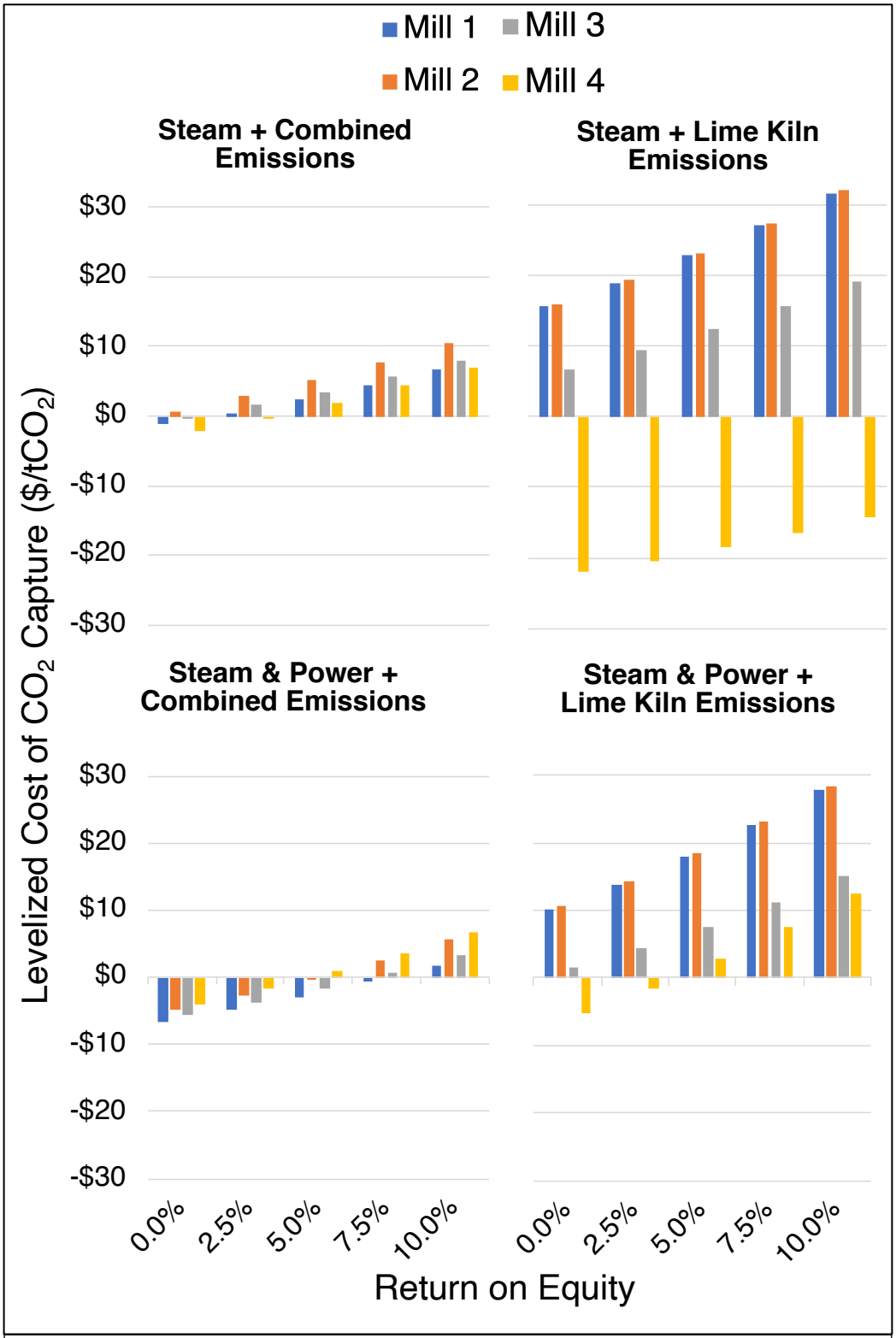

Figure 4.13 Sensitivity analysis showing levelized costs of CO_2 capture ($/t$CO_2$) with variation in return on equity. Year of cost estimation: 2026. 45Q tax credit: $50/t$CO_2$.

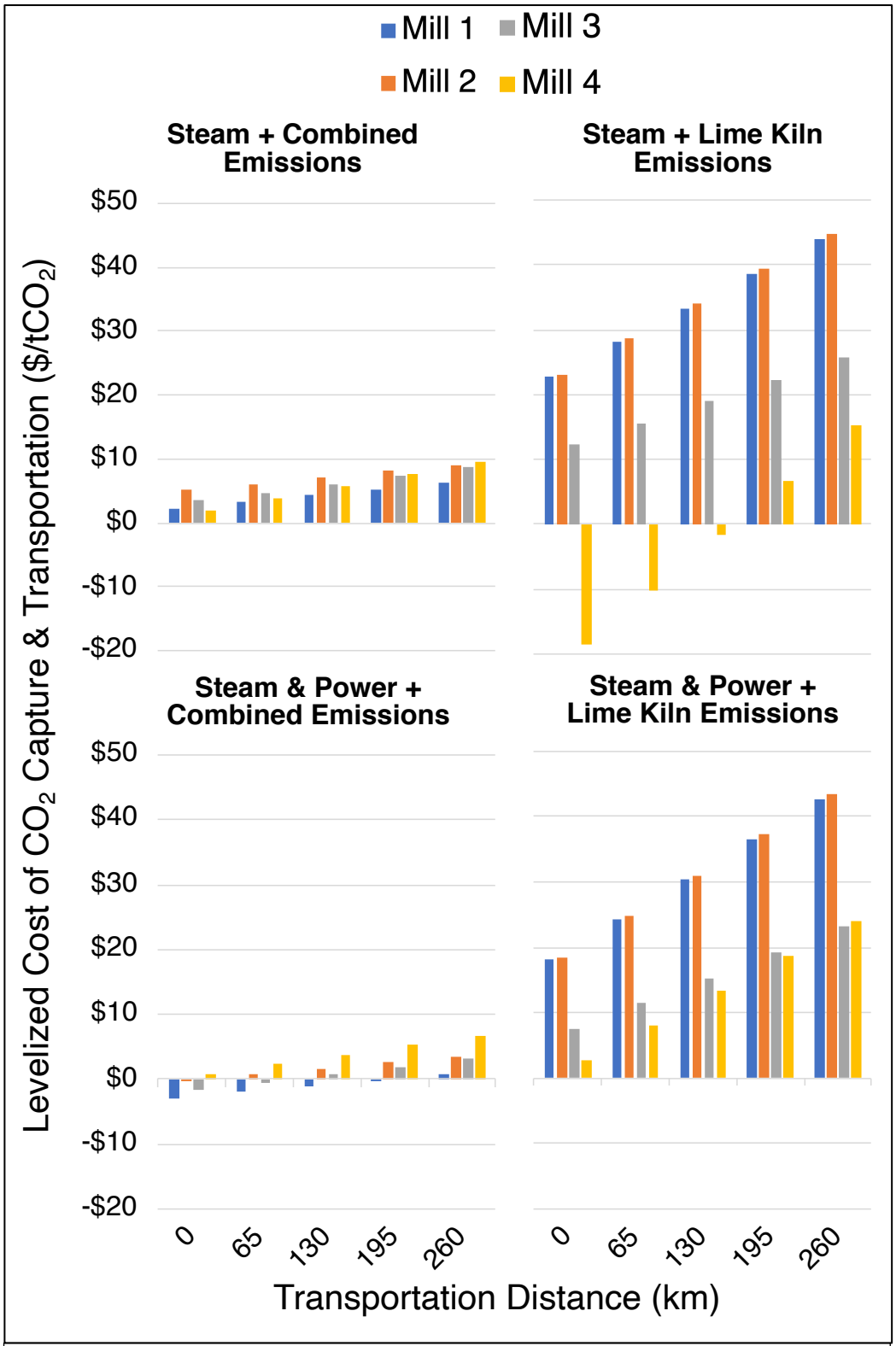

Figure 4.14 Sensitivity analysis showing levelized costs of CO_2 capture ($/t$CO_2$) with variation in transportation distance. Year of cost estimation: 2026. 45Q tax credit: $50/t$CO_2$.

Figure 4.15 shows the levelized costs of CO_2 capture for best and worst case scenarios in which the highest and lowest performing values from the sensitivity analyses are applied, respectively. These scenarios are not highly likely, but they show the range of potential costs. The best case scenario might be plausible with an optimized system using advanced amine solvents located in an area with an abundance of low cost biomass or curtailed solar/wind energy. The worst case scenario shows costs typically considered very high for post-combustion CO_2 capture, and would likely not be economical even with stringent carbon emission policies.

Figure 4.16 shows the levelized costs for scenarios in which idling boilers and turbines are brought online to provide the heat and power for CO_2 capture. To be conservative, 10% of the installed capital cost for a new boiler + turbogenerator system is assumed necessary to bring an idling boiler + turbogenerator system online. The reductions in costs compared to the baseline scenarios are significant. The largest reductions in costs are experienced by the Steam & Power Emissions scenarios, due primarily to the avoidance of steep capital costs for boilers and turbogenerators.

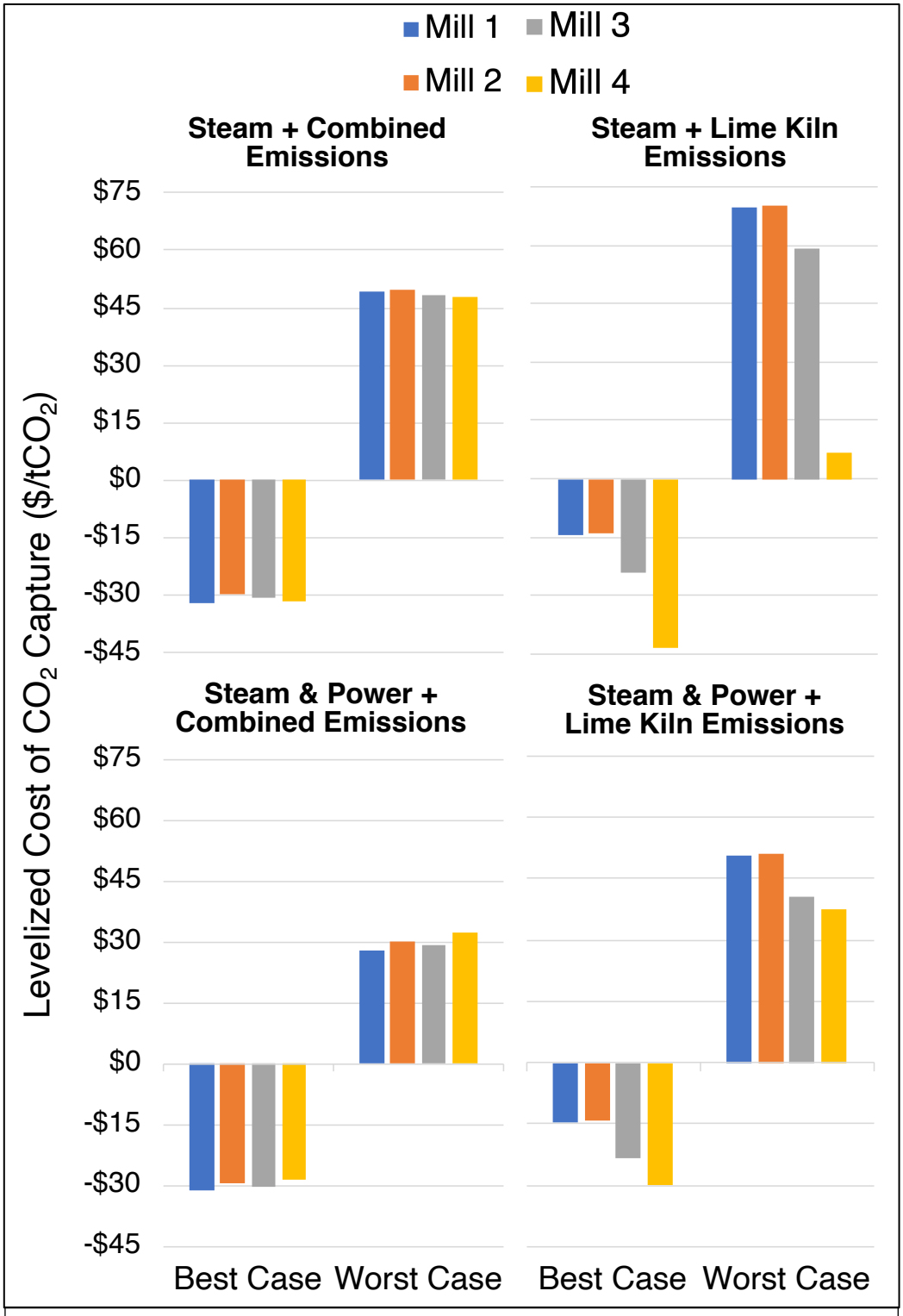

Figure 4.15 Levelized costs of CO_2 capture ($/tCO2) for best and worst case scenarios. Year of cost estimation: 2026. 45Q tax credit: $50/tCO2.

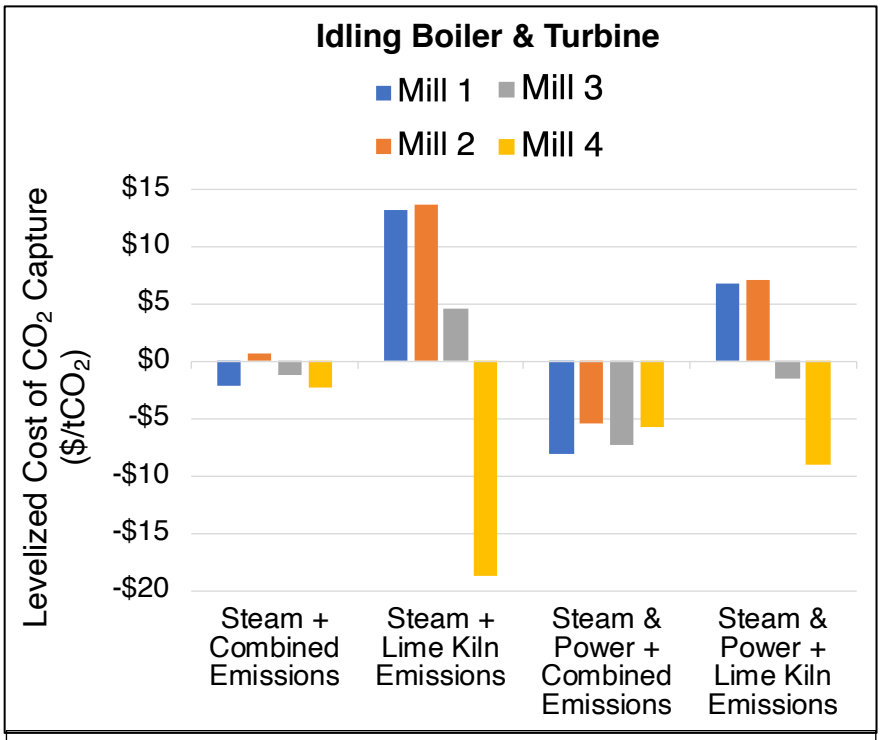

Figure 4.16 Levelized costs of CO_2 capture ($/t$CO_2$) for baseline scenarios with existing boiler and turbogenerator subsystems. Year of cost estimation: 2026. 45Q tax credit: $50/t$CO_2$.

4.3.3 Top-Down Analysis, Part II: Industry-Wide Cost Assessment

Results from the bottom-up analysis are used to construct a multivariate regression that is applied in a top-down fashion to estimate levelized costs of capturing CO_2 for all 205 mills in the year 2026, the results of which are shown in Table 4.8. To account for the 45Q tax credit, a $50 per tonne CO_2 reduction in cost is incorporated in each cost estimate shown. Costs range from -$0.6 to $12.7 per tonne CO_2, with recovery boiler- and lime kiln-derived CO_2 being the lowest cost options of the three main operations. Given that levelized costs are inversely proportional to CO_2 concentration and flowrate, the aforementioned trend in costs can largely be explained by the following: CO_2 concentrations of lime kiln emissions are significantly high, CO_2 concentrations and flow rates of recovery boiler emissions are moderately high, and CO_2

Table 4.8 Levelized costs of capturing CO_2 from operations at all sites (year 2026). \$50/tCO_2 reduction incorporated.

Operation	Min.	Max.	Avg.	Std. Dev.
Lime Kiln	\$2.1	\$5.0	\$4.6	\$0.6
Multi-Fuel Boiler	\$1.6	\$12.7	\$8.1	\$3.6
Recovery Boiler	\$1.2	\$5.9	\$4.0	\$1.1
Combined	-\$0.6	\$12.7	\$6.4	\$4.6

concentrations of multifuel boilers are moderately low, corroborated by Table 4.5. Compared with costs estimated in the bottom-up analysis, the top-down analysis provides similar cost estimates for capturing combined emissions, however, cost estimates for lime kiln emissions are relatively low. Thus, the regression is better suited for large flow rates of CO_2 wherein economies of scale are more readily achieved, including flue streams from multi-fuel boilers, recovery boilers, and combined emissions. If existing capital assets, such as boilers and turbines, can be utilized, the small scales of operation for lime kiln scenarios become more cost competitive since reduced capital costs make economies of scale less important. Overall, economic results from the top-down approach demonstrate the robustness of the regression and its ability to accurately estimate costs of capturing CO_2 emissions from a multitude of fuel types and large-scale industrial operations.

The costs of capturing CO_2 from combined emissions are analyzed on the basis of product mass (\$/tproduct) and CO_2 mass (\$/tCO_2), as shown in Figure 4.17A. Costs on the basis of product mass trend differently than those on the basis of CO_2 mass, which is due to the variation in emission intensities. For example, the cost of capturing CO_2 emitted from the production of containerboard is relatively moderate on the basis of CO_2 mass, but relatively low on the basis of product mass, which is because costs on the basis of product mass are proportional to emission intensities. Incremental costs (Figure 4.17B) are also proportional

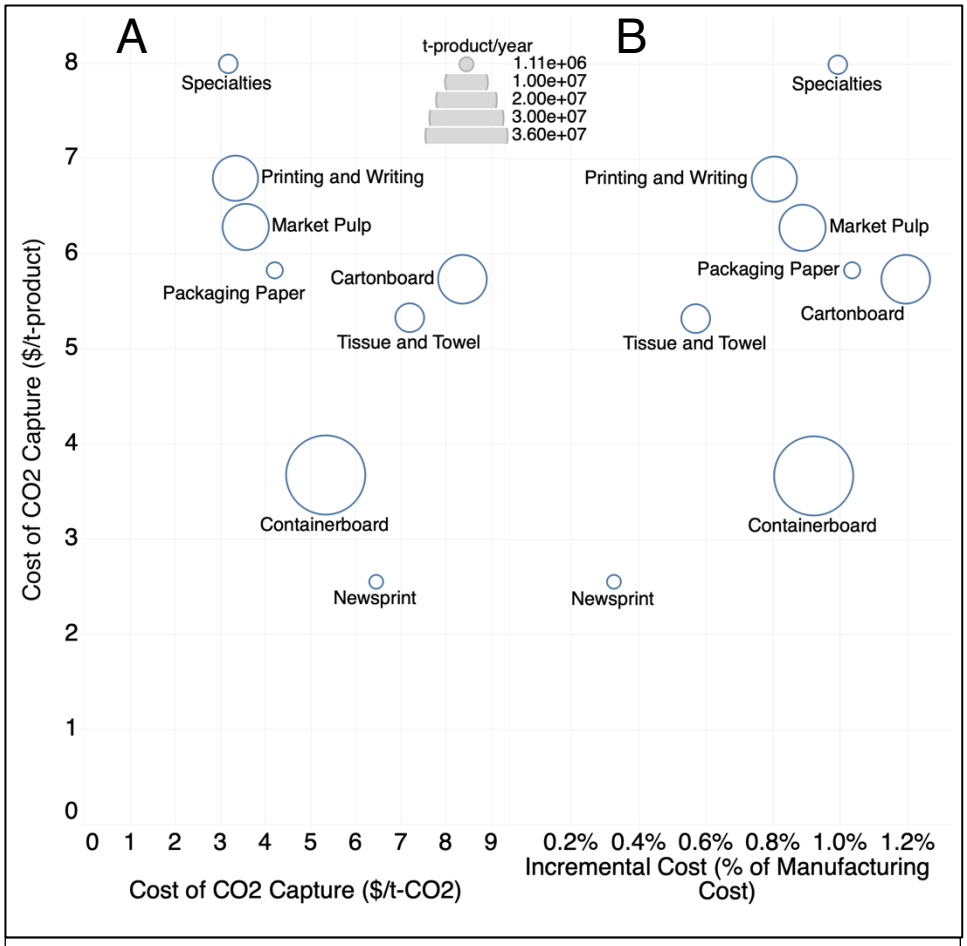

Figure 4.17 A) Costs of capturing combined CO_2 emissions on the basis of product mass ($/tproduct) and CO_2 mass ($/t$CO_2$). B) Costs of capturing combined CO_2 emissions on the basis of product mass and the resultant incremental cost in manufacturing cost expressed as percent increase in manufacturing cost. Year of cost estimates is 2026. To account for the 45Q sequestration tax credit, a $50/t$CO_2$ reduction in cost is incorporated in each cost estimate.

to emission intensities, but in addition, they are inversely proportional to manufacturing costs, and thus the dynamics are more complex. For example, tissue and towel products have relatively low emission intensities and high manufacturing costs, and thus incremental costs of capturing CO_2 are relatively low. Incremental cost data shown in Figure 4.17B provide stakeholders with an understanding of how the capture of combined CO_2 emissions would affect their margins. Overall, costs on the basis of product mass are relatively small and therefore incorporating the capture of combined CO_2 emissions would not add significant cost to pulping operations. Using

results from the geospatial analysis (Figure 4.7), costs are estimated for transporting CO_2 to suitable geology for long-term sequestration. The average cost of transportation among mills that do not sit atop suitable geology is $24.8 per tonne CO_2 in the year 2026 (assuming 2% rate of inflation and not accounting for the 45Q tax credit), and thus mills co-located with suitable geology should be prioritized for initial deployment of CO_2 capture and sequestration in the US pulp and paper industry.

4.4 Process Innovation

Two opportunities to reduce costs of CO_2 capture exist through process innovation at existing Kraft pulping mills: 1) partial oxy-fuel combustion of lime kilns with post-combustion CO_2 capture and 2) integrated alkaline solvent CO_2 capture.

4.4.1 Partial Oxy-Fuel Combustion of Lime Kiln

A substantial number of mills that utilize oxygen for delignification purchase oxygen from external suppliers because the quantities of oxygen demanded are not large enough to justify the acquisition and operation of large air separation units. A possible justification for the use of air separation units could be the reduction of CO_2 capture costs through partial oxy-fuel combustion in lime kilns. Therefore, Kraft pulping mills that utilize large quantities of pure oxygen for delignification might be suitable for CO_2 capture via partial oxy-fuel combustion in the lime kiln with post-combustion CO_2 capture. Partially substituting air intake with pure oxygen generates emissions with relatively high concentrations of CO_2 and thereby reduces the energy required for CO_2 capture, as shown in Figure 4.18; the increase in CO_2 concentration is due to the reduction in nitrogen introduced to the system via air. In addition, preliminary studies have demonstrated an increase in lime kiln capacity with oxy-fuel substitution.[4.8]

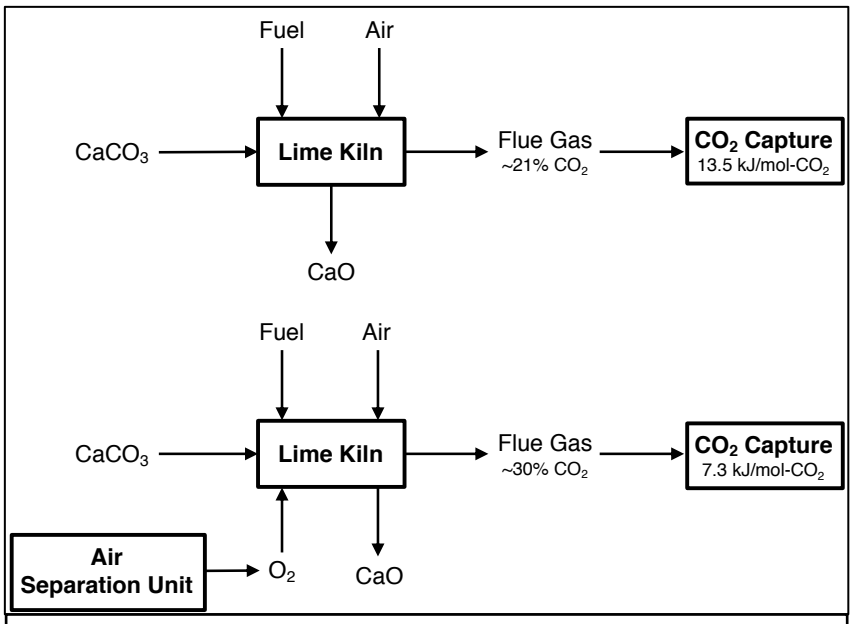

Figure 4.18 Process flow diagrams demonstrating the potential for process innovation to reduce costs of CO_2 capture at existing Kraft pulping mills that utilize oxygen delignification through partial oxy-fuel combustion of lime kilns.

4.4.2 Integrated Calcium Looping CO_2 Capture

Calcium looping CO_2 capture is an established method of separating CO_2 from a gaseous stream through four chemical reactions, as shown in Figure 4.19B.[4.2,4.39] The company Carbon Engineering is commercializing a technology to remove CO_2 from the air using chemistry similar to that shown in Figure 4.19B, with the main difference being the use of potassium hydroxide in place of sodium hydroxide.[4.14] An advantage to using alkaline chemistry for CO_2 capture is the ability for solvent regeneration; as shown in Figure 4.19, all chemicals are regenerated. Interestingly, Carbon Engineering's inspiration for capturing CO_2 using alkaline chemistry came from studying the Kraft pulping process, in which sodium and calcium hydroxides are used in a closed system for biomass pulping, as shown in Figure 4.19A.[4.40] Carbon Engineering chose potassium hydroxide over sodium hydroxide because the former

A

C = carbon in biomass

1. $2NaOH + C \rightarrow Na_2CO_3 + H_2O$
2. $Na_2CO_3 + Ca(OH)_2 \rightarrow 2NaOH + CaCO_3$
3. $CaCO_3 \rightarrow CaO + CO_2$
4. $CaO + H_2O \rightarrow Ca(OH)_2$

B

C = flue gas

1. $2NaOH + CO_2 \rightarrow Na_2CO_3 + H_2O$
2. $Na_2CO_3 + Ca(OH)_2 \rightarrow 2NaOH + CaCO_3$
3. $CaCO_3 \rightarrow CaO + CO_2$
4. $CaO + H_2O \rightarrow Ca(OH)_2$

Figure 4.19 Chemical reactions involved in A) Kraft pulping of biomass and B) calcium looping CO_2 capture.

is better at reacting with dilute concentrations of CO_2 in the air. Kraft chemistry for biomass pulping is very similar to that used for calcium looping CO_2 capture, as shown in Figure 4.19, except the substrate is biomass, instead of carbon dioxide. Figure 4.20A shows a simplified process flow diagram of Kraft pulping, and Figure 4.20B shows an altered process flow diagram wherein biomass is replaced with flue gas. Thus, Kraft pulping mills have the potential for calcium looping CO_2 capture through process intensification. The theoretical CO_2 absorption capacity of NaOH is higher than that of monoethanolamine (MEA), with 0.9 tonnes of NaOH and 1.39 tonnes of MEA required to capture 1 tonne of CO_2.[4.39] Many of the critical components necessary for large scale calcium looping CO_2 capture currently exist at Kraft pulping mills: alkali reactors, liquid/solid separators, alkali regenerators, lime kilns, and causticizing plants.

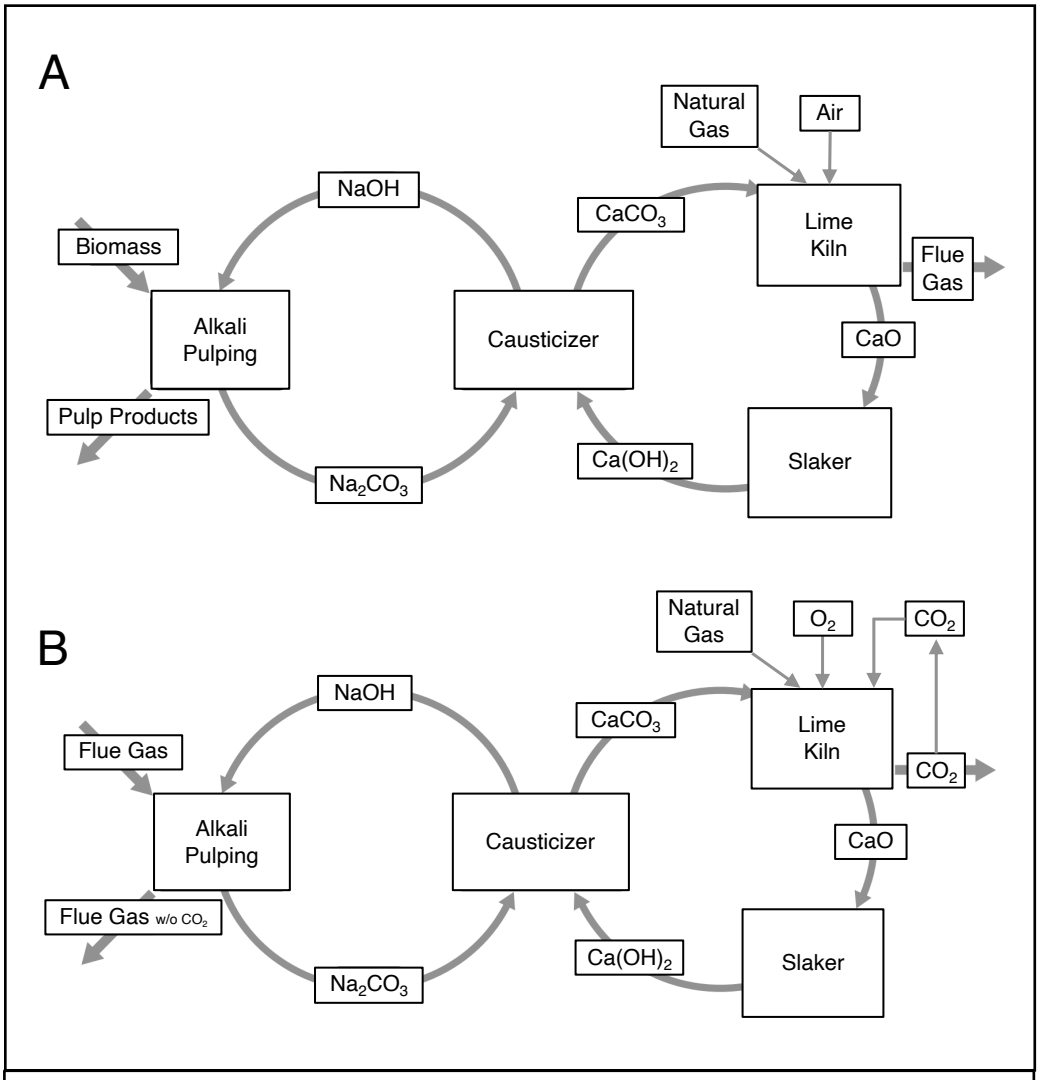

Figure 4.20 A) Generalized process flow diagram of the Kraft pulping process highlighting the alkaline chemistry used for biomass pulping. B) Generalized process flow diagram of the Kraft pulping process being utilized for calcium looping CO_2 capture.

Residual alkali (NaOH) that does not react with biomass during pulping in alkali reactors is available for reaction with CO_2 to form additional sodium carbonate. Flue gas from various on-site sources, such as recovery boilers and multi-fuel boilers, could be passed through pulping liquor to capture a percentage of the CO_2. The biomass- and CO_2-derived sodium carbonate would then move through the existing process with little to no modifications required. The operations in which alkali CO_2 capture could occur include the pulping digestor, recovery boiler,

or a new operation dedicated to CO_2 capture. The new operation could involve a mineralization reactor in which flue gas reacts with sodium hydroxide to form sodium carbonate, which could then combine with existing sodium carbonate prior to entering the causticizer. The CO_2-derived sodium carbonate transfers CO_2 to calcium carbonate which is then calcined to liberate CO_2. Figure 4.20B incorporates complete oxy-fuel combustion in the lime kiln to provide a pure stream of CO_2 post-calcination (and post-condensation of water vapor). Research shows the conversion of a lime kiln from air- to oxy-fuel increases kiln capacity, which would be necessary if additional $CaCO_3$ is being processed due to the incorporation of CO_2 capture in the upstream pulping process.[4.8] Therefore, the aforementioned synergies with Kraft pulping and calcium looping CO_2 capture create an opportunity for pulp and paper mills to cost-effectively integrate CO_2 capture at scale with minimal capital expenditure.

4.5 CO_2 Utilization

The Section 45Q tax credit provides the potential for pulp and paper mills to improve cash flow through on-site CO_2 utilization.[4.16] To be eligible for the utilization tax credits, taxpayers must prove through life cycle assessment that the CO_2 is captured and permanently isolated from the atmosphere or displaced from being emitted into the atmosphere. Two potential pathways for CO_2 utilization in pulp and paper manufacturing are lignin precipitation and calcium carbonate filling.

4.5.1 Lignin Precipitation

Lignin precipitation involves a process similar to that described in the previous section on calcium looping CO_2 capture wherein flue gas is bubbled through black liquor to lower the pH and precipitate lignin.[4.15,4.41] To achieve a high purity lignin product, sulfuric acid is used to remove inorganics. Valmet has patented a technology, Lignoboost, that achieves a high rate of

lignin precipitation through the use of CO_2 for pH adjustment. Domtar is using the lignoboost process at their pulping mill located in Plymouth, NC.[4.18] Typically, high purity CO_2 is purchased for lignin precipitation, and thus CO_2 captured onsite could substitute purchased CO_2 and thereby potentially qualify for the 45Q utilization tax credit.

4.5.2 Calcium Carbonate Filling

Pulp and paper mills that use calcium carbonate fillers typically employ a pathway similar to the one shown in Figure 4.21, wherein mined calcium carbonate is calcined to produce lime (CaO).[4.42] Lime (CaO), which is much lighter than calcium carbonate, is transported to a satellite site nearby to a pulp and paper mill where various grades of calcium carbonate filler are made using purchased CO_2. The calcium carbonate filler may be eligible for the 45Q utilization tax credit if CO_2 from a nearby pulp and paper mill is used instead of the purchased CO_2, because in this way CO_2 is displaced from being emitted into the atmosphere, as shown by the dashed stream in Figure 4.21. Lignin precipitation and calcium carbonate filling both require full life cycle assessments to guarantee eligibility with the Section 45Q utilization tax credit.

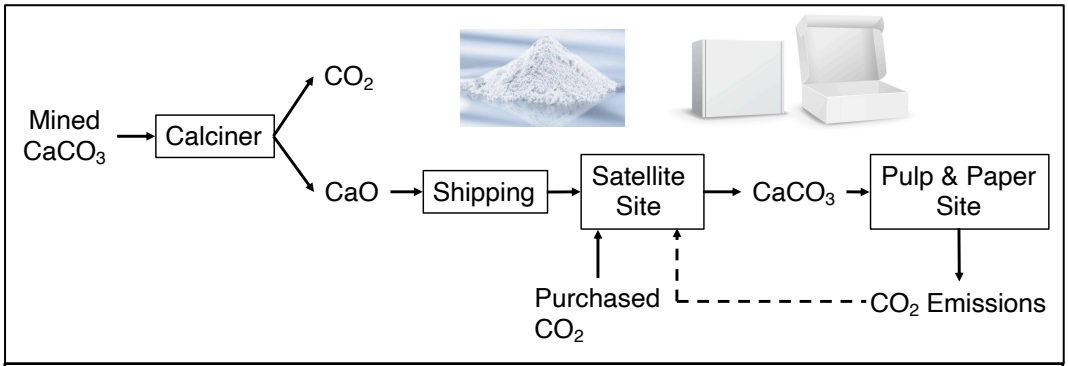

Figure 4.21 Generalized flow diagram showing how calcium carbonate filler is made for pulp and paper products.

4.6 Conclusions

The pulp & paper industry in the United States emits approximately 150 million metric tons of CO_2 per year, of which 77% is biogenically derived. Lime kilns, multi-fuel boilers, and recovery boilers are responsible for approximately 9%, 43%, and 48% of total CO_2 emissions. Approximately 90% of total CO_2 emissions are derived from the combustion of black liquor (~50%), wastewood (~25%), and natural gas (~15%). Lime kiln emissions are more concentrated in CO_2 than those from multi-fuel boilers and recovery boilers due to fuel- and calcium carbonate-derived CO_2. The top-down, industry-wide analysis indicates CO_2 concentration is the most influential variable when estimating energy demands of CO_2 capture. Fuels with high H/C ratios, such as natural gas, generate low concentrations of CO_2 via combustion, whereas fuels with low H/C ratios, such as coal and biomass, generate relatively high concentrations of CO_2. Therefore, within the scope of the top-down analysis, capturing CO_2 from coal and biomass combustion is generally less expensive than capturing CO_2 from natural gas combustion. Idling capital assets available at pulp and paper mills warrant further investigation into the feasibility of using such for CO_2 capture. 88 of the 205 mills assessed in the top-down, industry-wide analysis are located on geology suitable for sequestration and therefore do not require long-distance transportation of CO_2. The average distance to suitable geology for mills that are not co-located is ~130km. The bottom-up analysis estimates baseline costs of CO_2 capture for the four select mills to range from -$19 to $23 per tonne CO_2 (in year 2026 with $50 per tonne CO_2 tax credit applied). The bottom-up analysis shows operating costs dominating capital costs for CO_2 capture at all four mills. For all four mills in the bottom-up analysis, levelized costs of CO_2 capture are near to zero for the baseline combined emissions scenarios (in year 2026 with $50 per tonne CO_2 tax credit applied). Overall, the bottom-up analysis estimates the capture of CO_2 from combined

emissions to be less expensive than that of CO_2 from lime kiln emissions only, due primarily to differences in economies of scale; this observation contradicts energy demand trends from the top-down analysis. According to the bottom-up analysis, waste heat at Mill 4 enables low cost CO_2 capture, particularly for the small scale scenario: Steam + Lime Kiln Emissions, wherein the levelized cost is -$19 per tonne CO_2. Thus, waste heat, if of sufficient quality and availability, can substantially reduce costs of CO_2 capture. The Combined Emissions scenarios demand substantial quantities of biomass and thereby require investigation into local biomass resource availability. Sensitivity analyses indicate reboiler duty, biomass cost, electricity cost, rate of MEA loss, return on equity, and transportation distance affect levelized costs to varying degrees. Reboiler duty, biomass cost, and transportation distance are the most influential parameters analyzed. Lime Kiln Emissions scenarios are proven to be most sensitive to transportation distance due to their low flow rates of CO_2 and thus high pipeline cost intensities. Retrofitting idling biomass boilers and turbogenerators for CO_2 capture significantly lowers levelized costs, particularly for Steam & Power Emissions scenarios. The use of natural gas-fueled boiler and turbogenerator systems would likely reduce costs of CO_2 capture due to the very low cost of natural gas energy in the US, relative to biomass energy. However, the net removal of CO_2 from the atmosphere would be reduced if natural gas was used in place of biomass fuel. A multivariate regression is generated using data from the bottom-up analysis and data from the literature[4.11] to estimate costs of capturing CO_2 at all 205 mills selected for this study. Cost estimates of CO_2 capture from the top-down, industry-wide analysis range from -$0.6 to $12.7 per tonne CO_2 (in year 2026 with $50 per tonne CO_2 tax credit applied). The top-down economic analysis finds that, overall, capturing lime kiln- and recovery boiler-derived CO_2 is less costly than multi-fuel boiler-derived CO_2. For mills that are not co-located with suitable geology, the average cost of

transporting CO_2 to suitable geology is $24.8 per tonne CO_2 (in the year 2026, not accounting for the 45Q tax credit). The average incremental cost of capturing combined CO_2 emissions, expressed as percent of manufacturing cost, is ~1% for the different product grades assessed. Process intensification and innovation offer an opportunity to reduce the costs of CO_2 capture through 1) partial oxy-fuel combustion of lime kilns with post-combustion CO_2 capture and 2) integrated calcium looping CO_2 capture. Utilizing Kraft chemistry for large scale calcium looping CO_2 capture at existing pulp and paper mills is of particular interest due to the potential for innovation and thus high impact. Pathways for CO_2 utilization, such as lignin precipitation and calcium carbonate filling, hold the potential for cash flow improvement through the Section 45Q utilization tax credit. Detailed lifecycle assessments in compliance with the US Internal Revenue Service are required to validate eligibility for the utilization tax credit.

Chapter 5 – Carbon-Negative Carbon Fibers: Are Lignin-Derived Carbon Fibers Graphitic Enough?

5.1 Introduction

Commercial carbon fibers (CFs) are typically classified based on their tensile modulus, although other properties significantly influence performance. Low modulus carbon fibers (LMCFs) have modulus values typically under 350 GPa, whereas high modulus carbon fibers (HMCFs) have values above 350 GPa.[5.1] HMCFs are of high value due to their ability to reinforce lightweight composites in applications such as aviation and aerospace. Commercial HMCFs are often derived from polyacrylonitrile (PAN) and have excellent properties for high performance, high strength, lightweight materials. However, the PAN precursor is very expensive, accounting for 50% of the final CF product cost.[5.2] The high cost of PAN-derived CFs has encouraged researchers to look for inexpensive substitutes, such as lignins. Researchers have attempted to produce lignin-derived carbon fibers of two general classifications: 1) single component fibers in which lignin is the only precursor and 2) multi-component fibers in which lignin is blended with other polymers. The manufacturing operations involved in the production of LMCFs and HMCFs are basically the same aside from downstream operations in which HMCFs undergo high temperature graphitization (2000 - 3000°C), as shown in Figure 5.1.[5.1] During graphitization, carbon fiber tensile modulus increases while tensile strength usually decreases.[5.3] The high tensile modulus associated with HMCFs, as well as the high structural

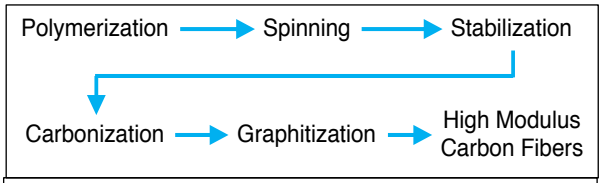

Figure 5.1 Generalized process for the production of high modulus carbon fibers.

rigidity and low coefficient of thermal expansion, are due in large part to the highly oriented, basal-plane-based graphitic crystallites that form along the fiber axes during high temperature treatment.[5.1] During graphitization of commercial HMCFs, disordered sp^3-hybridized polymeric clusters transition to ordered sp^2-hybdridized. This structural transition is clearly evident from X-ray diffraction (XRD) and Raman spectroscopy, as shown in Figures 5.2A & B.[5.4] As the temperature increases, the peak width of the X-ray diffractogram and the I_D/I_G ratio of the Raman spectra decrease, indicating an increase in graphitic crystallite size (L), quantified by Equations 1 & 2[5.5,5.6] and corroborated by Figure 5.2C.[5.7] Graphite has a characteristic (002) peak at $2\theta = 26.7°$ via XRD, and therefore ordered materials containing highly graphitic crystallites will have a large, narrow peak at this angle with a flat baseline; jagged baselines and turbulent curves for carbon materials indicate disorder. Thus, the average graphite crystallite size in high quality, commercially produced HMCFs is relatively large and easily identifiable and quantifiable through XRD and Raman spectroscopy. Moreover, the presence of large graphite crystallites in CFs indicates the proper structural arrangement for high tensile modulus.[5.8] In this review, we present evidence for the lack of graphitic structure in lignin-derived carbon fibers through discussion and presentation of both qualitative and quantitative information obtained from numerous studies focused on carbon fibers and lignin carbonization; the majority of data presented is qualitative from XRD and Raman spectroscopy since graphitic structure can be easily detected and broadly assessed with such methods. Given the lack of robust data in the literature, we do not delve deeply into the effects of varying lignin types and other parameters such as lignin isolation method and carbonization time; we do however discuss the effects of temperature on graphitic structure development. The scope of this review is primarily confined

to single-component lignin CFs to clearly illustrate the inability of lignin to graphitize in the same way as polymers used in commercial CF production.

5.2 Comparison of Lignin and Polyacrylonitrile Precursors

5.2.1 Sp^2/Sp^3 Hybridized Carbon Considerations

Lignin-derived CFs have been promoted as a sustainable, low-cost replacement to PAN-derived CFs. The performance of single component lignin-derived CFs has not come close to that of PAN-derived fibers, whereas CFs made from blends of lignin and other proven polymers, such as PAN, have come closer, but still require much improvement.[5.1] CFs derived from a mixture of lignin and PAN typically exhibit enhanced performance and graphitic structure relative to single component lignin CFs; the enhanced performance is due to the presence of PAN, not lignin.[5.1,5.9,5.10] Regardless of whether pure lignin or a polymer blend is used to produce CFs, most researchers assume some level of structural transformation of lignin from disordered sp^3-hybridized carbon to graphitic sp^2-hybridized carbon. However, this assumption is often made without proper validation through the appropriate analytical techniques, particularly XRD and Raman spectroscopy. Researchers often attribute the relatively poor performance of lignin-derived CFs on issues related to impurities in feedstock, improper fiber diameter and density, prevalence of defects, and non-homogeneity of spun fibers, to name a few.[5.1] An overlooked reason for poor performance is the lack of graphitic sp^2 hybridized structure in the final fiber product, especially for HMCFs. As early as 1951, various carbon precursors were extensively studied to determine the polymers best suited for forming graphite at elevated temperatures.[5.11] It was determined that polymers with heavily cross-linked, 3-dimensional structures are poorly suited for graphitization, whereas polymers with less cross-linking and more linear, 2-dimensional structures are better suited for

graphitization.[5.11] The reactions that take place during the initial thermal stabilization stage of carbon fiber production significantly influence the degree of graphitization during later stages.[5.11] Polyacrylonitrile is a suitable precursor for high modulus carbon fibers due its linear, 2-dimensional polymeric chains that arrange themselves for cross-linking cyclization reactions during the initial thermal stabilization stage, as shown in Figure 5.3[5.8,5.12]; the initial rearrangement and cyclization of PAN forms turbostratic structures suitable for graphitization

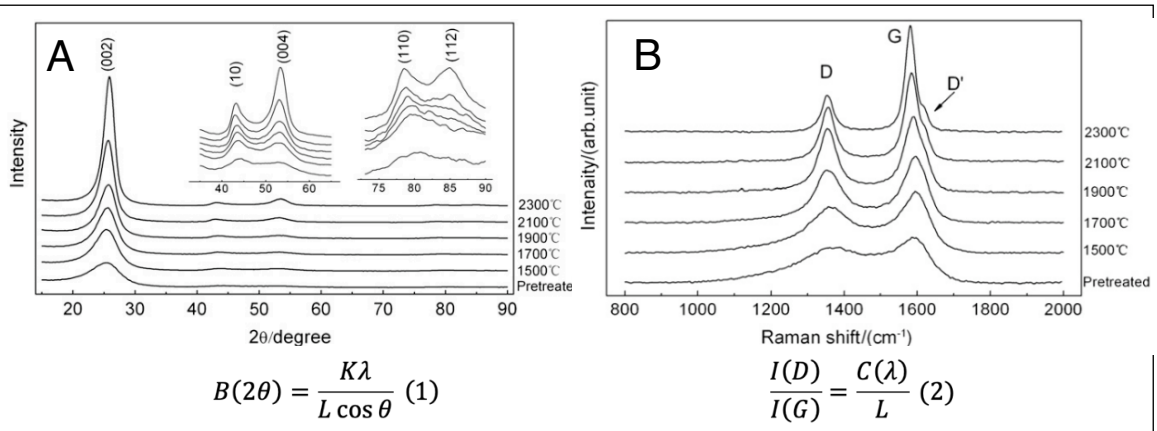

$$B(2\theta) = \frac{K\lambda}{L\cos\theta} \quad (1)$$

$$\frac{I(D)}{I(G)} = \frac{C(\lambda)}{L} \quad (2)$$

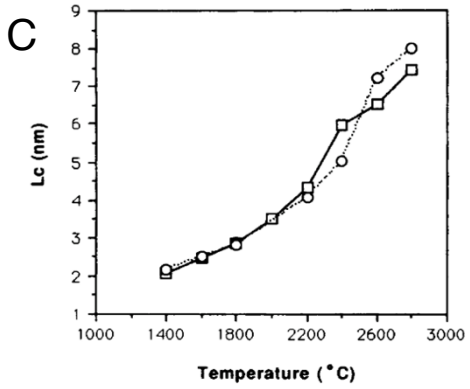

Figure 5.2 A) & B): X-Ray diffractograms & Raman spectra of PAN-derived carbon fibers treated at different temperatures, respectively.[5.4] Reprinted with permission from Elsevier. Equation 1 is the Scherer Equation which shows an inverse relationship between peak width (B) of XRD diffractogram and graphitic crystallite size (L). Equation 2 is the I_D/I_G ratio of Raman spectra intensity which is inversely related to graphitic crystallite size (L)[5.5,5.6]. C): Crystallite size (Lc) of PAN-derived carbon fibers graphitized at varying temperatures. Square: unmodified PAN precursor, Circle: PAN precursor modified with potassium permanganate.[5.7] Reprinted with permission from John Wiley & Sons.

at higher temperatures. It should be noted that high modulus, PAN-derived carbon fibers are not fibers of pure graphite, but rather fibers containing ribbon-like structures of ordered graphitic carbon interlocked with disordered domains of carbon.[5.13]

5.2.2 Chemical Considerations

Natural lignin polymers are synthesized by plants to act as a resin providing strength to cellulose fibers, and therefore lignin is a relatively non-oriented material.[5.14,5.15] Lignins vary in their molecular configuration and reactivity due to differences in plant genetics and isolation methods. Researchers have used a multitude of different isolated lignins to produce CFs, although the mechanical properties of such CFs have generally been poor regardless of the plant species and isolation method used, relative to commercial CFs.[5.16–5.20] Three of the most common methods for isolating lignins include the use of organic solvents (organosolv, Alcell lignin), alkali solvents (kraft lignin), and pyrolysis (pyrolytic lignin).[5.18] Lignin obtained from the kraft process corresponds to ~85% of lignin removed in the pulping industry.[5.21] Among other advantages, high lignin extraction yield and less than 1 - 2% residual sulfur content make kraft lignin an abundant and relatively cheap carbon fiber precursor.[5.22] Extracted from lignocellulosic biomass using organic solvent extraction methods, organosolv lignin more closely resembles native lignin compared to kraft lignin. Compared to kraft lignin, organosolv and pyrolytic lignins require less purification and pretreatment steps prior to fiber spinning.[5.20] Kraft lignin is typically desalted using acid solutions prior to organic solvent purification to enhance thermoelastic properties and allow for effective spinning.[5.18,5.20] The industrial Lignoboost and Lignoforce processes that isolate lignin from kraft liquor via CO_2 precipitation provide a relatively pure lignin that requires fewer pretreatment steps.[5.23–5.25] Hosseinaei et al. compared the mechanical properties of CFs made from woody (hardwood) and non-woody (grass)-derived lignins using an organosolv isolation method.[5.16] The grass-derived lignins volatized thermally labile acid groups during melt-spinning which led to defects in the CFs and ultimately poor strength, compared to the hard wood-derived lignins which were more stable.

Although lignins from various plant species and isolation methods have been used for producing CFs, there is a general lack of consensus regarding which lignin type provides optimal CF properties. The lack of consensus is partly due to the large number of process variables when producing CFs, particularly during purification, pretreatment, spinning, and stabilization. Moreover, there has yet to be a published study in which the graphitic structures of CFs made from various lignin types were analyzed and compared.

Irrespective of the type of lignin, thermal treatment yields condensed structures, although the proportion of linkages varies with lignin type.[5.26–5.28] Thermal treatment of kraft lignin at relatively low temperatures creates phenoxy radical resonance structures that enable a multitude of coupling reactions, two of such are shown in Figure 5.3.[5.28] The β-O-4 linkages present in kraft lignin give rise to two parallel reactions, one forming an enol ether [5.28,5.29] and the other forming phenoxy radicals which result in condensed structures through radical coupling.[5.27,5.28] Molecular rotation is restricted due to formation of carbon-carbon bonds, which maintain molecular position.[5.21] As the temperature increases to ~500°C during lignin carbonization, volatiles including H_2O, CO, CH_4 and CO_2 are liberated and oligomeric tars form on the surface of the carbon fibers.[5.30] Upon further increase in temperature, decomposition of side chains followed by aromatic condensation takes place. At 800 - 1000 °C, solid-state nuclear magnetic resonance and Fourier-transform infrared spectroscopy have been used to show some aromatic rings begin to rupture.[5.26,5.30] Zhang et al. proposed that these structures may further decompose and rearrange into non-graphitic, disordered domains during carbon fiber production.[5.30] However, there is no general consensus on the mechanisms involved in carbonization of lignin.

The regular structure of PAN coupled with the thermally induced elimination chemistry depicted in Figure 5.3A provides a consistently homogeneous chemical pattern composed of a high

number of sp^2 centers. However, when embarking from lignin, it becomes readily apparent that efforts to create such regular patterns, using the outlined limited mechanistic data, requires a lot more speculation for the creation of even a tenuous and unsubstantiated representation. While 5-5' carbon-carbon bonds may form via the coupling of C5 carbon centered radicals originating from the phenoxy radicals shown in Figure 5.3B, these may account for only but a fraction of the final structure. For lignin to become a regular carbonaceous material composed of a high number of sp^2 centers one needs additional documented detailed thermally induced coupling and elimination chemistry. One potential pathway for lignin graphitization is to induce the aforementioned chemistry via the installation of thermally reactive propargyl centers prior to high temperature thermal treatment as already exemplified by the effort of the Argyropoulos group.[5.31,5.32]

Numerous reactions take place during lignin carbonization, with the lack of uniform repeating units and abundance of irregular side chains promoting the development of disordered char. Therefore, the irregular, complex and variable structure of lignin likely inhibits rearrangement and cross-linking cyclization during carbonization — a necessity for highly graphitic carbon fibers. Nevertheless, many researchers assume lignin graphitizes similarly to PAN during carbon fiber production, even though the polymeric reactivity of PAN and lignin vary significantly during thermal treatment.

5.2.3 Temperature-Strength Relationship Considerations

As shown in Figure 5.4, the tensile modulus values for commercial PAN-derived CFs increase with temperature, as one would expect due to the development of graphitic crystallites along the fiber axes.[5.33,5.34] Researchers developing lignin-derived CFs use performance metrics of commercial CFs as

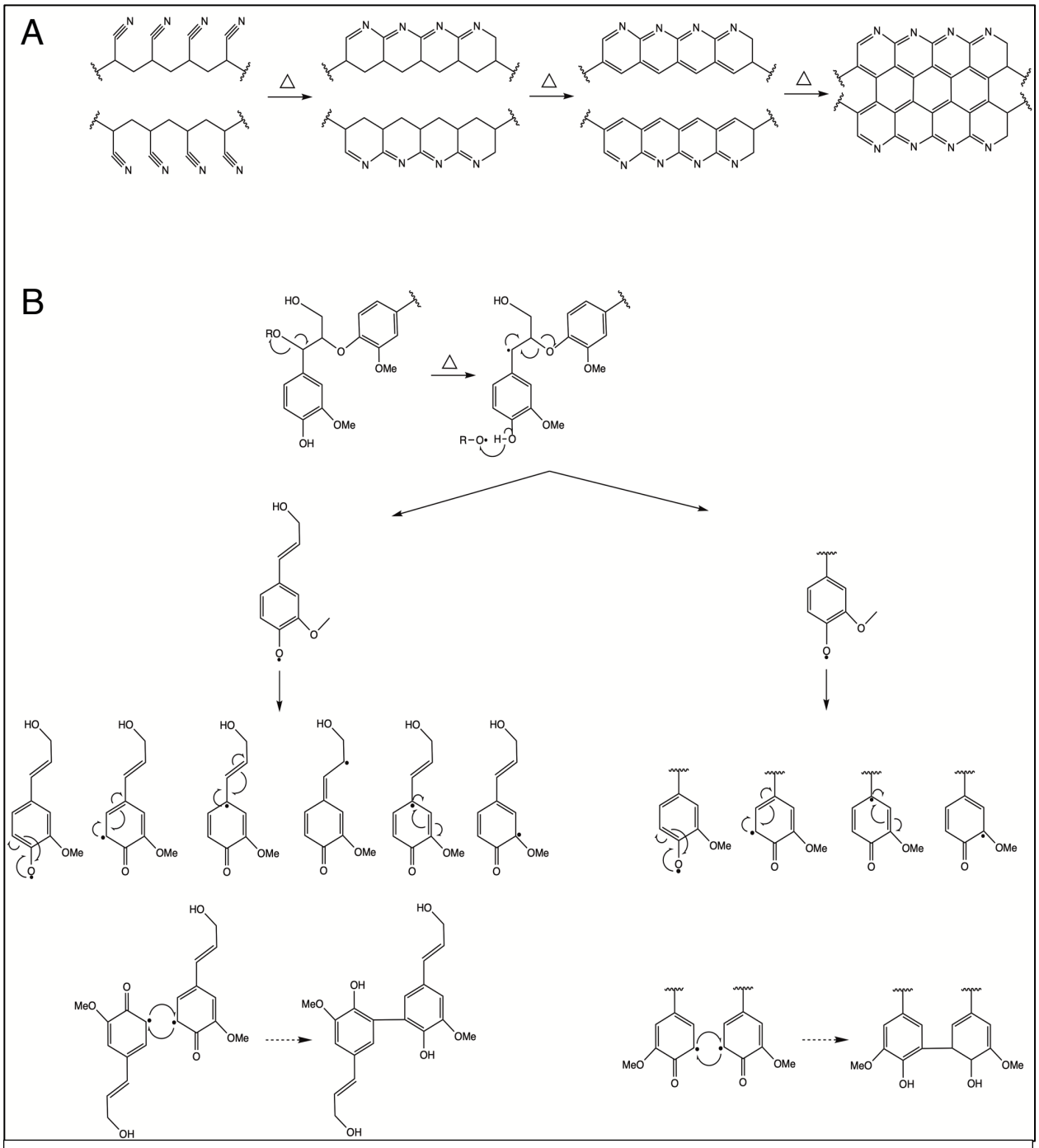

Figure 5.3 A) Cross-linking cyclization of PAN to form a 2-dimensional carbon lattice of graphitic structure.[5.8,5.12] B) Cleavage of the β-O-4 linkage with free radical resonance enabling a multitude of pathways for radical coupling. Two examples of radical coupling to produce 5-5' carbon-carbon bonds are provided.[5.28]

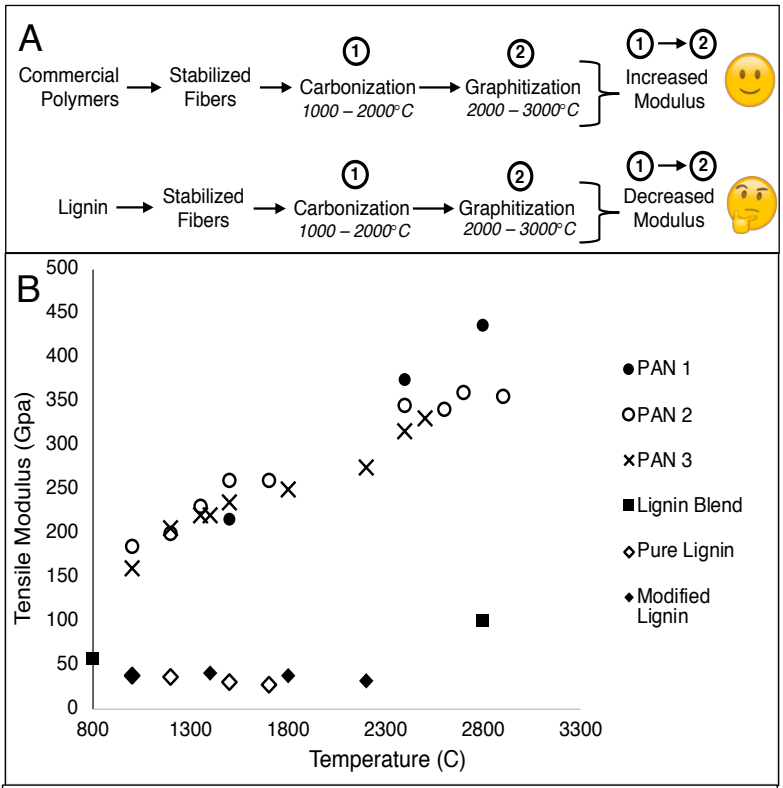

Figure 5.4 A) Schematic conveying an overlooked discrepancy in the temperature-modulus relationship among lignin-derived and commercial carbon fibers. B) A plot showing the change in tensile modulus with respect to temperature for six carbon fibers. PAN 1, 2, & 3: Polyacrylonitrile carbon fibers treated at 1000 – 2900°C[5.33,5.34], Lignin Blend: Carbon fibers derived from pyrolysis fuel oil blended with hardwood kraft lignin treated at 800 and 2800°C[5.36], Pure Lignin: Carbon fibers derived from softwood kraft lignin treated at 1000 – 1700°C [5.35], Modified Lignin: Carbon fibers derived from acylated softwood lignin treated at 1000 – 2200°C.[5.37]

benchmarks for further research and development. Given that the tensile modulus values of commercial CFs increase during high temperature treatment, one would expect the same from lignin-derived CFs; even if lignin-derived CFs have low starting modulus values relative to PAN, their modulus values should still increase at higher temperatures. Interestingly, data from the literature indicate that the tensile modulus values of lignin-derived CFs either minimally increase, stay the same, or decrease with increasing temperature, as shown in Figure 5.4.[5.35–5.37]

Unfortunately, the aforementioned statements regarding the lack of graphitic structure in lignin-derived CFs cannot be confidently validated due to a lack of published data showing evidence of such. However, there is an emerging field of research targeting the development of new methods to convert lignin and other bioresources into graphite for electrochemical applications, such as anodes for Li-ion batteries.[5.35,5.38–5.45] The lignin graphitization procedures used in these studies are similar to those used in carbon fiber studies, with the major exception being that strength properties are not optimized since electrode applications do not require such. Instead, lignin graphitization studies optimize for graphitic structure formation, and usually small graphitic particles are produced, not fibers. Nevertheless, significant insight can be gained from comparing graphite quality reported in lignin graphitization studies to the sought after graphite quality of commercial CFs.

5.3 Graphitization of Pure Lignin

Highly graphitic structure has been claimed to be present in organosolv lignin-derived CFs treated up to 2700°C, as shown by the XRD diffractograms, graphitic crystallite sizes, and decreasing interlayer spacings in Figure 5.5.[5.18,5.46] However, these studies found no increase in tensile modulus or other strength properties with increased treatment temperature, agreeing with the data provided in Figure 5.4. This discrepancy means that lignin-derived CFs likely graphitize much differently than PAN-derived CFs, which is corroborated with XRD diffractograms of lignin- and PAN-derived CFs treated at 1800°C; at 1800°C, PAN-derived fibers are quite graphitic (Fig. 2A), while lignin-derived CFs are quite disordered (Fig. 5A). As shown in Figure 5.5, the lignin-derived CFs do not show strong evidence of graphitic structure until 2700°C; a jagged baseline, broad peak, and low intensity indicate disorder. The T300 PAN-derived CF used for comparison is Toray's commercialized baseline CF with a relatively

low tensile modulus, and therefore it's not an ideal CF for comparison with the lignin-derived CFs treated at high temperatures [5.47]; the T300 PAN-derived CF is likely not produced at a high temperature, and therefore highly graphitic structure is not expected. As shown in Figure 5.2, the degree of graphitization for PAN-derived carbon fibers is significantly dependent upon treatment temperature, and therefore the use of T300 for comparison is probably not valid. It would be helpful if high modulus PAN-derived CFs, such Toray's M40J, were used to compare graphitic structure with lignin-derived CFs treated at high temperatures. Nowlak et al. (2018) recently published results on kraft lignin-derived carbon fibers for use in lithium-ion battery electrodes.[5.35] As shown in Figure 5.6, the degree of graphitization is quite poor up to 1700°C. The T1000 PAN-derived CF used for comparison is Toray's intermediate modulus CF, and therefore not an ideal CF for comparison with the lignin-derived CFs treated at high temperatures.[5.47] Tenhaeff et al. (2014) prepared organosolv lignin-derived carbon fibers for application in Li-ion battery anodes.[5.48] The CFs were carbonized at 1000, 1500, and 2000°C. As shown in Figure 5.7A, graphitic structure increased with temperature, however, the jagged baseline, low intensity, and wide peak indicate the degree of graphitization was less than that found in commercial, high modulus CFs. As shown in Figure 5.7B, the I_d/I_g ratio of the Raman spectra for the CFs treated at 2000°C appears to show stronger evidence of graphitic structure than its corresponding X-ray diffractogram. The reason for disagreement among XRD and Raman results might stem from the difference in detection mechanisms: XRD typically takes a bulk measurement of crystalline structure, whereas Raman measurements can vary from a single point to mapping of many points. A single point measurement via Raman that detects graphitic structure does not mean the entire material is graphitic, hence why large mapping should be done to avoid misleading results. Researchers should provide as much information

as possible with regards to the method used for Raman spectroscopy. Garcia-Negron et al. (2017) (Fig. 8) prepared carbon materials from kraft lignin for use in energy storage applications.[5.42] The kraft lignin underwent an initial carbonization at 1000°C under nitrogen

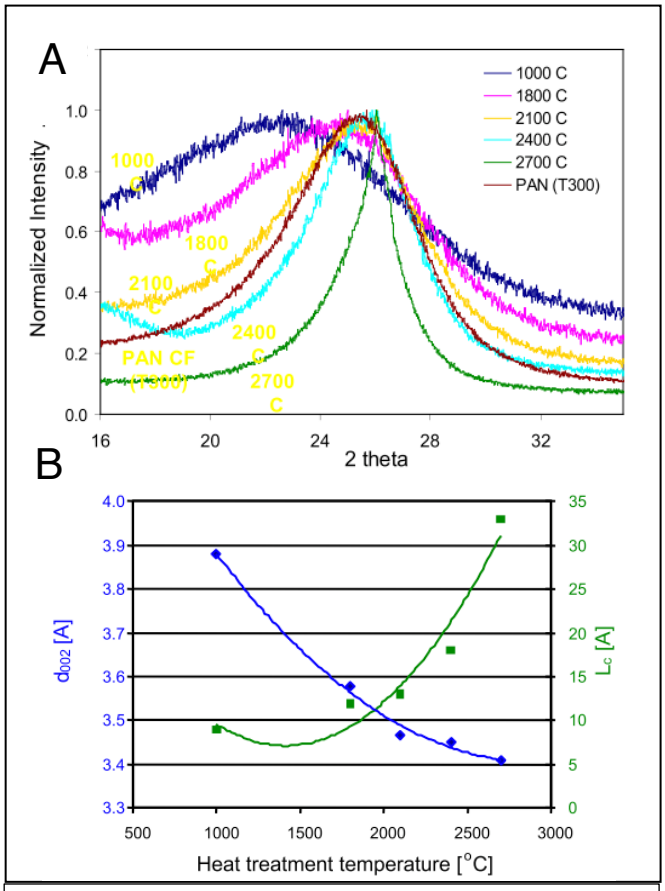

Figure 5.5 A) X-ray diffractograms of organosolv lignin-derived CFs treated at different temperatures. T300 represents Toray's commercial, baseline CF with a relatively low tensile modulus. B) Interlayer spacing and crystallite size of organosolv lignin-derived CFs as determined by the XRD results.[5.18,5.46] Plots are from a publicly available presentation given by the US Dept. of Energy.[5.46]

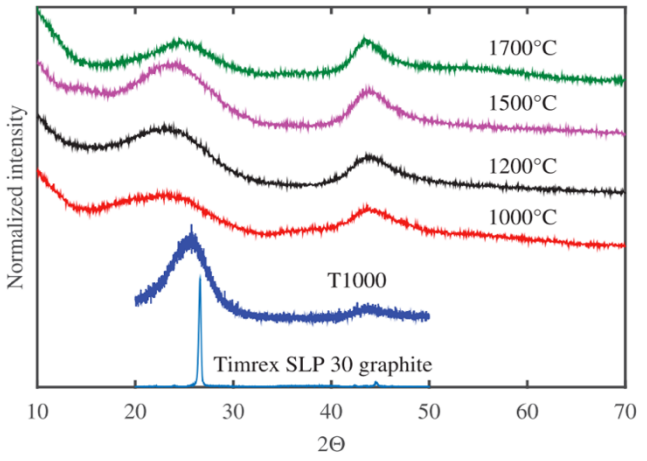

Figure 5.6 XRD diffractograms for kraft lignin-derived carbon fibers carbonized at varying temperatures. Timrex SLP 30 is a commercial graphite and T1000 is a commercial, intermediate modulus PAN-derived carbon fiber.[5.35] Reprinted with permission from Walter De Gruyter & Company.

gas, followed by ball milling to reduce particle size to nanometer range, and then finally a thermal reduction treatment in which the carbonized powder was heated to 1050 and 2000°C under hydrogen gas. As shown in Figure 5.8, the graphitic structure resultant from high temperature treatment was minimal. Köhnke et al. (2018) successfully graphitized kraft lignin at 2000°C, as shown in Figure 5.9.[5.38] Interestingly, sulfite lignin graphitized to a much lesser extent than kraft lignin, underlining the importance of starting polymer structure and composition. Notably, Köhnke et al. used fine lignin powders resultant from spray-drying, with spherical diameters on the order of 1 – 6 microns. Multiple studies that successfully graphitized lignin used intensive milling or other techniques to reduce particle size to the micron level prior to thermal treatment, indicating that initial particle size may play a major role in the degree of graphitization.[5.38,5.40,5.49] Yoon et al. (2018) carbonized acid hydrolysis lignin at 900 and 1300°C for use as anode material in a Na-ion battery.[5.43] As shown in Figure 5.10, the characteristic (002) peak of graphite (2θ = 26.7°) is not detectable. The broad 002 peak indicates the existence of small graphitic domains

present among the predominantly disordered carbon, but the total degree of graphitization is minimal. For comparison, X-ray diffractograms of PAN fibers carbonized at similar temperatures (1000 - 1500°C) do show evidence of graphitic structure (Figure 5.2A).

Ding et al. (2018) successfully isolated graphene quantum dots (GQDs) using alkali lignin as the feedstock.[5.50] The experimental procedure involved the partial depolymerization of alkali lignin via nitric acid treatment, followed with hydrothermal carbonization of the solids, and finally long-duration (1-week) dialysis of the solution resultant from hydrothermal carbonization to isolate water soluble GQDs. The authors were able to show graphitic structure in the quantum dots through the use of XRD, Raman spectroscopy, and ^{13}C cross-polarization magic angle spinning nuclear magnetic resonance (^{13}C CP MAS NMR). As shown in Figure 5.11, the peak at 130 ppm indicates an abundance of fused SP^2 carbons which is characteristic of graphitic materials. Solid state NMR, such as ^{13}C CP MAS NMR, provides more structural granularity than XRD and Raman spectroscopy for complex solid materials like carbonized biomass, and therefore this technique should be used by researchers focused on lignin-derived carbon fibers. Researchers should however use caution when analyzing solid state NMR spectra of carbonized materials due to the likelihood of misinterpretation from anisotropic shielding and overlapping lineshapes. Ding et al.'s work suggests the use of hydrothermal carbonization might be an avenue towards higher quality carbon fibers via the enhanced development of graphitic structure. Chu et al. (2013) used ^{13}C NMR to analyze amorphous char materials generated from pyrolysis of a lignin model compound and proposed a mechanism that involves random repolymerization of radical species, thus corroborating points made in our aforementioned discussion on the disordered rearrangement of lignin during high temperature treatment (Figure 5.3B).[5.51]

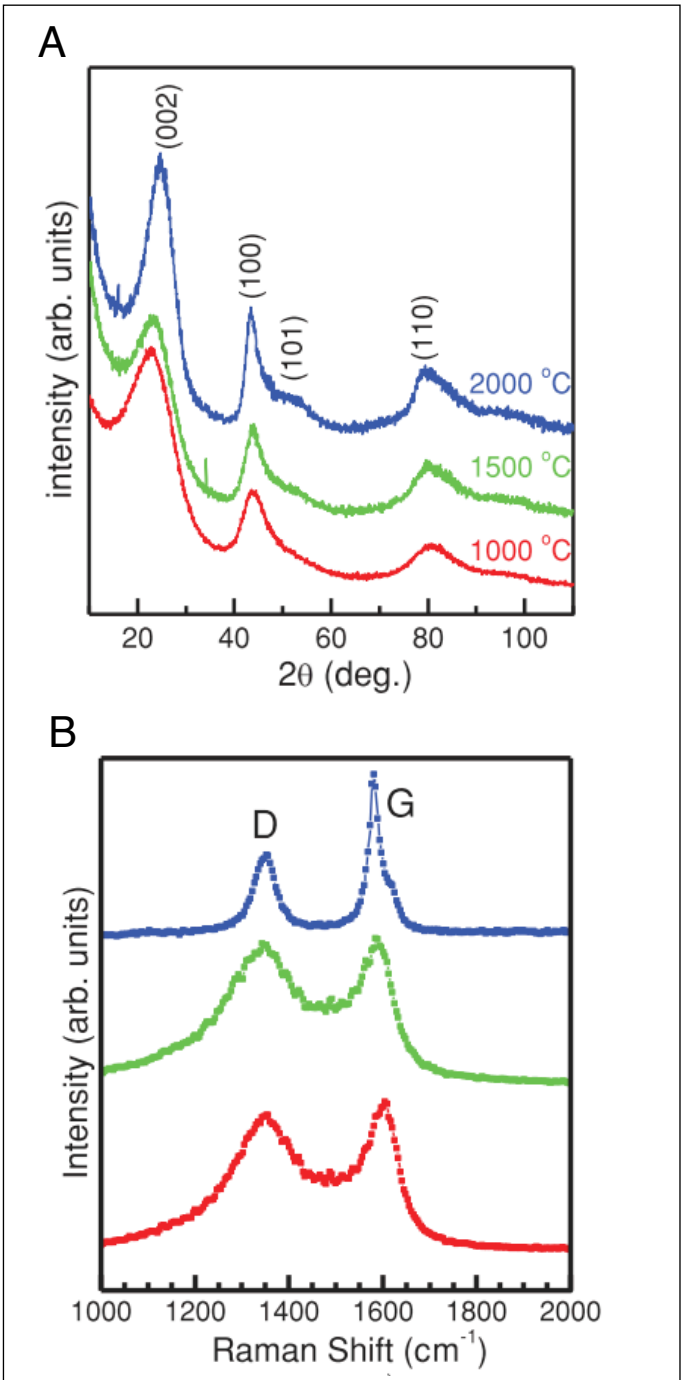

Figure 5.7 A) XRD diffractograms and B) Raman spectra of organosolv-lignin derived carbon fibers carbonized at different temperatures.[5.48] Reprinted with permission from John Wiley & Sons.

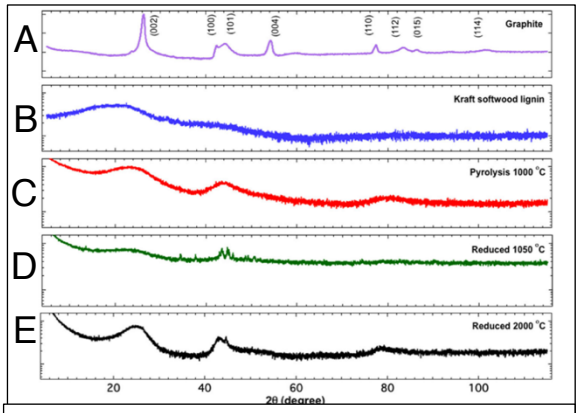

Figure 5.8 XRD diffractograms of A) graphite, B) kraft lignin, and carbon fibers treated at C) 1000°C, D) 1050°C, E) 2000°C.[5.42] Reprinted with permission from John Wiley & Sons.

Overall, the literature shows graphitization of single component lignin carbon fibers and raw lignin samples via thermal treatment alone is difficult to achieve. Evidence of graphitic structure is generally weak for various lignin types treated at temperatures ranging from 1000 – 2000°C. There appears to be an improvement in graphitization when lignin particle size is significantly reduced prior to thermal treatment. The lack of clear evidence for graphitic structure in lignin-derived carbon fibers indicates the carbonization chemistry of such fibers differs quite significantly when compared to PAN-derived carbon fibers.

5.4 Graphitization of Fractionated Lignin

Jin et al. (2018) isolated and fractionated softwood kraft lignin from black liquor using the ALPHA process, which uses liquid-liquid equilibrium present in an acetic acid-water solution.[5.52] This method allows for separating lignin by molecular weight through adjusting the ratio of acetic acid to water. The researchers used this feature to produce lignin-derived CFs from three samples with different molecular weights, and they found that tensile strength and modulus increase as molecular weight increases. The improved carbon fiber performance is most likely due in part by the increased level of graphitic structure present in the higher molecular weight lignin-derived

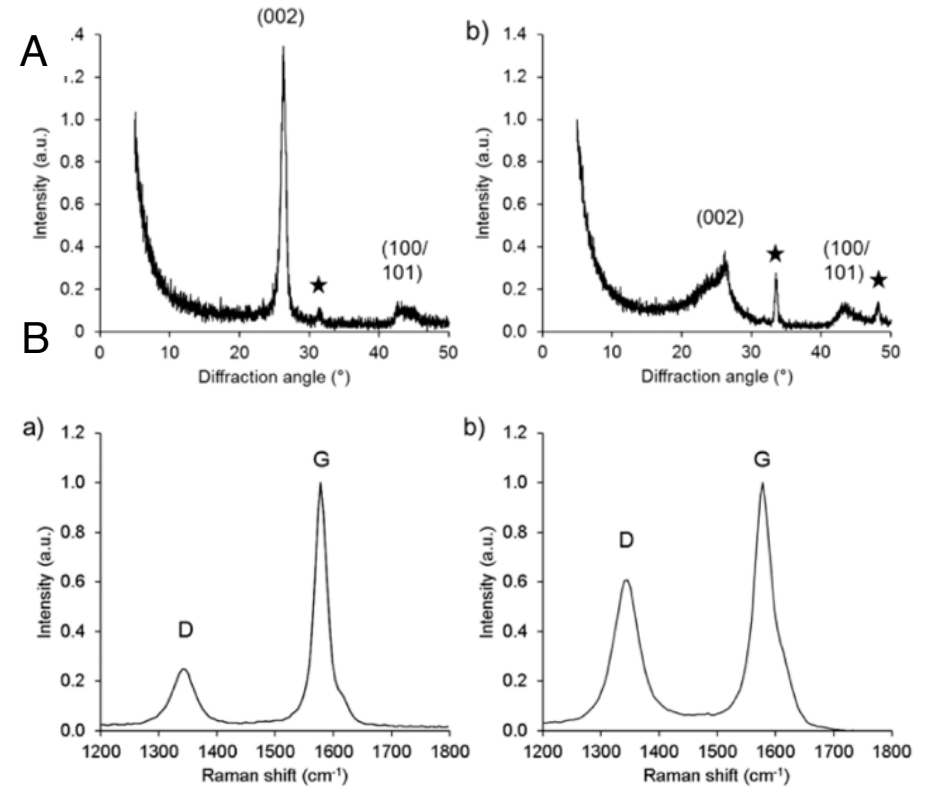

Figure 5.9 A) X-ray diffractograms and B) Raman spectra of fine (1 – 6um) kraft lignin particles (left) and sulfite lignin particles (right) graphitized at 2000°C.[5.38] Reprinted with permission from the American Chemical Society.

carbon fibers, as shown in Figure 5.12; a decrease in Id/Ig ratio corresponds to an increase in graphite crystallite size. Liu et al. (2018) extracted and fractionated lignin from corn stalk using differences in pH, and the resultant fractions were used as precursors mixed with PAN (1:1 ratio) prior to carbonization.[5.55] High molecular weight lignin (M_w: 8170 g/mol) produced carbon fibers with an elastic modulus of 4.5 ± 0.1 GPa, compared to those produced from low molecular weight lignin (M_w: 4467 g/mol) which had an elastic modulus of 2.6 ± 0.4.[5.55] Also, Li et al. (2017) developed a method of lignin fractionation using an enzyme treatment and further dialysis to study the effect of molecular weight and polydispersity on the properties of lignin-PAN carbon fibers.[5.56,5.57] The elastic modulus values for all lignin-derived CFs increased with molecular

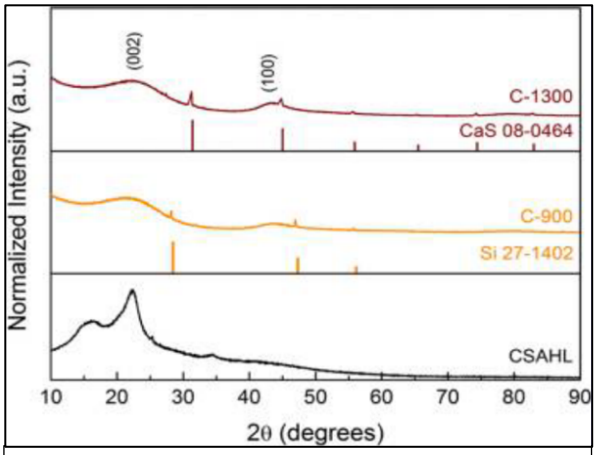

Figure 5.10 X-ray diffractograms showing normalized intensity for acid hydrolysis lignin (CSAHL), CSAHL carbonized at 900°C (C-900), and CSAHL carbonized at 1300°C (C-1300).[5.43]

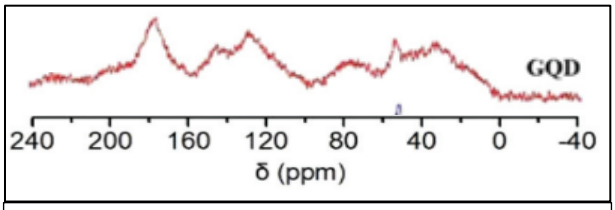

Figure 5.11 ^{13}C cross-polarization magic angle spinning NMR of lignin-derived graphene quantum dots[5.50] Reprinted with permission from the Royal Society of Chemistry.

weight. High molecular weight and low polydispersity enhances polymer uniformity and limits the formation of fiber defects during stabilization and carbonization.[5.52–5.54] Although higher molecular weight lignins were shown to enhance graphitic structure and improve performance, the mechanical properties were still inferior to those of PAN-derived CFs and thus the generalized observation of lignins' inability to graphitize persists. Treatment of fractioned lignins at higher temperatures might show a further increase in graphitic structure and thereby an increase in tensile moduli. Ideally, research into lignin-derived carbon fibers will continue to progress such that graphitic structure development can be achieved at relatively moderate temperatures (< 1500°C).

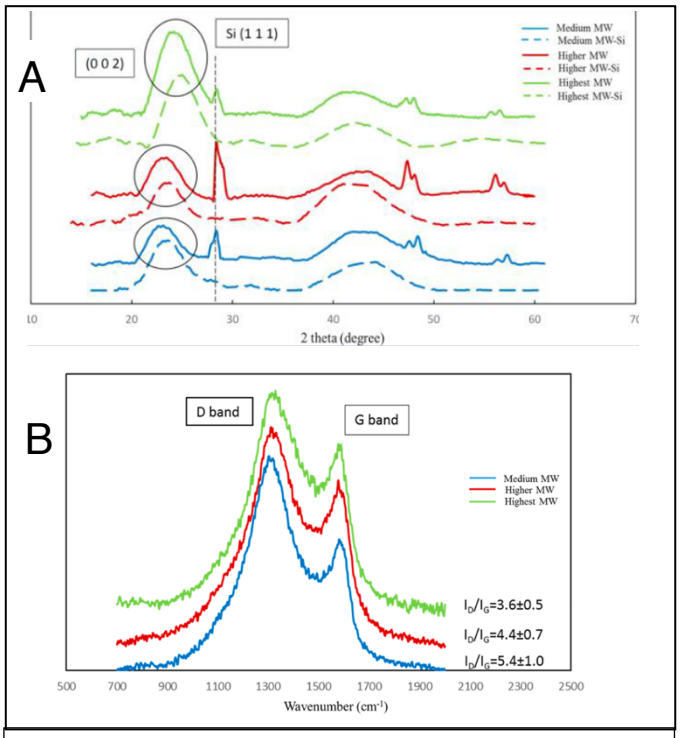

Figure 5.12 A) X-ray diffractograms and B) Raman spectra of carbon fibers derived from lignins of varying molecular weight.[5.52] Molecular weight scale: Green – highest, red – intermediate, blue – lowest. Reprinted with permission from the American Chemical Society.

5.5 Catalytic Graphitization of Lignin

Most studies that attempt graphitization of lignin use furnaces with temperature limits around 1500°C, and therefore transition metal catalysts are often used to obtain an improved graphitic structure. For example, Kubo et al. successfully graphitized acid hydrolysis lignin through the use of a nickel catalyst, as shown in Figure 5.13.[5.44] The mechanism by which transition metals catalyze the conversion of disordered lignin to graphitic carbon is still under investigation, but there are two emerging theories: 1) dissolution of carbon into nanosized catalyst particles followed by graphitic layering and 2) near-eutectic liquid droplets of metal carbide formation and then decomposition upon high temperature treatment resulting in graphite.[5.58] As shown in Figure 5.13, the degree of graphitization increases with catalyst loading. Neeli et al. (2018) conducted an interesting set of experiments in which they used iron

to catalytically graphitize different fractions of lignocellulose, namely cellulose, hemicellulose, and lignin.[5.59] As shown in Figure 5.14, essentially no graphitic structure was detected in lignin, whereas a moderate degree of graphitic structure was detected in hemicellulose and cellulose. The ability of cellulose to graphitize is not surprising since Rayon, a cellulose derivative, is a proven precursor for the production of carbon fibers.[5.1] However, the inability of lignin to graphitize is surprising given the extensive research done on lignin-derived CFs. Yan et.al (2018) investigated the effect

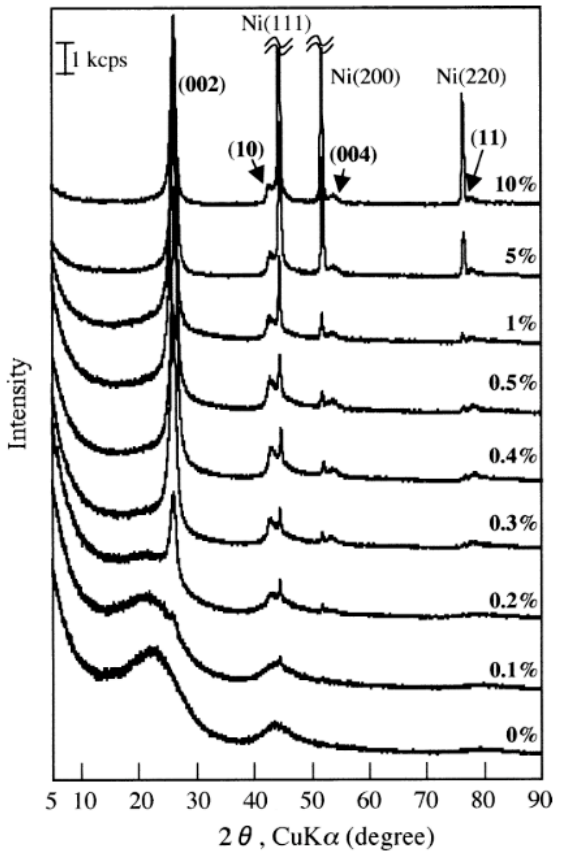

Figure 5.13 X-ray diffractograms of acid hydrolysis lignin carbonized at 1000°C with varying nickel catalyst loadings.[5.44] Reprinted with permission from Springer Japan.

different gases have on the formation of graphitic structure during catalytic graphitization of kraft lignin at 1000°C.[5.60] Methane and natural gas in the ambient gas phase were found to improve graphitic structure development, and hydrogen and carbon dioxide were found to have an etching effect on solid carbon species. The improved graphitic structure from natural gas and methane might be due to vapor deposition on the metal catalysts and subsequent graphitization. As shown in Figure 5.15, the X-ray diffractograms for kraft lignin carbonized under inert gases show poor graphitic structure development. Banek et al. (2018) recently developed an innovative method to catalytically graphitize multiple biomass resources, including whole biomass, cellulose, and lignin.[5.40] Their method involves vigorously ball milling a mixture of iron and lignin prior to a 2-step graphitization procedure: step 1 involves carbonization under nitrogen at 600°C for 30-minutes and step 2 involves laser irradiation to induce graphitization. As shown in Figure 5.16, Banek et al. achieved highly graphitic structure for all of the biomass resources tested; interestingly, wood flour and cellulose resulted in better graphitic structure than lignin. Similar to Köhnke et al.'s work[5.38], Banek et al. started with lignin of very small particle size. Garcia-Negron et al. also used small particles for high temperature graphitization[5.42], but obtained less graphitic materials than Köhnke and Banek. One possible reason for the discrepancy in results among the papers is that Köhnke and Banek reduced the particle size of raw lignin prior to any thermal treatment, whereas Garcia-Negron reduced particle size after an initial carbonization at 1000°C. Therefore, the use of small (1 - 50um) untreated lignin particles seems advantageous for subsequent graphitic structure development and warrants serious attention.

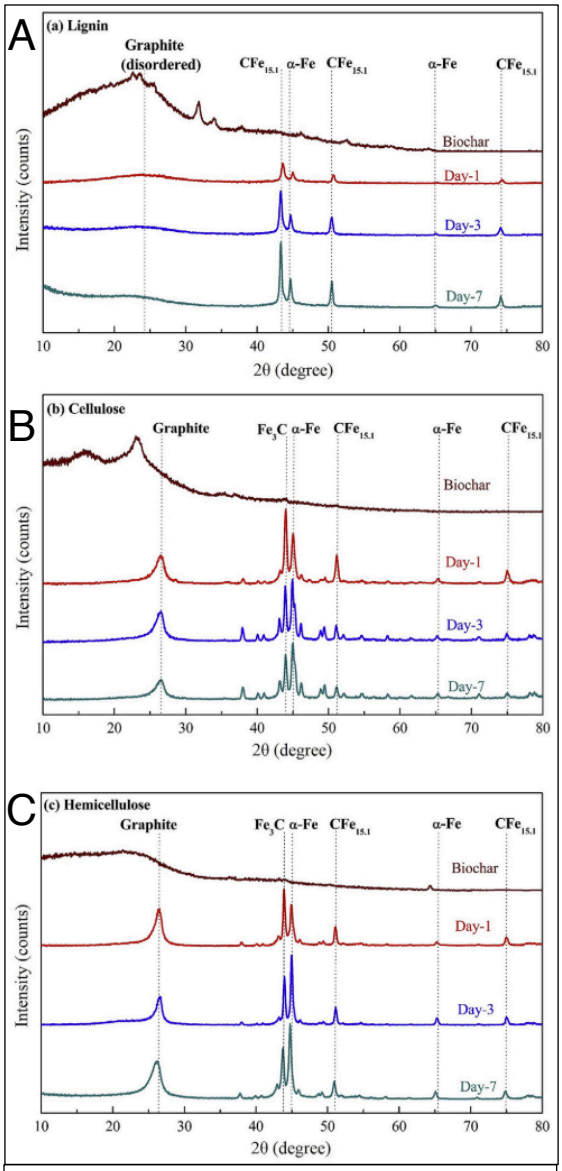

Figure 5.14 XRD diffractograms of iron catalyzed biomass fractions carbonized at 1000°C A) lignin, B) cellulose, and C) hemicellulose. Top diffractograms represent hydrochar samples prior to iron catalyzed pyrolysis. Day-1, 3, 7 refer to the number of days the iron impregnated hydrochar samples were left to dry in a 110°C oven prior to pyrolysis.[5.59] Reprinted with permission from Elsevier.

Several researchers have catalytically graphitized carbon nanotubes on the surface of PAN-derived CFs via chemical vapor deposition (CVD) to improve performance properties such as thermal stability and electrical conductivity, however, there has been little investigation into using such a technique on lignin-derived CFs.[5.61–5.64] Xu et al. (2014) decorated the surface of CFs derived from a mixture of lignin and PAN with carbon nanotubes to enhance thermal stability.[5.61] The carbon nanotubes were synthesized on the surface of the fibers via CVD using iron and palladium nanoparticles, and electron energy loss spectroscopy (EELS) was used to identify both amorphous and graphitic regions. Like solid state NMR, EELS is a powerful analytical tool that should be used more often by researchers focused on developing lignin-derived carbon fibers. Li et al. (2014) and Tan et al. (2012) also used EELS to quantify the sp^2 content and C-C bond lengths of bio-based graphene quantum dots thereby providing robust support to their hypotheses.[5.65,5.66]

Innovative techniques have been developed to decorate CF surfaces with graphitic carbon nanotubes, but there has been a lack of innovation in incorporating higher levels of graphitic domains within the bulk of fibers. Given that PAN-derived CFs possess graphitic domains within fibers and not only on their surfaces, researchers should use the aforementioned studies on catalytic graphitization to innovate new methods for enhancing graphitic structure throughout the bulk of lignin-derived CFs, but without hindering strength properties. The use of transition metals to catalyze the conversion of lignin to graphite has been primarily used for electrochemical applications, such as electrodes; however, the method might benefit researchers interested in high modulus lignin-derived carbon fibers. Catalysts significantly increase graphitic structure development during lignin carbonization, and therefore an opportunity exists to increase carbon fiber strength if utilized in an innovative fashion. Given that the catalytic mechanism is still under

investigation, there is uncertainty in how fiber strength properties will be affected by the presence of metals. In addition, the removal of metals post-thermal treatment would likely require strong acid washing of the fibers, which might negatively affect strength properties. Nonetheless, doping lignin with transition metals prior to carbon fiber production is an intriguing avenue for further research.

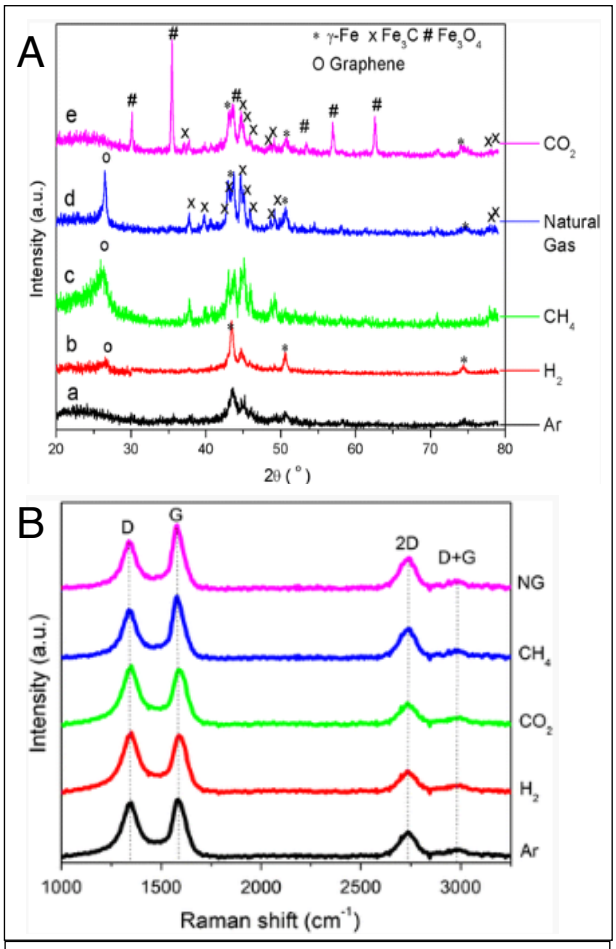

Figure 5.15 A) XRD diffractograms and B) Raman spectra for iron catalyzed kraft lignin at 1000°C under varying gases.[5.60] Reprinted with permission from Springer Nature.

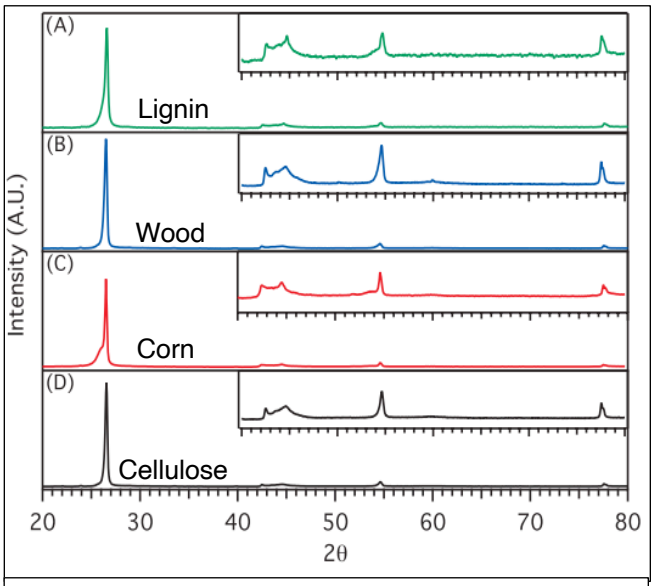

Figure 5.16 XRD diffractograms of A) lignin, B) wood flour, C) corn cob, and D) cellulose catalytically graphitized via a 2-step procedure involving carbonization at 600°C and laser irradiation.[5.40] Reprinted with permission from the American Chemical Society.

5.6 Conclusions

The use of lignin for high modulus carbon fibers may be fundamentally impaired due to the poor ability of lignin to graphitize relative to PAN and other commercial polymers. The amount of robust evidence supporting the claim that lignins graphitize similarly to PAN at high temperatures is minimal and must be expanded through the use of proper analytical techniques such as X-ray diffraction and Raman spectroscopy. Although X-ray diffraction and Raman spectroscopy are capable of evaluating the crystalline domains of graphitic carbon materials, their ability to evaluate molecular configurations present in disordered domains is weak. The complex transformations of lignin during graphitization result in ordered domains inter-mixed with disordered domains, thereby warranting the use of additional techniques that can evaluate particular molecular configurations present in the disordered domains. Solid-state nuclear

magnetic resonance and electron energy loss spectroscopy have been used by other researchers to determine the molecular configurations of disordered domains in activated carbons and related biochar materials, but the techniques have been underutilized on lignin-derived graphitic materials.[5.67,5.68] We recommend relevant research efforts to focus on understanding the development of graphitic (ordered) and amorphous (disordered) domains of carbon fibers via X-ray diffraction, Raman spectroscopy, solid-state nuclear magnetic resonance, and electron energy loss spectroscopy.

The literature shows lignin-derived carbon fiber tensile modulus values do not increase with treatment temperature in the same manner as PAN (Figure 5.4). We propose the poor ability of lignins to graphitize is the primary cause for this discrepancy, and we provide evidence from multiple studies aimed at producing graphite from lignin. Some researchers have successfully demonstrated the graphitization of various lignins through the use of small particle sizes, molecular weight fractions, and transition metal catalysts. Transition metal catalysts appear to provide highly graphitic structure at relatively low temperatures, but the applicability of these catalysts to lignin carbon fiber production may be limited. Nonetheless, the use of metal catalysts for lignin-derived, high modulus carbon fibers warrants attention. In addition, the effects of lignin particle size and molecular weight on graphitization and the resultant carbon fiber strength should be investigated further.

Chapter 6 – Carbon-Negative Batteries: A Simple Method for Producing Bio-Based Anode Materials for Lithium-Ion Batteries

6.1 Introduction

Graphite is a crystalline allotrope of carbon consisting of sp2 bonded carbon atoms densely arranged in parallel-stacked layers.[6.1] The highest demand for graphite currently comes from metals processing, however, growth in the manufacturing of lithium-ion cells for electric vehicles and stationary energy storage is rapidly increasing the demand for battery-grade graphite.[6.2–6.7] The anode of a lithium-ion cell is predominantly made of graphite, constituting 15 - 30% of the total cell mass and 11 - 23% of total cell manufacturing cost.[6.8] Production of battery-grade graphite is expensive ($10 - $20/kg), produces substantial greenhouse gas emissions (7.5 - 9.9 kg CO_2/kWh), utilizes harsh chemicals (e.g. hydrofluoric acid), and is geographically constrained.[6.1,6.6,6.9–6.12] Thus, the energy storage industry would greatly benefit from innovative technologies that convert domestic, low-cost, sustainable, and non-toxic carbonaceous materials, such as biomass, into high quality, low-cost graphite anodes. Most carbonaceous materials treated at high temperatures (> 2000°C) under inert atmospheres and without catalysts will carbonize to form disordered, amorphous carbon materials with cross-linked domains or ordered soft carbon materials with graphitic domains.[6.1] As early as 1951, glucose, cellulose, lignocellulosic biomass, and related biomaterials were proven to be non-graphitizing materials that form disordered, amorphous char when treated at high temperatures.[6.1,6.13,6.14] Although some carbonized biomaterials show evidence of graphitic structure, the crystallites are typically small and heavily diluted in disordered carbon, thus making them not suitable for lithium-ion anode applications.[6.13,6.15,6.16] Notably, multiple published studies have recently demonstrated catalytic conversion of lignocellulosic biomass and

other biomaterials to battery-grade biographite at relatively low temperatures (1000 - 2000°C).[6.17–6.22] The term "biographite" refers to graphite derived from biogenic carbon. Banek et al. (2018) used an iron catalyst to convert multiple lignocellulosic feedstocks to high quality biographite using a high intensity laser and thin carbon substrates.[6.18] The biographite produced was of high quality and performed well in a lithium-ion cell, however, the method of graphitization is difficult to scale due to the necessity of a high intensity laser and thin substrates. Zhao et al. (2018) converted glucose to battery-grade biographite by heating a mixture of glucose-derived biochar and magnesium at 800 - 1000°C for 3 - 20h using a tube furnace.[6.21] The biographite produced was of high quality and performed well in a lithium-ion cell, however, only glucose was assessed. Gomez-Martin (2018) converted medium-density fiberboard (MDF) to battery-grade biographite by impregnating iron chloride into the MDF via soaking in an aqueous solution prior to treatment at 850 - 2000°C in a tube furnace. The biographite produced at 2000°C was of high quality and performed reasonably well in a lithium-ion cell, however, soaking in iron chloride solution and treatment at such a high temperature decrease process viability.[6.19] Biomaterials vary significantly in their composition, and there is a lack of knowledge regarding how various components and building blocks, including glucose, cellulose, and lignin, affect graphitization. Notably, there has yet to be a study published in which a multitude of biomaterials of varying compositions and particle sizes are catalytically graphitized using a simplistic, dry mix, single-step process in a traditional tube furnace at relatively low temperatures (< 1200°C). In this contribution, we demonstrate such a method by using iron to catalytically graphitize a multitude of biomaterials to high quality biographite.

6.2 Experimental

6.2.1 Materials

The commercial synthetic graphite used as the primary reference for characterization is from Asbury Carbons. Several other graphite materials from the literature are used as references for electrochemical performance.[6.1-6.4] The softwood biomaterial is loblolly pine from the southeastern US and two particle sizes are used: 150 – 425um (baseline) and 710 – 1000um. The hardwood biomaterial is a mixture of hardwood obtained from the southeastern US and two particle sizes are used: 150 – 425um (baseline) and 710 – 1000um. The cellulose biomaterial is softwood market pulp from the southeastern US and one particle size is used: < 500um. The glucose and organosolv lignin biomaterials are from Sigma Aldrich and one particle size is used for both: < 500um. The hydrolysis lignin is from NCSU after autohydrolysis and enzymatic digestion of hardwood and one particle size is used: < 500um. The Kraft lignin is a softwood Kraft lignin from a pulp mill in the southeastern US (size < 500um). The iron catalyst is an iron powder of particle size < 10um and is from Sigma Aldrich. The hydrochloric acid is of 37 wt% and is from Fisher Scientific.

6.2.2 Catalytic Graphitization & Acid Washing

The baseline method of graphitization involves mixing dry biomaterial with iron powder catalyst (30 wt%) prior to graphitization in a tube furnace under nitrogen (1L/min). The "baseline" heating ramp is as follows: furnace on, 25 – 600°C at 3°C/min, 600 – 1200°C at 10°C/min, furnace off, natural cool down. The "fast" heat ramp is as follows: furnace on, 25 – 1200°C at 10°C/min, furnace off, natural cool down. The "hold" heat ramp is as follows: furnace on, 25 – 600°C at 3°C/min, 600 – 1200°C at 10°C/min, hold at 1200°C for 60 minutes, furnace off, natural cool down. The iron catalyst is removed from the biographite via reaction with

hydrochloric acid. The reflux is carried out in excess by lightly boiling a 5 wt% loading of biographite + iron in concentrated hydrochloric acid (37 wt%) for three hours. The purified graphite is separated via filtration and dried.

6.2.3 X-ray Diffraction

X-ray diffraction patterns of powdered samples are taken on a Rigaku Ultima IV X-ray diffractometer equipped with a copper X-ray source, K-beta filter, and dTex detector. Diffraction patterns are obtained using a data spacing of 0.02 degrees at a scan rate of 2.5° two-theta/minute. PDXL integrated X-ray powder diffraction software is used to estimate graphite crystal size based on the Scherrer Equation.

6.2.4 Raman Spectroscopy

Laser Raman spectra are obtained on powdered samples at room temperature using a Horiba Jobin-Yvon LabRam HR800 spectrometer with a 50x microscope objective microprobe in the back scattering geometry and a 532 nm Nd:YAG frequency-doubled laser (Torus). Raman spectra mapping (5-point) is conducted to ensure representative estimates of crystallite size and degrees of graphitization.

6.2.5 Scanning Electron Microscopy & Energy Dispersive X-ray Spectroscopy

Dry biographite samples with and without iron are used without further preparation for SEM. Samples are placed on aluminum stubs using two-sided carbon tape. The samples do not require coating due to the high electrical conductivity of the graphitic carbon. Imaging is performed using a FEI Quanta 400 FEG SEM instrument operating under vacuum (0.45 Torr) at a beam accelerating voltage of 20 keV and capturing secondary electrons with an Everhart-Thornley detector. The FEI Quanta 400 FEG SEM is coupled with an energy dispersive x-ray detector to obtain spectral maps that are interpreted via TEAM software developed by EDAX.

6.2.6 Electrochemical Tests

Softwood-derived biographite electrodes are prepared from slurry with the following composition: active material (92 wt%); Super C45 (2 wt%), which is used as a conductive agent, and a binder (polyvinylidenedifluoride, 6 wt%), which is dissolved in N-methyl-2-pyrrolidone (NMP). This slurry is pasted onto Cu-foil current collector and dried at 120°C for 12 h under vacuum. Electrodes with a diameter of 14 mm are punched, and the average active material loading density is 3.5 mg cm^{-2}. The electrochemical performance of the prepared electrodes is evaluated using CR2032 coin-type cells assembled in an Ar-filled glove box. Li metal is used as a counter and reference electrode, and a solution of 1.2M $LiPF_6$ + EC:EMC (3:7 by wt.) (Gen II electrolyte) is employed as the electrolyte. Galvanostatic discharge/charge tests are performed in a range of 0.005 to 1.5 V (*vs* Li/Li^+, hereafter) at a variety C-rate (1C corresponded to about 372 mAg^{-1}).

6.3 Results & Discussion

Softwood, hardwood, cellulose, glucose, organosolv lignin, hydrolysis lignin, and kraft lignin biomaterials are all investigated for their catalytic conversion to crystalline graphite. Evident from Figure 6.1, kraft lignin is the only biomaterial incapable of graphitization under the conditions used in this study, due to the presence of sulfur and its interaction with the iron catalyst. X-ray diffraction (XRD) and Raman spectroscopy are the two main methods used to qualify and quantify the graphite crystallinity of the biographite products. The 002 and 100 reflections of graphitic materials, which correspond to 2θ diffraction angles of 26.5° and 42.4°, allow for the quantification of graphitic crystallite size in the c-direction (Lc) and a-direction (La). Crystallite size (L) is inversely proportional to the XRD peak intensity full-width at half-height (B), as shown in Figure 6.2, Equation 1, and thus tall and narrow peaks indicate larger

graphite crystallites than short and wide peaks. Graphitic structure can also be characterized by measuring the Raman shifts from irradiating samples with light of particular wavelengths. Two primary Raman shifts are associated with graphitic materials: a small intensity shift at ~1350 cm^{-1} (*D* shift) and a large intensity shift at ~1575 cm^{-1} (*G* shift). The average graphite crystallite size (L) is inversely proportional to the ratio of D and G intensities (I_D/I_G), as shown in Equation 2. The degree of graphitization (α) can be estimated by using Equation 3.

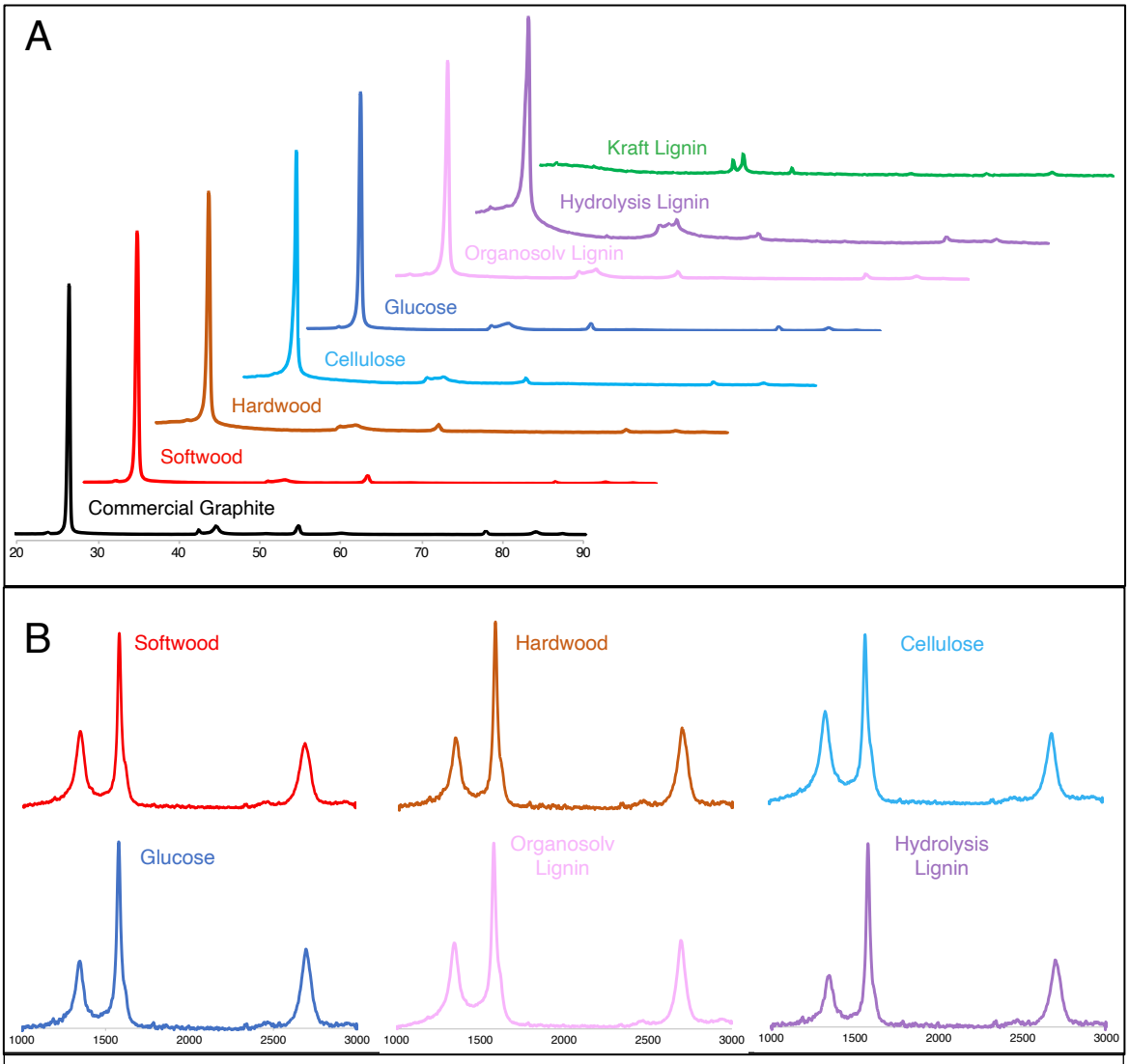

Figure 6.1 A) X-ray diffractograms with 2θ angles of diffraction on x-axis and intensity on y-axis and B) Rama spectra with chemical shift (cm^{-1}) on x-axis and intensity on y-axis of biographite materials produced from the baseline method of iron-catalyzed graphitization. Biographite materials had iron removed prior to analysis. See supporting information for descriptions of the biomaterial feedstocks.

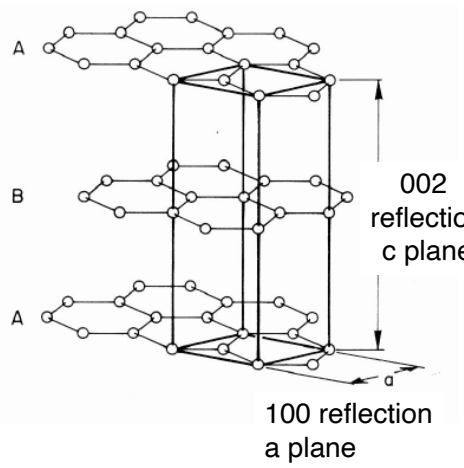

$$B(2\theta) = \frac{K\lambda}{Lcos(\theta)} \quad (1)$$

$$\frac{I(D)}{I(G)} = \frac{C(\lambda)}{L} \quad (2)$$

$$\alpha = \frac{I(G)}{I(D) + I(G)} \quad (3)$$

Figure 6.2 ABA stacking of sp2 hybridized graphene sheets in graphite with the 002 and 100 reflections highlighted. Equation 1: Scherrer equation used to estimate graphite crystallite size (L) from the full width at half height (B) of diffraction peaks at particular 2-theta angles. Equation 2: inverse relationship between Raman spectra D and G peak intensity ratio and graphite crystallite size (L). Equation 3: degree of graphitization as determined by D and G peak intensities.

Graphite crystallite size in the c-direction (Lc) and a-direction (La) are quantified for each biomaterial graphitized under baseline conditions, as shown in Figure 6.3A. Softwood produces graphite crystallites of the largest size in the a-direction and second largest size in the c-direction. Cellulose and glucose both produce graphite crystallites of relatively large size in the c-direction, but small size in the a-direction. Organosolv lignin and hydrolysis lignin produce graphite crystallites of relatively small size in the c-direction. Kraft lignin-derived materials are not included since kraft lignin produces non-graphitic disordered carbon. Cross sectional crystallite areas are estimated by multiplying Lc and La, and degrees of graphitization are determined using Raman data, as shown in Figure 6.3B. Standard deviations in degree of graphitization are also shown in Figure 6.3B. The standard deviation in degree of graphitization provides an understanding of the uniformity of graphitic structure within the bulk material: low standard deviation (small circles) indicates high degree of uniformity, whereas high standard

deviation (large circles) indicates a lesser degree of uniformity. Softwood generates graphite crystallites of the largest cross sectional areas and hydrolysis lignin generates a bulk material with the highest degree of graphitization. Thus, certain regions in softwood are amenable to large crystallite formation, whereas most regions in hydrolysis lignin are amenable to medium size crystallite formation. Interestingly, the biomaterials that melt to form a liquid intermediate phase during heating, namely the lignins and glucose, have smaller standard deviations and thus have relatively uniform distributions of graphitic structure relative to the non-melting biomaterials such as cellulose, softwood, and hardwood. The difference in trends observed indicates the process of graphitization is highly dependent on biomolecular structure, with the presence or absence of liquid intermediate phase being of particular importance. Hardwood and softwood biomaterials of two different particle sizes are assessed for graphite crystallite size and degree of graphitization, as shown in Figure 6.3C+D. Large particles react less with the iron catalyst than small particles, due to the decreased surface area of large particles. Notably, the increase in graphite quality from large to small particle size is much greater for softwood than for hardwood. Softwood of small particle size generates the highest quality graphite, nearly reaching that of commercial graphite. Glucose and softwood are graphitized using different heating methods to assess graphite crystallite size and degree of graphitization, as shown in Figure 6.3E+F; see Supporting Information for details regarding the different heating methods. The degree of graphitization for both glucose and softwood is highest with the longest heating method (hold). Glucose generates the largest crystallites with the fastest heating method, whereas softwood generates the largest crystallites with the baseline heating method. The difference in trends observed are complex and indicate that optimal heating method differs with biomolecular structure. To refine our knowledge of the relationship between biomolecular structure and

method of thermal treatment, we assess the graphitization of glucose and softwood at different maximum temperatures. As shown in Figure 6.3G, the onset temperature for graphitization of glucose (~600°C) is lower than that for softwood (~900°C). This observation corroborates findings from the assessment of different heating methods (Figure 6.3E+F), wherein glucose graphitizes more quickly due to the lower onset temperature for graphitization, relative to softwood. Product yield is an important parameter with regards to the economic viability of any biomass conversion process. Overall, lignin provides the highest graphite yield and glucose the lowest yield. Thus, biomaterials high in oxygen content have the lowest biographite yields. See Appendix (Figure A6.1) for more details regarding graphite mass yield.

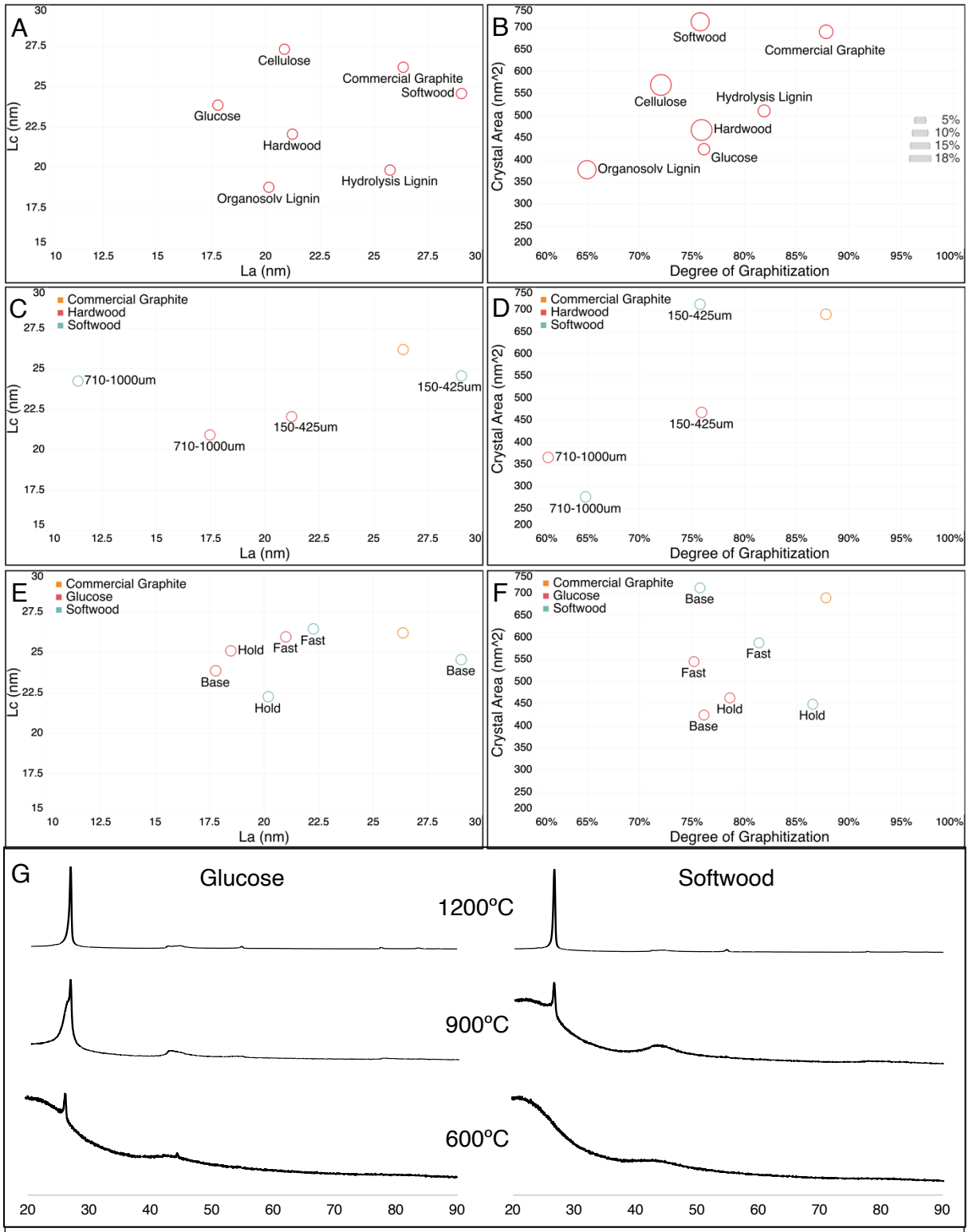

Figure 6.3 A – F) Graphite crystallite size in c-direction (Lc) vs. size in a-direction (La) (left panes) and graphite crystallite area (nm^2) vs. degree of graphitization (right panes) for various biographite materials (B has standard deviations of degree of graphitization inset). G) X-ray diffractograms of glucose- and softwood-derived biographite materials graphitized at different temperatures; 2θ angles of diffraction on x-axis and intensity on y-axis.

Insight into the mechanisms involved in iron-catalyzed graphitization of biomaterials can be gained from past studies on graphite crystallization in cast iron. Stefanescu et al. (2018) hypothesized a three-stage mechanism of graphite formation during cast iron heating and cooling[6.23]: 1) crystallite nucleation in molten iron, 2) crystallite growth during eutectic iron-carbon formation, and 3) continued crystallite growth via graphite precipitation during cool down as molten iron solidifies and the solubility of carbon decreases. The bulk of graphite crystallite growth takes place at temperatures in the range of 1100 – 1200°C, or the eutectic point at which iron carbide completes the transition from solid to liquid.[6.24] Generally, graphite grows from molten iron carbide in the form of platelets, which we have observed in our work (Figure 6.4A), but the final morphologies of the aggregated platelets vary depending on local composition and degrees of supersaturation and undercooling; the biographite platelets appear similar in structure to those in the commercial synthetic graphite product, as shown in Figure A6.2. Our work has identified three primary morphological transformations during catalytic graphitization of biomaterials, which agree with graphite morphologies identified in cast iron production: nucleation followed by growth of graphite crystallites forming 1) spheroids (Figure 6.4B), 2) foliated layers (Figure 6.4C), and 3) spiraling platelets (Figure 6.4D). Notably, the graphitization mechanism primarily progresses through liquid-solid interactions, with the molten liquid iron interacting with solid carbon and inducing crystallite growth.

High degrees of graphitization and large graphite crystallite formations (Figures 6.1 & 6.3) indicate that the iron catalyst particles melt and flow within the pores of the biomaterial cellular matrix during heating, thereby distributing the iron catalyst within the biomaterial structure. Figure 6.4E shows an iron-carbon phase diagram, with the eutectic transition point at ~1150°C. At ~1150°C, the semi-molten iron becomes saturated in carbon and transitions to a

full-molten liquid phase. Figure 6.4F shows a proposed mechanism for iron-catalyzed graphitization of biomaterials wherein 1) iron particle is resting on solid carbon (black circles) at temperature < 700°C, 2) temperature increases from 700 to 800°C, with iron particle beginning to transition from solid to liquid, 3) temperature increases from 800 to 900°C, with carbon beginning to solubilize in the semi-liquid iron particle, 4) temperature increases from 900 to 1000°C, with initial nucleation of graphite crystallites as the molten iron particle is partially saturated with carbon, 5) temperature increases from 1000 to 1200°C, with molten iron carbide fully saturated in carbon, 6) temperature remains constant at 1200°C, with molten iron carbide catalyzing the transformation of disordered carbon to graphitic carbon. At 1200°C, the activity of the iron catalyst reduces with time as graphitic carbon precipitation blocks access to disordered carbon.

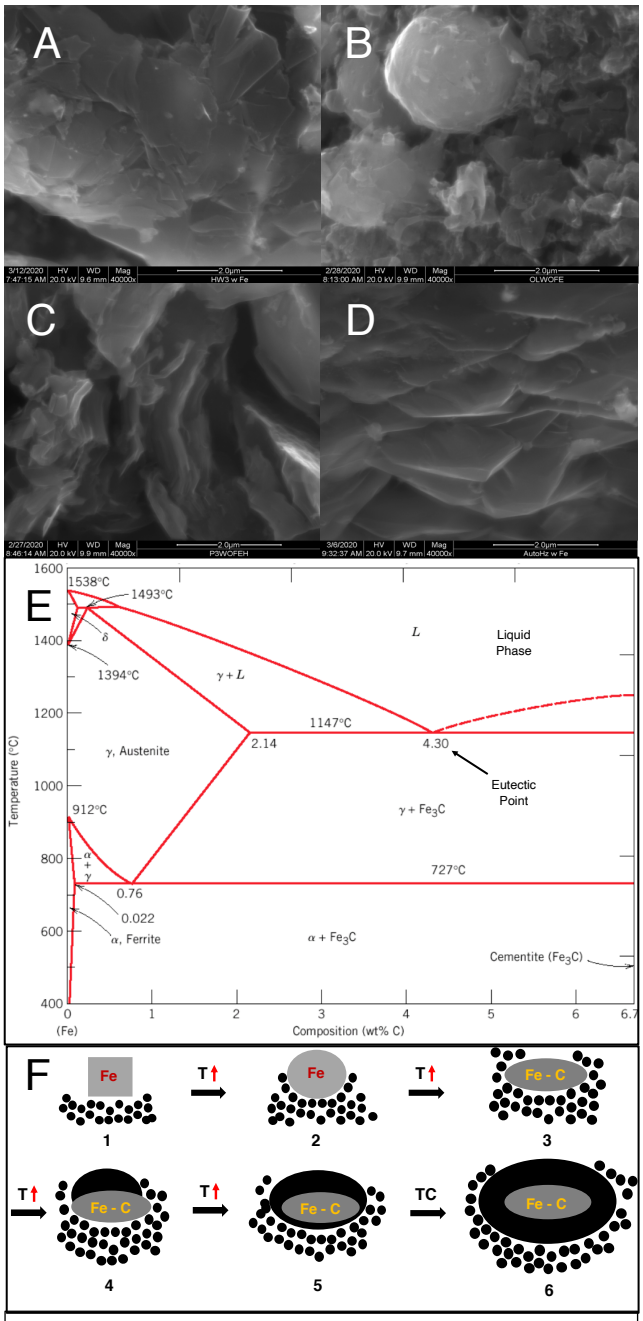

Figure 6.4 Scanning electron micrographs of A) graphite platelets grown from the iron catalyst during biomass graphitization, aggregated graphite platelets forming B) spheroid, C) foliated layering, and D) spiraling platelets. E) Iron-Iron Carbide (Fe-Fe_3C) phase diagram[6.24]. F) Proposed mechanism of iron-catalyzed graphitization of biomaterials wherein iron melts (1-2) before solubilizing carbon to form molten iron carbide (3) which precipitates graphite upon reaching carbon saturation (4-6).

Scanning electron microscopy is used to understand the morphologies of the various biomaterials treated in the study, as shown in Figure 6.5. The cellular structure morphology representative of woody biomass is evident in the cross sectional images shown in Figures 6.5A+B, wherein the depth of catalyst penetration is revealed. See Appendix (Figure A6.3) for scanning electron micrographs of cross sectional areas of biographite treated at temperatures lower than the baseline temperature (1200°C). Iron catalyst on the exterior of the hardwood fibers (Figure 6.5B) appears to catalyze graphitization of carbon several micrometers deep into the fiber walls. Interestingly, the depth of catalyst penetration is greater for softwood (Figure 6.5A) than for hardwood (Figure 6.5B). Hardwood cellular structure is more complex than softwood due to the large number of cell types and the variability among cell types, which likely inhibits molten catalyst transport in hardwood cells and thus results in less graphitization; this is corroborated with the relatively small crystallite size of hardwood (baseline particle size of 150 - 425um) biographite shown in Figure 6.3C+D.[6.25] Figures 6.5C, D, and E show micrographs of graphitized lignins, all of which form intermediate liquid phases during initial heating and result in a solidified material that resembles shattered glass upon crushing via mortar and pestle. Graphitic platelets are clearly observed in the materials derived from organosolv and hydrolysis lignins, as shown in Figures 6.5C and D. The morphology of carbonized kraft lignin (Figure 6.5E) shows no evidence of graphitic structure and appears similar to that of glucose carbonized at 600°C (Figure A6.3C), both of which have been proven to be constructed of nongraphitic, disordered carbon.

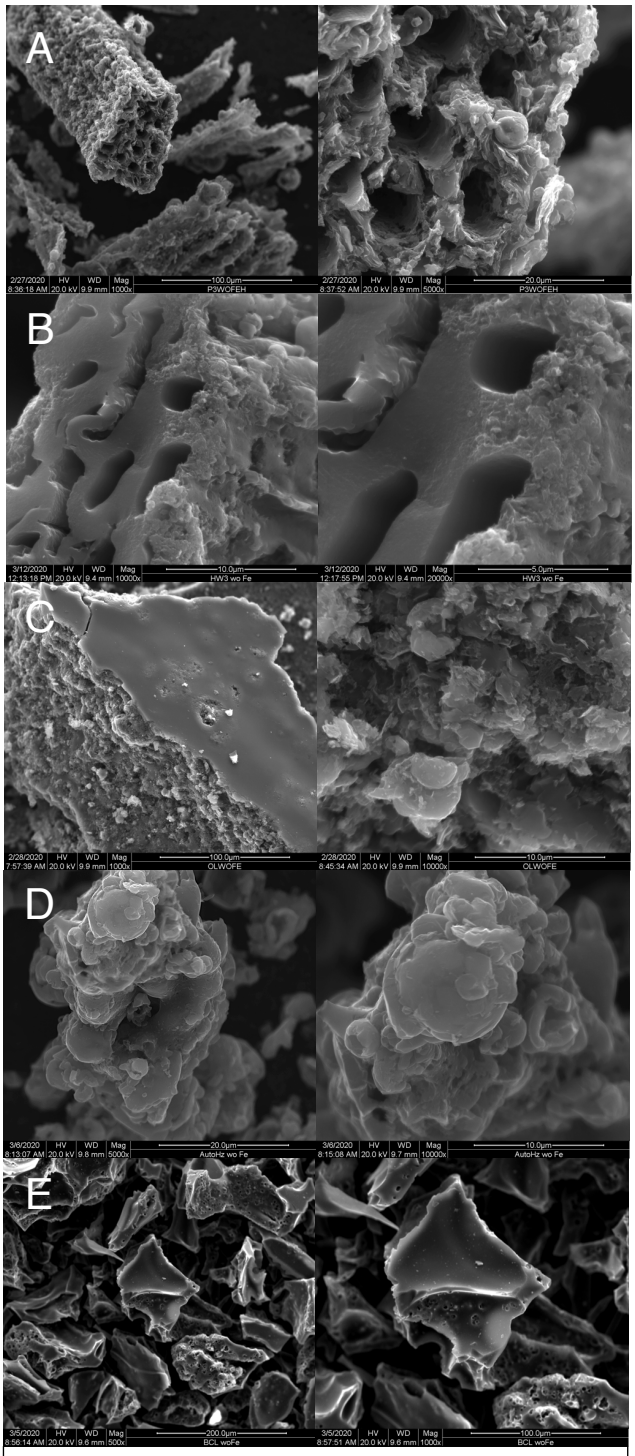

Figure 6.5 Scanning electron micrographs of biographite materials produced under baseline conditions with iron removal: A) softwood, B) hardwood, C) organosolv lignin, D) hydrolysis lignin, and E) kraft lignin.

Energy-dispersive x-ray spectral (EDS) mapping is used to understand the morphology and distribution of iron and carbon in graphitized materials prior to acid washing, as shown in Figure 6.6. The detection of iron and carbon is confined to several micrometers within the surface of the materials analyzed, and thus EDS does not provide insight into the composition of the inner mass within large particles. As shown in Figures 6.6A and B, the distribution of iron and carbon in graphitized softwood appears to be more uniform than that in hydrolysis lignin. According to Figure 6.6B, softwood-derived biographite is of larger crystallite size but smaller degree of graphitization compared with hydrolysis lignin. Therefore, large graphite crystallites are highly concentrated near the surface of softwood particles, with disordered regions concentrated within the core of the particles where iron catalyst has difficulty reaching. Hydrolysis lignin forms a liquid intermediate phase during heating which results in relatively small particles during graphitization, with iron distributed more uniformly within the core of the particles, relative to softwood. As shown in Figure 6.6B, iron and hydrolysis lignin-derived biographite are agglomerated together, indicating intimate contact during graphitization. As shown in the high magnification micrographs in Figure 6.6A+B, the irregular morphology of the iron indicates the initial spherical iron particles melt, react with carbon, precipitate graphite, and then solidify during cool down, thereby supporting the proposed mechanism of graphitization shown in Figure 6.4F. As shown in Figure 6.6C, the spherical iron catalyst particles in kraft lignin retain their initial shape and morphology throughout heating and never melt. The lack of iron phase change indicates iron never reaches the eutectic transition point in kraft lignin and thus never precipitates graphite platelets. The reason for the reduced reactivity of iron in kraft lignin appears to be the presence of sulfur and the gamma allotrope (Figure A6.4), both of which prevent the iron from transitioning phases and catalyzing the production of graphite platelets.

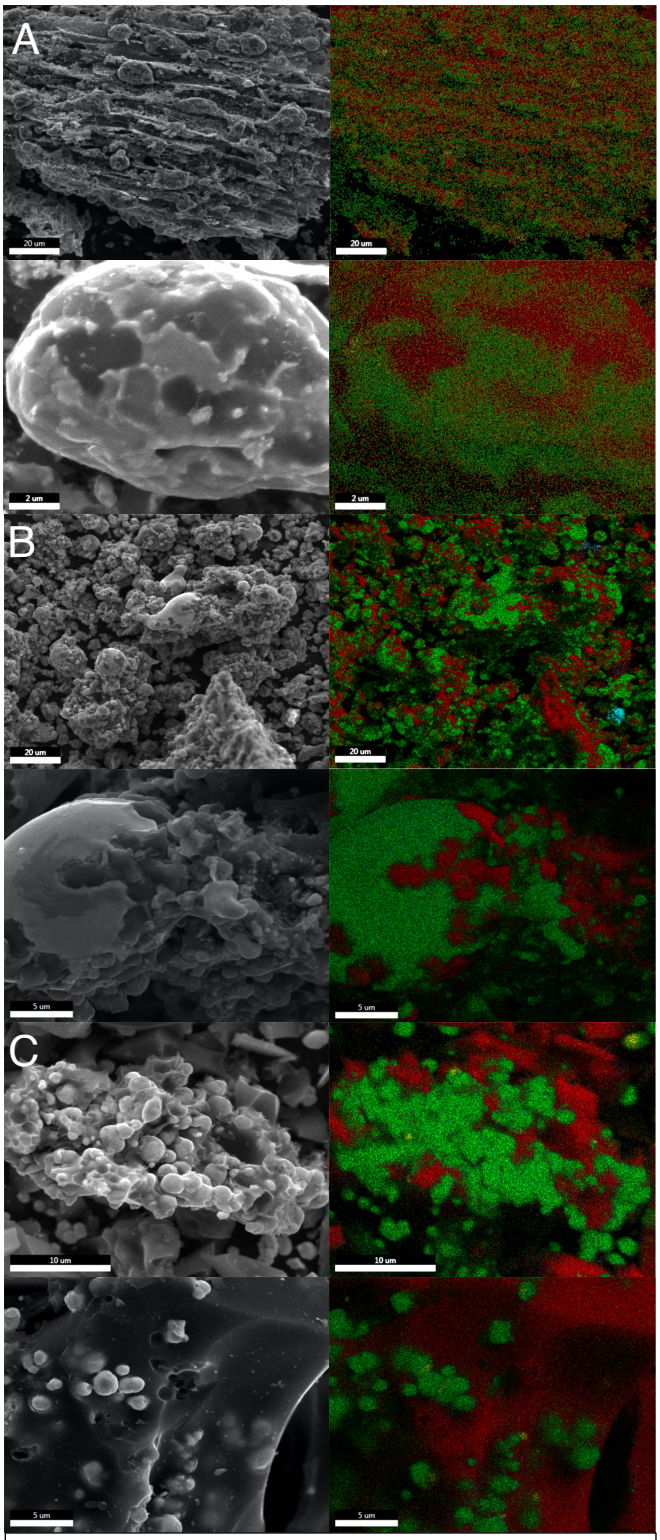

Figure 6.6 Scanning electron micrographs and corresponding energy-dispersive x-ray spectral mapping of biographite materials produced using the baseline procedure without iron removal. Green and red represent presence of iron and carbon, respectively. A) softwood, B) hydrolysis lignin, and C) kraft lignin.

The main motivation behind this study is to develop a simple, scalable, and green alternative to the current method of producing graphite anode material for lithium-ion batteries, and the only way to ensure new graphite materials are adequate for battery application is to test electrochemical performance. Softwood-derived biographite is selected for electrochemical performance testing in a coin-type half-cell due to its overall large graphite crystallite size and degree of graphitization (Figures 6.1 & 6.3), as well as softwood's viability as a low-cost, sustainable biomass resource. Figure 6.7A shows the galvanostatic discharge and charge profiles of the biographite tested at 0.1C in the voltage window of 0.005-1.5 V. During the first cycle, the characteristic voltage plateaus due to the staging mechanism are observed with discharge and charge capacities of 399.08 and 335.09 $mAhg^{-1}$, respectively. The calculated initial Coulombic efficiency (CE) is 83.96%, and most capacity loss is attributed to the reduction of electrolyte and the formation of a stable solid-electrolyte interphase (SEI) layer.[6.26,6.27] The electrochemical reactions related to the SEI formation are inferred by sloping voltage profile from 0.8 to 0.3 V. Irreversibility of the SEI formation is well supported by the disappearance of the cathodic peaks originated from SEI formation reactions in subsequent cycles (Figure 6.7B). CE of the second cycle is drastically increased up to 98.08% based on discharge and charge capacities of 344.33 and 335.09 $mAhg^{-1}$, respectively.

To understand the detailed storage mechanism of Li^+ ions—intercalation and de-intercalation with biographite—the differential capacity (dQ/dV) of the 1st and 2nd discharge and charge cycles are analyzed, as shown in Figure 6.7B. During initial Li^+ ion intercalation (discharge), the cathodic peaks at around 0.74 and 0.67 V (*vs* Li/Li^+, hereafter) are shown in the green color-highlighted inset. These initial peaks are observed during the first cycle and are attributed to the irreversible SEI formation as discussed above. Below 0.3 V, three additional

cathodic peaks are observed at around 0.20 (blue color-highlighted inset), 0.11 and 0.07 V, respectively. These peaks originate from the Li^+ ion staging mechanisms, including phase transitions that are dependent on the content of intercalated Li^+ ions.[6.28,6.29] Specifically, three cathodic peaks correspond to the following phase transitions: 1) diluted stage I to stage IV, 2) stage IV to stage II and III, and 3) stage II to stage I. During the subsequent Li^+ ion de-intercalation (charge), three anodic peaks from the reverse staging processes are observed, which demonstrate the electrochemical reversibility of the biographite. During the second cycle, the dQ/dV peaks relate to staging mechanisms and shift to relatively high voltages, with electrochemical reactions occurring readily at lower overpotentials mainly due to the formation of stable SEI with high Li^+ ion transport property.

The rate capability of the biographite is tested to understand the reversible Li^+ ion intercalation and de-intercalation behaviors at high C-rate, as shown in Figure 6.7C. The specific reversible capacities of approximately 340, 300, 245, 120, 40 and 15 $mAhg^{-1}$ are observed at 0.1C, 0.5C, 1C, 2C, 4C and 8C, respectively. The detailed discharge and charge profiles with varying C-rate are shown in Figure 6.7D. The biographite shows large capacity reduction with high C-rate, but demonstrates outstanding capacity self-recovery. In addition, galvanostatic long-term cycling test (at 0.5C) is performed to evaluate the cyclability of the biographite material, as shown in Figure 6.7E and F. Two formation cycles (0.1C) prior to faster cycling (0.5C) are incorporated to form the stable SEI layer and activate the electrode. The capacity retention is 89% at 100 cycles with >99% of Coulombic efficiency. These results conclude that the well-synthesized biographite has a great potential as an anode material for lithium-ion batteries compared with previously reported results (Table A6.1).

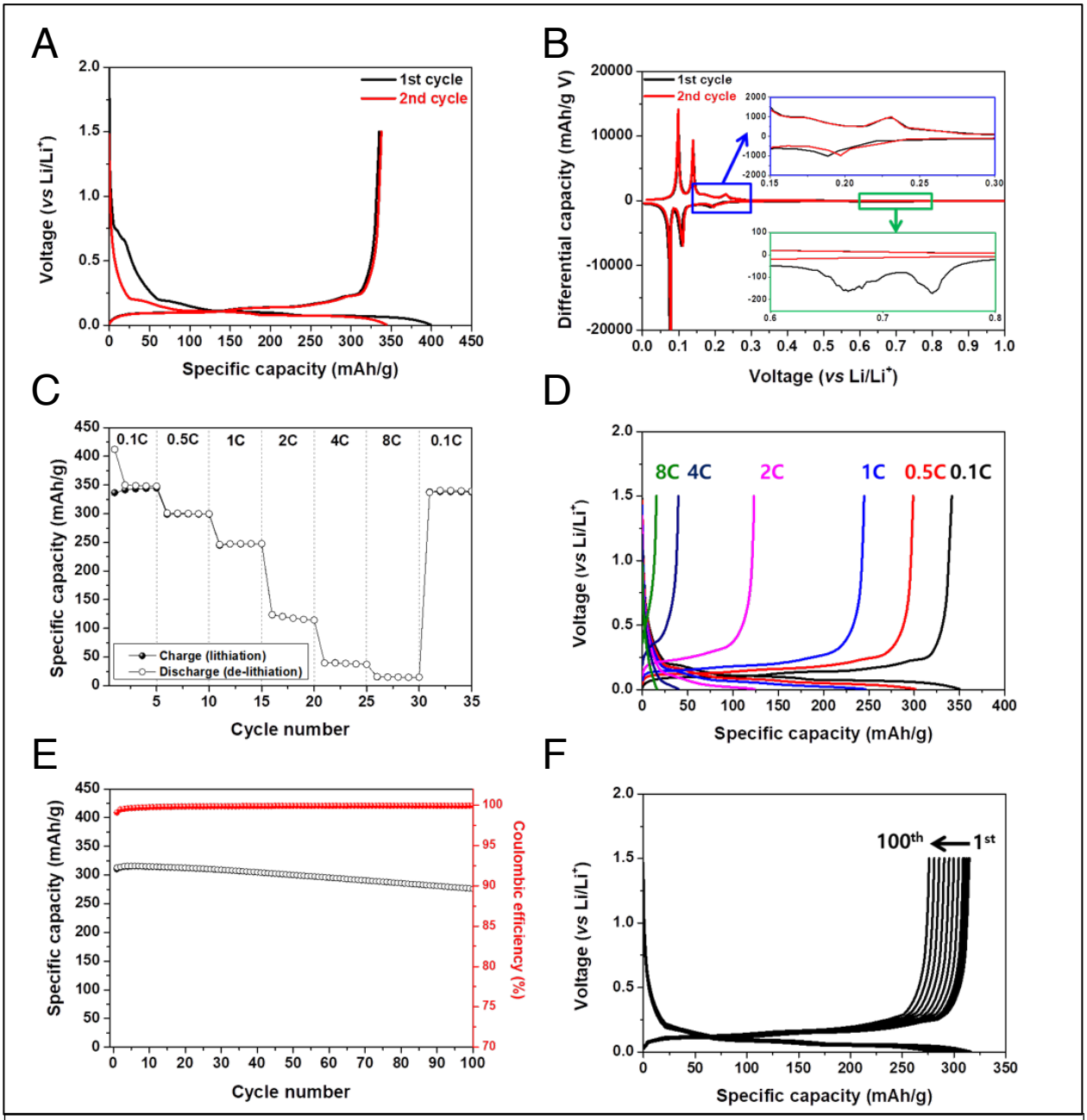

Figure 6.7 Electrochemical performance of softwood biographite: A) galvanostatic discharge and charge profiles and B) differential capacity (dQ/dV) plots at 0.1C in the voltage window of 0.005-1.5 V for the 1st and 2nd cycles. C) rate capability plot and D) corresponding galvanostatic discharge and charge profiles at varying C-rates from 0.1C to 8C. E) cycling stability plot and F) corresponding galvanostatic discharge and charge profiles at 0.5C over 100 cycles.

6.4 Conclusions

In summary, a multitude of biomaterials, including softwood, hardwood, cellulose, glucose, organosolv lignin, and hydrolysis lignin, are successfully converted to high quality graphite using a simple and scalable iron-catalyzed process. Small biomaterial particles result in better quality graphite, relative to large particles, due to increased surface area and more reactivity between biomaterial and catalyst. Graphite mass yield is highest for biomaterials with low oxygen content, such as lignin, and lowest for biomaterials with high oxygen content, such as glucose. The onset temperature of graphitization is lower for glucose (~600°C) than for lignocellulose (~900°C), and optimal heating rates vary with biomolecular structure. Softwood generates the largest graphite crystallites and hydrolysis lignin generates a bulk material with the highest degree of graphitization. Biomaterials that melt to form a liquid intermediate phase during heat ramp, such as glucose and lignin, have higher graphite uniformity than those without melting points, such as lignocellulose. At the eutectic transition point (~1100 – 1200°C), molten iron-iron carbide complexes catalyze the conversion of disordered, amorphous carbon to graphite in the form of aggregated platelets. Graphite platelets aggregate to form three primary morphologies: spheroids, foliated layers, and spiraling towers. Of the seven biomaterials assessed, kraft lignin is the only material incapable of graphitization due to inadequate phase transition of the iron catalyst. Softwood-derived biographite demonstrates excellent electrochemical performance in a lithium-ion coin cell with capacity retention of 89% over 100 cycles and >99% Coulombic efficiency, and thus has great potential as a green anode material for lithium-ion batteries.

Chapter 7 – Discussion & Future Work

In this dissertation, we assess five biomass-enabled carbon-negative technology areas through systems-level modeling: 1) enhanced carbon dioxide removal from coupled direct air capture-bioenergy systems, 2) synergistic biosystems to decarbonize agriculture through the conversion of organic waste to dietary protein and ammonia fertilizer, and 3) bioenergy with carbon capture in the US pulp and paper industry, as well as product development: 4) lignin-derived carbon fibers and 5) bio-based anode materials for lithium-ion batteries. The carbon-negative technologies assessed all have the capability of generating products that result in a net reduction in atmospheric CO_2. Potential CO_2 reductions are directly quantified for the three system-level assessments and indirectly qualified for the two product assessments. In future work, biomass-derived graphitic materials should undergo extensive emissions accounting to fully understand their carbon-negative potential. Nonetheless, the five assessments provide stakeholders in carbon-negative technology development and deployment with valuable information that could be used to advance the U.S. bioeconomy through technology innovation and policy adoption.

7.1 Systems-Level Modeling of Carbon-Negative Technologies

Our granular approach to designing, modeling, and analyzing complex biomass-enabled carbon-negative systems has brought new concepts into the academic literature that will help technologists, environmentalists, policy makers, and the public understand and appreciate the roles biomass can play in industrial decarbonization. Coupled direct air capture-bioenergy systems have profound potential for low-cost gigaton scale CO_2 removal in the U.S. Biomass is a suitable energy source for direct air capture through its ability to provide high, medium, and low temperature thermal energy at relatively low cost while enhancing CO_2 removal capacity, as well

as its inability to provide electricity at costs competitive with other renewable resources, such as wind and solar. However, direct air capture technologies are in their infancy and require substantial development to increase technical readiness and decrease uncertainty prior to integration with bioenergy with carbon capture technologies. In addition, social acceptance, environmental protection, and appropriate political incentives are necessary for large-scale deployment of CO_2 removal systems fueled by biomass. Future work should aim at bridging these gaps in research.

An integrated, synergistic biosystem that converts readily available organic waste to dietary protein and ammonia fertilizer shows great potential for drastically reducing the environmental impacts of animal agriculture and fertilizer production in the U.S. The public is showing increasing levels of awareness around environmental impacts of animal agriculture and acceptance for non-animal based protein products, and therefore the biosystem presented in this dissertation has a high probability of social acceptance. Further comprehensive investigation into the economic viability of the biosystem is required, and should be the focus of future work. In addition, a thorough lifecycle assessment is required to understand the potential for a truly carbon-negative biosystem.

Prospects for bioenergy with carbon capture in the U.S. pulp and paper industry are assessed and shown to have exciting potential for large-scale and relatively low cost CO_2 removal. Up until this point, there has been no granular assessment of the potential role the pulp and paper industry could play in industrial decarbonization. The results presented in this dissertation show several potentially low-cost opportunities for CO_2 capture, utilization, and/or sequestration. In the near-term, idling assets and waste heat should be leveraged to capture CO_2 from lime kilns. Additionally, innovative methods of integrating CO_2 capture into existing Kraft

pulp mills through calcium looping are intriguing and warrant further attention. Future work should also involve detailed lifecycle assessments to ensure the CO_2 utilization opportunities highlighted in this dissertation are eligible for the federal 45Q tax credit. In addition, scientists and engineers in the pulp and paper industry should be consulted to refine the process models and critique proposed concepts for innovative CO_2 capture and utilization.

7.2 Product Development for Carbon-Negative Technologies

Graphitic carbon products, including carbon fibers and battery anodes, are experiencing rapid growth in demand and require new, sustainable methods of production. Innovative technologies are currently under development to produce the aforementioned graphitic carbon products from renewable biomass resources. In this dissertation, we assess the current state of innovation in lignin-derived carbon fibers and offer future avenues for improvement. Overall, lignin-derived carbon fiber products have been unable to compete with commercial PAN-derived carbon fiber products on both cost and performance. Future work in this area should focus on increasing the graphitic structure of lignin-derived carbon fibers, since this characteristic has been largely overlooked.

Although carbon fibers are experiencing an increase in demand, electrochemical battery anodes are experiencing a substantially higher increase in demand, specifically in the lithium-ion battery market. The production of graphite for lithium-ion battery anodes is highly polluting, largely based outside the U.S., and expensive. In this dissertation, we develop and assess a new method for converting low-cost, sustainable biomass resources into high quality graphite for use in lithium-ion battery anodes. The electrochemical performance of the biographite anode material is close to that of commercial anodes, and with further process refinement the performance should match if not exceed that of commercial anodes. Preliminary results from an

ongoing techno-economic analysis indicate the biographite product could compete with commercially produced synthetic graphite. Future work should focus on optimizing the catalytic graphitization process to generate a graphite product that meets or exceeds the electrochemical performance of commercial lithium-ion anodes. In addition, a thorough techno-economic-lifecycle assessment should be completed to demonstrate the potential economic and environmental benefits of the biographite product.

References

2.1 D. L. Sanchez, J. H. Nelson, J. Johnston, A. Mileva and D. M. Kammen, *Nat. Clim. Chang.*, 2015, **5**, 230–234.

2.2 D. Sandalow, J. Friedmann and C. McCormick, Direct Air Capture of Carbon Dioxide: ICEF Roadmap 2018, https://www.icef-forum.org/pdf2018/roadmap/ICEF2018_Roadmap_Draft_for_Comment_20181012.pdf.

2.3 M. Allen, M. Babiker, Y. Chen, H. de Coninck, S. Connors, R. van Diemen and O. P. Dube, *Intergov. Panel Clim. Chang.*

2.4 D. L. Sanchez and D. M. Kammen, *Nat. Energy*, 2016, **1**, 1–4.

2.5 G. P. Peters and O. Geden, *Nat. Clim. Chang.*, 2017, **7**, 619–621.

2.6 National Academy of Sciences, *Natl. Acad. Press*, 2018, 131–171.

2.7 D. L. Sanchez, G. Amador, J. Funk and K. J. Mach, *Environ. Res. Lett.*, , DOI:10.1088/1748-9326/aaa08f.

2.8 E. Baik, D. L. Sanchez, P. A. Turner, K. J. Mach, C. B. Field and S. M. Benson, *Proc. Natl. Acad. Sci.*, , DOI:10.1073/pnas.1720338115.

2.9 H. J. Buck, *Clim. Change*, 2016, **139**, 155–167.

2.10 K. S. Lackner, *Science (80-.).*

2.11 E. S. Sanz-Pérez, C. R. Murdock, S. A. Didas and C. W. Jones, *Chem. Rev.*, 2016, **116**, 11840–11876.

2.12 D. W. Keith, G. Holmes, D. St. Angelo and K. Heidel, *Joule*, 2018, **2**, 1–22.

2.13 2014, No. 14715962.8 (European Patent).

2.14 2015, No. 2015/0283501 (US Patent).

2.15 C. Bataille, C. Guivarch, S. Hallegatte, J. Rogelj and H. Waisman, *Nat. Clim. Chang.*, 2018, **8**, 648–650.

2.16 F. Creutzig, C. Breyer, J. Hilaire, J. Minx, G. P. Peters and R. Socolow, *Energy Environ. Sci.*, , DOI:10.1039/c8ee03682a.

2.17 McKinsey & Company, Decarbonization of industrial sectors: the next frontier, https://www.mckinsey.com/~/media/McKinsey/Business Functions/Sustainability and Resource Productivity/Our Insights/How industry can move toward a low carbon future/Decarbonization-of-industrial-sectors-The-next-frontier.ashx.

2.18 EU Biomass Availability and Sustainability Information System, Report on conversion efficiency of biomass, http://www.basisbioenergy.eu/fileadmin/BASIS/D3.5_Report_on_conversion_efficiency_of_biomass.pdfAhttp://www.basisbioenergy.eu/%0Ahttp://www.basisbioenergy.eu/%0Ahttp://www.basisbioenergy.eu/.

2.19 R. M. Swanson, J. Satrio, R. C. Brown, A. Platon and D. D. Hsu, *NREL*, , DOI:10.2172/994017.

2.20 D. Humbird, R. Davis, L. Tao, C. Kinchin, D. Hsu, A. Aden, P. Schoen, J. Lukas, B. Olthof, M. Worley, D. Sexton and D. Dudgeon, *NREL*, , DOI:10.2172/1013269.

2.21 J. Wilcox, P. C. Psarras and S. Liguori, *Environ. Res. Lett.*, , DOI:10.1088/1748-9326/aa6de5/meta.

2.22 X. Zhao, H. Zhou, V. S. Sikarwar, M. Zhao, A.-H. A. Park, P. S. Fennell, L. Shen and L.-S. Fan, *Energy Environ. Sci.*, 2017, **10**, 1885–1910.

2.23 J. C. Abanades, B. Arias, A. Lyngfelt, T. Mattisson, D. E. Wiley, H. Li, M. T. Ho, E. Mangano and S. Brandani, *Int. J. Greenh. Gas Control*, 2015, **40**, 126–166.

2.24 Oak Ridge National Laboratory, *2016 Billion-Ton-Report: Advancing Domestic Resources for a Thriving Bioeconomy*, 2016, vol. 1.

2.25 M. Peters, *Plant Design and Economics for Chemical Engineers*, 1991.

2.26 M. K. Mann and P. L. Spath, *NREL*.

2.27 T. Asano, *Integr. Gasif. Comb. Cycle Technol.*, 2017, 799–815.

2.28 V. S. Sikarwar, M. Zhao, P. Clough, J. Yao, X. Zhong, M. Z. Memon, N. Shah, E. J. Anthony and P. S. Fennell, *Energy Environ. Sci.*, 2016, **9**, 2939–2977.

2.29 V. Sivaram and S. Kann, *Nat. Energy*, 2016, **1**, 1–3.

2.30 F. A. Felder, *Electr. J.*, 2011, **24**, 34–46.

2.31 O. Ellabban, H. Abu-Rub and F. Blaabjerg, *Renew. Sustain. Energy Rev.*, 2014, **39**, 748–764.

2.32 M. Bui, C. S. Adjiman, A. Bardow, E. J. Anthony, A. Boston, S. Brown, P. S. Fennell, S. Fuss, A. Galindo, L. A. Hackett, J. P. Hallett, H. J. Herzog, G. Jackson, J. Kemper, S. Krevor, G. C. Maitland, M. Matuszewski, I. S. Metcalfe, C. Petit, G. Puxty, J. Reimer, D. M. Reiner, E. S. Rubin, S. A. Scott, N. Shah, B. Smit, J. P. M. Trusler, P. Webley, J. Wilcox and N. Mac Dowell, *Energy Environ. Sci.*, 2018, 1062–1176.

2.33 D. W. Keith, *Sci. Perspect.*, 2009, **325**, 1654–1655.

2.34 US Dept. of the Treasury and Internal Revenue Service, *Carbon Oxide Sequestration Credit*, 2018.

3.1 U.S. Environmental Protection Agency, Sources of Greenhouse Gas Emissions, https://www.epa.gov/ghgemissions/sources-greenhouse-gas-emissions.

3.2 M. Richardson and P. Kumar, *Earth's Futur.*, 2017, **5**, 617–632.

3.3 U.S. Geological Survey, Mineral Commodity Summaries: Ammonia, https://minerals.usgs.gov/minerals/pubs/commodity/iron_ore/mcs-2017-feore.pdf.

3.4 D. Graham-Rowe, *Nature*, 2011, **474**, 3–5.

3.5 U.S. Natural Resources Conservation Service, Range and Pastureland Overview, https://www.nrcs.usda.gov/wps/portal/nrcs/detail/national/landuse/rangepasture/?cid=nrcs dev11_ 001074.

3.6 B. Tiwari, M. Henchion, A. Mullen, M. Fenelon and M. Hayes, *Foods*, 2017, **6**, 53.

3.7 M. Kent, H. M. Welladsen, A. Mangott and Y. Li, *PLoS One*, 2015, **10**, 1–15.

3.8 M. L. Wells, P. Potin, J. S. Craigie, J. A. Raven, S. S. Merchant, K. E. Helliwell, A. G. Smith, M. E. Camire and S. H. Brawley, *J. Appl. Phycol.*, 2017, **29**, 949–982.

3.9 M. P. Caporgno and A. Mathys, *Front. Nutr.*, 2018, **5**, 1–10.

3.10 M. L. Drewery, J. E. Sawyer, W. E. Pinchak and T. A. Wickersham, *J. Anim. Sci.*, 2014, **92**, 4642–4649.

3.11 R. Ekmay, S. Gatrell, K. Lum, J. Kim and X. G. Lei, *J. Agric. Food Chem.*, 2014, **62**, 9783–9791.

3.12 S. Gatrell, K. Lum, J. Kim and X. G. Lei, *J. Anim. Sci.*, 2014, **92**, 1306–1314.

3.13 V. Kiron, M. Sørensen, M. Huntley, G. K. Vasanth, Y. Gong, D. Dahle and A. M.

Palihawadana, 2016, **3**, 1–12.

3.14 M. S. Madeira, C. Cardoso, P. A. Lopes, D. Coelho and C. Afonso, *Livest. Sci.*, 2017, **205**, 111–121.

3.15 Y. Gong, T. Bandara, M. Huntley, Z. I. Johnson and J. Dias, *Aquaculture*, 2019, **501**, 455–464.

3.16 S. Bleakley and M. Hayes, *Foods*, 2017, **6**, 33.

3.17 R. Davis, J. Markham, C. Kinchin, N. Grundl, E. C. D. Tan and D. Humbird, , DOI:10.2172/1239893.

3.18 National Renewable Energy Laboratory, Biogas Potential in the United States, http://www.nrel.gov/docs/fy14osti/60178.pdf.

3.19 C. E. Berryman, H. R. Lieberman, V. L. Fulgoni and S. M. Pasiakos, *Am. J. Clin. Nutr.*, 2018, **108**, 405–413.

3.20 Oak Ridge National Laboratory, *2016 Billion-Ton-Report: Advancing Domestic Resources for a Thriving Bioeconomy*, 2016, vol. 1.

3.21 S. Zhu, S. Feng, Z. Xu, L. Qin and C. Shang, *Bioresour. Technol.*, 2019, **285**, 121353.

3.22 L. Moreno-garcia, Y. Gariépy, N. Bourdeau, S. Barnabé and G. S. V Raghavan, *Bioresour. Technol.*, 2019, **283**, 168–173.

3.23 W. A. V Stiles, D. Styles, S. P. Chapman, S. Esteves, A. Bywater, L. Melville, A. Silkina, I. Lupatsch, C. Fuentes, R. Lovitt, T. Chaloner, A. Bull, C. Morris and C. A. Llewellyn, *Bioresour. Technol.*, 2018, **267**, 732–742.

3.24 thyssenkrupp, Small-scale green ammonia plants open up new storage possibilities for wind and solar power, https://insights.thyssenkrupp-industrial-solutions.com/small-scale-green-ammonia-plants-open-up-new-storage-possibilities-for-wind-and-solar-power/.

3.25 M. K. Conaway, H.R.2 - Agriculture Improvement Act of 2018, https://www.congress.gov/bill/115th-congress/house-bill/2/text.

4.1 G. P. Peters and O. Geden, *Nat. Clim. Chang.*, 2017, **7**, 619–621.

4.2 National Academy of Sciences, *Natl. Acad. Press*, 2018, 131–171.

4.3 D. Sanchez, N. Johnson and S. McCoy, *Proc. Natl. Acad. Sci.*, , DOI:10.1073/pnas.1719695115.

4.4 G. F. Nemet, M. W. Callaghan, F. Creutzig, S. Fuss, J. Hartmann, J. Hilaire, W. F. Lamb, J. C. Minx, S. Rogers and P. Smith, *Environ. Res. Lett.*, , DOI:10.1088/1748-9326/aabff4.

4.5 D. Brack, *Chatham House*.

4.6 D. P. Hanak, E. J. Anthony and V. Manovic, *Energy Environ. Sci.*, 2015, **8**, 2199–2249.

4.7 X. Zhao, H. Zhou, V. S. Sikarwar, M. Zhao, A.-H. A. Park, P. S. Fennell, L. Shen and L.-S. Fan, *Energy Environ. Sci.*, 2017, **10**, 1885–1910.

4.8 D. A. Granados, F. Chejne and J. M. Mejía, *Appl. Energy*, 2015, **158**, 107–117.

4.9 K. Onarheim, S. Santos, P. Kangas and V. Hankalin, *Int. J. Greenh. Gas Control*, 2017, **59**, 58–73.

4.10 K. Onarheim, S. Santos, P. Kangas and V. Hankalin, *Int. J. Greenh. Gas Control*, 2017, **66**, 60–75.

4.11 P. Psarras, S. Comello, P. Bains, P. Charoensawadpong, S. Reichelstein and J. Wilcox, *Environ. Sci. Technol.*, 2017, acs.est.7b01723.

4.12 M. Bui, C. S. Adjiman, A. Bardow, E. J. Anthony, A. Boston, S. Brown, P. S. Fennell, S.

Fuss, A. Galindo, L. A. Hackett, J. P. Hallett, H. J. Herzog, G. Jackson, J. Kemper, S. Krevor, G. C. Maitland, M. Matuszewski, I. S. Metcalfe, C. Petit, G. Puxty, J. Reimer, D. M. Reiner, E. S. Rubin, S. A. Scott, N. Shah, B. Smit, J. P. M. Trusler, P. Webley, J. Wilcox and N. Mac Dowell, *Energy Environ. Sci.*, 2018, **11**, 1062–1176.

4.13 D. Y. C. Leung, G. Caramanna and M. M. Maroto-valer, *Renew. Sustain. Energy Rev.*, 2014, **39**, 426–443.

4.14 D. W. Keith, G. Holmes, D. St. Angelo and K. Heidel, *Joule*, 2018, **2**, 1–22.

4.15 P. Tomani, *Cellul. Chem. Technol.*, 2010, **44**, 53–58.

4.16 US Dept. of the Treasury and Internal Revenue Service, *Carbon Oxide Sequestration Credit*, 2018.

4.17 U.S. Department of Energy, Loan Guarantee Program, https://www.energy.gov/lpo/loan-programs-office.

4.18 Domtar, First LignoBoost plants producing large volumes of kraft lignin to the market place, https://www.valmet.com/media/articles/up-and-running/new-technology/PEERS1stLignoBoostPlants/.

4.19 A. Nabinger, K. Tomberlin, R. Venditti and Y. Yao, *Procedia CIRP*, 2019, **80**, 689–692.

4.20 U.S. Environmental Protection Agency, .

4.21 Fisher International, http://www.fisheri.com/.

4.22 J. Wilcox, *Carbon Capture*, Springer, 2012.

4.23 E. Baik, D. L. Sanchez, P. A. Turner, K. J. Mach, C. B. Field and S. M. Benson, *Proc. Natl. Acad. Sci.*, , DOI:10.1073/pnas.1720338115.

4.24 Aspen Tech, Aspen Hysys v10, https://www.aspentech.com/.

4.25 Aspen Tech, Aspen Plus v10, https://www.aspentech.com/.

4.26 D. Humbird, R. Davis, L. Tao, C. Kinchin, D. Hsu, A. Aden, P. Schoen, J. Lukas, B. Olthof, M. Worley, D. Sexton and D. Dudgeon, *NREL*, , DOI:10.2172/1013269.

4.27 Asian Development Bank, Beijing Jiaotong University and North China Electric Power University, .

4.28 R. Sakwattanapong, A. Aroonwilas and A. Veawab, *Ind. Eng. Chem. Res.*, 2005, **44**, 4465–4473.

4.29 EU Biomass Availability and Sustainability Information System, Report on conversion efficiency of biomass, http://www.basisbioenergy.eu/fileadmin/BASIS/D3.5_Report_on_conversion_efficiency_of_biomass.pdfAhttp://www.basisbioenergy.eu/%0Ahttp://www.basisbioenergy.eu/%0Ahttp://www.basisbioenergy.eu/.

4.30 G. T. Rochelle, *Curr. Opin. Chem. Eng.*, 2012, **1**, 183–190.

4.31 W. J. Sagues, S. Park, H. Jameel and D. L. Sanchez, *Sustain. Energy Fuels*, , DOI:10.1039/c9se00384c.

4.32 R. M. Swanson, J. Satrio, R. C. Brown, A. Platon and D. D. Hsu, *NREL*, , DOI:10.2172/994017.

4.33 Oak Ridge National Laboratory, *2016 Billion-Ton-Report: Advancing Domestic Resources for a Thriving Bioeconomy*, 2016, vol. 1.

4.34 Gekko Python Package - Optimization suite, https://gekko.readthedocs.io/en/latest/.

4.35 D. R. Sanchez, *Kraft Recover. Short Course*, 2000, 17–74.

4.36 Carnegie Mellon University, Integrated Environmental Control Module, https://www.cmu.edu/epp/iecm/iecm_dl.html.

4.37 C. S. Galik, R. Abt and Y. Wu, *J. For.*, 2009, **107**, 69–77.

4.38 D. L. Sanchez and D. S. Callaway, *Appl. Energy*, 2016, **170**, 437–444.

4.39 M. Yoo, S. Han and J. Wee, *J. Environ. Manage.*, 2013, **114**, 512–519.

4.40 H. Tran and E. K. Vakkilainnen, *TAPPI Kraft Recover. Course*, 2012, 1–8.

4.41 W. Zhu, G. Westman and H. Theliander, *J. Wood Chem. Technol.*, 2014, **34**, 77–97.

4.42 M. A. Hubbe and R. Gill, *BioResources*.

5.1 H. Brünig, D. Fischer, M. Al Aiti, G. Heinrich and D. Jehnichen, *Prog. Mater. Sci.*, 2018, **98**, 477–551.

5.2 W. Fang, S. Yang, X.-L. Wang, T.-Q. Yuan and R.-C. Sun, *Green Chem.*, 2017, **19**, 1794–1827.

5.3 X. Huang, *Materials.*, 2009, **2**, 2369–2403.

5.4 A. Gao, C. Su, S. Luo, Y. Tong and L. Xu, *J. Phys. Chem. Solids*, 2011, **72**, 1159–1164.

5.5 S. Speakman, *MIT Cent. Mater. Sci. Eng.*, 2015, 1–66.

5.6 A. C. Ferrari, *Solid State Commun.*, 2007, **143**, 47–57.

5.7 T. H. Ko, *J. Appl. Polym. Sci.*, 1996, **59**, 577–580.

5.8 C. D. Warren, Carbon Fiber Precursors and Conversion, https://www.energy.gov/sites/prod/files/2016/09/f33/fcto_h2_storage_700bar_workshop_3_warren.pdf.

5.9 J. Jin and A. A. Ogale, *J. Appl. Polym. Sci.*, 2018, **135**, 1–9.

5.10 Q. Li, S. Xie, W. K. Serem, M. T. Naik, L. Liu and J. S. Yuan, *Green Chem.*, 2017, **19**, 1628–1634.

5.11 R. E. Franklin, *Proc. R. Soc.*, 1951, **209**, 196–218.

5.12 M. S. A. Rahaman, A. F. Ismail and A. Mustafa, *Polym. Degrad. Stab.*, 2007, **92**, 1421–1432.

5.13 D. Li, C. Lu, S. Du, G. Wu, Y. Yang and L. Wang, *Appl. Phys. A Mater. Sci. Process.*, 2016, **122**, 1–10.

5.14 L. Salmén, A. M. Olsson, J. S. Stevanic, J. Simonovic and K. Radotic, *BioResources*, 2012, **7**, 521–532.

5.15 C. Crestini, H. Lange, M. Sette and D. S. Argyropoulos, *Green Chem.*, 2017, **19**, 4104–4121.

5.16 O. Hosseinaei, D. P. Harper, J. J. Bozell and T. G. Rials, *ACS Sustain. Chem. Eng.*, 2016, **4**, 5785–5798.

5.17 Q. Yu, A. Bahi and F. Ko, *Macromol. Mater. Eng.*, 2015, **300**, 1023–1032.

5.18 D. A. Baker and T. G. Rials, *J. Appl. Polym. Sci.*, 2013, **130**, 713–728.

5.19 J. M. Rosas, R. Berenguer, M. J. Valero-Romero, J. RodrÃ-guez-Mirasol and T. Cordero, *Front. Mater.*, 2014, **1**, 1–17.

5.20 W. Qin and J. F. Kadla, *J. Appl. Polym. Sci.*, 2012, **126**, 203–212.

5.21 F. Souto, V. Calado and N. Pereira, *Mater. Res. Express*, 2018, **5**, 1–30.

5.22 S. Laurichesse and L. Avérous, *Prog. Polym. Sci.*, 2014, **39**, 1266–1290.

5.23 L. Kouisni, P. Holt-Hindle, K. Maki and M. Paleologou, *Pulp Pap. Canada*, 2014, **115**, 18–22.

5.24 P. Tomani, *Cellul. Chem. Technol.*, 2010, **44**, 53–58.

5.25 Y. Nordström, I. Norberg, E. Sjöholm and R. Drougge, *J. Appl. Polym. Sci.*, 2013, **129**, 1274–1279.

5.26 M. Foston, G. A. Nunnery, X. Meng, Q. Sun, F. S. Baker and A. Ragauskas, *Carbon*, 2013, **52**, 65–73.

5.27 Q. Sun, R. Khunsupat, K. Akato, J. Tao, N. Labbé, N. C. Gallego, J. J. Bozell, T. G. Rials,

G. A. Tuskan, T. J. Tschaplinski, A. K. Naskar, Y. Pu and A. J. Ragauskas, *Green Chem.*, 2016, **18**, 5015–5024.

5.28 C. Cui, H. Sadeghifar, S. Sen and D. S. Argyropoulos, *BioResources*, 2013, **8**, 864–886.

5.29 I. Norberg, Y. Nordström, R. Drougge, G. Gellerstedt and E. Sjöholm, *J. Appl. Polym. Sci.*, 2013, **128**, 3824–3830.

5.30 X. Zhang, Q. Yan, W. Leng, J. Li, J. Zhang, Z. Cai and E. B. Hassan, *Materials*, 2017, **10**, 1–15.

5.31 S. Sen, H. Sadeghifar and D. S. Argyropoulos, *Biomacromolecules*, 2013, **14**, 3399–3408.

5.32 H. Sadeghifar, S. Sen, S. V. Patil and D. S. Argyropoulos, *ACS Sustain. Chem. Eng.*, 2016, **4**, 5230–5237.

5.33 M. Fitzer E, *Carbon reinforcements and carbon/carbon composites*, Springer-Verlag Berlin Heidelberg, 1998.

5.34 A. Galiguzov, A. Malakho, V. Kulakov, A. Kenigfest, E. Kramarenko and V. Avdeev, *Carbon Lett.*, 2013, **14**, 22–26.

5.35 A. P. Nowak, J. Hagberg, S. Leijonmarck, H. Schweinebarth, D. Baker, A. Uhlin, P. Tomani and G. Lindbergh, *Holzforschung*, 2018, **72**, 81–90.

5.36 M. S. Kim, D. H. Lee, C. H. Kim, Y. J. Lee, J. Y. Hwang, C. M. Yang, Y. A. Kim and K. S. Yang, *Carbon*, 2015, **85**, 194–200.

5.37 L. M. Steudle, E. Frank, A. Ota, U. Hageroth, S. Henzler, W. Schuler, R. Neupert and M. R. Buchmeiser, *Macromol. Mater. Eng.*, 2017, **302**, 1–11.

5.38 J. Köhnke, H. Rennhofer, H. Lichtenegger, A. raj Mahendran, C. Unterweger, B. Prats-Mateu, N. Gierlinger, E. Schwaiger, A.-K. Mahler, A. Potthast and W. Gindl-Altmutter, *ACS Sustain. Chem. Eng.*, 2018, **6**, 3385–3391.

5.39 D. Yoon, J. Hwang, W. Chang and J. Kim, *ACS Appl. Mater. Interfaces*, 2018, **10**, 569–581.

5.40 N. A. Banek, D. T. Abele, K. R. McKenzie and M. J. Wagner, *ACS Sustain. Chem. Eng.*, 2018, **6**, 13199–13207.

5.41 H. Qin, Y. Zhou, J. Huang, C. Zhang, B. Wang and S. Jin, *Int. J. Electrochem. Sci.*, 2017, **12**, 10599–10604.

5.42 V. Garcia-Negron, N. D. Phillip, J. Li, C. Daniel, D. Wood, D. J. Keffer, O. Rios and D. P. Harper, *Energy Technol.*, 2017, **5**, 1311–1321.

5.43 D. Yoon, J. Hwang, W. Chang and J. Kim, *ACS Appl. Mater. Interfaces*, 2018, **10**, 569–581.

5.44 S. Kubo, Y. Uraki and Y. Sano, *J. Wood Sci.*, 2003, **49**, 188–192.

5.45 M. Demir, Z. Kahveci, B. Aksoy, N. K. R. Palapati, A. Subramanian, H. T. Cullinan, H. M. El-kaderi, C. T. Harris and R. B. Gupta, *Ind. Eng. Chem. Res.*, 2015, **54**, 10731–10739.

5.46 F. S. Baker, Low Cost Carbon Fiber From Renewable Resources, https://www1.eere.energy.gov/vehiclesandfuels/pdfs/merit_review_2010/lightweight_materials/lm005_baker_2010_o.pdf.

5.47 TORAY CARBON FIBERS AMERICA INC., Technical data sheet, https://www.toray.us/products/prod_004.html.

5.48 W. E. Tenhaeff, O. Rios, K. More and M. A. McGuire, *Adv. Funct. Mater.*, 2014, **24**, 86–94.

5.49 X. Zhao, Y. Yao, A. E. George, R. A. Dunlap and M. N. Obrovac, *J. Electrochem. Soc.*, 2016, **163**, A858–A866.

5.50 Z. Ding, F. Li, J. Wen, X. Wang and R. Sun, *Green Chem.*, 2018, **20**, 1383–1390.

5.51 S. Chu, A. V. Subrahmanyam and G. W. Huber, *Green Chem.*, 2013, **15**, 125–136.

5.52 J. Jin, J. Ding, A. Klett, M. C. Thies and A. A. Ogale, *ACS Sustain. Chem. Eng.*, 2018, **6**, 14135–14142.

5.53 E. Frank, F. Hermanutz and M. R. Buchmeiser, *Macromol. Mater. Eng.*, 2012, **297**, 493–501.

5.54 D. A. Baker, N. C. Gallego and F. S. Baker, *J. Appl. Polym. Sci.*, 2012, **124**, 227–234.

5.55 H. Liu, Z. Dai, Q. Cao, X. Shi, X. Wang, H. Li, Y. Han, Y. Li and J. Zhou, *ACS Sustain. Chem. Eng.*, 2018, **6**, 8554–8562.

5.56 Q. Li, S. Xie, W. K. Serem, M. T. Naik, L. Liu and J. S. Yuan, *Green Chem.*, 2017, **19**, 1628–1634.

5.57 Q. Li, W. K. Serem, W. Dai, Y. Yue, M. T. Naik, S. Xie, P. Karki, L. Liu, H. J. Sue, H. Liang, F. Zhou and J. S. Yuan, *J. Mater. Chem. A*, 2017, **5**, 12740–12746.

5.58 A. Gomez-Martin, J. Martinez-Fernandez, M. Ruttert, A. Heckmann, M. Winter, T. Placke and J. Ramirez-Rico, *ChemSusChem*, 2018, **11**, 2776–2787.

5.59 S. T. Neeli and H. Ramsurn, *Carbon*, 2018, **134**, 480–490.

5.60 Q. Yan, X. Zhang, J. Li, E. B. Hassan, C. Wang, J. Zhang and Z. Cai, *J. Mater. Sci.*, 2018, **53**, 8020–8029.

5.61 X. Xu, J. Zhou, L. Jiang, G. Lubineau, S. A. Payne and D. Gutschmidt, *Carbon*, 2014, **80**, 91–102.

5.62 S. A. Steiner, R. Li and B. L. Wardle, *ACS Appl. Mater. Interfaces*, 2013, **5**, 4892–4903.

5.63 K. J. Kim, J. Kim, W. R. Yu, J. H. Youk and J. Lee, *Carbon*, 2013, **54**, 258–267.

5.64 F. J. Garcia-Mateos, T. Cordero-Lanzac, R. Berenguer, E. Morallon, D. Cazorla-Amoros, J. Rodriguez-Mirasol and T. Cordero, *Appl. Catal. B Environ.*, 2017, **211**, 18–30.

5.65 X. Li, S. P. Lau, L. Tang, R. Ji and P. Yang, *Nanoscale*, 2014, **6**, 5323–5328.

5.66 L. Tang, R. Ji, X. Cao, J. Lin, H. Jiang, X. Li, K. S. Teng, C. M. Luk, S. Zeng, J. Hao and S. P. Lau, *ACS Nano*, 2012, **6**, 5102–5110.

5.67 X. Cao and K. Schmidt-Rohr, *Environ. Sci. Technol. Lett.*, 2018, **5**, 476–480.

5.68 C. E. Brewer, K. Schmidt-Rohr, J. A. Satiro and R. C. Brown, *AIChE J.*, 2010, **28**, 386–396.

6.1 H. Pierson, *Handbook of Carbon, Graphite, Diamond and Fullerenes*, Noyes Publications, **1993**.

6.2 S. Moores, *Benchmark Miner. Intell.* **2019**.

6.3 M. Burton, E. Van Der Walt, *Bloomberg* **2017**.

6.4 A. Mayyas, *Natl. Renew. Energy Lab.* **2018**.

6.5 D. Bogdanov, J. Farfan, K. Sadovskaia, A. Aghahosseini, M. Child, A. Gulagi, A. S. Oyewo, L. de Souza Noel Simas Barbosa, C. Breyer, *Nat. Commun.* **2019**, *10*, 1.

6.6 E. A. Olivetti, G. Ceder, G. G. Gaustad, X. Fu, *Joule* **2017**, *1*, 229.

6.7 G. Crabtree, *Science (80-.).* **2019**.

6.8 J. B. Dunn, L. Gaines, M. Barnes, J. Sullivan, M. Wang, *Argonne Natl. Lab.* **2012**, 10.

6.9 N. Lebedeva, F. Persio, L. Boon-Brett, *Eur. Comm. JRC Sci. Policy* **2016**.

6.10 A. D. Jara, A. Betemariam, G. Woldetinsae, J. Y. Kim, *Int. J. Min. Sci. Technol.* **2019**, *29*, 671.

6.11 J. Whiteside, D. Finn-Foley, *Wood Mackenzie* **2019**.

6.12 M. Romare, L. Dahllöf, *The Life Cycle Energy Consumption and Greenhouse Gas Emissions from Lithium-Ion Batteries*, **2017**.

6.13 J. S. McDonald-Wharry, M. Manley-Harris, K. L. Pickering, *Energy and Fuels* **2016**, *30*,

7811.

6.14 R. E. Franklin, *Proc. R. Soc.* **1951**, *209*, 196.

6.15 J. R. Dahn, T. Zheng, Y. Liu, J. S. Xue, *Science (80-.).* **1995**, *270*, 590.

6.16 W. J. Sagues, A. Jain, D. Brown, S. Aggarwal, A. Suarez, M. Kollman, S. Park, D. S. Argyropoulos, *Green Chem.* **2019**, DOI 10.1039/C9GC01806A.

6.17 Q. Hu, Q. Mao, X. Ren, H. Yang, H. Chen, *Bioresour. Technol.* **2019**, *275*, 53.

6.18 N. A. Banek, D. T. Abele, K. R. McKenzie, M. J. Wagner, *ACS Sustain. Chem. Eng.* **2018**, *6*, 13199.

6.19 A. Gomez-Martin, J. Martinez-Fernandez, M. Ruttert, A. Heckmann, M. Winter, T. Placke, J. Ramirez-Rico, *ChemSusChem* **2018**, *11*, 2776.

6.20 E. Thompson, A. E. Danks, L. Bourgeois, Z. Schnepp, *Green Chem.* **2015**, *17*, 551.

6.21 L. Zhao, J. C. Bennett, M. N. Obrovac, *Carbon N. Y.* **2018**, *134*, 507.

6.22 L. Zhao, X. Zhao, L. T. Burke, J. C. Bennett, R. A. Dunlap, M. N. Obrovac, *ChemSusChem* **2017**, *10*, 3409.

6.23 D. M. Ştefănescu, G. Alonso, P. Larrañaga, E. de La Fuente, R. Suárez, *Mater. Sci. Forum* **2018**, *925*, 36.

6.24 Department of Materials Science & Engineering, *Univ. Tennessee* **2018**.

6.25 A. C. Wiedenhoeft, *Handb. Wood Chem. Wood Compos. Second Ed.* **2012**, 9.

6.26 J. S. Gnanaraj, R. W. Thompson, S. N. Iaconatti, J. F. Dicarlo, K. M. Abraham, *Electrochem. Solid-State Lett.* **2005**, *8*, DOI 10.1149/1.1850390.

6.27 D. Aurbach, B. Markovsky, I. Weissman, E. Levi, Y. Ein-Eli, *Electrochim. Acta* **1999**, *45*, 67.

6.28 M. D. Levi, D. Aurbach, *J. Electroanal. Chem.* **1997**, *421*, 79.

6.29 D. Aurbach, *J. Electrochem. Soc.* **1995**, *142*, 2882.

APPENDIX

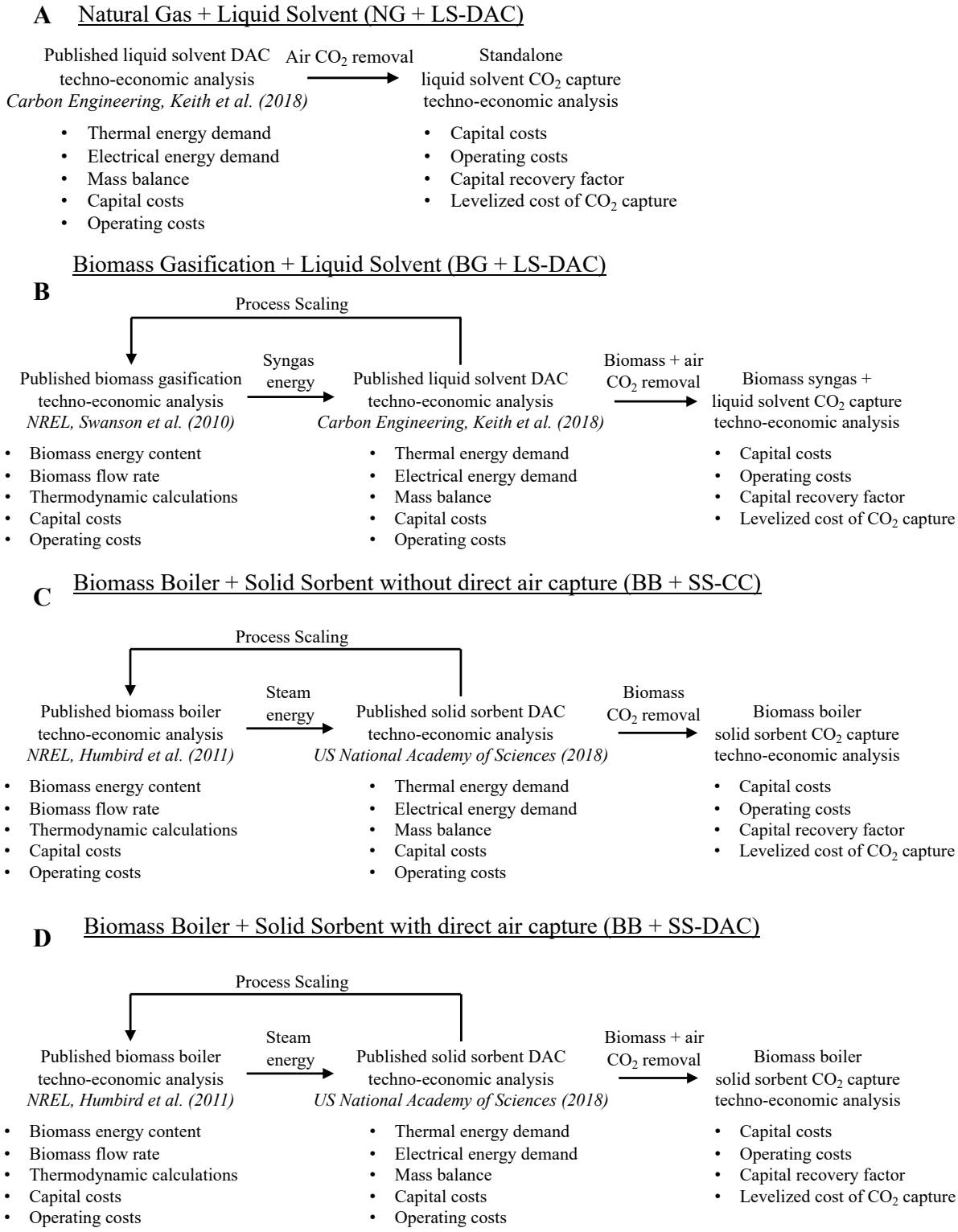

Figure A2.1 Approaches taken to design, model, and analyze the four CO_2 removal systems.

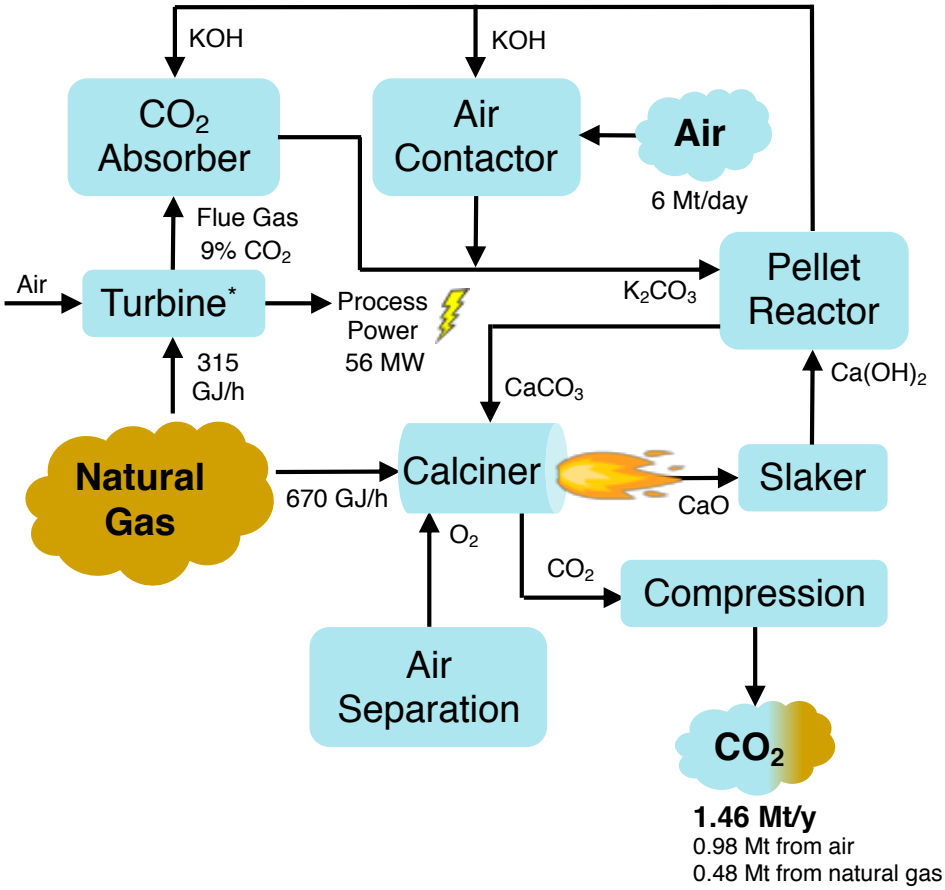

Figure A2.2 A generalized process flow diagram of the Natural Gas plus Liquid Solvent DAC system (NG + LS-DAC) adapted from Carbon Engineering. Turbine* includes a gas turbogenerator and a heat recovery steam generator.

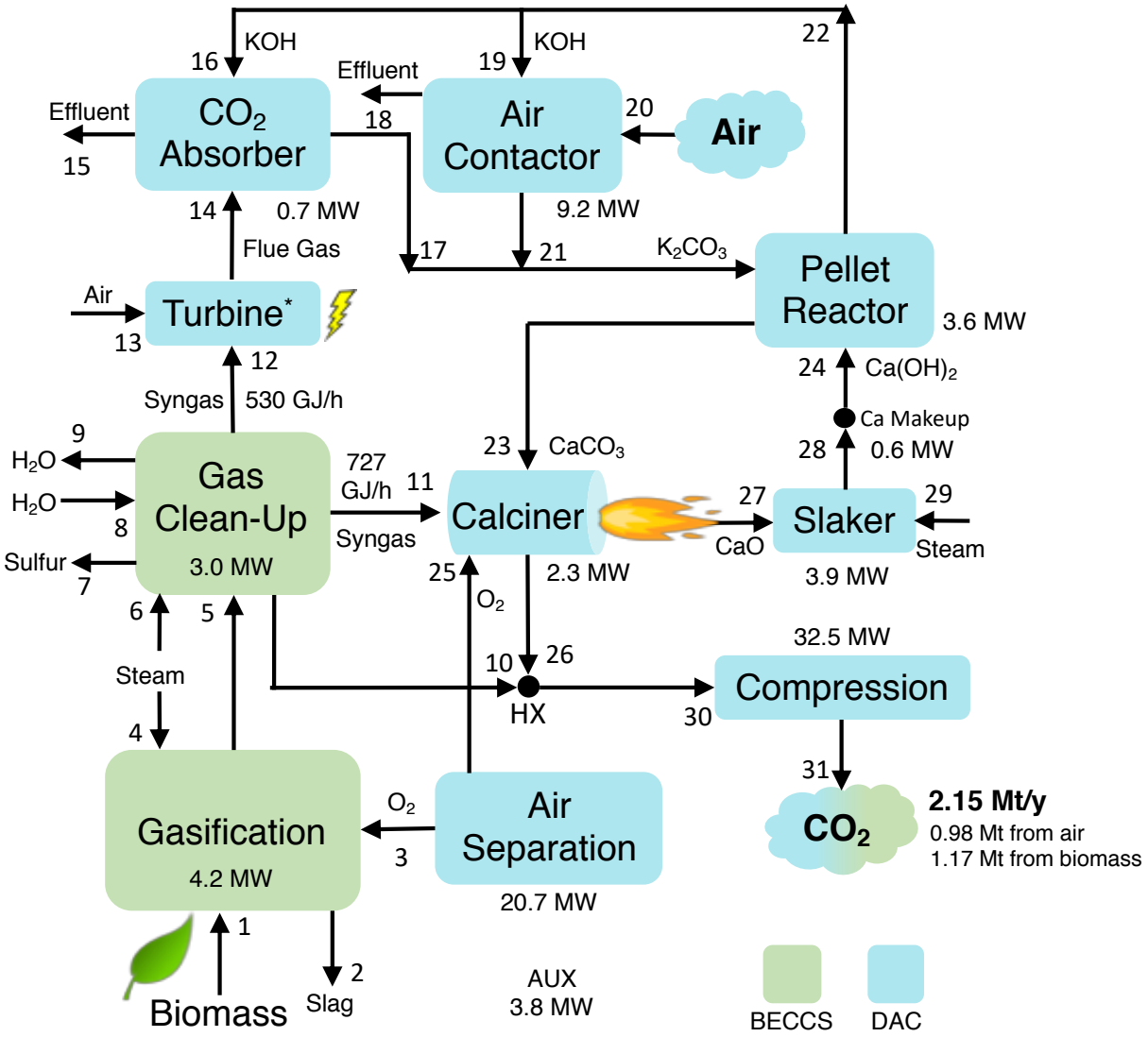

Figure A2.3 A generalized process flow diagram of the Biomass Gasification + Liquid Solvent Direct Air Capture (BG + LS-DAC) system. Only major streams shown, with minor make-up streams not shown. Turbine* includes a gas turbogenerator and a heat recovery steam system. Preprocessing (drying) and several minor streams are not shown for the gasification subsystem. Calciner includes heat exchange between hot flue gas and incoming $CaCO_3$, as well as water knockout. Air separation includes oxygen pre-heating. Power demanded by major process areas shown.

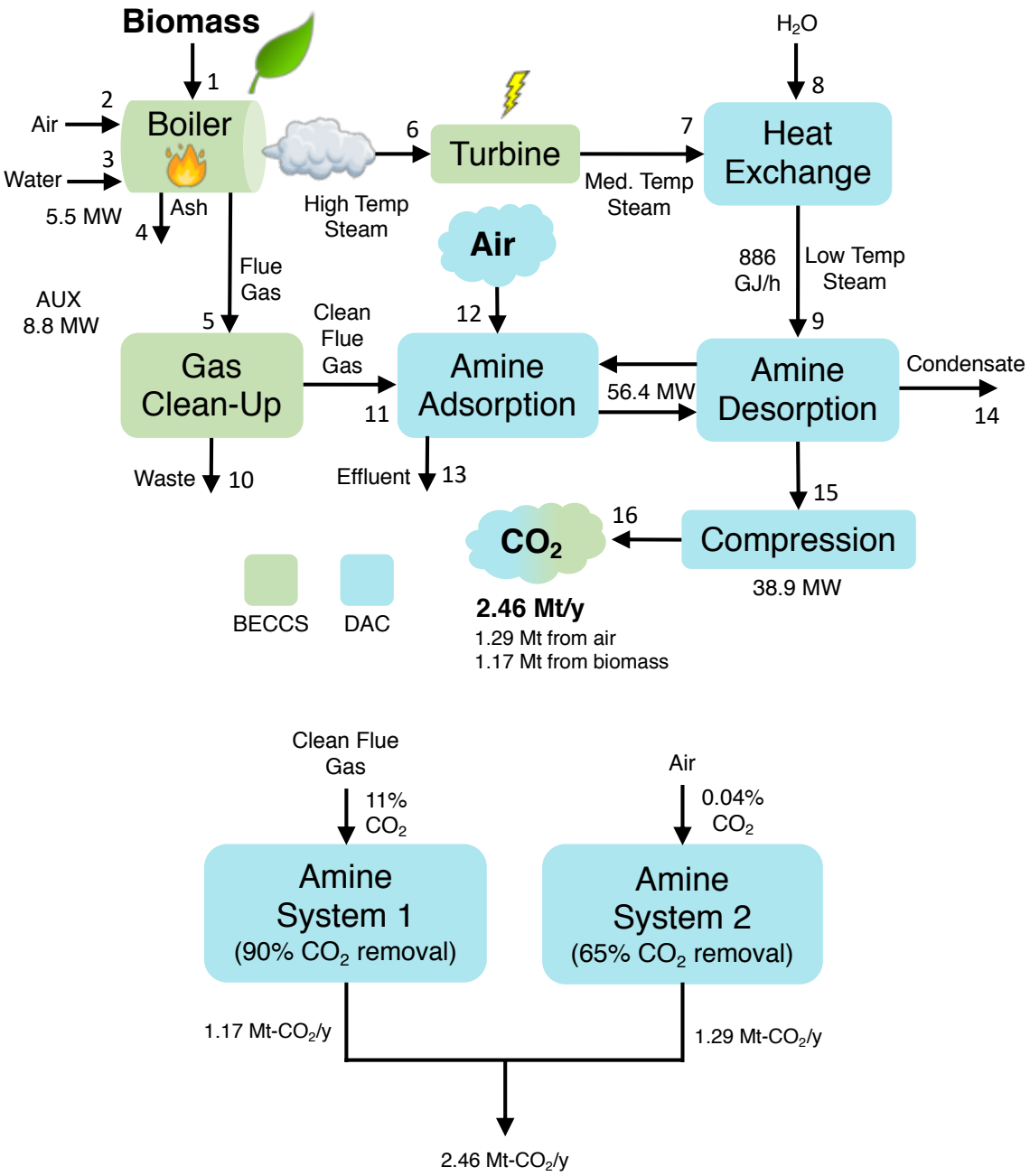

Figure A2.4 A generalized process flow diagram of the Biomass Boiler plus Solid Sorbent Direct Air Capture (BB + SS-DAC) system**.** Only major streams shown, with most make-up streams not shown. Power demanded by major process areas shown.

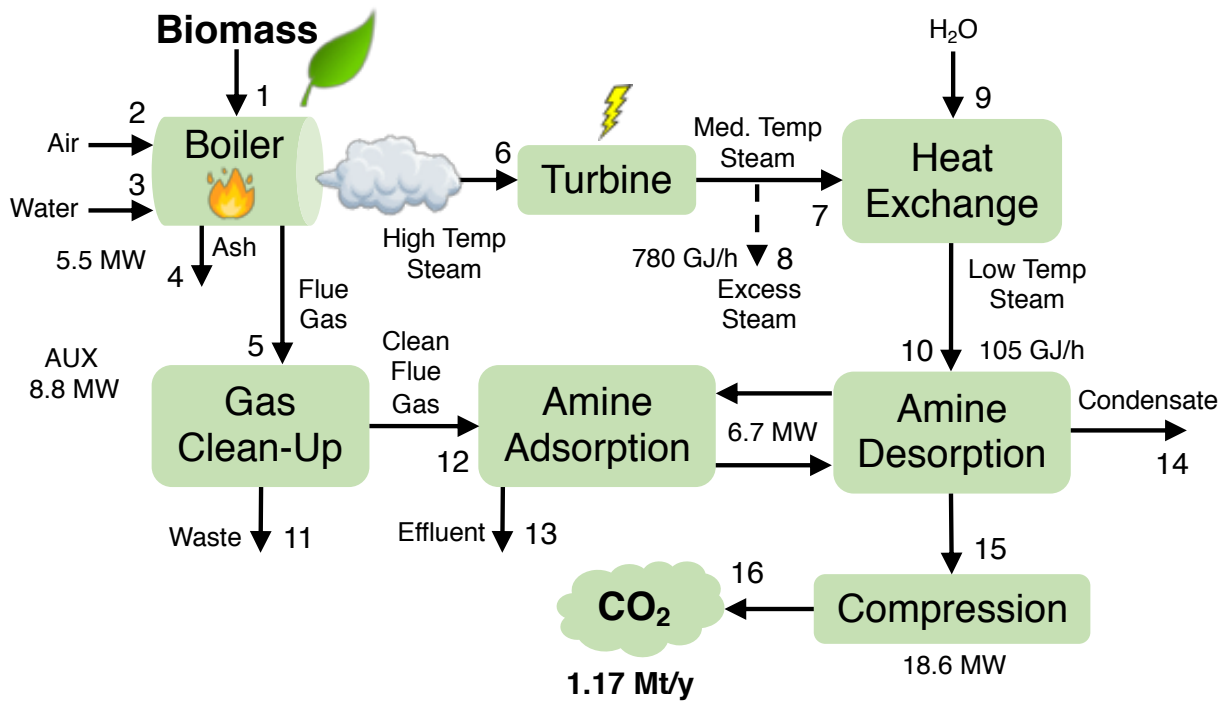

Figure A2.5 A generalized process flow diagram of the Biomass Boiler plus Solid Sorbent Carbon Capture (BB + SS-CC) system**.** Only major streams shown, with most make-up streams not shown. Power demanded by major process areas shown.

Table A2.1 An overview of the four CO_2 removal systems analyzed in this study.

System	Acronym	Feedstock for Combustion	CO_2 Capture Technology	Flue Gas CO_2 Capture?	Direct Air CO_2 Capture?
Natural Gas plus Liquid Solvent Direct Air Capture	NG + LS-DAC	Natural Gas	Liquid Alkaline Solvent	Yes	Yes
Biomass Gasification plus Liquid Solvent Direct Air Capture	BG + LS-DAC	Biomass	Liquid Alkaline Solvent	Yes	Yes
Biomass Boiler plus Solid Sorbent Carbon Capture	BB + SS-CC	Biomass	Solid Amine Sorbent	Yes	No
Biomass Boiler plus Solid Sorbent Direct Air Capture	BB + SS-DAC	Biomass	Solid Amine Sorbent	Yes	Yes

Table A2.2 Capital recovery factors (CRF) with varying weighted average costs of capital (i) and project life (years).

Capital Recovery Factor (CRF) Values						
Weighted Average Cost of Capital (i)	Project Life (years) (N)					
	5	10	15	20	25	30
1%	21%	11%	7%	6%	5%	4%
5%	23%	13%	10%	8%	7%	7%
10%	26%	16%	13%	12%	11%	11%
15%	30%	20%	17%	16%	15%	15%
20%	33%	24%	21%	21%	20%	20%

Table A2.3 Itemized capital costs and scaling factors for the NG + LS-DAC system.

Equipment Name	Original installed cost	Reference	Year of quote	Scaling Value	Units	Scaling exponent	Scaling stream	New value	Size ratio	Scaled installation cost	Index base year (2016)	Index project year (2016)	Installed cost in project year
Air contactor	$ 132,800,000	*(10)*	2016	1.45	Mt-CO2/y	0.80	CO2 Capacity	1.45	1	$ 132,800,000	541.7	541.7	$ 132,800,000
Pellet reactor	$ 94,800,000	*(10)*	2016	1.45	Mt-CO2/y	0.80	CO2 Capacity	1.45	1	$ 94,800,000	541.7	541.7	$ 94,800,000
Calciner-slaker	$ 63,600,000	*(10)*	2016	1.45	Mt-CO2/y	0.80	CO2 Capacity	1.45	1	$ 63,600,000	541.7	541.7	$ 63,600,000
Air separation unit	$ 46,700,000	*(10)*	2016	1.45	Mt-CO2/y	0.80	CO2 Capacity	1.45	1	$ 46,700,000	541.7	541.7	$ 46,700,000
CO2 compressor	$ 15,500,000	*(10)*	2016	1.45	Mt-CO2/y	0.80	CO2 Capacity	1.45	1	$ 15,500,000	541.7	541.7	$ 15,500,000
Steam turbine	$ 5,800,000	*(10)*	2016	1.45	Mt-CO2/y	0.80	CO2 Capacity	1.45	1	$ 5,800,000	541.7	541.7	$ 5,800,000
Power plant	$ 26,700,000	*(10)*	2016	1.45	Mt-CO2/y	0.80	CO2 Capacity	1.45	1	$ 26,700,000	541.7	541.7	$ 26,700,000
Fines filter	$ 24,800,000	*(10)*	2016	1.45	Mt-CO2/y	0.80	CO2 Capacity	1.45	1	$ 24,800,000	541.7	541.7	$ 24,800,000
Other equipment	$ 77,000,000	*(10)*	2016	1.45	Mt-CO2/y	0.80	CO2 Capacity	1.45	1	$ 77,000,000	541.7	541.7	$ 77,000,000
Buildings	$ 5,800,000	*(10)*	2016	1.45	Mt-CO2/y	0.80	CO2 Capacity	1.45	1	$ 5,800,000	541.7	541.7	$ 5,800,000
Transformer	$ 16,700,000	*(10)*	2016	1.45	Mt-CO2/y	0.80	CO2 Capacity	1.45	1	$ 16,700,000	541.7	541.7	$ 16,700,000
Indirect costs		*(10)*											$ 180,800,000
Contingency		*(10)*											$ 86,800,000
												Total Direct Costs:	$ 510,200,000
												Total Indirect Costs:	$ 267,600,000
												Total Capital Costs:	$ 777,800,000
												Capital Intensity ($/t-CO2-year)	$ 793

Table A2.4 A summary of results from the Natural Gas plus Liquid Solvent Direct Air Capture (NG + LS-DAC) techno-economic analysis showing levelized costs of CO_2 removal with a natural gas cost of $3.5/GJ and CRF values of 7.5% and 12.5%. These results compare nicely with those determined in Keith et al.'s techno-economic analysis of Carbon Engineering's baseline process.

Natural Gas + Liquid Solvent Direct Air Capture NG + LS-DAC Economic Summary		
Direct air CO2 capacity (Mt-CO2/y)		0.98
Biogenic CO2 capacity (Mt-CO2/y)		0.00
Total capacity (Mt-CO2/y)		0.98
Specific biogenic CO2 capacity (t-CO2/t-biomass)		N/A
Natural gas cost ($/GJ)	$	3.50
Equipment Costs (2016$)		**Installed Capital Cost**
Air contactor	$	132,800,000
Pellet reactor	$	94,800,000
Calciner-slaker	$	63,600,000
Air separation unit	$	46,700,000
CO2 compressor	$	15,500,000
Steam turbine	$	5,800,000
Power plant	$	26,700,000
Fines filter	$	24,800,000
Other equipment	$	77,000,000
Buildings	$	5,800,000
Transformer	$	16,700,000
Indirect costs	$	180,800,000
Contingency	$	86,800,000
Total Installed Capital	$	777,800,000
Capital Intensity ($/t-CO2-year)	$	793
Levelized Capital Cost (CRF 7.5%) ($/t-CO2)	**$**	**66**
Levelized Capital Cost (CRF 12.5%) ($/t-CO2)	**$**	**110**
Operating Costs (2016$)		**Annual Cost ($/y)**
Natural gas	$	30,252,835
Non-energy O&M	$	29,433,600
Electricity to grid	$	-
Net Operating Costs	$	59,686,435
Net Operating Costs ($/t-CO2)	**$**	**61**
Total Costs (CRF 7.5%) ($/t-CO2)	**$**	**127**
Total Costs (CRF 12.5%) ($/t-CO2)	**$**	**171**

Table A2.5 Mass balance of the BG + LS-DAC system.

Stream	Approx. Temp (C)	Mass flow (t/day)	Biomass	H2O	CO	H2	CO2	O2	N2	KOH	K2CO3	Ca(OH)2	CaCO3	CaO	H2S	S	Slag
1	90	2556	2300	256	0	0	0	0	0	0	0	0	0	0	0	0	0
2	50	131	0	0	0	0	0	0	0	0	0	0	0	0	0	0	131
3	149	856	0	0	0	0	0	805	0	0	0	0	0	0	0	0	0
4	200	1104	0	1104	0	0	0	0	0	0	0	0	0	0	0	0	0
5	1300	4399	0	1137	1676	141	1362	0	0	0	0	0	0	0	0	0	0
6	190	633	0	633	0	0	0	0	0	0	0	0	0	0	0	0	0
7	50	8	0	5	0	0	0	0	0	0	0	0	0	0	0	4	0
8	30	115	0	115	0	0	0	0	0	0	0	0	0	0	0	0	0
9	40	1726	0	1550	25		147		0	0	0	0	0	0	1	0	0
10	53	2032	0	29	5	0	1976	0	18	0	0	0	0	0	0	0	0
11	52	799	0	30	661	102	9	0	0	0	0	0	0	0	0	0	0
12	52	583	0	22	481	75	7	0	0	0	0	0	0	0	0	0	0
13	25	3761	0	0	0	0	0	873	2836	0	0	0	0	0	0	0	0
14	90	4294	0	694	0	0	764	0	2836	0	0	0	0	0	0	0	0
15	25	3607	0	0	0	0	76	0	0	0	0	0	0	0	0	0	0
16	21	17370	0	15617	0	0	0	0	0	1752	0	0	0	0	0	0	0
17	31	18057	0	15899	0	0	0	0	0	0	2158	0	0	0	0	0	0
18	21	6021307	0	59035	0	0	922	1385520	4575830	0	0	0	0	0	0	0	0
19	21	68065	0	61198	0	0	0	0	0	6866	0	0	0	0	0	0	0
20	21	6024000	0	59035	0	0	3614	1385520	4575830	0	0	0	0	0	0	0	0
21	31	70758	0	62300	0	0	0	0	0	0	8458	0	0	0	0	0	0
22	21	84573	0	76816	0	0	0	0	0	7757	0	0	0	0	0	0	0
23	21	6913	0	0	0	0	0	0	0	0	0	0	6913	0	0	0	0
24	21	20277	0	15161	0	0	0	0	0	0	0	5116	0	0	0	0	0
25	674	1197	0	0	0	0	0	1197	0	0	0	0	0	0	0	0	0
26	900	4876	0	952	0	0	3924	0	0	0	0	0	0	0	0	0	0
27	674	3794	0	0	0	0	0	0	0	0	0	0	0	3794	0	0	0
28	300	19423	0	15161	0	0	0	0	0	0	0	4262	0	0	0	0	0
29	253	16198	0	16198	0	0	0	0	0	0	0	0	0	0	0	0	0
30	30	6439	0	0	0	0	6246	0	193	0	0	0	0	0	0	0	0
31	40	6439	0	0	0	0	6246	0	193	0	0	0	0	0	0	0	0

Overall Mass Balance			
	Mass in	Mass out	% diff
Gasification	4515	4530	-0.33%
Syngas Cleaning	5146	5149	-0.06%
Turbine	4344	4294	1.16%
CO2 Absorber	21664	21664	0.00%
Air Contactor	6092065	6092065	0.00%
Pellet reactor	91035	91486	-0.50%
Calciner	8910	8670	2.69%
Slaker	19992	19423	2.85%
Total	6247670	6247280	0.01%

Table A2.6 Itemized capital costs and scaling factors for the BG + LS-DAC system.

Equipment	Original installed cost	Reference	Year of quote	Scaling stream	Scaling value	Units	Scaling exponent	New value	Size ratio	Scaled installed cost	Cost index base year	Cost index project year (2016)	Installed cost in project year
Preprocessing	$ 22,700,000	*(15)*	2007	Biomass feed	2000	dry tonne/day	0.80	2300	1.15	$ 25,385,407	525.4	541.7	$ 26,172,963
Gasification	$ 67,800,000	*(15)*	2007	Biomass feed	2000	dry tonne/day	0.80	2300	1.15	$ 75,820,731	525.4	541.7	$ 78,172,992
Syngas cleaning	$ 33,500,000	*(15)*	2007	Biomass feed	2000	dry tonne/day	0.80	2300	1.15	$ 37,463,045	525.4	541.7	$ 38,625,298
Power Plant	$ 45,564,672	*(15)*	2007	Power Generation	36	MW	0.80	85	2.4	$ 90,497,884	525.4	541.7	$ 93,305,489
Air contactor	$ 132,800,000	*(10)*	2016	CO2 capacity	0.98	Mt-CO2/y	0.80	0.98	1	$ 132,800,000	541.7	541.7	$ 132,800,000
Pellet reactor	$ 94,800,000	*(10)*	2016	CO2 to pellets	1.13	Mt-CO2/y	0.80	1.23	1.08	$ 101,176,251	541.7	541.7	$ 101,176,251
Calciner-slaker	$ 63,600,000	*(10)*	2016	Total CO2 capacity	1.45	Mt-CO2/y	0.80	2.15	1.48	$ 86,921,315	541.7	541.7	$ 86,921,315
Air separation unit	$ 46,700,000	*(10)*	2016	O2 demand	1284	tonne/day	0.80	2002	1.56	$ 66,626,224	541.7	541.7	$ 66,626,224
CO2 compressor	$ 15,500,000	*(10)*	2016	Total CO2 capacity	1.45	Mt-CO2/y	0.80	2.15	1.48	$ 21,183,654	541.7	541.7	$ 21,183,654
Fines filter	$ 24,800,000	*(10)*	2016	CO2 to pellets	1.13	Mt-CO2/y	0.80	1.23	1.08	$ 26,468,049	541.7	541.7	$ 26,468,049
Other equipment	$ 77,000,000	*(10)*	2016	Total CO2 capacity	1.45	Mt-CO2/y	0.80	2.15	1.48	$ 105,234,925	541.7	541.7	$ 105,234,925
Buildings	$ 5,800,000	*(10)*	2016	Total CO2 capacity	1.45	Mt-CO2/y	0.80	2.15	1.48	$ 7,926,787	541.7	541.7	$ 7,926,787
Transformer	$ 16,700,000	*(10)*	2016	Power Generation	55.80	MW	0.80	84.60	1.52	$ 23,297,066	541.7	541.7	$ 23,297,066
Indirect costs		*(10)*											$ 286,300,100
Contingency													$ 218,842,222
										Total Direct Costs:			$ 807,911,012
										Total Indirect Costs:			$ 505,142,322
										Total Capital Costs:			$ 1,313,053,334
										Capital Intensity ($/t-CO2-year)			$ 611

Table A2.7 A summary of results from the Biomass Gasification plus Liquid Solvent Direct Air Capture (BG + LS-DAC) techno-economic analysis showing levelized costs of CO_2 removal with a biomass cost of $70/dry short ton and CRF values of 7.5% and 12.5%.

Biomass Gasification + Liquid Solvent Direct Air Capture BG + LS-DAC Economic Summary		
Direct air CO2 capacity (Mt-CO2/y)		0.98
Biogenic CO2 capacity (Mt-CO2/y)		1.17
Total capacity (Mt-CO2/y)		2.15
Specific biogenic CO2 capacity (t-CO2/t-biomass)		1.55
Biomass cost ($/short t-biomass)	$	70
Equipment Costs (2016$)		**Installed Capital Cost**
Preprocessing	$	26,172,963
Gasification	$	78,172,992
Syngas cleaning	$	38,625,298
Power Plant	$	93,305,489
Air contactor	$	132,800,000
Pellet reactor	$	101,176,251
Calciner-slaker	$	86,921,315
Air separation unit	$	66,626,224
CO2 compressor	$	21,183,654
Fines filter	$	26,468,049
Other equipment	$	105,234,925
Buildings	$	7,926,787
Transformer	$	23,297,066
Indirect costs	$	286,300,100
Contingency	$	218,842,222
Total Installed Capital	$	1,313,053,334
Capital Intensity ($/t-CO2-year)	$	611
Levelized Capital Cost (CRF 7.5%) ($/t-CO2)	**$**	**51**
Levelized Capital Cost (CRF 12.5%) ($/t-CO2)	**$**	**85**
Operating Costs (2016$)		**Annual Cost ($/y)**
Biomass feedstock	$	58,299,522
Non-energy O&M Costs	$	62,967,699
Electricity to grid	$	-
Net Operating Costs	$	121,267,221
Net Operating Costs ($/t-CO2)	**$**	**56**
Total Costs (w/ CRF 7.5%) ($/t-CO2)	**$**	**107**
Total Costs (w/ CRF 12.5%) ($/t-CO2)	**$**	**141**

Table A2.8 Mass balance of the BB + SS-DAC system.

Stream	Approx. Temp (C)	Mass flow (t/day)	Biomass	H2O	CO2	O2	N2	Ash	S
1	47	3067	2300	624	0	0	0	138	5
2	192	21795	0	0	0	5056	16434	0	0
3	114	9279	0	9279	0	0	0	0	0
4	25	138	0	0	0	0	0	138	0
5	278	23418	0	1035	3971	1973	16434	0	5
6	454	9279	0	9279	0	0	0	0	0
7	230	9279	0	9279	0	0	0	0	0
8	25	53526	0	53526	0	0	0	0	0
9	100	62804	0	62804	0	0	0	0	0
10	25	1040	0	1035	0	0	0	0	5
11	60	22378	0	0	3971	1973	16434	0	0
12	25	10214528	0	100102	6129	2349342	7758956	0	0
13	30	10229201	0	100102	2625	2351315	7775158	0	0
14	40	62804	0	62804	0	0	0	0	0
15	30	7705	0	0	7474	0	231	0	0
16	40	7705	0	0	7474	0	231	0	0

Overall Mass Balance			
	Mass in	Mass out	% diff
Boiler	34140	32835	3.82%
Turbine	9279	9279	0.00%
Heat Exchange	62804	62804	0.00%
Gas Clean-Up	23418	23418	0.00%
Amine System	10299710	10299710	0.00%
Total	10429351	10428046	0.01%

Table A2.9 Itemized capital costs and scaling factors for the BB + SS-DAC system.

Equipment Name	Original installed price	Reference	Year of quote	Scaling stream	Scaling Value	Units	Scaling exponent	New value	Size ratio	Scaled installed cost	Index base year	Index project year (2016)	Installed cost in project year
Preprocessing	$ 24,155,013	*(16)*	2009	Biomass Feed	2000	dry tonne/day	0.8	2300	1.15	$ 27,012,548	521.9	541.7	$ 28,037,358
Boiler	$ 48,652,589	*(16)*	2010	High Quality Steam Production	235	tonne/h	0.8	387	1.65	$ 72,508,866	550.8	541.7	$ 71,310,917
Turbine/generator	$ 16,145,591	*(16)*	2010	Power Production	41	MW	0.8	109.6	2.67	$ 35,453,254	550.8	541.7	$ 34,867,515
Boiler accessories + gas cleaning	$ 1,161,393	*(16)*	2010	Biomass Feed	622	dry tonne/day	0.8	2300	3.70	$ 3,305,273	550.8	541.7	$ 3,250,665
Cooling tower system/HX	$ 2,186,673	*(16)*	2010	High Quality Steam Production	235	tonne/h	0.8	387	1.65	$ 3,258,885	550.8	541.7	$ 3,205,043
Blower	$ 21,000,000	*(5)*	2016	Gas Flow Rate	10.2	Mt-gas/day	0.8	10.2	1.00	$ 21,033,213	541.7	541.7	$ 21,033,213
Vacuum pump	$ 26,000,000	*(5)*	2016	CO2 Capacity	1	Mt-CO2/y	0.8	2.46	2.46	$ 53,340,397	541.7	541.7	$ 53,340,397
Contactor	$ 13,000,000	*(5)*	2016	CO2 Capacity	1	Mt-CO2/y	0.8	2.46	2.46	$ 26,670,198	541.7	541.7	$ 26,670,198
Compressor	$ 15,500,000	*(10)*	2016	CO2 Capacity	1.45	Mt-CO2/y	0.8	2.46	1.69	$ 23,559,576	541.7	541.7	$ 23,559,576
Indirect costs		*(10)*											$ 94,005,682
Contingency													$ 107,784,169
												Total Direct Costs:	$ 265,274,882
												Total Indirect Costs:	$ 201,789,851
												Total Capital Costs:	$ 467,064,733
												Capital Intensity ($/t-CO2-year)	$ 190

Table A2.10 A summary of results from the Biomass Boiler plus Solid Sorbent Direct Air Capture (BB + SS-DAC) techno-economic analysis showing levelized costs of CO_2 removal with a biomass cost of $70/dry short ton and CRF values of 7.5% and 12.5%.

Biomass Boiler + Solid Sorbent with Direct Air Capture BB + SS-DAC Economic Summary		
Direct air CO2 capacity (Mt-CO2/y)		1.28
Biogenic CO2 capacity (Mt-CO2/y)		1.17
Total capacity (Mt-CO2/y)		2.46
Specific biogenic CO2 capacity (t-CO2/t-biomass)		1.55
Biomass cost ($/short t-biomass)	$	70
Electricity cost ($/kWh)	$	0.05
Equipment Costs (2016$)		**Installed Capital Cost**
Preprocessing	$	28,037,358
Boiler	$	71,310,917
Turbine/generator	$	34,867,515
Boiler accessories + gas cleaning	$	3,250,665
Cooling tower system	$	3,205,043
Blower	$	21,033,213
Vacuum pump	$	53,340,397
Contactor	$	26,670,198
Compressor	$	23,559,576
Indirect costs	$	94,005,682
Contingency	$	107,784,169
Total Installed Capital	$	467,064,733
Capital Intensity ($/t-CO2-year)	$	190
Levelized Capital Cost (CRF 7.5%) ($/t-CO2)	**$**	**16**
Levelized Capital Cost (CRF 12.5%) ($/t-CO2)	**$**	**26**
Operating Costs (2016$)		**Annual Cost ($/y)**
Biomass feestock	$	58,299,522
Sorbent material (6-month life span)	$	188,743,957
Non-energy O&M	$	42,993,151
Electricity to grid	$	-
Process steam byproduct	$	-
Net Operating Costs	$	290,036,631
Net Operating Costs ($/t-CO2)	**$**	**118**
Total Costs (CRF 7.5%) ($/t-CO2)	**$**	**134**
Total Costs (CRF 12.5%) ($/t-CO2)	**$**	**145**

Table A2.11 Mass balance of the BB + SS-CC system.

Stream	Approx. Temp (C)	Mass flow (t/day)	Biomass	H2O	CO2	O2	N2	Ash	S
1	47	3067	2300	624	0	0	0	138	5
2	192	21795	0	0	0	5056	16434	0	0
3	114	9279	0	9279	0	0	0	0	0
4	25	138	0	0	0	0	0	138	0
5	278	23418	0	1035	3971	1973	16434	0	5
6	454	9279	0	9279	0	0	0	0	0
7	230	1104	0	1104	0	0	0	0	0
8	230	8175	0	8175	0	0	0	0	0
9	25	6370	0	6370	0	0	0	0	0
10	100	7474	0	7474	0	0	0	0	0
11	25	1040	0	1035	0	0	0	0	5
12	60	22378	0	0	3971	1973	16434	0	0
13	30	18694	0	0	398	1973	16323	0	0
14	40	7474	0	1104	0	0	0	0	0
15	30	3683	0	0	3573	0	110	0	0
16	40	3683	0	0	3573	0	110	0	0

Overall Mass Balance			
	Mass in	Mass out	% diff
Boiler	34140	32835	3.82%
Turbine	9279	9279	0.00%
Heat Exchange	7474	7474	0.00%
Gas Clean-Up	23418	23418	0.00%
Amine System	29851	29851	0.00%
Total	104162	102856	1.25%

Table A2.12 Itemized capital costs and scaling factors for the BB + SS-CC system.

Equipment Name	Original installed price	Reference	Year of quote	Scaling stream	Scaling Value	Units	Scaling exponent	New value	Size ratio	Scaled installed cost	Index base year	Index project year (2016)	Installed cost in project year
Preprocessing	$ 24,155,013	*(16)*	2009	Biomass Feed	2000	dry tonne/day	0.8	2300	1.15	$ 27,012,548	521.9	541.7	$ 28,037,358
Boiler	$ 48,652,589	*(16)*	2010	High Quality Steam Production	235	tonne/h	0.8	387	1.65	$ 72,508,866	550.8	541.7	$ 71,310,917
Turbine/generator	$ 16,145,591	*(16)*	2010	Power Production	41	MW	0.8	110	2.67	$ 35,453,254	550.8	541.7	$ 34,867,515
Boiler accessories + gas cleaning	$ 1,161,393	*(16)*	2010	Biomass Feed	622.2	dry tonne/day	0.8	2300	3.70	$ 3,305,273	550.8	541.7	$ 3,250,665
Cooling tower system/HX	$ 2,186,673	*(16)*	2010	High Quality Steam Production	235	tonne/h	0.8	387	1.65	$ 3,258,885	550.8	541.7	$ 3,205,043
Blower	$ 21,000,000	*(5)*	2016	Gas flow rate	10.2	Mt-gas/day	0.8	0.02	0.00	$ 162,336	541.7	541.7	$ 162,336
Vacuum Pump	$ 26,000,000	*(5)*	2016	CO2 Capacity	1	Mt-CO2/y	0.8	1.17	1.17	$ 29,553,222	541.7	541.7	$ 29,553,222
Contactor	$ 13,000,000	*(5)*	2016	CO2 Capacity	1	Mt-CO2/y	0.8	1.17	1.17	$ 14,776,611	541.7	541.7	$ 14,776,611
Compressor	$ 15,500,000	*(10)*	2016	CO2 Capacity	1.45	Mt-CO2/y	0.8	1.17	0.81	$ 13,053,172	541.7	541.7	$ 13,053,172
Indirect costs		*(10)*											$ 70,242,267
Contingency													$ 80,537,732
												Total Direct Costs:	$ 198,216,839
												Total Indirect Costs:	$ 150,779,998
												Total Capital Costs:	$ 348,996,837
												Capital Intensity ($/t-CO2-year)	$ 297

Table A2.13 A summary of results from the Biomass Boiler plus Solid Sorbent Carbon Capture (BB + SS-CC) techno-economic analysis showing levelized costs of CO_2 removal with a biomass cost of $70/dry short ton and CRF values of 7.5% and 12.5%.

Biomass Boiler + Solid Sorbent with Carbon Capture BB + SS-CC Economic Summary		
Direct air CO2 capacity (Mt-CO2/y)		0.00
Biogenic CO2 capacity (Mt-CO2/y)		1.17
Total capacity (Mt-CO2/y)		1.17
Specific biogenic CO2 capacity (t-CO2/t-biomass)		1.55
Biomass cost ($/short t-biomass)	$	70
Electricity cost ($/kWh)	$	0.05
Equipment Costs (2016$)		**Installed Capital Cost**
Preprocessing	$	28,037,358
Boiler	$	71,310,917
Turbine/generator	$	34,867,515
Boiler accessories + gas cleaning	$	3,250,665
Cooling tower system	$	3,205,043
Blower	$	162,336
Vacuum Pump	$	29,553,222
Contactor	$	14,776,611
Compressor	$	13,053,172
Indirect costs	$	70,242,267
Contingency	$	80,537,732
Total Installed Capital	$	348,996,837
Capital Intensity ($/t-CO2-year)	$	297
Levelized Capital Cost (CRF 7.5%) ($/t-CO2)	**$**	**25**
Levelized Capital Cost (CRF 12.5%) ($/t-CO2)	**$**	**41**
Operating Costs (2016$)		**Annual cost ($/y)**
Biomass feedstock	$	58,299,522
Sorbent material (6-month life span)	$	90,221,241
Non-energy O&M	$	28,519,718
Electricity to grid	$	(27,610,545)
Process steam byproduct	$	(23,832,413)
Net Operating Costs	$	125,597,522
Net Operating Costs ($/t-CO2)	**$**	**107**
Total Costs (w/ CRF 7.5%) ($/t-CO2)	**$**	**132**
Total Costs (w/ CRF 12.5%) ($/t-CO2)	**$**	**148**

Table A2.14 A) Levelized costs of CO_2 removal by the NG + LS-DAC system with variation in natural gas price and capital recovery factor (CRF). Baseline scenario assumes no natural gas leakage. Penalty scenario assumes a quantity of carbon equivalent to 3% of the natural gas-carbon captured on-site is emitted to the atmosphere during extraction and transportation. Natural gas is taken to have a global warming potential of 25. Relative to Baseline, the Penalty scenario increases levelized cost by 15%. **B)** Levelized costs of CO_2 removal by the BB + SS-CC system with variation in biomass price and CRF. Baseline scenario assumes biomass is carbon neutral. Penalty scenario assumes a quantity of carbon equivalent to 15% of the biogenic carbon captured on-site is emitted to the atmosphere during cultivation, harvest, and transportation of biomass. Relative to Baseline, the Penalty scenario increases costs by 18%.

A

Levelized Cost of CO_2 Removal ($/t-$CO_2$)
NG +LS-DAC

	Natural Gas Price ($/GJ)									
	$1.50		$3.50		$5.50		$7.50		$9.50	
CRF	Baseline	Penalty	Baseline	Penalty	Baseline	Penalty	Baseline	Penalty	Baseline	Penalty
2.5%	$65	$75	$83	$95	$100	$116	$118	$136	$136	$156
7.5%	$109	$126	$127	$146	$145	$166	$162	$187	$180	$207
12.5%	$153	$177	$171	$197	$189	$217	$206	$237	$224	$258
17.5%	$197	$227	$215	$248	$233	$268	$250	$288	$268	$308

B

Levelized Cost of CO_2 Removal ($/t-$CO_2$)
BB + SS-CC

	Biomass Prices ($/short ton)									
	$20		$40		$60		$80		$100	
CRF	Baseline	Penalty	Baseline	Penalty	Baseline	Penalty	Baseline	Penalty	Baseline	Penalty
2.5%	$80	$94	$94	$111	$108	$127	$122	$144	$137	$161
7.5%	$96	$113	$111	$130	$125	$147	$139	$163	$153	$180
12.5%	$113	$133	$127	$149	$141	$166	$155	$183	$170	$200
17.5%	$129	$152	$144	$169	$158	$186	$172	$202	$186	$219

Table A2.15 Levelized costs of CO_2 removal by the BB + SS-CC system with variation in biomass price and capital recovery factor (CRF). No revenue from excess steam.

Levelized Cost of CO2 Removal ($/t-CO2)
BB + SS-CC (no steam byproduct)

	Biomass Price ($/ short ton)				
CRF	$20	$40	$60	$80	$100
2.5%	$100	$114	$128	$143	$157
7.5%	$117	$131	$145	$159	$173
12.5%	$133	$147	$162	$176	$190
17.5%	$150	$164	$178	$192	$206

Table A3.1 Nutrient inputs to the algae farm (Davis et al., 2016).

	Input (t/day)	Input (mol/day)
NH3	2.1	122995
DAP	1.0	7741
NH3 in DAP	0.3	15482
Phos. Acid in DAP	0.8	7741
CO2	230	5227273

Table A3.2 U.S. ammonia production, import, & export (metric ton/year) (U.S. Geological Survey, 2017.).

Production	1.05E+07
Imports	3.30E+06
Exports	5.30E+05
Net Consumption	1.33E+07

Table A3.3 Total protein consumption by males of all ages in the U.S. for year 2017 (Berryman et al., 2018).

0	2015150	15.9	7.2	14571671.8	12677	12.7	0.005
1	2031718	21.3	9.7	19670724.3	17114	17.1	0.006
2	2056625	27.5	12.5	25707812.5	22366	22.4	0.008
3	2050474	31	14.1	28893042.7	25137	25.1	0.009
4	2042001	36	16.4	33414561.8	25395	25.4	0.009
5	2045050	40.5	18.4	37647511.4	28612	28.6	0.010
6	2069201	45.5	20.7	42794838.9	32524	32.5	0.012
7	2063003	50.5	23.0	47355296.1	35990	36.0	0.013
8	2062172	56.5	25.7	52960326.4	40250	40.2	0.015
9	2128715	63	28.6	60958656.8	46329	46.3	0.017
10	2140682	70.5	32.0	68599127.7	52135	52.1	0.019
11	2123819	78.5	35.7	75781723.4	57594	57.6	0.021
12	2116260	88	40.0	84650400	64334	64.3	0.023
13	2119558	100	45.5	96343545.5	73221	73.2	0.027
14	2104753	112	50.9	107151062	77149	77.1	0.028
15	2098809	123.5	56.1	117819505	84830	84.8	0.031
16	2155909	134	60.9	131314457	94546	94.5	0.035
17	2197871	142	64.5	141862583	102141	102.1	0.037
18	2169468	147.5	67.0	145452968	104726	104.7	0.038
19	2178434	152	69.1	150509985	99337	99.3	0.036
20	2187409	155	70.5	154112907	101715	101.7	0.037
21	2213975	197.8	89.9	199056480	131377	131.4	0.048
22	2270148	197.8	89.9	204106943	134711	134.7	0.049
23	2318784	197.8	89.9	208479761	137597	137.6	0.050
24	2358826	197.8	89.9	212079901	139973	140.0	0.051
25	2413370	197.8	89.9	216983903	143209	143.2	0.052
26	2443974	197.8	89.9	219735481	145025	145.0	0.053
27	2432679	197.8	89.9	218719957	144355	144.4	0.053
28	2335023	197.8	89.9	209939795	138560	138.6	0.051
29	2277184	197.8	89.9	204739543	135128	135.1	0.049
30	2236352	197.8	89.9	201068375	132705	132.7	0.048
31	2241759	197.8	89.9	201554514	133026	133.0	0.049
32	2248948	197.8	89.9	202200870	133453	133.5	0.049
33	2168114	197.8	89.9	194933159	128656	128.7	0.047
34	2193958	197.8	89.9	197256769	130189	130.2	0.048
35	2185895	197.8	89.9	196531832	129711	129.7	0.047
36	2156347	197.8	89.9	193875198	127958	128.0	0.047
37	2204181	197.8	89.9	198175910	130796	130.8	0.048
38	2056619	197.8	89.9	184908745	122040	122.0	0.045
39	2012943	197.8	89.9	180981875	119448	119.4	0.044
40	1985267	197.8	89.9	178493551	117806	117.8	0.043
41	1927055	197.8	89.9	173259763	114351	114.4	0.042
42	1987507	197.8	89.9	178694948	117939	117.9	0.043
43	1916102	197.8	89.9	172274989	113701	113.7	0.042
44	1937184	197.8	89.9	174170452	114952	115.0	0.042
45	2025025	197.8	89.9	182068157	120165	120.2	0.044
46	2136737	197.8	89.9	192112081	126794	126.8	0.046
47	2169762	197.8	89.9	195081329	128754	128.8	0.047
48	2050739	197.8	89.9	184380079	121691	121.7	0.044
49	2003912	197.8	89.9	180169906	118912	118.9	0.043
50	1997485	197.8	89.9	179592060	118531	118.5	0.043
51	2032379	197.8	89.9	182729348	120601	120.6	0.044
52	2148966	197.8	89.9	193211579	127520	127.5	0.047
53	2175762	197.8	89.9	195620783	129110	129.1	0.047
54	2165590	197.8	89.9	194706228	128506	128.5	0.047
55	2154452	197.8	89.9	193704821	127845	127.8	0.047
56	2171286	197.8	89.9	195218350	128844	128.8	0.047
57	2190232	197.8	89.9	196921768	129968	130.0	0.047
58	2102988	197.8	89.9	189077739	124791	124.8	0.046
59	2081562	197.8	89.9	187151347	123520	123.5	0.045
60	2047375	197.8	89.9	184077625	121491	121.5	0.044
61	1963253	197.8	89.9	176514292	116499	116.5	0.043
62	1938979	197.8	89.9	174331839	115059	115.1	0.042
63	1843702	197.8	89.9	165765571	109405	109.4	0.040
64	1763974	197.8	89.9	158597299	104674	104.7	0.038
65	1688983	197.8	89.9	151854926	100224	100.2	0.037
66	1626011	197.8	89.9	146193171	96487	96.5	0.035
67	1583631	197.8	89.9	142382824	93973	94.0	0.034
68	1527330	197.8	89.9	137320852	90632	90.6	0.033
69	1503913	197.8	89.9	135215451	89242	89.2	0.033
70	1558707	197.8	89.9	140141929	92494	92.5	0.034
71	1136177	197.8	89.9	102152641	67421	67.4	0.025
72	1108765	197.8	89.9	99688053.2	65794	65.8	0.024
73	1066091	197.8	89.9	95851272.6	63262	63.3	0.023
74	1077532	197.8	89.9	96879922.5	63941	63.9	0.023
75	923942	197.8	89.9	83070785.3	54827	54.8	0.020
76	827432	197.8	89.9	74393658.9	49100	49.1	0.018
77	769612	197.8	89.9	69195115.3	45669	45.7	0.017
78	713055	197.8	89.9	64110126.8	42313	42.3	0.015
79	664775	197.8	89.9	59769315.9	39448	39.4	0.014
80	596081	197.8	89.9	53593100.8	35371	35.4	0.013
81	552132	197.8	89.9	49641686.2	32764	32.8	0.012
82	510165	197.8	89.9	45868471.4	30273	30.3	0.011
83	441701	197.8	89.9	39712935.4	26211	26.2	0.010
84	408980	197.8	89.9	36771020	24269	24.3	0.009
85	371580	197.8	89.9	33408420	22050	22.0	0.008
86	334790	197.8	89.9	30100664.5	19866	19.9	0.007
87	301527	197.8	89.9	27110018.5	17893	17.9	0.007
88	254258	197.8	89.9	22860105.6	15088	15.1	0.006
89	219994	197.8	89.9	19779460.5	13054	13.1	0.005
90	185145	197.8	89.9	16646218.6	10987	11.0	0.004
91	150011	197.8	89.9	13487352.6	8902	8.9	0.003
92	122401	197.8	89.9	11004962.6	7263	7.3	0.003
93	96053	197.8	89.9	8636037.91	5700	5.7	0.002
94	73785	197.8	89.9	6633942.27	4378	4.4	0.002
95	54785	197.8	89.9	4925669.55	3251	3.3	0.001
96	40626	197.8	89.9	3652646.73	2411	2.4	0.001
97	27000	197.8	89.9	2427545.45	1602	1.6	0.001
98	17926	197.8	89.9	1611710.36	1064	1.1	0.000
99	11894	197.8	89.9	1069378.73	706	0.7	0.000
100	17894	197.8	89.9	1608833.27	1062	1.1	0.000

Table A3.4 Total protein consumption by females of all ages in the U.S. for year 2017 (Berryman et al., 2018).

0	1924145	15.2	6.9	13301381.2	11572	11.6	0.004
1	1943534	20.4	9.3	18021860.7	15679	15.7	0.006
2	1965150	26.5	12.0	23671125	20594	20.6	0.008
3	1956281	31.5	14.3	28010387	24369	24.4	0.009
4	1953782	34	15.5	30194812.7	22948	22.9	0.008
5	1956268	39.5	18.0	35123902.7	26694	26.7	0.010
6	1976331	44	20.0	39526620	30040	30.0	0.011
7	1979376	49.5	22.5	44535960	33847	33.8	0.012
8	1980666	57	25.9	51317255.5	39001	39.0	0.014
9	2043456	62	28.2	57588305.5	43767	43.8	0.016
10	2051237	70.5	32.0	65732822	49957	50.0	0.018
11	2034143	81.5	37.0	75355752	57270	57.3	0.021
12	2029693	91.5	41.6	84416777	64157	64.2	0.023
13	2035757	101	45.9	93459753.2	71029	71.0	0.026
14	2022552	105	47.7	96530890.9	69502	69.5	0.025
15	2015751	115	52.3	105368802	75866	75.9	0.028
16	2066782	118	53.6	110854671	79815	79.8	0.029
17	2098704	120	54.5	114474764	82422	82.4	0.030
18	2071758	125	56.8	117713523	84754	84.8	0.031
19	2078174	126	57.3	119022693	78555	78.6	0.029
20	2089336	128	58.2	121561367	80231	80.2	0.029
21	2104329	170.5	77.5	163085498	107636	107.6	0.039
22	2150615	170.5	77.5	166672663	110004	110.0	0.040
23	2196524	170.5	77.5	170230610	112352	112.4	0.041
24	2228689	170.5	77.5	172723398	113997	114.0	0.042
25	2295484	170.5	77.5	177900010	117414	117.4	0.043
26	2350352	170.5	77.5	182152280	120221	120.2	0.044
27	2351456	170.5	77.5	182237840	120277	120.3	0.044
28	2260383	170.5	77.5	175179683	115619	115.6	0.042
29	2210555	170.5	77.5	171318013	113070	113.1	0.041
30	2174279	170.5	77.5	168506623	111214	111.2	0.041
31	2183649	170.5	77.5	169232798	111694	111.7	0.041
32	2204770	170.5	77.5	170869675	112774	112.8	0.041
33	2142863	170.5	77.5	166071883	109607	109.6	0.040
34	2177520	170.5	77.5	168757800	111380	111.4	0.041
35	2179052	170.5	77.5	168876530	111459	111.5	0.041
36	2157640	170.5	77.5	167217100	110363	110.4	0.040
37	2190170	170.5	77.5	169738175	112027	112.0	0.041
38	2063849	170.5	77.5	159948298	105566	105.6	0.039
39	2025301	170.5	77.5	156960828	103594	103.6	0.038
40	2009156	170.5	77.5	155709590	102768	102.8	0.038
41	1948683	170.5	77.5	151022933	99675	99.7	0.036
42	2003193	170.5	77.5	155247458	102463	102.5	0.037
43	1947353	170.5	77.5	150919858	99607	99.6	0.036
44	1981873	170.5	77.5	153595158	101373	101.4	0.037
45	2066554	170.5	77.5	160157935	105704	105.7	0.039
46	2183846	170.5	77.5	169248065	111704	111.7	0.041
47	2201202	170.5	77.5	170593155	112591	112.6	0.041
48	2089271	170.5	77.5	161918503	106866	106.9	0.039
49	2046810	170.5	77.5	158627775	104694	104.7	0.038
50	2053593	170.5	77.5	159153458	105041	105.0	0.038
51	2089015	170.5	77.5	161898663	106853	106.9	0.039
52	2214239	170.5	77.5	171603523	113258	113.3	0.041
53	2261664	170.5	77.5	175278960	115684	115.7	0.042
54	2262401	170.5	77.5	175336078	115722	115.7	0.042
55	2258814	170.5	77.5	175058085	115538	115.5	0.042
56	2290060	170.5	77.5	177479650	117137	117.1	0.043
57	2303341	170.5	77.5	178508928	117816	117.8	0.043
58	2232903	170.5	77.5	173049983	114213	114.2	0.042
59	2222318	170.5	77.5	172229645	113672	113.7	0.041
60	2202546	170.5	77.5	170697315	112660	112.7	0.041
61	2128409	170.5	77.5	164951698	108868	108.9	0.040
62	2111180	170.5	77.5	163616450	107987	108.0	0.039
63	2032205	170.5	77.5	157495888	103947	103.9	0.038
64	1956079	170.5	77.5	151596123	100053	100.1	0.037
65	1878995	170.5	77.5	145622113	96111	96.1	0.035
66	1825058	170.5	77.5	141441995	93352	93.4	0.034
67	1778116	170.5	77.5	137803990	90951	91.0	0.033
68	1723919	170.5	77.5	133603723	88178	88.2	0.032
69	1700425	170.5	77.5	131782938	86977	87.0	0.032
70	1765955	170.5	77.5	136861513	90329	90.3	0.033
71	1307666	170.5	77.5	101344115	66887	66.9	0.024
72	1290521	170.5	77.5	100015378	66010	66.0	0.024
73	1255382	170.5	77.5	97292105	64213	64.2	0.023
74	1280269	170.5	77.5	99220847.5	65486	65.5	0.024
75	1115294	170.5	77.5	86435285	57047	57.0	0.021
76	1019726	170.5	77.5	79028765	52159	52.2	0.019
77	959502	170.5	77.5	74361405	49079	49.1	0.018
78	894185	170.5	77.5	69299337.5	45738	45.7	0.017
79	853738	170.5	77.5	66164695	43669	43.7	0.016
80	782413	170.5	77.5	60637007.5	40020	40.0	0.015
81	741699	170.5	77.5	57481672.5	37938	37.9	0.014
82	706475	170.5	77.5	54751812.5	36136	36.1	0.013
83	626409	170.5	77.5	48546697.5	32041	32.0	0.012
84	599235	170.5	77.5	46440712.5	30651	30.7	0.011
85	562977	170.5	77.5	43630717.5	28796	28.8	0.011
86	526296	170.5	77.5	40787940	26920	26.9	0.010
87	494385	170.5	77.5	38314837.5	25288	25.3	0.009
88	434161	170.5	77.5	33647477.5	22207	22.2	0.008
89	395817	170.5	77.5	30675817.5	20246	20.2	0.007
90	349357	170.5	77.5	27075167.5	17870	17.9	0.007
91	299362	170.5	77.5	23200555	15312	15.3	0.006
92	259808	170.5	77.5	20135120	13289	13.3	0.005
93	214903	170.5	77.5	16654982.5	10992	11.0	0.004
94	172001	170.5	77.5	13330077.5	8798	8.8	0.003
95	136983	170.5	77.5	10616182.5	7007	7.0	0.003
96	105967	170.5	77.5	8212442.5	5420	5.4	0.002
97	76874	170.5	77.5	5957735	3932	3.9	0.001
98	53197	170.5	77.5	4122767.5	2721	2.7	0.001
99	38571	170.5	77.5	2989252.5	1973	2.0	0.001
100	68354	170.5	77.5	5297435	3496	3.5	0.001

The nonlinear regression (Figure A4.1) is computed using the Gekko package in Python and a total of 39 data sets (Table A4.1), with each set containing four data points: CO_2 flow rate, CO_2 capture rate, CO_2 concentration, and levelized cost of capturing CO_2. The Python code is based on a non-linear regression for predicting oil prices, which is available via APMonitor's open source repositories. As shown in Figure A4.1, the nonlinear fit is acceptable with an R^2 correlation of 0.853. Of the 39 data sets used in the regression, 15 are from the bottom-up analysis conducted in this study, and the remaining 24 are derived from work published by Psarras et al. wherein techno-economic studies were conducted on CO_2 capture systems for power generation via 1) natural gas combined cycle (NGCC) with post-combustion monoethanolamine (MEA) chemisorption capture, 2) subcritical pulverized coal (PC) with post-combustion MEA chemisorption capture, and 3) integrated gasification combined cycle (IGCC) with a water gas shift reactor and Selexol unit. One data set from the bottom-up analysis (Mill 4, Steam + Lime Kiln Emissions) is not included in the regression because this particular scenario has a very low cost of CO_2 capture due to the lack of new boiler installation and no biomass consumption, thereby making it an outlier. All other data sets from the bottom-up analysis are included in the regression. The multivariate regression accounts for direct contact cooling of gases to condense water soluble components, but does not account for additional gas treating including desulfurization. The lack of additional gas treatment is deemed acceptable since gas streams at pulp and paper mills typically have concentrations of sulfur containing species (SOx) acceptable to amine chemisorption.

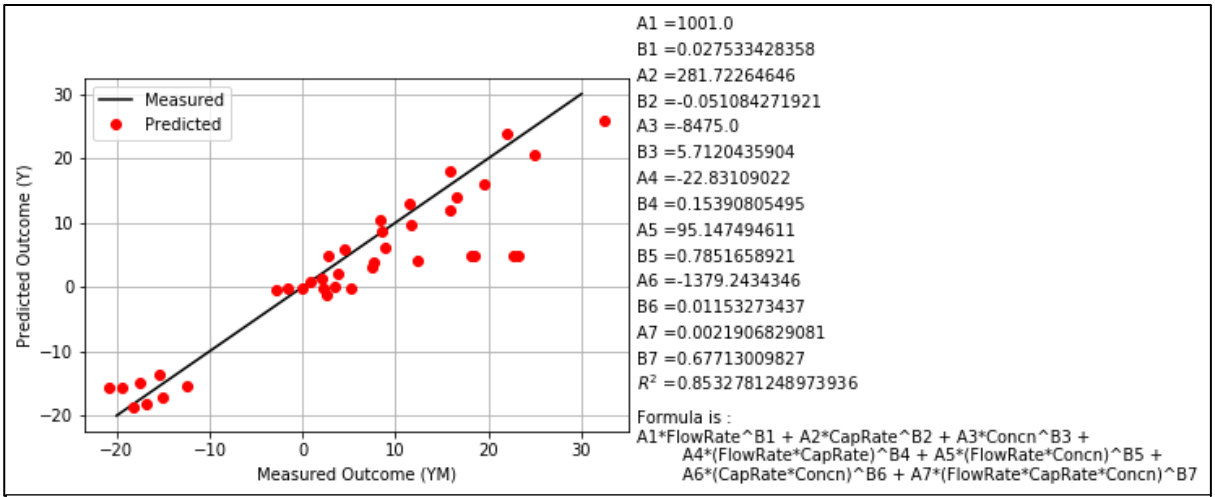

Figure A4.1 Nonlinear regression developed in Python to estimate costs of CO_2 capture for 205 pulp and paper mills across the US.

Table A4.1 Data sets used to construct the multivariate regression for top-down, industry-wide cost estimation. Flow rate: t-CO_2/year | Capture rate: CO_2 captured/total CO_2 | Concentration: CO_2 mol% | Cost: USD/t-CO_2 in year 2026 with \$50/t-CO_2 tax credit applied.

Flow_Rate	Capture_Rate	Concentration	Cost
3.13E+06	90%	37.7%	-20.7
2.06E+06	90%	13.6%	0.82
3.80E+06	70%	13.0%	4.45
3.13E+06	80%	37.7%	-19.4
3.12E+05	90%	18.3%	2.76
3.13E+06	70%	37.7%	-17.5
1.60E+06	90%	13.1%	2.01
1.53E+06	80%	37.7%	-16.9
3.13E+06	60%	37.7%	-15.3
7.05E+05	90%	20.8%	7.59
1.53E+06	70%	37.7%	-15.0
4.36E+06	90%	15.1%	-2.90
1.53E+06	60%	37.7%	-12.4
6.45E+05	90%	21.4%	12.3
3.80E+06	90%	13.0%	2.62
3.80E+06	80%	13.0%	3.79
3.37E+06	90%	14.9%	-1.67
1.53E+06	90%	37.7%	-18.2
9.51E+05	90%	13.0%	7.49
3.11E+06	90%	14.9%	3.50
3.80E+06	60%	13.0%	8.41
1.25E+06	90%	4.19%	8.49
3.41E+05	90%	18.3%	18.4
9.51E+05	80%	13.0%	8.88
3.16E+05	90%	18.8%	22.7
1.25E+06	80%	4.19%	11.5
3.10E+05	90%	18.6%	23.1
9.51E+05	70%	13.0%	11.7
6.26E+05	90%	4.19%	15.8
2.61E+06	90%	12.8%	-0.12
1.25E+06	70%	4.19%	15.9
4.01E+06	90%	15.1%	2.31
1.25E+06	60%	4.19%	22.0
2.61E+06	90%	12.7%	5.13
6.26E+05	80%	4.19%	19.6
6.26E+05	60%	4.19%	32.4
3.47E+05	90%	18.4%	18.0
6.26E+05	70%	4.19%	24.9
9.51E+05	60%	13.0%	16.5

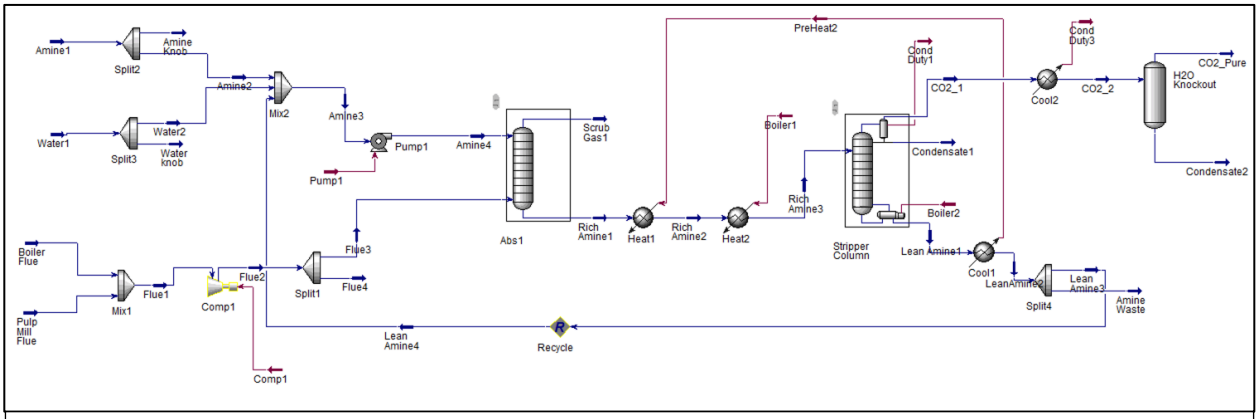

Figure A4.2 CO_2 Capture Amine System Model in Aspen Hysys.

Table A4.2 Techno-economic summary of Mill 1, Baseline Scenario 1.

Mill 1 **Baseline Scenario 1: Steam + Combined Emissions**		
P&P Site Biomass Input (dry short t-biomass/day)		4225
CO2 capture capacity (kt-CO2/y)		4005
CO2 capture rate (CO2 captured/CO2 input)		90%
Concentration of CO2 input (mol%)		15.1%
Biomass Input (dry short t-biomass/day)		3140
Biomass cost ($/short t-biomass)	$	60
Electricity cost ($/kWh)	$	0.07
LP steam cost ($/t-steam)	$	8.6
Reboiler Duty (GJ/tCO2)		3.5
Equipment Costs (2026$)		**Installed Capital Cost**
Biomas Boiler		
Biomass Preprocessing	$	39,149,860
Biomass Boiler	$	110,191,339
Turbine/generator	$	-
Boiler accessories + gas cleaning	$	4,038,839
Amine Capture System		
Compressors	$	38,479,067
Pumps	$	11,337,909
Heat Exchangers	$	28,120,818
Absorber Columns	$	16,719,920
Stripper Column	$	33,810,834
Water Knockout	$	599,264
Indirect costs	$	98,856,748
Contingency	$	38,130,460
Total Installed Capital	$	419,435,057
Capital Intensity ($/t-CO2-year)	$	105
Levelized Capital Cost (CRF 8%) ($/t-CO2)	**$**	**9**
Operating Costs (2026$)		**Annual cost ($/y)**
Biomass feedstock	$	61,896,026
MEA Absorbent	$	54,337,562
Cooling Water	$	3,173,003
Electricity	$	33,734,316
Low Pressure Steam	$	(54)
Other O&M	$	6,640,189
Fixed Costs	$	12,353,588
Net Operating Costs	$	172,134,630
Net Operating Costs ($/t-CO2)	**$**	**43**
45Q Tax Credit (y2026) ($/tCO2)	$	50
Total Costs (w/ CRF 8%) ($/t-CO2)	**$**	**2**

Table A4.3 Techno-economic summary of Mill 1, Baseline Scenario 2.

Mill 1		
Baseline Scenario 2: Steam & Power + Combined Emissions		
P&P Site Biomass Input (dry short t-biomass/day)		4225
CO2 capture capacity (kt-CO2/y)		4363
CO2 capture rate (CO2 captured/CO2 input)		90%
Concentration of CO2 input (mol%)		15%
Biomass Input (dry short t-biomass/day)		3932
Biomass cost ($/short t-biomass)	$	60
Electricity cost ($/kWh)	$	0.07
LP steam cost ($/t-steam)	$	8.6
Reboiler Duty (GJ/tCO2)		3.5
Equipment Costs (2026$)		**Installed Capital Cost**
Biomas Boiler		
Biomass Preprocessing	$	45,819,715
Biomass Boiler	$	116,278,923
Turbine/generator	$	29,959,742
Boiler accessories + gas cleaning	$	4,726,925
Amine Capture System		
Compressors	$	40,850,295
Pumps	$	12,036,595
Heat Exchangers	$	29,853,731
Absorber Columns	$	17,750,265
Stripper Column	$	35,894,388
Water Knockout	$	636,193
Indirect costs	$	116,832,370
Contingency	$	45,063,914
Total Installed Capital	$	495,703,058
Capital Intensity ($/t-CO2-year)	$	114
Levelized Capital Cost (CRF 8%) ($/t-CO2)	**$**	**10**
Operating Costs (2026$)		**Annual cost ($/y)**
Biomass feedstock	$	77,493,605
MEA Absorbent	$	59,183,562
Cooling Water	$	3,455,981
Electricity	$	8
Low Pressure Steam	$	366,774
Other O&M	$	7,170,388
Fixed Costs	$	13,605,713
Net Operating Costs	$	161,276,031
Net Operating Costs ($/t-CO2)	**$**	**37**
45Q Tax Credit (y2026) ($/tCO2)	$	50
Total Costs (w/ CRF 8%) ($/t-CO2)	**$**	**(3)**

Table A4.4 Techno-economic summary of Mill 1, Baseline Scenario 3.

Mill 1		
Baseline Scenario 3: Steam + Lime Kiln Emissions		
P&P Site Biomass Input (dry short t-biomass/day)		4225
CO2 capture capacity (kt-CO2/y)		316
CO2 capture rate (CO2 captured/CO2 input)		90%
Concentration of CO2 input (mol%)		18.8%
Biomass Input (dry short t-biomass/day)		247
Biomass cost ($/short t-biomass)	$	60
Electricity cost ($/kWh)	$	0.07
LP steam cost ($/t-steam)	$	8.6
Reboiler Duty (GJ/tCO2)		3.5
Equipment Costs (2026$)		**Installed Capital Cost**
Biomas Boiler		
Biomass Preprocessing	$	6,610,627
Biomass Boiler	$	18,606,294
Turbine/generator	$	-
Boiler accessories + gas cleaning	$	681,976
Amine Capture System		
Compressors	$	6,497,360
Pumps	$	438,616
Heat Exchangers	$	5,257,233
Absorber Columns	$	1,962,317
Stripper Column	$	5,195,355
Water Knockout	$	189,622
Indirect costs	$	15,903,790
Contingency	$	6,134,319
Total Installed Capital	$	67,477,510
Capital Intensity ($/t-CO2-year)	$	214
Levelized Capital Cost (CRF 8%) ($/t-CO2)	**$**	**19**
Operating Costs (2026$)		**Annual cost ($/y)**
Biomass feedstock	$	4,876,510
MEA Absorbent	$	4,281,012
Cooling Water	$	752,633
Electricity	$	2,699,549
Low Pressure Steam	$	(4)
Other O&M	$	523,151
Fixed Costs	$	3,800,124
Net Operating Costs	$	16,932,975
Net Operating Costs ($/t-CO2)	**$**	**54**
45Q Tax Credit (y2026) ($/tCO2)	$	50
Total Costs (w/ CRF 8%) ($/t-CO2)	**$**	**23**

Table A4.5 Techno-economic summary of Mill 1, Baseline Scenario 4.

Mill 1		
Baseline Scenario 4: Steam & Power + Lime Kiln Emissions		
P&P Site Biomass Input (dry short t-biomass/day)		4225
CO2 capture capacity (kt-CO2/y)		347
CO2 capture rate (CO2 captured/CO2 input)		90%
Concentration of CO2 input (mol%)		18.4%
Biomass Input (dry short t-biomass/day)		318
Biomass cost ($/short t-biomass)	$	60
Electricity cost ($/kWh)	$	0.07
LP steam cost ($/t-steam)	$	8.6
Reboiler Duty (GJ/tCO2)		3.5
Equipment Costs (2026$)		**Installed Capital Cost**
Biomas Boiler		
Biomass Preprocessing	$	7,881,360
Biomass Boiler	$	20,000,913
Turbine/generator	$	5,153,317
Boiler accessories + gas cleaning	$	813,069
Amine Capture System		
Compressors	$	6,950,284
Pumps	$	469,191
Heat Exchangers	$	5,623,709
Absorber Columns	$	2,099,108
Stripper Column	$	5,557,517
Water Knockout	$	202,841
Indirect costs	$	19,162,959
Contingency	$	7,391,427
Total Installed Capital	$	81,305,696
Capital Intensity ($/t-CO2-year)	$	234
Levelized Capital Cost (CRF 8%) ($/t-CO2)	**$**	**21**
Operating Costs (2026$)		**Annual cost ($/y)**
Biomass feedstock	$	6,268,920
MEA Absorbent	$	4,713,619
Cooling Water	$	828,689
Electricity	$	(2)
Low Pressure Steam	$	(23,905)
Other O&M	$	580,055
Fixed Costs	$	4,027,147
Net Operating Costs	$	16,394,524
Net Operating Costs ($/t-CO2)	**$**	**47**
45Q Tax Credit (y2026) ($/tCO2)	$	50
Total Costs (w/ CRF 8%) ($/t-CO2)	**$**	**18**

Table A4.6 Techno-economic summary of Mill 2, Baseline Scenario 1.

Mill 2 **Baseline Scenario 1: Steam + Combined Emissions**		
P&P Site Biomass Input (dry short t-biomass/day)		5263
CO2 capture capacity (kt-CO2/y)		4,032
CO2 capture rate (CO2 captured/CO2 input)		90%
Concentration of CO2 input (mol%)		13%
Biomass Input (dry short t-biomass/day)		3162
Biomass cost ($/short t-biomass)	$	60
Electricity cost ($/kWh)	$	0.07
LP steam cost ($/t-steam)	$	8.6
Reboiler Duty (GJ/tCO2)		3.5
Equipment Costs (2026$)		**Installed Capital Cost**
Biomas Boiler		
Biomass Preprocessing	$	39,334,782
Biomass Boiler	$	110,711,823
Turbine/generator	$	-
Boiler accessories + gas cleaning	$	4,057,917
Amine Capture System		
Compressors	$	38,660,821
Pumps	$	64,048,312
Heat Exchangers	$	52,823,747
Absorber Columns	$	23,400,191
Stripper Column	$	20,602,663
Water Knockout	$	605,508
Indirect costs	$	123,986,017
Contingency	$	47,823,178
Total Installed Capital	$	526,054,958
Capital Intensity ($/t-CO2-year)	$	130
Levelized Capital Cost (CRF 8%) ($/t-CO2)	**$**	**12**
Operating Costs (2026$)		**Annual cost ($/y)**
Biomass feedstock	$	62,314,110
MEA Absorbent	$	54,704,591
Cooling Water	$	3,067,235
Electricity	$	34,515,204
Low Pressure Steam	$	(54)
Other O&M	$	6,685,041
Fixed Costs	$	14,104,013
Net Operating Costs	$	175,390,139
Net Operating Costs ($/t-CO2)	**$**	**43**
45Q Tax Credit (y2026) ($/tCO2)	$	50
Total Costs (w/ CRF 8%) ($/t-CO2)	**$**	**5**

Table A4.7 Techno-economic summary of Mill 2, Baseline Scenario 2.

Mill 2	
Baseline Scenario 2: Steam & Power + Combined Emissions	
P&P Site Biomass Input (dry short t-biomass/day)	5263
CO2 capture capacity (kt-CO2/y)	4,442
CO2 capture rate (CO2 captured/CO2 input)	90%
Concentration of CO2 input (mol%)	13%
Biomass Input (dry short t-biomass/day)	4068
Biomass cost ($/short t-biomass)	$ 60
Electricity cost ($/kWh)	$ 0.07
LP steam cost ($/t-steam)	$ 8.6
Reboiler Duty (GJ/tCO2)	3.5
Equipment Costs (2026$)	**Installed Capital Cost**
Biomas Boiler	
Biomass Preprocessing	$ 46,927,113
Biomass Boiler	$ 119,089,223
Turbine/generator	$ 30,683,827
Boiler accessories + gas cleaning	$ 4,841,169
Amine Capture System	
Compressors	$ 41,367,183
Pumps	$ 68,531,866
Heat Exchangers	$ 56,521,551
Absorber Columns	$ 25,038,267
Stripper Column	$ 22,044,905
Water Knockout	$ 647,896
Indirect costs	$ 145,492,550
Contingency	$ 56,118,555
Total Installed Capital	$ 617,304,106
Capital Intensity ($/t-CO2-year)	$ 139
Levelized Capital Cost (CRF 8%) ($/t-CO2)	**$ 12**
Operating Costs (2026$)	**Annual cost ($/y)**
Biomass feedstock	$ 80,182,988
MEA Absorbent	$ 60,256,259
Cooling Water	$ 3,378,512
Electricity	$ (27)
Low Pressure Steam	$ (330,024)
Other O&M	$ 7,419,233
Fixed Costs	$ 15,602,090
Net Operating Costs	$ 166,509,030
Net Operating Costs ($/t-CO2)	**$ 37**
45Q Tax Credit (y2026) ($/tCO2)	$ 50
Total Costs (w/ CRF 8%) ($/t-CO2)	**$ (0)**

Table A4.8 Techno-economic summary of Mill 2, Baseline Scenario 3.

Mill 2		
Baseline Scenario 3: Steam + Lime Kiln Emissions		
P&P Site Biomass Input (dry short t-biomass/day)		5263
CO2 capture capacity (kt-CO2/y)		310
CO2 capture rate (CO2 captured/CO2 input)		90%
Concentration of CO2 input (mol%)		18.6%
Biomass Input (dry short t-biomass/day)		243
Biomass cost ($/short t-biomass)	$	60
Electricity cost ($/kWh)	$	0.07
LP steam cost ($/t-steam)	$	8.6
Reboiler Duty (GJ/tCO2)		3.5
Equipment Costs (2026$)		**Installed Capital Cost**
Biomas Boiler		
Biomass Preprocessing	$	6,529,129
Biomass Boiler	$	18,376,910
Turbine/generator	$	-
Boiler accessories + gas cleaning	$	673,568
Amine Capture System		
Compressors	$	6,417,259
Pumps	$	438,510
Heat Exchangers	$	5,256,080
Absorber Columns	$	1,961,844
Stripper Column	$	5,194,103
Water Knockout	$	189,577
Indirect costs	$	15,762,943
Contingency	$	6,079,992
Total Installed Capital	$	66,879,914
Capital Intensity ($/t-CO2-year)	$	216
Levelized Capital Cost (CRF 8%) ($/t-CO2)	**$**	**19**
Operating Costs (2026$)		**Annual cost ($/y)**
Biomass feedstock	$	4,790,853
MEA Absorbent	$	4,205,815
Cooling Water	$	754,525
Electricity	$	2,653,428
Low Pressure Steam	$	(4)
Other O&M	$	513,961
Fixed Costs	$	3,790,313
Net Operating Costs	$	16,708,891
Net Operating Costs ($/t-CO2)	**$**	**54**
45Q Tax Credit (y2026) ($/tCO2)	$	50
Total Costs (w/ CRF 8%) ($/t-CO2)	**$**	**23**

Table A4.9 Techno-economic summary of Mill 2, Baseline Scenario 4.

Mill 2		
Baseline Scenario 4: Steam & Power + Lime Kiln Emissions		
P&P Site Biomass Input (dry short t-biomass/day)		5263
CO2 capture capacity (kt-CO2/y)		341
CO2 capture rate (CO2 captured/CO2 input)		90%
Concentration of CO2 input (mol%)		18.3%
Biomass Input (dry short t-biomass/day)		313
Biomass cost ($/short t-biomass)	$	60
Electricity cost ($/kWh)	$	0.07
LP steam cost ($/t-steam)	$	8.6
Reboiler Duty (GJ/tCO2)		3.5
Equipment Costs (2026$)		**Installed Capital Cost**
Biomas Boiler		
Biomass Preprocessing	$	7,788,738
Biomass Boiler	$	19,765,861
Turbine/generator	$	5,092,755
Boiler accessories + gas cleaning	$	803,514
Amine Capture System		
Compressors	$	6,866,254
Pumps	$	469,191
Heat Exchangers	$	5,623,831
Absorber Columns	$	2,099,108
Stripper Column	$	5,557,517
Water Knockout	$	202,841
Indirect costs	$	18,994,364
Contingency	$	7,326,398
Total Installed Capital	$	80,590,373
Capital Intensity ($/t-CO2-year)	$	236
Levelized Capital Cost (CRF 8%) ($/t-CO2)	**$**	**21**
Operating Costs (2026$)		**Annual cost ($/y)**
Biomass feedstock	$	6,163,939
MEA Absorbent	$	4,632,418
Cooling Water	$	831,057
Electricity	$	(2)
Low Pressure Steam	$	(25,143)
Other O&M	$	570,342
Fixed Costs	$	4,015,404
Net Operating Costs	$	16,188,016
Net Operating Costs ($/t-CO2)	**$**	**47**
45Q Tax Credit (y2026) ($/tCO2)	$	50
Total Costs (w/ CRF 8%) ($/t-CO2)	**$**	**18**

Table A4.10 Techno-economic summary of Mill 3, Baseline Scenario 1.

Mill 3 **Baseline Scenario 1: Steam + Combined Emissions**		
P&P Site Biomass Input (dry short t-biomass/day)		7320
CO2 capture capacity (kt-CO2/y)		3,110
CO2 capture rate (CO2 captured/CO2 input)		90%
Concentration of CO2 input (mol%)		15%
Biomass Input (dry short t-biomass/day)		2438
Biomass cost ($/short t-biomass)	$	60
Electricity cost ($/kWh)	$	0.07
LP steam cost ($/t-steam)	$	8.6
Reboiler Duty (GJ/tCO2)		3.5
Equipment Costs (2026$)		**Installed Capital Cost**
Biomas Boiler		
Biomass Preprocessing	$	32,793,928
Biomass Boiler	$	92,301,910
Turbine/generator	$	-
Boiler accessories + gas cleaning	$	3,383,139
Amine Capture System		
Compressors	$	32,232,038
Pumps	$	2,937,532
Heat Exchangers	$	21,843,947
Absorber Columns	$	12,686,435
Stripper Column	$	27,626,824
Water Knockout	$	479,783
Indirect costs	$	79,199,937
Contingency	$	30,548,547
Total Installed Capital	$	336,034,019
Capital Intensity ($/t-CO2-year)	$	108
Levelized Capital Cost (CRF 8%) ($/t-CO2)	**$**	**10**
Operating Costs (2026$)		**Annual cost ($/y)**
Biomass feedstock	$	48,056,605
MEA Absorbent	$	42,188,149
Cooling Water	$	4,001,875
Electricity	$	26,041,826
Low Pressure Steam	$	(42)
Other O&M	$	5,155,500
Fixed Costs	$	10,984,357
Net Operating Costs	$	136,428,270
Net Operating Costs ($/t-CO2)	**$**	**44**
45Q Tax Credit (y2026) ($/tCO2)	$	50
Total Costs (w/ CRF 8%) ($/t-CO2)	**$**	**4**

Table A4.11 Techno-economic summary of Mill 3, Baseline Scenario 2.

Mill 3		
Baseline Scenario 2: Steam & Power + Combined Emissions		
P&P Site Biomass Input (dry short t-biomass/day)		7320
CO2 capture capacity (kt-CO2/y)		3,374
CO2 capture rate (CO2 captured/CO2 input)		90%
Concentration of CO2 input (mol%)		15%
Biomass Input (dry short t-biomass/day)		3023
Biomass cost ($/short t-biomass)	$	60
Electricity cost ($/kWh)	$	0.07
LP steam cost ($/t-steam)	$	8.6
Reboiler Duty (GJ/tCO2)		3.5
Equipment Costs (2026$)	**Installed Capital Cost**	
Biomas Boiler		
Biomass Preprocessing	$	38,122,553
Biomass Boiler	$	96,745,461
Turbine/generator	$	24,926,865
Boiler accessories + gas cleaning	$	3,932,859
Amine Capture System		
Compressors	$	34,124,666
Pumps	$	3,110,020
Heat Exchangers	$	23,126,599
Absorber Columns	$	13,431,368
Stripper Column	$	29,249,040
Water Knockout	$	507,955
Indirect costs	$	93,547,085
Contingency	$	36,082,447
Total Installed Capital	$	396,906,918
Capital Intensity ($/t-CO2-year)	$	118
Levelized Capital Cost (CRF 8%) ($/t-CO2)	**$**	**10**
Operating Costs (2026$)		**Annual cost ($/y)**
Biomass feedstock	$	59,588,889
MEA Absorbent	$	45,771,106
Cooling Water	$	4,341,746
Electricity	$	11
Low Pressure Steam	$	471,313
Other O&M	$	5,513,686
Fixed Costs	$	11,983,734
Net Operating Costs	$	127,670,485
Net Operating Costs ($/t-CO2)	**$**	**38**
45Q Tax Credit (y2026) ($/tCO2)	$	50
Total Costs (w/ CRF 8%) ($/t-CO2)	**$**	**(2)**

Table A4.12 Techno-economic summary of Mill 3, Baseline Scenario 3.

Mill 3 **Baseline Scenario 3: Steam + Lime Kiln Emissions**		
P&P Site Biomass Input (dry short t-biomass/day)		7320
CO2 capture capacity (kt-CO2/y)		645
CO2 capture rate (CO2 captured/CO2 input)		90%
Concentration of CO2 input (mol%)		21%
Biomass Input (dry short t-biomass/day)		506
Biomass cost ($/short t-biomass)	$	60
Electricity cost ($/kWh)	$	0.07
LP steam cost ($/t-steam)	$	8.6
Reboiler Duty (GJ/tCO2)		3.5
Equipment Costs (2026$)		**Installed Capital Cost**
Biomas Boiler		
Biomass Preprocessing	$	10,906,052
Biomass Boiler	$	30,696,215
Turbine/generator	$	-
Boiler accessories + gas cleaning	$	1,125,107
Amine Capture System		
Compressors	$	10,719,188
Pumps	$	645,994
Heat Exchangers	$	7,924,913
Absorber Columns	$	2,781,819
Stripper Column	$	7,494,517
Water Knockout	$	219,608
Indirect costs	$	25,379,695
Contingency	$	9,789,311
Total Installed Capital	$	107,682,419
Capital Intensity ($/t-CO2-year)	$	167
Levelized Capital Cost (CRF 8%) ($/t-CO2)	**$**	**15**
Operating Costs (2026$)		**Annual cost ($/y)**
Biomass feedstock	$	9,970,482
MEA Absorbent	$	8,752,931
Cooling Water	$	875,371
Electricity	$	5,460,210
Low Pressure Steam	$	(9)
Other O&M	$	1,069,631
Fixed Costs	$	4,460,186
Net Operating Costs	$	30,588,802
Net Operating Costs ($/t-CO2)	**$**	**47**
45Q Tax Credit (y2026) ($/tCO2)	$	50
Total Costs (w/ CRF 8%) ($/t-CO2)	**$**	**12**

Table A4.13 Techno-economic summary of Mill 3, Baseline Scenario 4.

Mill 3		
Baseline Scenario 4: Steam & Power + Lime Kiln Emissions		
P&P Site Biomass Input (dry short t-biomass/day)		7320
CO2 capture capacity (kt-CO2/y)		705
CO2 capture rate (CO2 captured/CO2 input)		90%
Concentration of CO2 input (mol%)		21%
Biomass Input (dry short t-biomass/day)		638
Biomass cost ($/short t-biomass)	$	60
Electricity cost ($/kWh)	$	0.07
LP steam cost ($/t-steam)	$	8.6
Reboiler Duty (GJ/tCO2)		3.5
Equipment Costs (2026$)		**Installed Capital Cost**
Biomas Boiler		
Biomass Preprocessing	$	12,836,694
Biomass Boiler	$	32,576,305
Turbine/generator	$	8,393,419
Boiler accessories + gas cleaning	$	1,324,279
Amine Capture System		
Compressors	$	11,406,099
Pumps	$	687,391
Heat Exchangers	$	8,432,760
Absorber Columns	$	2,960,084
Stripper Column	$	7,974,783
Water Knockout	$	233,681
Indirect costs	$	30,388,923
Contingency	$	11,721,442
Total Installed Capital	$	128,935,861
Capital Intensity ($/t-CO2-year)	$	183
Levelized Capital Cost (CRF 8%) ($/t-CO2)	**$**	**16**
Operating Costs (2026$)		**Annual cost ($/y)**
Biomass feedstock	$	12,584,572
MEA Absorbent	$	9,565,101
Cooling Water	$	956,595
Electricity	$	1
Low Pressure Steam	$	26,291
Other O&M	$	1,164,435
Fixed Costs	$	4,809,113
Net Operating Costs	$	29,106,109
Net Operating Costs ($/t-CO2)	**$**	**41**
45Q Tax Credit (y2026) ($/tCO2)	$	50
Total Costs (w/ CRF 8%) ($/t-CO2)	**$**	**8**

Table A4.14 Techno-economic summary of Mill 4, Baseline Scenario 1.

Mill 4		
Baseline Scenario 1: Steam + Combined Emissions		
P&P Site Biomass Input (dry short t-biomass/day)		3444
CO2 capture capacity (kt-CO2/y)		1,602
CO2 capture rate (CO2 captured/CO2 input)		90%
Concentration of CO2 input (mol%)		13%
Biomass Input (dry short t-biomass/day)		831
Biomass cost ($/short t-biomass)	$	60
Electricity cost ($/kWh)	$	0.07
LP steam cost ($/t-steam)	$	8.6
Reboiler Duty (GJ/tCO2)		3.5
Equipment Costs (2026$)		**Installed Capital Cost**
Biomas Boiler		
Biomass Preprocessing	$	15,433,007
Biomass Boiler	$	43,437,799
Turbine/generator	$	-
Boiler accessories + gas cleaning	$	1,592,124
Amine Capture System		
Compressors	$	20,259,413
Pumps	$	2,015,265
Heat Exchangers	$	14,881,627
Absorber Columns	$	9,298,772
Stripper Column	$	23,790,777
Water Knockout	$	343,208
Indirect costs	$	45,868,197
Contingency	$	17,692,019
Total Installed Capital	$	194,612,209
Capital Intensity ($/t-CO2-year)	$	121
Levelized Capital Cost (CRF 8%) ($/t-CO2)	**$**	**11**
Operating Costs (2026$)		**Annual cost ($/y)**
Biomass feedstock	$	16,372,704
MEA Absorbent	$	21,732,188
Cooling Water	$	3,977,162
Electricity	$	13,457,879
Low Pressure Steam	$	(0)
Other O&M	$	1,756,459
Fixed Costs	$	8,662,574
Net Operating Costs	$	65,958,967
Net Operating Costs ($/t-CO2)	**$**	**41**
45Q Tax Credit (y2026) ($/tCO2)	$	50
Total Costs (w/ CRF 8%) ($/t-CO2)	**$**	**2**

Table A4.15 Techno-economic summary of Mill 4, Baseline Scenario 2.

Mill 4	
Baseline Scenario 2: Steam & Power + Combined Emissions	
P&P Site Biomass Input (dry short t-biomass/day)	3444
CO2 capture capacity (kt-CO2/y)	2,065
CO2 capture rate (CO2 captured/CO2 input)	90%
Concentration of CO2 input (mol%)	14%
Biomass Input (dry short t-biomass/day)	1856
Biomass cost ($/short t-biomass)	$ 60
Electricity cost ($/kWh)	$ 0.07
LP steam cost ($/t-steam)	$ 8.6
Reboiler Duty (GJ/tCO2)	3.5
Equipment Costs (2026$)	**Installed Capital Cost**
Biomas Boiler	
Biomass Preprocessing	$ 27,094,799
Biomass Boiler	$ 68,759,792
Turbine/generator	$ 17,716,243
Boiler accessories + gas cleaning	$ 2,795,196
Amine Capture System	
Compressors	$ 24,199,011
Pumps	$ 2,407,148
Heat Exchangers	$ 17,775,474
Absorber Columns	$ 11,106,990
Stripper Column	$ 28,417,076
Water Knockout	$ 409,948
Indirect costs	$ 70,238,587
Contingency	$ 27,092,026
Total Installed Capital	$ 298,012,290
Capital Intensity ($/t-CO2-year)	$ 144
Levelized Capital Cost (CRF 8%) ($/t-CO2)	**$ 13**
Operating Costs (2026$)	**Annual cost ($/y)**
Biomass feedstock	$ 36,585,905
MEA Absorbent	$ 28,012,212
Cooling Water	$ 5,126,456
Electricity	$ (5)
Low Pressure Steam	$ (5,096,774)
Other O&M	$ 3,385,249
Fixed Costs	$ 10,360,138
Net Operating Costs	$ 78,373,180
Net Operating Costs ($/t-CO2)	**$ 38**
45Q Tax Credit (y2026) ($/tCO2)	$ 50
Total Costs (w/ CRF 8%) ($/t-CO2)	**$ 1**

Table A4.16 Techno-economic summary of Mill 4, Baseline Scenario 3.

Mill 4		
Baseline Scenario 3: Steam + Lime Kiln Emissions		
P&P Site Biomass Input (dry short t-biomass/day)		3444
CO2 capture capacity (kt-CO2/y)		183
CO2 capture rate (CO2 captured/CO2 input)		90%
Concentration of CO2 input (mol%)		21%
Biomass Input (dry short t-biomass/day)		0
Biomass cost ($/short t-biomass)	$	60
Electricity cost ($/kWh)	$	0.07
LP steam cost ($/t-steam)	$	8.6
Reboiler Duty (GJ/tCO2)		3.5
Equipment Costs (2026$)		**Installed Capital Cost**
Biomas Boiler		
Biomass Preprocessing	$	-
Biomass Boiler	$	-
Turbine/generator	$	-
Boiler accessories + gas cleaning	$	-
Amine Capture System		
Compressors	$	4,436,053
Pumps	$	243,056
Heat Exchangers	$	2,981,700
Absorber Columns	$	1,200,768
Stripper Column	$	3,705,667
Water Knockout	$	140,615
Indirect costs	$	4,447,751
Contingency	$	1,715,561
Total Installed Capital	$	18,871,172
Capital Intensity ($/t-CO2-year)	$	103
Levelized Capital Cost (CRF 8%) ($/t-CO2)	**$**	**9**
Operating Costs (2026$)		**Annual cost ($/y)**
Biomass feedstock	$	-
MEA Absorbent	$	2,481,845
Cooling Water	$	530,697
Electricity	$	1,566,366
Low Pressure Steam	$	(3,526,498)
Other O&M	$	-
Fixed Costs	$	3,002,133
Net Operating Costs	$	4,054,542
Net Operating Costs ($/t-CO2)	**$**	**22**
45Q Tax Credit (y2026) ($/tCO2)	$	50
Total Costs (w/ CRF 8%) ($/t-CO2)	**$**	**(19)**

Table A4.17 Techno-economic summary of Mill 4, Baseline Scenario 4.

Mill 4		
Baseline Scenario 4: Steam & Power + Lime Kiln Emissions		
P&P Site Biomass Input (dry short t-biomass/day)		3444
CO2 capture capacity (kt-CO2/y)		312
CO2 capture rate (CO2 captured/CO2 input)		90%
Concentration of CO2 input (mol%)		18%
Biomass Input (dry short t-biomass/day)		286
Biomass cost ($/short t-biomass)	$	60
Electricity cost ($/kWh)	$	0.07
LP steam cost ($/t-steam)	$	8.6
Reboiler Duty (GJ/tCO2)		3.5
Equipment Costs (2026$)		**Installed Capital Cost**
Biomas Boiler		
Biomass Preprocessing	$	7,313,067
Biomass Boiler	$	18,558,726
Turbine/generator	$	4,781,732
Boiler accessories + gas cleaning	$	754,442
Amine Capture System		
Compressors	$	6,445,250
Pumps	$	353,143
Heat Exchangers	$	4,332,184
Absorber Columns	$	1,744,625
Stripper Column	$	5,384,055
Water Knockout	$	204,303
Indirect costs	$	17,455,034
Contingency	$	6,732,656
Total Installed Capital	$	74,059,216
Capital Intensity ($/t-CO2-year)	$	237
Levelized Capital Cost (CRF 8%) ($/t-CO2)	**$**	**21**
Operating Costs (2026$)		**Annual cost ($/y)**
Biomass feedstock	$	5,633,286
MEA Absorbent	$	4,232,047
Cooling Water	$	904,945
Electricity	$	1
Low Pressure Steam	$	(5,345,208)
Other O&M	$	521,241
Fixed Costs	$	3,908,179
Net Operating Costs	$	9,854,491
Net Operating Costs ($/t-CO2)	**$**	**32**
45Q Tax Credit (y2026) ($/tCO2)	$	50
Total Costs (w/ CRF 8%) ($/t-CO2)	**$**	**3**

Assessing Graphite Mass Yields

As shown in Figure A6.1, biographite yields vary considerably with biomaterial precursor. Lignin provides the highest graphite product yields (~25%). Mixed hardwood and softwood have approximately equal biographite yields (~17%). Cellulose (15.9%) and glucose (13.6%) have the lowest biographite yields.

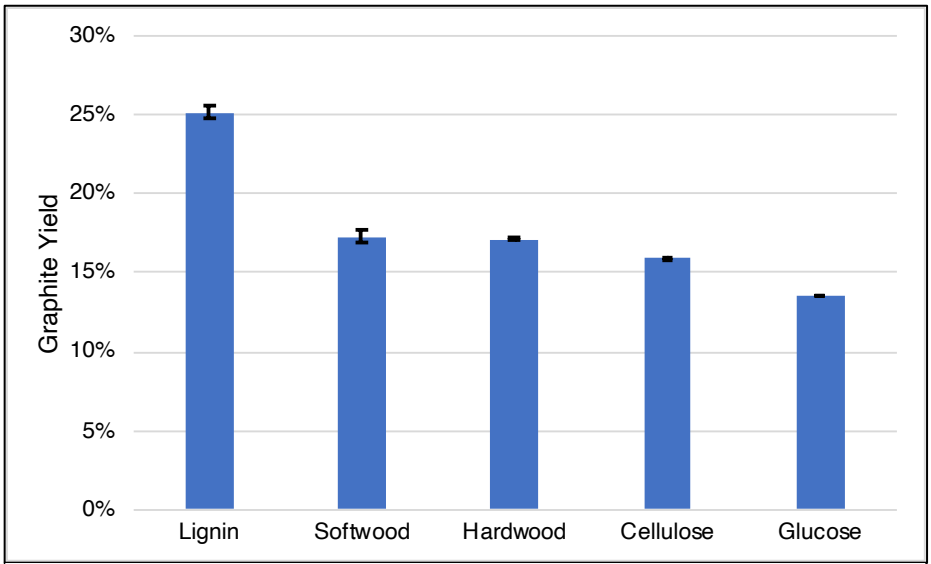

Figure A6.1 Biographite mass yields of the various biomaterials treated under baseline conditions, reported as percent of starting mass. Lignin refers to organosolv lignin.

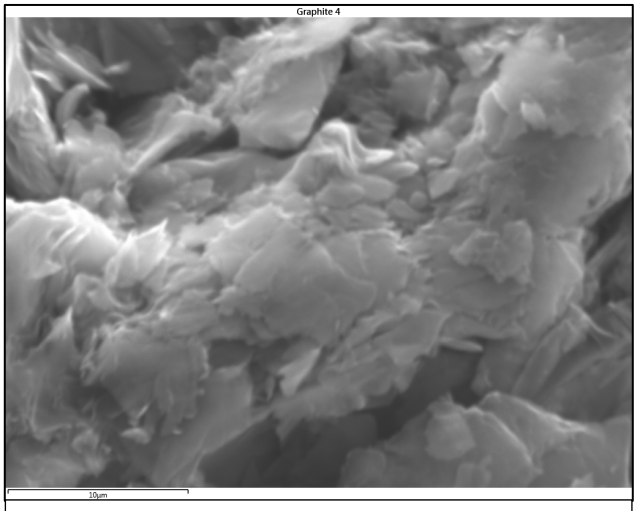

Figure A6.2 Scanning electron micrograph of commercial synthetic graphite.

Assessing Morphology of Biomaterials Treated at Low Temperatures

Notably, graphitic structure is readily detected through observation and comparison of biomaterials treated at different temperatures. Softwood and glucose treated at 600°C (Figure A6.3A+C) have been proven to be nongraphitic, disordered carbon via XRD (Figure 6.2G). In Figure A6.3A+C, indentations and thin shell casings where iron particles were located prior to acid washing are evident, but there is an overall lack of observable evidence indicating high reactivity between the iron catalyst and biomaterial. However, Figure A6.3B+D shows evidence of flaky graphite platelets forming from reaction between the iron particles and biomaterial treated at 1200°C, with validation from XRD and Raman data (Figure 6.1).

Assessing Kraft Lignin Carbonization

Kraft lignin's inability to graphitize under the conditions tested in this study appears to be due to the presence of sulfur and inadequate phase change of iron during thermal treatment. After a successful graphitization, the iron catalyst is of the allotropic form alpha, as shown in Figure A6.4A. Kraft lignin is the only biomaterial that contains iron catalyst of two allotropic forms after thermal treatment: alpha and gamma, as shown in Figure A6.4A. In addition, kraft lignin is the only biomaterial with a significant concentration of sulfur, as shown in Figure A6.4B. Sulfur and iron are highly reactive, and thus their interaction reduces the efficacy of the catalyst.

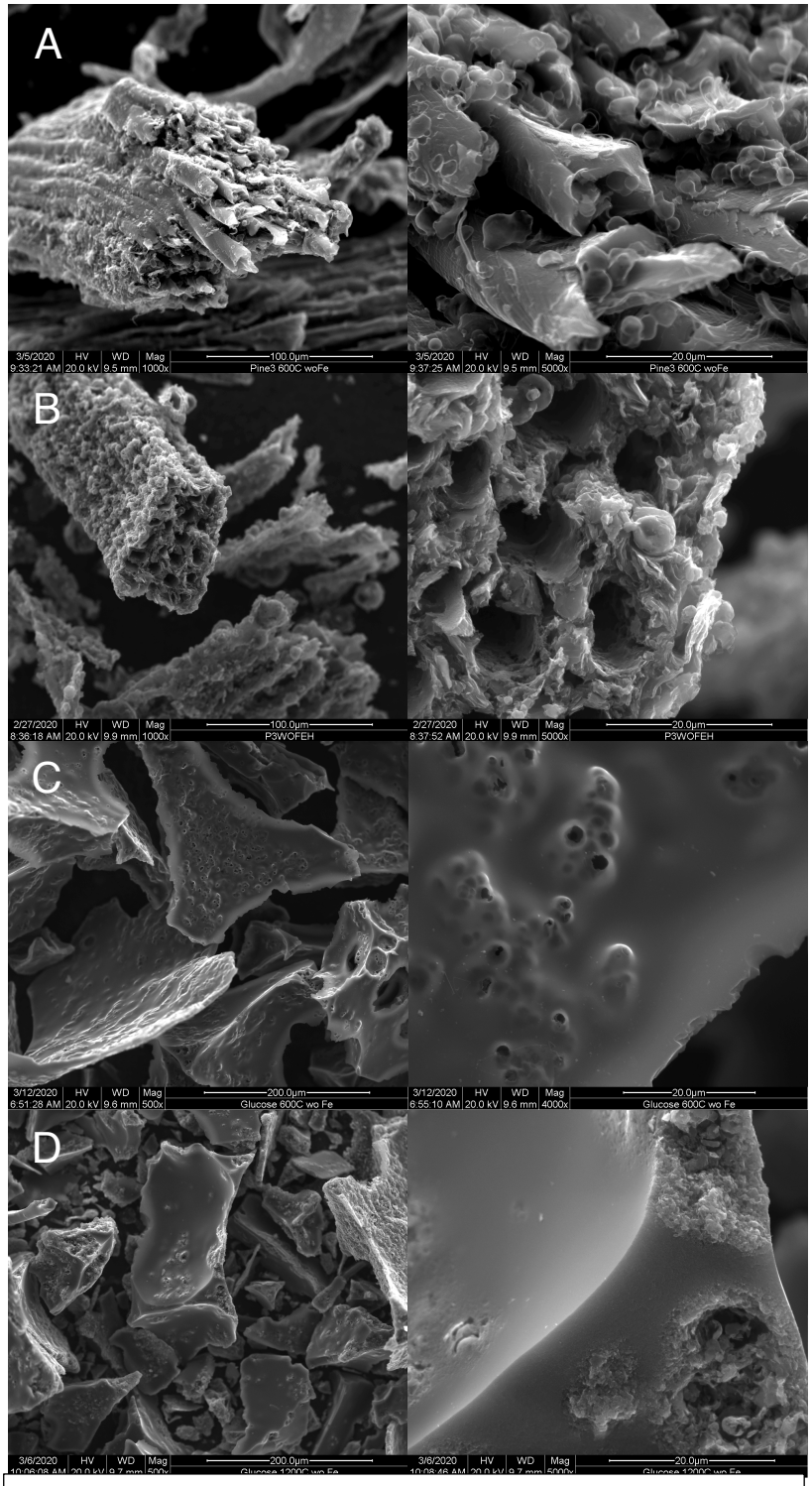

Figure A6.3 Scanning electron micrographs of biographite materials after iron removal via acid washing: A) softwood graphitized at 600°C, B) softwood graphitized at 1200°C, C) glucose graphitized at 600°C, and D) glucose graphitized at 1200°C.

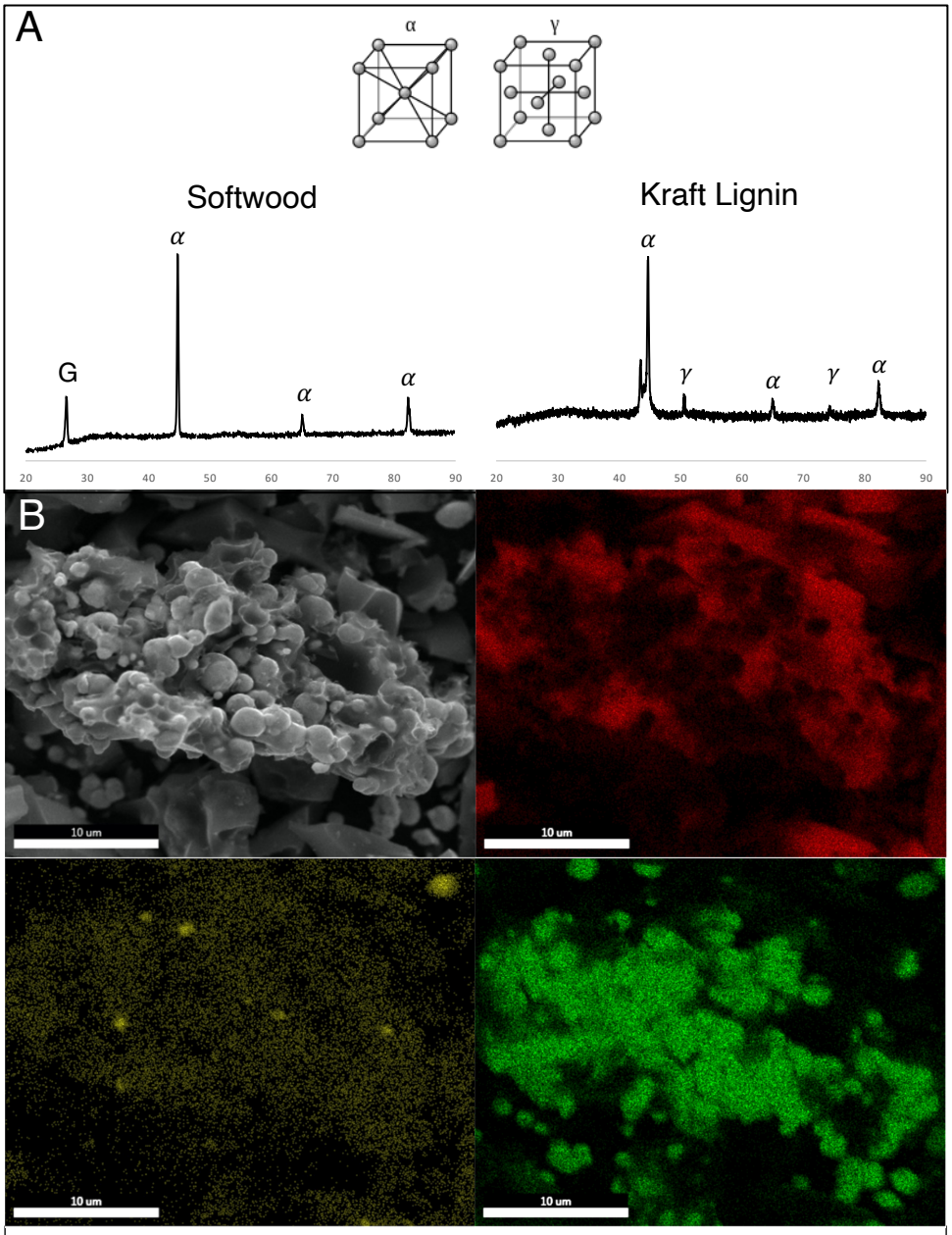

Figure A6.4 A) X-ray diffractograms of softwood- and kraft-lignin derived biographite materials (prior to iron removal) with peaks highlighted for graphite (G), the alpha allotrope of iron (α), and the gamma allotrope of iron (γ), with 2θ angles of diffraction on the x-axis and intensity on the y-axis. B) Energy-dispersive x-ray spectral mapping of kraft lignin-derived biographite materials produced using baseline procedure (prior to iron removal). Red, yellow, and green represent carbon, sulfur, and iron, respectively.

Table A6.1 Summary of electrochemical performance of biographite (this work) and other graphite materials reported in previous studies.

Sample	Voltage window (V)	1st CE (%)	1st delithiation capacity ($mAhg^{-1}$)	Rate capability ($mAhg^{-1}$)	Capacity Retention (%)	Reference
Biographite	0.005-1.5	84.0	335 (at 0.1C)	40 (at 4C) 15 (at 8C)	89 (100 cycles at 0.5C)	This work
Natural graphite	0.001-2.5	80.0	314 (at 0.1C)	~25 (at 1.2C)	52 (30 cycles at 0.1C)	[1]
PVC-coated natural graphite	0.001-2.5	87.0	330 (at 0.1C)	~120 (at 1.2C)	101 (30 cycles at 0.1C)	[1]
Natural graphite	0.00-2.0	83.9	253 (at 0.5C)	-	-	[2]
Na_2CO_3 coated natural graphite	0.00-2.0	86.2	316 (at 0.5C)	-	-	[2]
Artificial graphite	0.00-2.0	53.0	310 (at 30 mAg^{-1})	-	-	[3]
Natural graphite	0.01-2.0	94.5	352.6 (at 0.2C)	~330 (at 5C)	84 (50 cycles at 0.5C)	[4]
H_3PO_4-treated natural graphite	0.01-2.0	92.5	352.5 (at 0.2C)	~338 (at 5C)	94 (50 cycles at 0.5C)	[4]

Appendix References

[1] H. L. Zhang, F. Li, C. Liu, H. M. Cheng, *J. Phys. Chem. C* **2008**, *112*, 7767.
[2] S. Komaba, M. Watanabe, H. Groult, N. Kumagai, *Carbon N. Y.* **2008**, *46*, 1184.
[3] S. Yoon, H. Kim, S. M. Oh, *J. Power Sources* **2001**, *94*, 68.
[4] M. S. Park, J. Lee, J. W. Lee, K. J. Kim, Y. N. Jo, S. G. Woo, Y. J. Kim, *Carbon N. Y.* **2013**, *62*, 278.